



ATLAS Note

ANA-HDBS-2020-09-INT1

22nd March 2023



Draft version 1.2

1

2 Search for $t\bar{b}$ resonance using boosted top-quark 3 topology in the lepton+jets final state at $\sqrt{s} = 13$ 4 TeV with the ATLAS detector

5

De La Torre Perez, Hector^a, Gombas, Jason Peter^a, Schwienhorst, Reinhard^a,
6 Sato, Koji^b, Hirose, Shigeki^b, Yamauchi, Hiroki^b, Salvador Salas, Adrian^c, Riu,
7 Imma^c, Mir Martinez, Lluisa Maria^c

8

^a*Michigan State University (US)*

9

^b*University of Tsukuba (JP)*

10

^c*The Barcelona Institute of Science and Technology (BIST) (ES)*

11

A search for $t\bar{b}$ resonances with a boosted top tagging technique is presented, focusing on a final state consisting of a single charged lepton and multiple jets as well as a top-tagged large- R jet. The analysis is based on the pp collision data at the centre-of-mass energy of 13 TeV collected with the ATLAS detector with an integrated luminosity of 139 fb^{-1} . As a hypothetical particle with spin-0(1), a charged Higgs boson (a W' boson) scenario is searched in the mass range from 1 TeV up to 5 TeV.

17

© 2023 CERN for the benefit of the ATLAS Collaboration.

18

Reproduction of this article or parts of it is allowed as specified in the CC-BY-4.0 license.

19 **Contents**

20	1 Introduction	6
21	2 Data and MonteCarlo Simulated Events	8
22	2.1 Data Sample	8
23	2.2 Signal Samples	8
24	2.2.1 $\bar{t}bH^+$ Samples	9
25	2.2.2 $\bar{t}bW'$ Samples	9
26	2.3 Background Samples	10
27	2.3.1 $t\bar{t}$ +jets	11
28	2.3.2 $t\bar{t}H$	12
29	2.3.3 $t\bar{t}V$	12
30	2.3.4 Single top	12
31	2.3.5 tH	13
32	2.3.6 Rare t processes	14
33	2.3.7 Vector bosons plus jets	14
34	2.3.8 Dibosons	15
35	3 Object Reconstruction	16
36	3.1 Electrons	16
37	3.2 Muons	16
38	3.3 Taus	16
39	3.4 Small- R jets and b -tagging	16
40	3.5 Large- R jets and top-tagging	17
41	3.6 Overlap Removal	18
42	4 Analysis Strategy	19
43	4.1 Analysis strategy below 3 TeV	19
44	4.1.1 Event Selection	19
45	4.1.2 Multivariable analysis using BDT	23
46	4.2 Analysis strategy above 3 TeV	33
47	5 Background modeling	37
48	5.1 Blind strategy	37
49	5.2 Data/MC comparison for BDT input variables	37
50	5.3 Data/MC comparison for BDT outputs	40
51	5.4 Reweighting technique	42
52	6 Systematics Uncertainties	49
53	6.1 Luminosity and pile-up modeling	50
54	6.1.1 Luminosity	50
55	6.1.2 Pile-up modeling	50
56	6.2 Reconstructed objects	51
57	6.2.1 Charged leptons	51
58	6.2.2 Small- R jets, Large- R jets	51
59	6.3 Signal modeling	53

60	6.4	Background modeling	54
61	6.4.1	$t\bar{t}$ +jets	54
62	6.4.2	Other backgrounds	56
63	7	Profile Likelihood Fit	58
64	7.1	Method	58
65	7.2	Pruning and smoothing of systematic uncertainties	58
66	7.3	Asimov fit	59
67	7.3.1	Pre-fit plots	59
68	7.3.2	Asimov fit results	75
69	7.3.3	Post-fit plots	132
70	7.3.4	Asimov fit results summary	147
71	7.4	Data fit	149
72	7.4.1	Pre-fit plots	149
73	7.4.2	Fit results	154
74	7.5	Post-fit plots	165
75	7.6	Upper cross-section limits as a function of signal mass	169
76	8	Summary and Conclusions	173
77	Appendices		178
78	A	TOPQ1 DAOD list	178
79	A.1	Data	178
80	A.2	$\bar{t}bH^+$	178
81	A.3	$\bar{t}bW'$	178
82	A.4	$t\bar{t}$ + jets	179
83	A.5	$t\bar{t}H$	180
84	A.6	$t\bar{t}V$	181
85	A.7	Single top	181
86	A.8	tH	182
87	A.9	Rare t processes	182
88	A.10	Vector bosons plus jets	182
89	A.10.1	W + jets	182
90	A.10.2	Z + jets	183
91	A.11	Diboson	185
92	B	Signal/background comparisons	186
93	B.1	BDT input variables	186
94	B.2	BDT outputs	189
95	B.3	H_T^{jets} in the CR	191
96	C	Fit test	192
97	C.1	Data fit with $t\bar{t}$ + light constrained	192
98	C.1.1	Pre-fit plots	192
99	C.1.2	Fit results	195

100 List of contributions

De La Torre Perez, Hector	W' vs H+ comparisons, W' generation
Gombas, Jason Peter	W' NLO model, W' vs H+ comparisons, W' generation
Schwienhorst, Reinhard	W' NLO model, Jason supervision
Sato, Koji	Analysis contact, supervision of Hiroki
Hirose, Shigeki	Analysis contact, ntuple production, BDT training, MC production, supervision of Hiroki
101 Yamauchi, Hiroki	Main analyser: ntuple production, fit studies and limits extraction
Salvador Salas, Adrian	Main analyser of resolved analysis, providing technical support; ntuple production
Riu, Imma	Signal AODs and TOPQ1s production; provision of other technical support from resolved analysis
102 Mir Martinez, Lluisa Maria	Monte Carlo production

103 Version log with major updates:

104 **v1.1:**

- 105 • Added information of $t\bar{b}W'$ MC samples (Section 2.2)
- 106 • Changed analysis regions (Section 4.1.1)
- 107 • Compared BDT distributions between H^+ and W' signals (Section 4.1.2)
- 108 • Adopted the cut-and-counting approach for the signal above 3 TeV (Section 4.2)
- 109 • Performed reweighting to improve $t\bar{t} + \text{jets}$ MC prediction (Section 5.4)
- 110 • Some systematics are included or updated (Section 6)
 - 111 – b -tagging calibration uncertainty sources of PCBT are replaced into the ones of FixedCut to consider p_T extrapolation (Section 6.2.2).
 - 113 – Systematic uncertainties from the reweighting are included (Section 6.4.1).
 - 114 – $t\bar{t} + \geq 1b$ fraction uncertainty to the whole of $t\bar{t} + \text{HF}$ is included. (Section 6.4.1)
 - 115 – Uncertainty of the difference between 4FS and 5FS for $t\bar{t} + \geq 1b$ is included (Section 6.4.1).
- 116 • Estimated the cross-section upper limits for $W'_{L/R}$ signals (Section 7.6)

117 **v1.2:**

- 118 • Added theoretical motivations for $W'_{L(R)} \rightarrow tb$ searches (Section 1)
- 119 • Updated analysis regions to SR ($\geq 2b$) region and CR ($1b$) region (Section 4)
- 120 • Updated BDT comparison plots between data and MC in association with the update of analysis regions (Section 5.3)
- 122 • Updated the reweighting strategy to correct only the shape of $t\bar{t} + \text{jets}$ MC distributions (Section 5.4)
- 124 • Updated Asimov fit results and expected upper limits on each signal mass hypothesis in association with the update of analysis regions (Section 7)

126 Remaining to do:

- 128 • Fix the pre-fit plot on 2500 GeV H^+ mass hypothesis, and update the fit result and expected upper limit.
- 130 • Compare the fit results between when and when not constraining $t\bar{t} + \text{light}$ normalization to the result of $t\bar{t} + \text{jets}$ differential cross-section measurement analysis [1].

132 1 Introduction

133 The discovery of a neutral boson with a measured mass of around 125 GeV at the Large Hadron Collider
 134 (LHC) in 2012 [2–4] opens the question of whether this is the Higgs boson of the Standard Model (SM)
 135 or part of an extended scalar sector. Indeed, charged Higgs bosons¹ are predicted in several extensions
 136 of the SM, which add a second doublet [5–8] or triplets [8–12] to its scalar sector. In CP-conserving
 137 Two-Higgs-Doublet Models (2HDMs) H^+ production and decay at tree level depend on its mass and
 138 two parameters: the mixing angle α of the neutral CP-even Higgs bosons, and the ratio of the vacuum
 139 expectation values of the two Higgs doublets ($\tan \beta$).

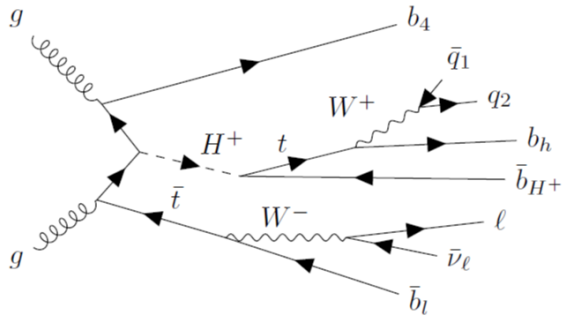


Figure 1: Feynman diagram for $pp \rightarrow tbH^+ \rightarrow tb(tb)$

140 For H^+ masses above the top-quark mass the leading production mode is $gg \rightarrow tbH^+$ and, close to the
 141 alignment limit when $\cos(\beta - \alpha) \approx 0$, the dominant decay mode is $H^+ \rightarrow tb$. For lower H^+ masses, the
 142 dominant decay mode is $H^+ \rightarrow \tau\nu$, as well as for large values of $\tan \beta$ irrespective of the charged Higgs
 143 mass. Therefore, the two decay modes naturally complement each other in searches for charged Higgs
 144 bosons.

145 The ATLAS and CMS collaborations have searched for charged Higgs bosons in pp collisions at $\sqrt{s} = 7, 8$
 146 and 13 TeV, probing the mass range below the top-quark mass in the $\tau\nu$ [13–18], cs [19, 20], and cb [21]
 147 decay modes, as well as above the top-quark mass in the $\tau\nu$ and tb decay modes [15, 17, 18, 22–28]. In
 148 addition, $H^+ \rightarrow WZ$ was searched for in the vector-boson-fusion production mode [29, 30]. No evidence for
 149 charged Higgs bosons was found in any of these searches.

150 This note presents a search for H^+ production in the $H^+ \rightarrow tb$ decay mode using pp collisions at $\sqrt{s} = 13$
 151 TeV. Events with one charged lepton ($l = e, \mu$) and jets in the final state are considered. Compared with the
 152 previous analysis using the same final state and the dataset [25] (so-called ‘resolved analysis’), boosted top
 153 tagging technique is used to identify a hadronically decaying top quark originated from the decay of the
 154 heavy H^+ . This technique allows to improve sensitivities in the high mass regions, where all top decay
 155 products are merged into a single large-R jet, and, therefore, cannot be reconstructed in the resolved analysis
 156 [25]. To separate the signal from the SM background, multivariate discriminants are employed in the
 157 regions where the signal rate is expected to be the largest. Limits on the $H^+ \rightarrow tb$ production cross-section
 158 are set by a simultaneous fit of BDT distributions.

¹ Charge-conjugate is implied elsewhere in this note.

159 Furthermore, the analysis technique is extended to a search for the $W' \rightarrow tb$ decay, where W' is produced
160 in association with tb . Several theories beyond the SM predict heavy-charged gauge bosons, which are
161 usually referred to as W' bosons[31–36]. Such W' bosons can be heavy enough to decay into a top quark
162 and a bottom quark. Some models predict W' bosons that preferably couple to quarks or third-generation
163 fermions [37–40]. Unlike the W boson, which only couples to left-handed fermions, the chirality of the
164 interaction of the W' boson can be left or right-handed, or a mixture of the two. In models where the
165 right-handed neutrinos are heavier than the right-handed W' boson, such W' bosons cannot be searched for
166 in the leptonic decay modes. We search for W' bosons produced in association with a top quark and a
167 bottom quark: Figure 1 illustrates this production process if we replace H^+ with W' .

168 Formerly, W' bosons decaying into a top quark and a bottom quark were searched for in collisions between
169 a quark and an antiquark of any flavour, where the W' boson is singly produced without a top quark. D0
170 [41] and CDF [42] Collaborations at the Tevatron and CMS [43–46] and ATLAS [47–50] experiments at
171 the LHC have published such search results.

172 The analysis relies on ATLAS official background as well as requested H^+ and W' signal samples, as
173 detailed in Section 2, with the TOPQ1 derivation. The ntuples are produced using the TTHbbAnalysis
174 software package.² These ntuples are used as inputs to TRExFitter to perform statistical analysis.³

² https://gitlab.cern.ch/atlasHTop/TTHbbAnalysis/-/tree/user/hyamauch/pflow_dev_HplusBoosted

³ <https://gitlab.cern.ch/hyamauch/TRExFitter>

175 2 Data and MonteCarlo Simulated Events

176 2.1 Data Sample

177 This analysis uses pp collision data collected from 2015 to 2018 by the ATLAS detector at $\sqrt{s} = 13$ TeV.
 178 Selected events are recorded using unprescaled triggers, as detailed in Table 1. Only runs with stable
 179 colliding beams and all ATLAS subsystems operational are used. These are summarized in the Good
 180 Run Lists (GRL) shown in Table 2, together with the integrated luminosity collected each year. The total
 181 integrated luminosity is 139 fb^{-1} [51].

Year		Single-electron triggers
2015	e24_lhmedium_L1EM20VH_OR_e60_lhmedium_OR_e120_lhloose	
2016-2018	e26_lhtight_nod0_ivarloose_OR_e60_lhmedium_nod0_OR_e140_lhloose_nod0	

(a)

Year		Single-muon triggers
2015	mu20_iloose_L1MU15_OR_mu50	
2016-2018	mu26_ivarmedium_OR_mu50	

(b)

Table 1: Single-electron (a) and single-muon (b) trigger menus used depending on the year of data-taking.

Year	Luminosity (pb^{-1})	GRL
2015	3219.6	data15_13TeV/20170619/physics_25ns_21.0.19.xml
2016	32988.1	data16_13TeV/20180129/physics_25ns_21.0.19.xml
2017	44307.4	data17_13TeV/20180619/physics_25ns_Triggerno17e33prim.xml
2018	58450.1	data18_13TeV/20190318/physics_25ns_Triggerno17e33prim.xml

Table 2: Integrated luminosity for each year of data-taking, computed with the OffLumi-13TeV-010 luminosity tag [52], together with the corresponding GRLs [53].

182 2.2 Signal Samples

183 This paragraph describes MC samples used for each signal event's estimation. The summary is shown in
 184 Table 3.

Physics process	Generator	PS generator	Normalisation	PDF set
$t b H^+$ ($M_{H^+} \leq 3.0$ TeV)	MG5_aMC 2.6.2	Pythia 8.212	NLO	NNPDF2.3NLO
$t b H^+$ ($M_{H^+} = 4.0, 5.0$ TeV)	MG5_aMC 2.8.1	Pythia 8.244	NLO	NNPDF3.0NLO
$t b W'$	MG5_aMC 2.9.9	Pythia 8.307	NLO	NNPDF3.0NLO

Table 3: Nominal simulated signal event samples. The generator, parton shower generator and cross-section used for normalization are shown together with the applied PDF set.

185 **2.2.1 $\bar{t}bH^+$ Samples**

186 The H^+ signal samples are generated with MadGraph5_aMCatNLO (MG5_aMC) [54], which is a generator
187 based on a four-flavor scheme (4FS) next-to-leading order (NLO) in QCD [55]. The NNPDF2.3NLO
188 [56] parton distribution function (PDF) set is used.⁴ The width of the H^+ is set to zero. Dynamic QCD
189 factorisation and renormalisation scales (μ_f and μ_r) are set to $\frac{1}{3} \sum_i \sqrt{m(i)^2 + p_T(i)^2}$, where i runs over the
190 final state particles (H^+ , t and b) used in the generation. The events are showered with Pythia 8.212 [58]
191 with the A14 [59] set of underlying-event related parameters tuned to ATLAS. Ten different H^+ mass points
192 between 1000 and 5000 GeV are generated as detailed in Table 4. The table also shows cross sections from
193 MG5_aMC and Santander-matched cross sections for 2HDM type-II (a la MSSM), but without SUSY
194 QCD corrections [54, 60–62]. All samples are fully simulated with the proportions of mc16a, mc16d,
195 and mc16e corresponding to the amount of data recorded in the 2015-2016, 2017, and 2018 data-taking
196 years.

DSID	H^+ mass [GeV]	Size	$\sigma^{\text{MG5_aMC}}$ [fb]	$\sigma^{\text{MSSM}}_{\tan\beta=1}$ [fb]	$\sigma^{\text{MSSM}}_{\tan\beta=60}$ [fb]
450004	1000	1.0M	3.28	40.9	37.8
450598	1200	1.0M	1.31	16.4	15.1
450599	1400	1.0M	5.62×10^{-1}	7.1	6.5
450600	1600	1.2M	2.54×10^{-1}	3.2	3.0
450601	1800	1.3M	1.21×10^{-1}	1.5	1.4
450602	2000	1.9M	5.90×10^{-2}	0.8	0.7
451490	2500	1.9M	1.11×10^{-2}	<i>Not available</i>	
451491	3000	1.9M	2.34×10^{-3}	<i>Not available</i>	
508710	4000	1.9M	9.75×10^{-5}	<i>Not available</i>	
508711	5000	1.9M	4.28×10^{-6}	<i>Not available</i>	

Table 4: List of the generated H^+ samples. All samples are simulated with FullSim and available in the appropriate proportions of mc16a, mc16d, and mc16e. The cross-section values for $\tan\beta = 1$ or $\tan\beta = 60$ take into account the production of H^\pm .

197 **2.2.2 $\bar{t}bW'$ Samples**

198 The left- and right-handed W' (W'_L and W'_R) signal samples are generated with the same options (QCD
199 scales, PDF, NLO, and 4FS) as the H^+ signal sample generations. Nine different W' mass points between
200 1000 and 4000 GeV are generated, where the mass points are the same (except the 5000 GeV sample) as the
201 H^+ signal samples as detailed in Table 5⁵. The table also shows cross-sections calculated with MG5_aMC.
202 All samples are fully simulated with the proportions of mc16a, mc16d, and mc16e corresponding to the
203 amount of data recorded in the 2015-2016, 2017, and 2018 data-taking years.

⁴ The samples with masses of 4 and 5 TeV are generated using NNPDF3.0NLO [57] PDF set.

⁵ Only 5000 GeV mass sample aren't generated, because it is difficult technically due to its very narrow mass width.

DSID	W'_L mass [GeV]	Size	$\sigma^{\text{MG5_aMC}}$ [fb]
510889	1000	0.5M	22.54
510890	1200	0.5M	8.56
510891	1400	0.5M	3.50
510892	1600	0.5M	1.53
510893	1800	0.5M	7.03×10^{-1}
510894	2000	0.5M	3.33×10^{-1}
510895	2500	0.5M	5.98×10^{-2}
510896	3000	0.5M	1.19×10^{-2}
510897	4000	0.5M	5.50×10^{-4}

(a)

DSID	W'_R mass [GeV]	Size	$\sigma^{\text{MG5_aMC}}$ [fb]
510898	1000	0.5M	22.66
510899	1200	0.5M	8.52
510900	1400	0.5M	3.50
510901	1600	0.5M	1.52
510902	1800	0.5M	6.98×10^{-1}
510903	2000	0.5M	3.33×10^{-1}
510904	2500	0.5M	5.94×10^{-2}
510905	3000	0.5M	1.19×10^{-2}
510906	4000	0.5M	5.48×10^{-4}

(b)

Table 5: List of the generated W'_L (a) and W'_R (b) samples. All samples are simulated with FullSim and available in the appropriate proportions of mc16a, mc16d, and mc16e.

204 2.3 Background Samples

205 This paragraph describes MC samples used for each background event's estimation. The summary is shown
206 in Table 6.

Physics process	Generator	PS generator	Normalisation	PDF set
$t\bar{t}$ + jets	PowhegBox v2	Pythia 8.230	NNLO+NNLL	NNPDF3.0NLO
$t\bar{t}H$	PowhegBox v2	Pythia 8.230	NNLO	NNPDF3.0NLO
$t\bar{t}V$	MG5_aMC 2.3.3	Pythia 8.210	NLO	NNPDF3.0NLO
Single top t-chan.	PowhegBox v2	Pythia 8.230	aNNLO	NNPDF3.0NLOnf4
Single top s-chan.	PowhegBox v2	Pythia 8.230	aNNLO	NNPDF3.0NLO
Single top tW	PowhegBox v2	Pythia 8.230	aNNLO	NNPDF3.0NLO
$tHjb$	MG5_aMC 2.6.X	Pythia 8.230	NLO	NNPDF3.0NLOnf4
tHW	MG5_aMC 2.6.2	Pythia 8.235	NLO	NNPDF3.0NLO
tZq	MG5_aMC 2.3.3	Pythia 8.212	NLO	CTEQ6L1LO
tZW	MG5_aMC 2.3.3	Pythia 8.212	NLO	NNPDF3.0NLO
4 tops	MG5_aMC 2.3.3	Pythia 8.230	NLO	NNPDF3.1NLO
V + jets	Sherpa 2.2.1	Sherpa 2.2.1	NNLO	NNPDF3.0NLO
Diboson	Sherpa 2.2	Sherpa 2.2	NLO	NNPDF3.0NLO

Table 6: Nominal simulated background event samples. The generator, parton shower generator and cross-section used for normalisation are shown together with the applied PDF set.

2.3.1 $t\bar{t}$ +jets

The production of $t\bar{t}$ events is modeled using the PowhegBox [63–66] v2 generator, which provides matrix element (ME) at NLO in the strong coupling constant (α_S) with the NNPDF3.0NLO PDF set [57] and the h_{damp} parameter⁶ set to $1.5m_{\text{top}}$ [67]. The functional form of μ_f and μ_r is set to the default scale $\sqrt{m_t^2 + p_{T,t}^2}$. The events are showered with Pythia 8.230 [68].

The uncertainty due to initial-state-radiation (ISR) is estimated using weights in the ME and in the parton shower (PS). To simulate higher parton radiation μ_f and μ_r are varied by a factor of 0.5 in the ME while using the *Var3c* upward variation from the A14 tune. For lower parton radiation, μ_f and μ_r varied by a factor of 2.0 while using the *Var3c* downward variation in the PS. The impact of final-state-radiation (FSR) is evaluated using PS weights which vary μ_r for QCD emission in the FSR by a factor of 0.5 and 2.0, respectively. The impact of the PS and hadronisation model is evaluated by changing the showering of the nominal PowhegBox events from Pythia to Herwig 7.04 [69, 70].

To assess the uncertainty due to the choice of the matching scheme, the Powheg sample is compared to a sample of events generated with MG5_aMC v2.6.0 and the NNPDF3.0NLO PDF set showered with Pythia 8.230. The shower starting scale has the functional form $\mu_q = H_T/2$ [71], where H_T is defined as the scalar sum of the p_T of all outgoing partons. Choice of μ_f and μ_r is the same as that for the Powheg setup.

To enhance the statistics in the phase-space relevant for this analysis, for all the samples described above, dedicated filtered samples were produced, requiring b - or c -hadrons in addition to those arising from the decays of the top quarks, as follows:

- One sample was produced with at least two additional b -hadrons with $p_T > 15$ GeV.

⁶ The h_{damp} parameter controls the transverse momentum of the first additional emission beyond the LO Feynman diagram in the parton shower and therefore regulates the high- p_T emission against which the $t\bar{t}$ system recoils.

- One sample was produced with at least one additional b -hadron with $p_T > 5$ GeV and failing the previous requirement.
- One sample was produced with at least one additional c -hadron with $p_T > 15$ GeV and failing the previous two requirements.

The combined use of the unfiltered and filtered samples is done by assuring no overlap between them (by the use of the heavy flavour filter flag, *TopHeavyFlavorFilterFlag*) and weighted with the appropriate cross-section and filter efficiencies.

2.3.2 $t\bar{t}H$

The production of $t\bar{t}H$ events is modeled in the 5F scheme using PowhegBox [72] at NLO in α_S with the NNPDF3.0NLO PDF set. The h_{damp} parameter is set to $3/4 \times (m_t + m_{\bar{t}} + m_H) = 352.5$ GeV. The events are showered with Pythia 8.230. The uncertainties due to ISR, FSR, PS and hadronisation model, as well as that due to the matching scheme, are evaluated with the same procedures used for the $t\bar{t}$ + jets background.

2.3.3 $t\bar{t}V$

The production of $t\bar{t}V$ events is modeled using the MG5_aMC v2.3.3 generator, which provides ME at NLO in α_S with the NNPDF3.0NLO PDF set. The functional form of μ_f and μ_r is set to the default scale $0.5 \times \sum_i \sqrt{m_i^2 + p_{T,i}^2}$ where the sum runs over all the particles generated from the ME calculation. The events are showered with Pythia 8.210.

Additional $t\bar{t}V$ samples are produced with Sherpa 2.2.0 [73] at LO accuracy, using the MEPS@LO setup [74, 75] with up to one additional parton for the $t\bar{t}V$ sample and two additional partons for the others. A dynamic μ_r is used, defined similarly to that of the nominal MG5_aMC+Pythia samples. The CKKW matching scale of the additional emissions is set to 30 GeV. The default Sherpa 2.2.0 PS is used along with the NNPDF3.0NNLO PDF set.

2.3.4 Single top

t -channel

Single-top t -channel production is modeled using the PowhegBox v2 generator, which provides ME at NLO in α_S in the 4F scheme with the NNPDF3.0NLOnf4 PDF set. The functional form of μ_f and μ_r is set to $\sqrt{m_b^2 + p_{T,b}^2}$, following the recommendation of Ref. [76]. The events are showered with Pythia 8.230.

The impact of the PS and hadronisation model is evaluated by comparing the nominal generator setup with a sample produced with the PowhegBox v2 generator at NLO in QCD in the 4FS using the NNPDF3.0NLOnf4 PDF set. The same events produced for the nominal PowhegBox+Pythia8 sample are used. The events are showered with Herwig 7.04.

260 To assess the uncertainty due to the choice of the matching scheme, the nominal sample is compared
 261 to a sample generated with the MG5_aMC v2.6.2 generator at NLO in QCD in the 4FS, using the
 262 NNPDF3.0NLOnf4 PDF set. Top quarks are decayed at LO using MadSpin [77, 78] to preserve all
 263 spin correlations. The events are showered with Pythia 8.230.

264 **s-channel**

265 Single-top *s*-channel production is modeled using the PowhegBox v2 generator, which provides ME
 266 at NLO in α_S in the 5F scheme with the NNPDF3.0NLO PDF set. The functional form of μ_f and μ_r
 267 is set to the default scale, which is equal to the top quark mass. The events are showered with Pythia
 268 8.230.

269 The impact of the PS and hadronisation model is evaluated by comparing the nominal generator
 270 setup with a sample produced with the PowhegBox v2 generator at NLO in QCD in the 5FS using the
 271 NNPDF3.0NLO PDF set. The same events produced for the nominal PowhegBox+Pythia8 sample
 272 are used. The events are showered with Herwig 7.04.

273 To assess the uncertainty due to choice of the matching scheme, the nominal sample is compared
 274 to a sample generated with the MG5_aMC v2.6.2 generator at NLO in QCD in the 5FS, using
 275 the NNPDF3.0NLO PDF set. Top quarks are decayed at LO using MadSpin to preserve all spin
 276 correlations. The events are showered with Pythia 8.230.

277 ***tW***

278 Single-top *tW* associated production is modeled using the PowhegBox v2 generator, which provides ME
 279 at NLO in α_S in the 5F scheme with the NNPDF3.0NLO PDF set. The functional form of μ_f and μ_r
 280 is set to the default scale, which is equal to the top quark mass. The diagram removal scheme
 281 [79] is employed to handle the interference with $t\bar{t}$ production [67]. The events are showered with
 282 Pythia 8.230.

283 The nominal Powheg+Pythia8 sample is compared to an alternative sample generated using the
 284 diagram subtraction scheme [67, 79] to estimate the uncertainty due to the interference with $t\bar{t}$
 285 production.

286 The impact of the PS and hadronisation model is evaluated by comparing the nominal generator
 287 setup with a sample produced with the Powheg v2 generator at NLO in QCD in the 5FS using the
 288 NNPDF3.0NLO PDF set. The same events produced for the nominal Powheg+Pythia8 sample are
 289 used. The events are showered with Herwig 7.04.

290 To assess the uncertainty due to the choice of the matching scheme, the nominal sample is compared
 291 to a sample generated with the MG5_aMC v2.6.2 generator at NLO in QCD in the 5FS, using the
 292 NNPDF2.3NLO PDF set. The events are showered with Pythia 8.230.

293 **2.3.5 *tH***

294 ***tHjb* production**

295 The production of *tHjb* events is modeled in the 4F scheme using the MG5_aMCv2.6.0 with
 296 the NNPDF3.0NLOnf4 PDF set. The functional form of μ_f and μ_r is set to the default scale
 297 $1/2 \times \sum_i \sqrt{m_i^2 + p_{T,i}^2}$, where the sum runs over all the particles generated from the ME calculation.

298 The shower starting scale has the functional form $\mu_q = H_T/2$, where H_T is defined as the scalar sum
 299 of the p_T of all outgoing partons. The events are showered with Pythia 8.230.

300 ***tHW* production**

301 The production of *tHW* events is modeled in the 5F scheme using the MG5_aMCv2.6.2 with the
 302 NNPDF3.0NLO PDF set. The functional form μ_f and μ_r is set to the default scale $1/2 \times \sum_i \sqrt{m_i^2 + p_{T,i}^2}$
 303 where the sum runs over all the particles generated from the ME calculation. The shower starting
 304 scale has the functional form $\mu_q = H_T/2$, where H_T is defined as the scalar sum of the p_T of all
 305 outgoing partons. The events are showered with Pythia 8.235.

306 **2.3.6 Rare *t* processes**

307 ***tZq***

308 The *tZq* MC samples [80] are generated at LO in α_S using MG5_aMC 2.3.3 in the 4F scheme,
 309 with the CTEQ6L1 [81] LO PDF set. Following the recommendations taken from Ref. [76], the
 310 renormalisation and factorisation scales are set to $4 \times \sum_b \sqrt{m_i^2 + p_{T,b}^2}$, where the *b*-quark is the one
 311 coming from the gluon splitting. The events are showered with Pythia 8.212.

312 ***tZW***

313 The *tZW* sample is simulated using the MG5_aMC v2.3.3 generator at NLO in α_S with the
 314 NNPDF3.0NLO PDF set. The top quark is decayed inclusively while the *Z* boson decays to a pair of
 315 leptons, by means of Pythia 8.212. The 5F scheme is used where all the quark masses are set to zero,
 316 except for the top quark. μ_f and μ_r are set to the top quark mass. The DR1 scheme [79] is employed
 317 to handle the interference between *tWZ* and *ttZ*, and is applied to the *tWZ* sample.

318 **4 tops**

319 The production of 4 tops events is modeled using the MG5_aMC v2.3.3 generator, which provides
 320 ME at NLO in α_S with the NNPDF3.1NLO PDF set. The functional form of μ_f and μ_r is set to
 321 $0.25 \times \sum_i \sqrt{m_i^2 + p_{T,i}^2}$, where the sum runs over all the particles generated from the ME calculation,
 322 following the Ref.[82]. The events are showered with Pythia 8.230.

323 **2.3.7 Vector bosons plus jets**

324 QCD vector bosons plus jets production is simulated with the Sherpa v2.2.1 PS Monte Carlo generator. In
 325 this setup, NLO-accurate ME for up to two jets, and LO-accurate ME for up to four jets are calculated with
 326 the Comix [83] and OpenLoops [84, 85] libraries. The default Sherpa PS [86] based on Catani-Seymour
 327 dipoles and the cluster hadronisation model [87] are used. They employ the dedicated set of tuned
 328 parameters developed by the Sherpa authors for this version based on the NNPDF3.0nnlo set. The NLO ME
 329 of a given jet-multiplicity are matched to the PS using a colour-exact variant of the MC@NLO algorithm
 330 [88]. Different jet multiplicities are then merged into an inclusive sample using an improved CKKW
 331 matching procedure [74, 75], which is extended to NLO accuracy using the MEPS@NLO prescription
 332 [89]. The merging cut is set to $Q_{\text{cut}} = 20$ GeV.

333 QCD scale uncertainties are evaluated on-the-fly [90] using 7-point variations of μ_f and μ_r in the ME. The
 334 scales are varied independently by factors of 0.5 and 2 but avoiding opposite factors. PDF uncertainties for
 335 the nominal PDF set are evaluated using the 100 variation replicas, as well as ± 0.001 shifts of α_S .

336 2.3.8 Dibosons

337 Diboson samples are simulated with the Sherpa v2.2 generator. In this setup multiple ME are matched
338 and merged with the Sherpa PS based on Catani-Seymour dipole using the MEPS@NLO prescription.
339 For semileptonically and fully leptonically decaying diboson samples, as well as loop-induced diboson
340 samples, the virtual QCD correction for ME at NLO accuracy are provided by the OpenLoops library.
341 For electroweak $VVjj$ production, the calculation is performed in the G_μ scheme, ensuring an optimal
342 description of pure electroweak interactions at the electroweak scale. All samples are generated using
343 the NNPDF3.0nnlo set, along with the dedicated set of tuned PS parameters developed by the Sherpa
344 authors.

3 Object Reconstruction

This analysis requires exactly one lepton (electron or muon). Tau leptons are not used, but they are reconstructed only for overlap removals. Large-R jets originated from a top quark and small-R jets originated from b -quarks are also required. The large-R jets from top quarks are identified using a top-tagger based on DNN. Only the leading top-tagged large-R jet of all top-tagged large-R jets is used. On the other hand, the small-R jets originated from b -quarks are identified using a DL1r b -tagging and are required to be $\Delta R > 1.0$ to the leading top-tagged large-R jet to make sure the b -tagged jets are not sub-jets of the leading top-tagged large-R jet. The following describes the requirements for these object reconstructions in detail.

3.1 Electrons

Electrons are reconstructed from energy clusters in the electromagnetic calorimeter matched to tracks reconstructed in the inner detector (ID) [91, 92], and are required to have $p_T > 10$ GeV and $|\eta| < 2.47$. Candidates in the barrel–endcap transition region of the calorimeter ($1.37 < |\eta| < 1.52$) are excluded. Electrons must satisfy the *tight* identification criterion based on a likelihood discriminant described in Ref. [92] and the following constraints in the longitudinal and transverse impact parameters: $|z_0| < 0.5$ mm and $|d_0|/\sigma_{d_0} < 5$. The impact parameters are defined with respect to the beamline. Electrons are required to satisfy the *FCTight* isolate criteria [93].

3.2 Muons

Muons are reconstructed from either track segments or full tracks in the muon spectrometer, which are matched to tracks in the ID [94]. Tracks are then re-fitted using information from both detector systems. Muons are required to have $p_T > 10$ GeV and $|\eta| < 2.5$ and the following constraints in the longitudinal and transverse impact parameters: $|z_0| < 0.5$ mm and $|d_0|/\sigma_{d_0} < 3$. Muons should satisfy the *medium* identification and the *FCTightTrackOnly* isolation criteria [93].

3.3 Taus

Hadronically decaying tau leptons (τ_{had}) are distinguished from jets using the track multiplicity and the τ_{had} identification algorithm based on a recurrent neural network [95]. This algorithm exploits the track collimation, jet substructure, kinematic information and so on. These τ_{had} candidates are required to have $p_T > 25$ GeV, $|\eta| < 2.5$ and pass the *Medium τ* -identification working point. Although taus are not used in the analysis, the consistent configuration with the resolved analysis as well as the $t\bar{t}H(\rightarrow bb)$ analysis is kept.

3.4 Small- R jets and b -tagging

Jets are reconstructed using the anti- k_t clustering algorithm [96] on particle-flow objects [97] with a radius of $R = 0.4$. Jets are calibrated using the standard jet calibration procedure, which corrects the jet energy to match on average the true jet energy at the particle level and applies an in-situ correction for data [98]. The

379 jet collection name in ATLAS is `AntiKt4EMPflowJets_BTagging201903`. Jets are required to have
 380 $|\eta| < 2.5$ such that they are within the acceptance of the ID and the recommended jet vertex tagging (JVT)
 381 requirement [99] is applied to jets with $p_T < 60$ GeV in order to remove jets originating from the pile-up.

382 Small- R jets originating from the hadronization of b -quarks (referred to as b -jets hereafter) are identified
 383 using an algorithm based on multivariate techniques to combine information from the impact parameters
 384 of displaced tracks as well as properties of secondary and tertiary decay vertices reconstructed within the
 385 jets. In this analysis, b -tagging relies on the *DL1r* tagger [100], trained on simulated $t\bar{t}$ events, and the
 386 event selection makes use of jets b -tagged with the *DL1r* algorithm at the 70% efficiency working point.

387 3.5 Large- R jets and top-tagging

388 Top quarks with high transverse momentum ($p_T \gtrsim 2m_t$) are expected to result in decay products that
 389 are collimated. For top quarks decaying hadronically (bqq'), the three quarks may not be resolved as
 390 three separate jets. In order to reconstruct these boosted hadronically-decaying top quarks, large-radius
 391 (large- R) jets are used. The large- R jets are formed from the topological clusters of calorimeter cells
 392 which are calibrated to the hadronic energy scale using the local calibration weighting method [101] and
 393 reconstructed using the anti- k_t algorithm with radius parameter of $R = 1.0$. The jet collection name in
 394 ATLAS is `AntiKt10LCTopoTrimmedPtFrac5SmallR20Jets`. These jets are further trimmed to remove
 395 the effects of pile-up and underlying events. The trimming [102] is done by reclustering the original
 396 constituents of a large- R jet into a collection of R_{sub} subjets using k_t algorithm [103]. The subjets are
 397 then discarded if they carry less than a specific fraction (f_{cut}) of the p_T of the original large- R jet. In this
 398 analysis, the optimized values ($R_{\text{sub}} = 0.2$, $f_{\text{cut}} = 5\%$) are used [104]. The large- R jet energy and mass
 399 scale are then calibrated using correction factors derived from simulation. The mass of the large- R jets is
 400 calculated using tracking and calorimeter information, the so-called combined mass technique [105]. Only
 401 the large- R jets that satisfy $200 < p_T < 3000$ GeV, $|\eta| < 2.0$ and $40 < m_{\text{comb}} < 600$ GeV are considered in
 402 this analysis as recommended by the JetEtMiss group [106].

403 The identification of hadronically decaying top quarks that are reconstructed as large- R jets is performed
 404 using a multivariate classification algorithm employed in a deep neural network [107]. In the kinematic
 405 region of interest in this search, a single large- R jet captures the top quark decay products, resulting in a
 406 characteristic multi-core structure within the jet, in contrast to a typical single-core structure associated with
 407 jets in multijet. In order to exploit this characteristic behavior for top quark identification, a multivariate
 408 top-tagging classifier was developed. The tagger uses multiple jet-level discriminants as inputs, such as
 409 calibrated jet p_T and mass, information about the dispersion of the jet constituents such as N -subjettiness
 410 [108], splitting scales [109] and energy correlation functions [110]. Top-tagging, associated scale factors,
 411 and uncertainties are only provided for jets with $350 < p_T < 2500$ GeV. The tagger used is optimized for
 412 the contained top definition, in which the signal category is defined using jets matched to a truth top quark.
 413 In addition, a truth jet matched to the reconstructed jet is required to have a mass above 140 GeV and at
 414 least one b -hadron ghost matched to it.

415 In this analysis, large- R jets which pass the 80% efficiency working point of the contained top-tagging
 416 criterion ($J_{\text{top-tagged}}$) are chosen as the boosted top candidates. Especially, the leading boosted top candidate
 417 out of them is represented by $J_{\text{top-tagged}}^{\text{1st}}$ in the following sections.

418 3.6 Overlap Removal

419 In order to avoid counting a single detector response as more than one lepton or jet, the following overlap
 420 removal procedure is applied.

421 To prevent double-counting of electron energy deposits as jets, the small- R jet within $\Delta R_y = \sqrt{(\Delta y)^2 + (\Delta\phi)^2} =$
 422 0.2 of a selected electron is removed. Here, the rapidity is defined as $y = \frac{1}{2} \ln \frac{E+p_z}{E-p_z}$, where E is the energy
 423 and p_z is the longitudinal component of the momentum along the beam pipe. If the nearest small- R jet
 424 surviving that selection is within $\Delta R_y = 0.4$ of the electron, the electron is discarded. In the case that a
 425 large- R jet is found within $\Delta R = 1.0$ of the electron, the large- R jet is removed.⁷

426 Muons are removed if their distance from the nearest small- R jet is within $\Delta R_y < 0.4$. This treatment
 427 reduces the background from heavy-flavor decays inside small- R jets. However, if this small- R jet has
 428 fewer than three associated tracks, the muon is kept and the small- R jet is removed instead. This avoids an
 429 inefficiency for high-energy muons undergoing significant energy loss in the calorimeter.

430 A τ_{had} candidate is rejected if it is within $\Delta R_y < 0.2$ from any selected electron or muon. Also, small- R
 431 jets with $\Delta R_y < 0.2$ around a τ_{had} candidate are rejected. The overlap removal with τ_{had} is applied in order
 432 to keep consistency with the $t\bar{t}H(\rightarrow bb)$ analysis as well as the $H^+ \rightarrow tb$ analysis.

433 Small- R jets within $\Delta R < 1.0$ of a leading top-tagged large- R jet are removed⁶ to prevent double-counting
 434 of jet energy deposits. All of the above overlap removal procedures are summarized in Table 7.

Reject	Against	Criteria
Small- R jet	Electron	$\Delta R_y < 0.2$
Electron	Small- R jet	$0.2 < \Delta R_y < 0.4$
Small- R jet	Muon	$N_{track} < 3$ in jet and $\Delta R_y < 0.4$
Muon	Small- R jet	$\Delta R_y < 0.4$
τ_{had}	Electron	$\Delta R_y < 0.2$
τ_{had}	Muon	$\Delta R_y < 0.2$
Small- R jet	τ_{had}	$\Delta R_y < 0.2$
Large- R jet	Electron	$\Delta R < 1.0$
Small- R jet	Leading top-tagged large- R jet	$\Delta R < 1.0$

Table 7: Summary of overlap removal procedures in this analysis.

⁷ Following the recommendation for ATLAS analyses in Run 2 [111], the overlap removal implemented in the *AssociationUtils* package [112] is based on ΔR_y . It is found more appropriate in the case of non-massless objects [113]. However, overlap removal for large- R jets is performed in the ttHOffline software and is computed based on ΔR .

435 4 Analysis Strategy

436 We take different analysis approaches between the below and above 3 TeV signal mass samples. In the
 437 analyses below 3 TeV, we adopt the multivariable analyses by training boosted decision tree (BDT) on
 438 every mass point. On the other hand, for the mass points above 3 TeV, we adopt the cut-and-counting
 439 approach. We describe these strategies below.

440 4.1 Analysis strategy below 3 TeV

441 4.1.1 Event Selection

442 To analyse signals with the mass below 3 TeV, one signal region (SR) and one control region (CR) are
 443 defined according to the numbers of leptons, top tagged large- R jets, and b -tagged small- R jets.

444 Figure 2 shows the schematic of boosted event topology of an $H^+ \rightarrow tb$ event. A signal event is expected to
 445 have one $J_{\text{top-tag}}$, three b -jets, and one lepton+MET. However, the b -jet originated from the gluon (b_4 in
 446 Figure 1) is typically not detectable because it tends to fly in the forward directions and outside the detector
 447 acceptance. Therefore, at least two b -jets are required in this analysis.

448 Events in the SR are required to have exactly one lepton (e or μ), as shown in Figure 2. The lepton is
 449 also required to match the object that fired the single lepton trigger. Events must also have at least one
 450 top-tagged large- R jet, at least two small- R jets, and at least two b -tagged small- R jets. These small- R
 451 jets must additionally satisfy $\Delta R(J_{\text{top-tag}}^{1\text{st}}, \text{jet}) > 1.0$ to ensure these small- R jets are not constituent of the
 452 leading top-tagged jet. This analysis does not require missing E_T .

453 The requirements for events in the CR are almost the same as the SR, but only the required number of
 454 b -tagged small- R jets is different. Exactly one b -tagged small- R jet is required in the CR.

455 After the above selections, the SR and CR are enriched in $t\bar{t} +$ heavy flavour jets (HF) (i.e., $t\bar{t} + \geq 1b$,
 456 $t\bar{t} + \geq 1c$) and $t\bar{t} +$ light events, respectively. Therefore, these regions are used to control $t\bar{t} +$ jets in the
 457 final fit.

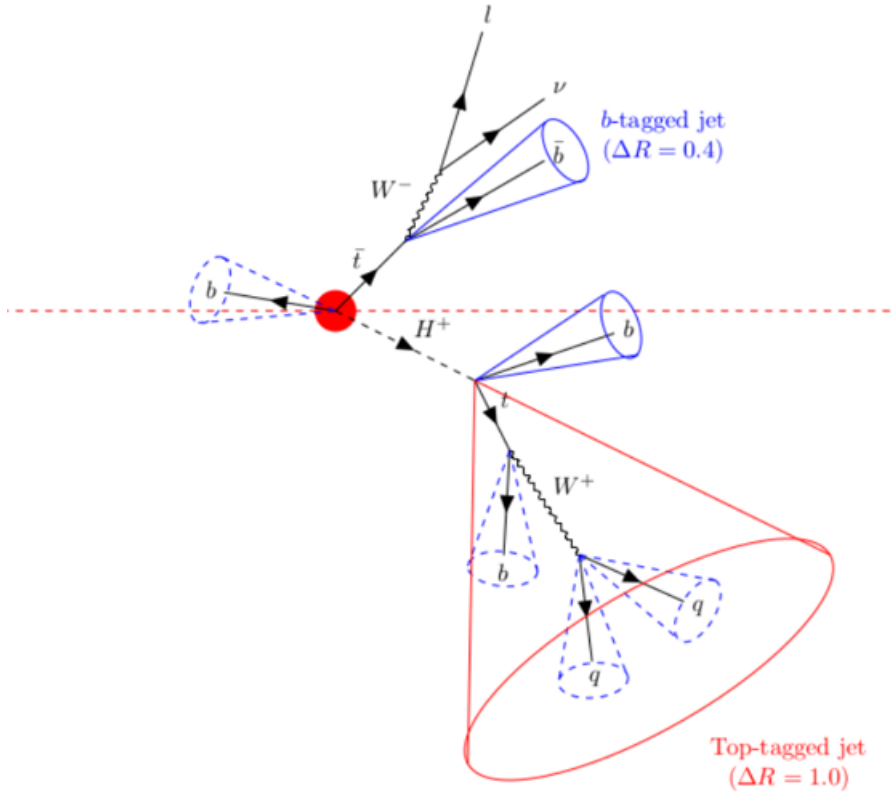


Figure 2: Schematic of boosted event topology. Signal event has one $J_{\text{top-tag}}$ and at least two b -tagged small- R jets.

Cut	SR	CR
leptons	<ul style="list-style-type: none"> - $N_{\text{lepton}} = 1$ <u>Electron</u> <u>Muon</u> - $p_T > 27 \text{ GeV}$ $- p_T > 27 \text{ GeV}$ - $\eta < 1.37$ or $1.52 < \eta < 2.47$ $- \eta < 2.5$ 	Same as SR
Top-tagged large- R jets	<ul style="list-style-type: none"> - $N_{J_{\text{top-tag}}} \geq 1$ - $350 \text{ GeV} < p_T < 2500 \text{ GeV}$ - $m > 40 \text{ GeV}$ 	Same as SR
Small- R jets	<ul style="list-style-type: none"> - $N_{\text{jet}} \geq 2$ - $p_T > 25 \text{ GeV}$ - $\eta < 2.5$ - $\Delta R(J_{\text{top-tag}}^{1\text{st}}, \text{jet}) > 1.0$ 	$N_{\text{jet}} \geq 1$ (Kinematic requirements are same as SR)
b -tagged small- R jets	$N_{b-\text{jet}} \geq 2$	$N_{b-\text{jet}} = 1$

Table 8: Event selections in the SR and CR. After these selections, the SR becomes enriched in $t\bar{t} + \text{HF}$, and the CR becomes enriched in $t\bar{t} + \text{light}$

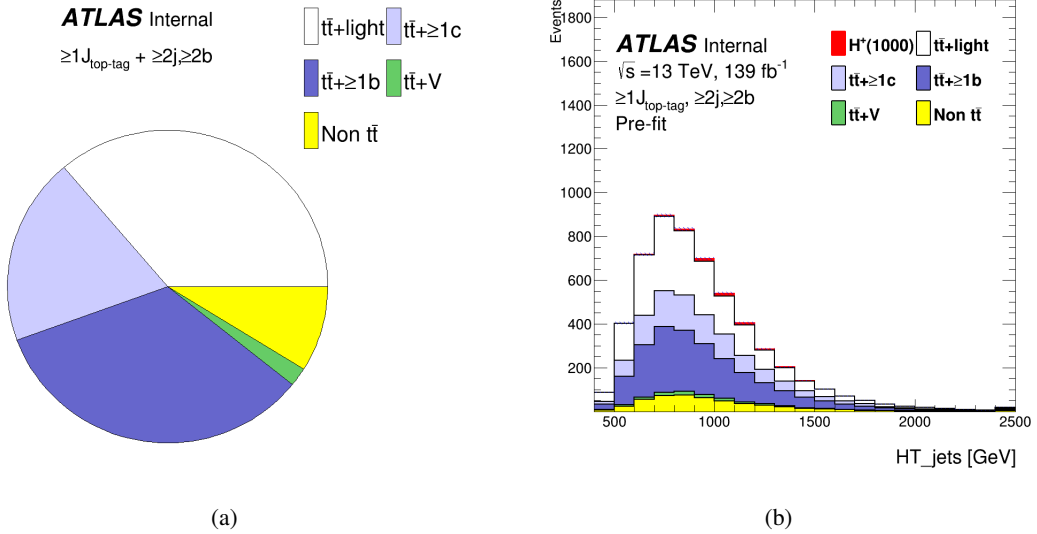


Figure 3: Background composition in the SR is shown in the pie chart (a) and the H_T^{jets} distributions (b).

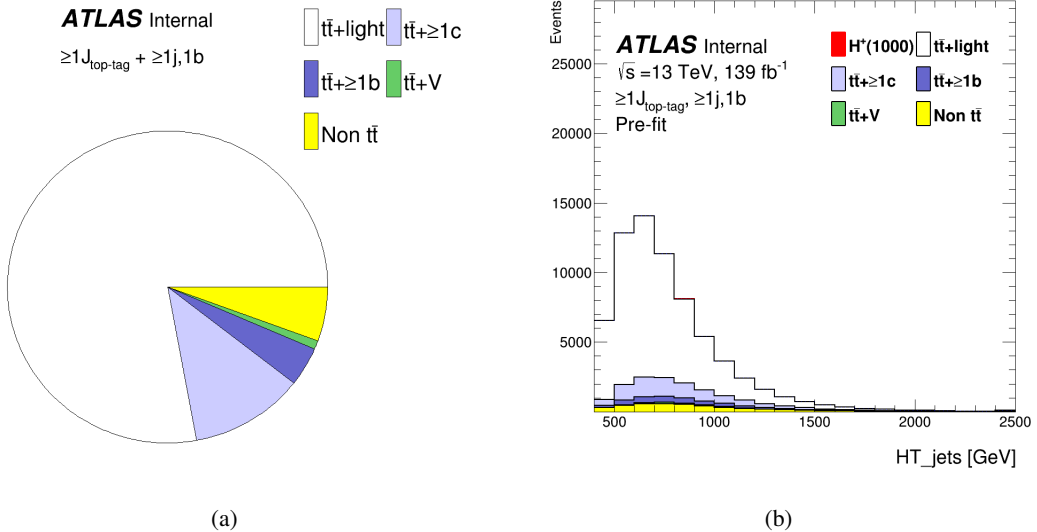


Figure 4: Background composition in the CR is shown in the pie chart (a) and the H_T^{jets} distributions (b).

458 The expected number of signal and background events in the SR and CR are shown in Table 9. For the
 459 predicted number of H^+ signal events with the 1000 and 3000 GeV mass hypothesis, the cross-section of
 460 $\sigma(pp \rightarrow tbH^+) \times Br(H^+ \rightarrow tb) = 0.046$ pb is assumed. This corresponds to the upper limit at $M_{H^+} = 1000$
 461 GeV obtained from the resolved analysis [25]. As discussed later in Section 5.1, we use the signal $\sigma \times Br$ to
 462 define the blinded regions. Table 10 shows the cut flow for each signal sample.

	SR	CR
$t\bar{t} + \text{light}$	1990 ± 95	54008 ± 2667
$t\bar{t} + \geq 1c$	1063 ± 925	8011 ± 1450
$t\bar{t} + \geq 1b$	1853 ± 931	2793 ± 1402
$t\bar{t} + W$	38 ± 6	312 ± 41
$t\bar{t} + Z$	67 ± 11	294 ± 38
Wt channel	184 ± 107	1995 ± 742
t channel	37 ± 27	172 ± 56
Other top sources	8 ± 1	34 ± 5
$VV, V+jets$	152 ± 55	1529 ± 530
$t\bar{t}H$	103 ± 4	176 ± 5
Total	5497 ± 270	69324 ± 3338
H^+ 1000 GeV	56 ± 5	56 ± 10
H^+ 3000 GeV	72 ± 17	96 ± 23

Table 9: Number of expected events in each analysis region. The quoted uncertainties include both statistical and systematic uncertainties before fitting. The signal cross-section of $\sigma(pp \rightarrow tbH^+) \times Br(H^+ \rightarrow tb) = 0.046$ pb is assumed (See text for detail).

Mass	Gen	Reco	TrigDec	1ℓ	TrigMatch	$\geq 1J$	$\geq 1j$	$\geq 1b^{85}$	$\geq 1J_{\text{non el}}$	$\geq 1J_{\text{top-tag}}$	$\geq 1j_{\text{add}}$	$\geq 1b^{70}_{\text{add}}$	$\geq 2b^{70}_{\text{add}}$	
1000	N _{MC}	998000	541248	529780	342999	337300	256596	256595	254364	225152	38298	38259	32751	15801
	Cut eff.	-	0.542	0.979	0.647	0.983	0.761	1.000	0.991	0.885	0.170	0.999	0.856	0.482
1200	N _{MC}	985000	544241	534601	335452	329187	269093	269093	266707	237410	48012	47968	40768	19536
	Cut eff.	-	0.553	0.982	0.627	0.981	0.817	1.000	0.991	0.890	0.202	0.999	0.850	0.479
1400	N _{MC}	999000	560829	551672	335009	328190	280389	280389	277776	249152	54672	54626	45817	21893
	Cut eff.	-	0.561	0.984	0.607	0.980	0.854	1.000	0.991	0.897	0.219	0.999	0.839	0.478
1600	N _{MC}	997000	565351	556595	328781	321427	282873	282873	280064	253245	58398	58374	48659	23140
	Cut eff.	-	0.567	0.985	0.591	0.978	0.880	1.000	0.990	0.904	0.231	1.000	0.834	0.476
1800	N _{MC}	978000	559240	550740	315454	307841	277151	277151	273951	250241	59500	59468	49081	22671
	Cut eff.	-	0.572	0.985	0.573	0.976	0.900	1.000	0.988	0.913	0.238	0.999	0.825	0.462
2000	N _{MC}	996000	570655	562595	312270	304274	278522	278522	274935	253344	62084	62056	50375	23076
	Cut eff.	-	0.573	0.986	0.555	0.974	0.915	1.000	0.987	0.921	0.245	1.000	0.812	0.458
2500	N _{MC}	999000	574372	566804	294566	286030	268297	268297	263948	248193	64809	64780	51192	22231
	Cut eff.	-	0.575	0.987	0.520	0.971	0.938	1.000	0.984	0.940	0.261	1.000	0.790	0.434
3000	N _{MC}	999000	570796	563605	277515	268587	255972	255972	250995	239429	66834	66826	51600	21345
	Cut eff.	-	0.571	0.987	0.492	0.968	0.953	1.000	0.981	0.954	0.279	1.000	0.772	0.413

(a)

Mass		Gen	Reco	TrigDec	1ℓ	TrigMatch	$\geq 1J$	$\geq 1j$	$\geq 1b^{85}$	$\geq 1J_{\text{non el}}$	$\geq 1J_{\text{top-tag}}$	$\geq 1j_{\text{add}}$	$\geq 1b_{\text{add}}^{70}$	$\geq 2b_{\text{add}}^{70}$
1000	N_{MC}	498000	248196	241900	151833	148932	118640	118640	117932	107739	18538	18534	16264	8623
	Cut eff.	-	0.498	0.975	0.628	0.981	0.797	1.000	0.994	0.914	0.172	1.000	0.878	0.530
1200	N_{MC}	497000	254395	248661	152134	148969	125935	125935	125170	114663	22658	22653	19664	10291
	Cut eff.	-	0.512	0.977	0.612	0.979	0.845	1.000	0.994	0.916	0.198	1.000	0.868	0.523
1400	N_{MC}	499000	260545	255004	151933	148562	130183	130183	129327	118716	24673	24667	21203	11079
	Cut eff.	-	0.522	0.979	0.596	0.978	0.876	1.000	0.993	0.918	0.208	1.000	0.860	0.523
1600	N_{MC}	497000	263865	258714	150482	146957	131867	131867	130959	121196	26420	26412	22631	11616
	Cut eff.	-	0.531	0.980	0.582	0.977	0.897	1.000	0.993	0.925	0.218	1.000	0.857	0.513
1800	N_{MC}	490000	263070	258072	145536	141752	129382	129382	128408	119539	27016	27014	22925	11728
	Cut eff.	-	0.537	0.981	0.564	0.974	0.913	1.000	0.992	0.931	0.226	1.000	0.849	0.512
2000	N_{MC}	500000	269918	265056	145830	141828	131486	131486	130372	122004	28059	28053	23583	11914
	Cut eff.	-	0.540	0.982	0.550	0.973	0.927	1.000	0.992	0.936	0.230	1.000	0.841	0.505
2500	N_{MC}	497000	271566	267051	137291	133192	125774	125774	124454	117931	29003	28999	23868	11596
	Cut eff.	-	0.546	0.983	0.514	0.970	0.944	1.000	0.990	0.948	0.246	1.000	0.823	0.486
3000	N_{MC}	489000	267310	262927	126289	121989	116513	116513	115007	109992	28753	28750	23174	10622
	Cut eff.	-	0.547	0.984	0.480	0.966	0.955	1.000	0.987	0.956	0.261	1.000	0.806	0.458

(b)

Mass		Gen	Reco	TrigDec	1ℓ	TrigMatch	$\geq 1J$	$\geq 1j$	$\geq 1b^{85}$	$\geq 1J_{\text{non el}}$	$\geq 1J_{\text{top-tag}}$	$\geq 1j_{\text{add}}$	$\geq 1b_{\text{add}}^{70}$	$\geq 2b_{\text{add}}^{70}$
1000	N_{MC}	499000	294866	290492	186576	183583	147606	147606	146329	131251	24304	24293	21011	10895
	Cut eff.	-	0.591	0.985	0.642	0.984	0.804	1.000	0.991	0.897	0.185	1.000	0.865	0.519
1200	N_{MC}	500000	300323	296365	185318	181937	154413	154413	153000	138404	29012	28997	24801	12811
	Cut eff.	-	0.601	0.987	0.625	0.982	0.849	1.000	0.991	0.905	0.210	1.000	0.855	0.517
1400	N_{MC}	500000	303573	299866	181675	178152	156905	156905	155480	141630	32480	32470	27571	13870
	Cut eff.	-	0.607	0.988	0.606	0.981	0.881	1.000	0.991	0.911	0.229	1.000	0.849	0.503
1600	N_{MC}	498000	304438	300981	177434	173574	156104	156104	154405	141953	34356	34336	28999	14487
	Cut eff.	-	0.611	0.989	0.590	0.978	0.899	1.000	0.989	0.919	0.242	0.999	0.845	0.500
1800	N_{MC}	488000	299636	296508	170489	166656	152480	152480	150711	139586	34423	34413	28710	14220
	Cut eff.	-	0.614	0.990	0.575	0.978	0.915	1.000	0.988	0.926	0.247	1.000	0.834	0.495
2000	N_{MC}	488000	300376	297075	166140	162131	150247	150247	148297	138313	35279	35265	29166	14182
	Cut eff.	-	0.616	0.989	0.559	0.976	0.927	1.000	0.987	0.933	0.255	1.000	0.827	0.486
2500	N_{MC}	498000	305572	302770	159971	155580	146930	146930	144597	136696	36850	36841	29578	13558
	Cut eff.	-	0.614	0.991	0.528	0.973	0.944	1.000	0.984	0.945	0.270	1.000	0.802	0.458
3000	N_{MC}	499000	304217	301493	152213	147658	140988	140988	138344	132052	37948	37944	29674	13047
	Cut eff.	-	0.610	0.991	0.504	0.970	0.955	1.000	0.981	0.955	0.287	1.000	0.782	0.440

(c)

Table 10: Cut flow for the H^+ (a), W'_{LH} (b), and W'_{RH} (c) signal: for each sample the corresponding mass, the number of generated events (Gen), the number of reconstructed events (Reco), the number of events that pass lepton triggers (TrigDec), the number of events that have an electron or muon with p_T larger than 27 GeV (1ℓ), the number of events that the lepton matches to the one detected with the trigger (TrigMatch), the number of events that have at least one large-R jets with p_T larger than 200 GeV ($\geq 1J$), the number of events that have at least one small-R jets with p_T larger than 25 GeV ($\geq 1j$), the number of events that have at least one b -tagged jets at the 85% efficiency working point ($\geq 1b^{85}$), the number of events that have at least one large-R jets with ΔR to the electron smaller than 1.0 ($\geq 1J_{\text{non el}}$), the number of events that have at least one top-tagged large-R jets with contained top-tagger at the 80% efficiency working point ($\geq 1J_{\text{top-tag}}$), the number of events that have at least additional small-R jets with ΔR to the leading top-tagged large-R jet larger than 1.0 ($\geq 1j_{\text{add}}$), the number of events that have at least one or two b -tagged additional small-R jets at the 70% efficiency working point ($\geq 1b_{\text{add}}^{70}$, $\geq 2b_{\text{add}}^{70}$) are shown in the top rows (N_{MC}). Each cut efficiency is also shown in the bottom rows (Cut eff.).

4.1.2 Multivariable analysis using BDT

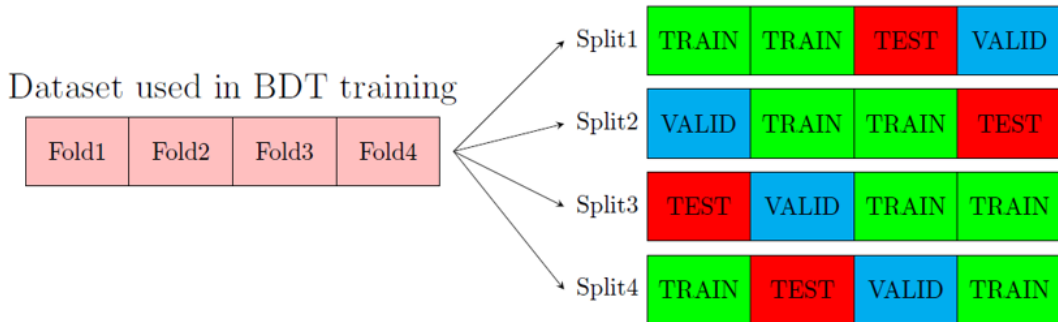
In this search, the most important background is $t\bar{t} + \text{jets}$ as discussed in Section 4.1. To enhance the separation between signal and background, multivariable analysis is performed using Boosted Decision Trees (BDT) technique of TMVA [114]. Obtained BDT score distribution is used in the profile likelihood fit as a final discriminant (Section 7).

468 **Signal and background definition in BDT training**

469 To classify signal (H^+ and W') and $t\bar{t}$ + jets background events, BDTs are trained using the simulated
 470 H^+ signal and $t\bar{t}$ + jets background samples. This analysis under 3 TeV mass points considers eight
 471 different mass hypotheses, and the training is performed on each mass hypothesis. On the other
 472 hand, the $t\bar{t}$ + jets background samples are common in each training. Since kinematics of H^+ signals
 473 become harder in higher mass hypotheses, the BDTs trained using the higher H^+ mass samples
 474 typically have greater separation power. These signal events and background events used in training
 475 are required to pass either SR criteria. These BDTs optimized using H^+ signal samples can be
 476 also used in $W' \rightarrow tb$ analysis because the difference between a H^+ and W' is only their spin and
 477 the kinematic characteristics of $W' \rightarrow tb$ events are similar to the ones of $H^+ \rightarrow tb$ events. This
 478 validation is done in the section below. BDTs are also trained using 4 and 5 TeV mass point samples.
 479 These BDT outputs are only used for the study in Section 5.4.

480 **BDT training settings**

481 To fully use the simulation samples' statistics, we adopt the 4-fold cross-validation method in the
 482 BDT training (Figure 5). Each simulation sample is divided into four sub-datasets (Fold1, Fold2,
 483 Fold3, and Fold4). For each MC event, a random number is generated with the MC event number as
 484 a seed, and the event is categorized into one of the sub-datasets according to the generated number.
 485 Two of the four sub-datasets are labelled "TRAIN," which are used for BDT training. One of the
 486 other sub-datasets is labelled "VALID" and is used to optimize the BDT performance. The last
 487 sample, "TEST", is used to construct a fit template. Four combinations of sub-dataset usage (Split1
 488 to Split4 in Figure 5) are tried, and we obtain four statistically-independent BDTs and fit templates.
 489 They are combined into one fit template used in the profile likelihood fit (Section 7).



490 Figure 5: Scheme of 4-fold cross-validation of BDT in this analysis.
 491

Hyperparameters for the BDTs are summarized in Table. 11. Those hyperparameters are chosen to
 obtain the best sensitivity.

Configuration	
Algorithm	Gradient boosting
<i>Hyperparameters</i>	
NTrees	100
MinNodeSize	2.5
MaxDepth	3
nCuts	20

Table 11: List of hyperparameters used in the training of a BDT

492 Input variables in BDT

493 Jets originating from a H^+ (W') decay have higher p_T comparing with $t\bar{t}$ + jets events due to its
 494 heavy mass. Additionally, angular and kinematics correlation among jets are different between H^+
 495 (W') and $t\bar{t}$ + jets events because these bosons create a resonance. The BDT is trained to exploit
 496 these kinematic characteristics fully. The variables used in BDT training are summarized in Table
 497 [12](#). Any variables for missing E_T are not used in BDT training. In Figure [6](#), each distribution in the
 498 H^+ sample with a mass of 3000 GeV is compared with the $t\bar{t}$ + jets background. Table [13](#) shows the
 499 ranking of these variables.

Symbol	Description
HT_jets	Scalar sum of the transverse energy of all jets
LeadingJet_pt	Leading jet p_T
Mjjj_MaxPt	Invariant mass of the jet triplet with maximum p_T
Mbb_MaxPt	Invariant mass of the b-jet pair with maximum p_T
Muu_MinR	Invariant mass of the untagged jet-pair with minimum ΔR
dRlepb_MinR	ΔR between the lepton and the pair of b -jets with smallest ΔR
dRbb_avg	Average ΔR between all b -jet pairs in the event
Centrality_all	Centrality calculated using all jets and leptons
H1_all	Second Fox-Wolfram moment calculated using all jets and lepton
LeadingTop_pt	Leading top-tagged jet p_T
LeadingTop_m	Invariant mass of leading top-tagged jet
Pt_tb	p_T of the pair of leading top-tagged jet and leading b -jet
M_tb	Invariant mass of the pair of leading top-tagged jet and leading b -jet
PtAsymm_tb	p_T asymmetry between leading top-tagged jet and leading b -jet

Table 12: List of variables included in the training of the BDT

Ranking	Variable	Importance				
		Fold1	Fold2	Fold3	Fold4	Avg.
1	HT_jets	9.509E-02	1.118E-01	1.216E-01	1.073E-01	1.089E-01
2	Centrality_all	1.053E-01	9.995E-02	1.126E-01	1.012E-01	1.048E-01
3	M_tb	9.192E-02	9.473E-02	8.282E-02	8.014E-02	8.740E-02
4	LeadingTop_pt	8.710E-02	8.107E-02	6.472E-02	7.292E-02	7.645E-02
5	Pt_tb	7.944E-02	7.816E-02	7.888E-02	6.795E-02	7.611E-02
6	LeadingJet_pt	6.180E-02	7.860E-02	6.628E-02	7.577E-02	7.061E-02
7	dRlepb_MindR	6.997E-02	7.842E-02	6.968E-02	6.393E-02	7.050E-02
8	dRbb_avg	6.236E-02	6.435E-02	5.331E-02	7.843E-02	6.461E-02
9	Mbb_MaxPt	5.348E-02	6.657E-02	7.339E-02	5.552E-02	6.224E-02
10	PtAsymm_tb	5.209E-02	6.526E-02	5.843E-02	6.620E-02	6.050E-02
11	Mjjj_MaxPt	6.439E-02	6.248E-02	5.503E-02	5.577E-02	5.942E-02
12	H1_all	6.316E-02	4.577E-02	4.876E-02	6.291E-02	5.515E-02
13	LeadingTop_m	5.868E-02	3.864E-02	5.567E-02	5.748E-02	5.262E-02
14	Muu_MindR	4.438E-02	3.422E-02	5.889E-02	5.439E-02	4.797E-02

Table 13: Importance ranking of variables used in BDT training on 3000 GeV H+ mass hypothesis. Importance values are output from TMVA.

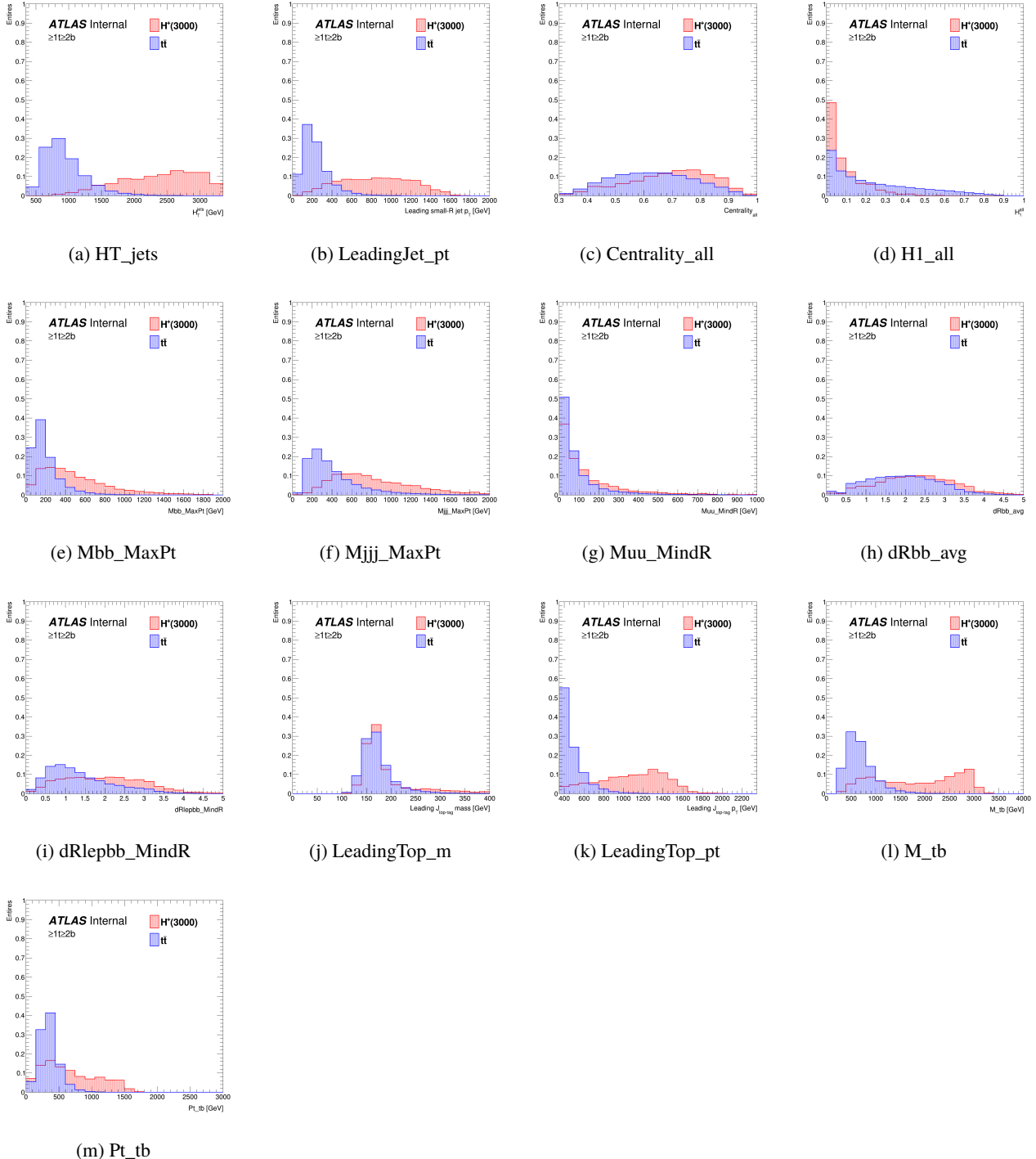


Figure 6: Comparison of input variables for BDT training between H^+ and $t\bar{t} + \text{jets}$ events under 3000 GeV H^+ mass hypothesis in the SR.

500 **Results of BDT training**

501 The BDT output distributions for H^+ signal and background events in the SR for different values

502 of the H^+ mass are shown in Figure 7 to 14, together with receiver operating characteristic (ROC)
 503 curves.

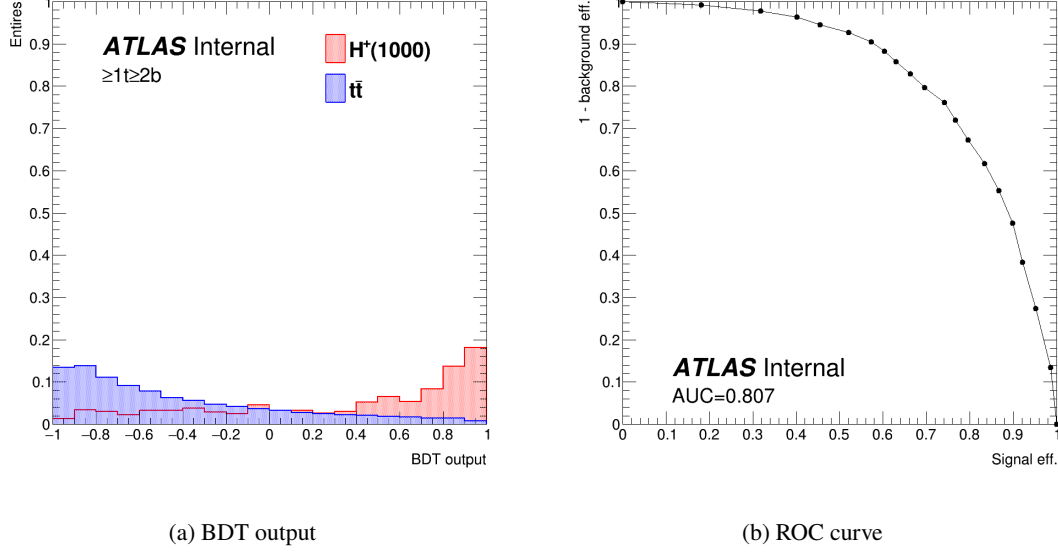


Figure 7: BDT distribution and ROC curve for the 1000 GeV H^+ mass hypothesis.

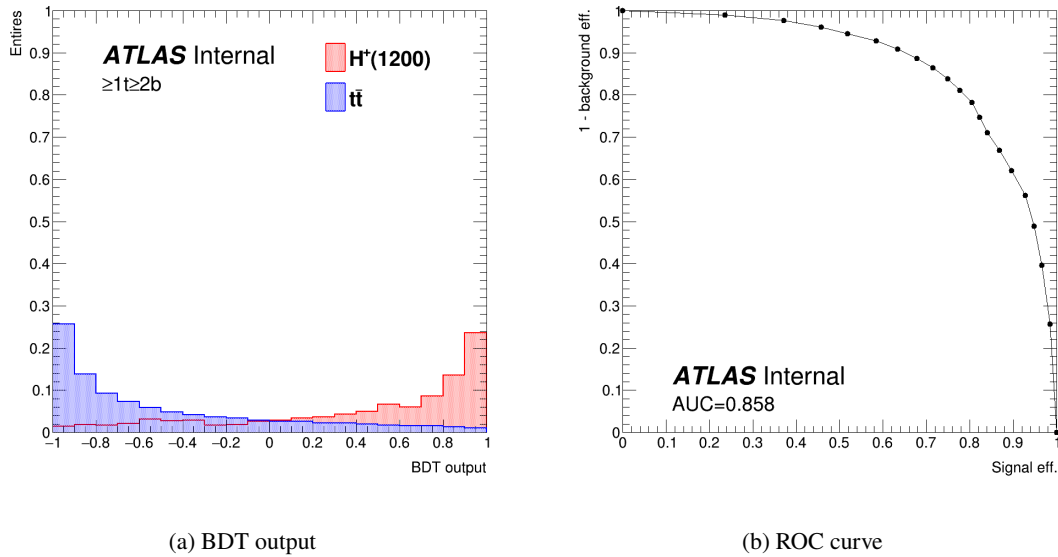


Figure 8: BDT distribution and ROC curve for the 1200 GeV H^+ mass hypothesis.

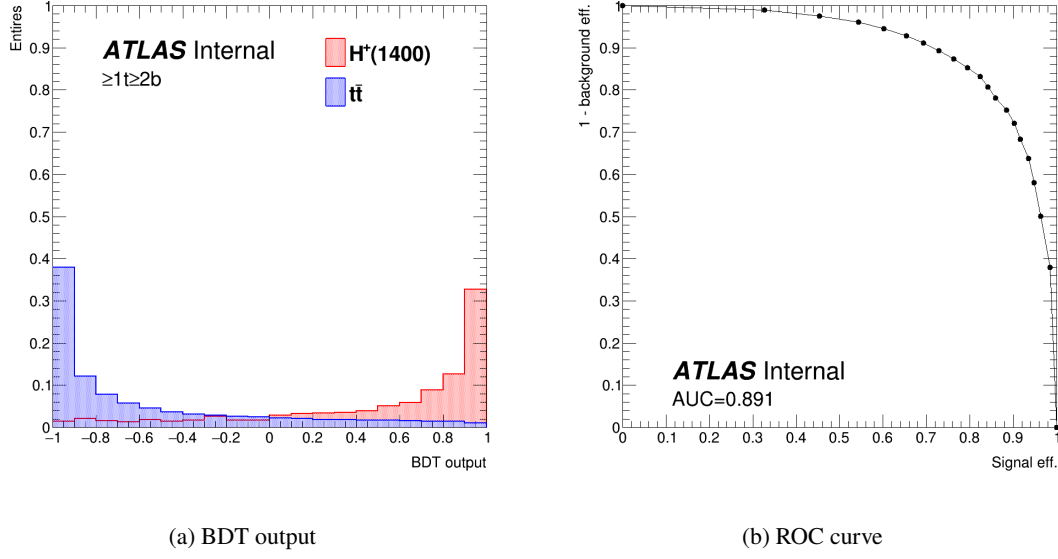


Figure 9: BDT distribution and ROC curve for the 1400 GeV H^+ mass hypothesis.

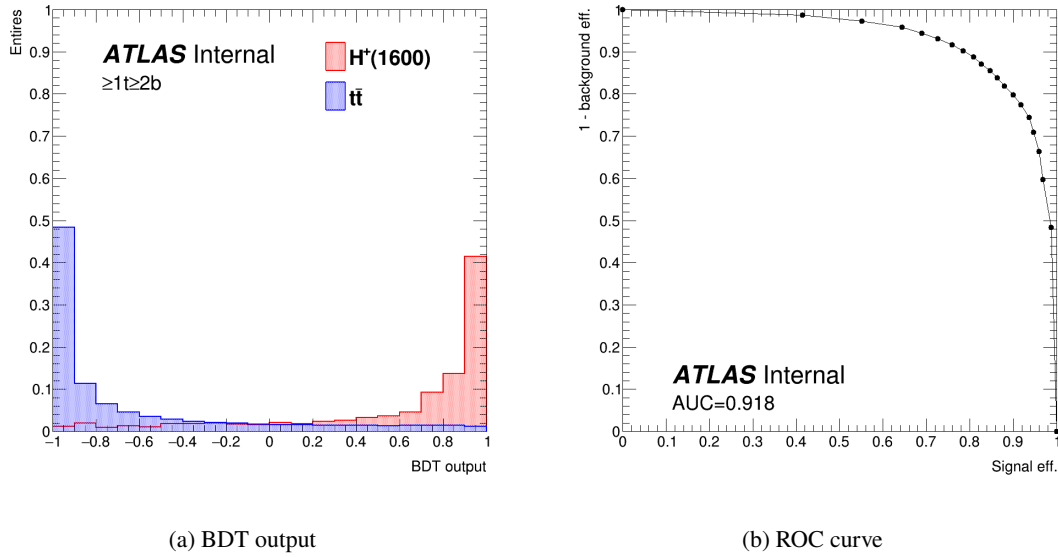


Figure 10: BDT distribution and ROC curve for the 1600 GeV H^+ mass hypothesis.

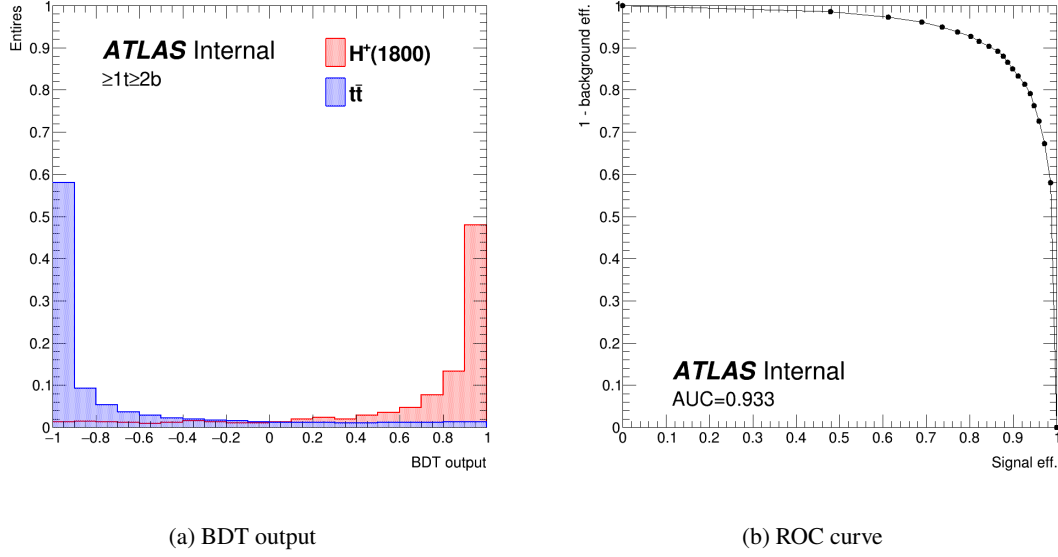


Figure 11: BDT distribution and ROC curve for the 1800 GeV H^+ mass hypothesis.

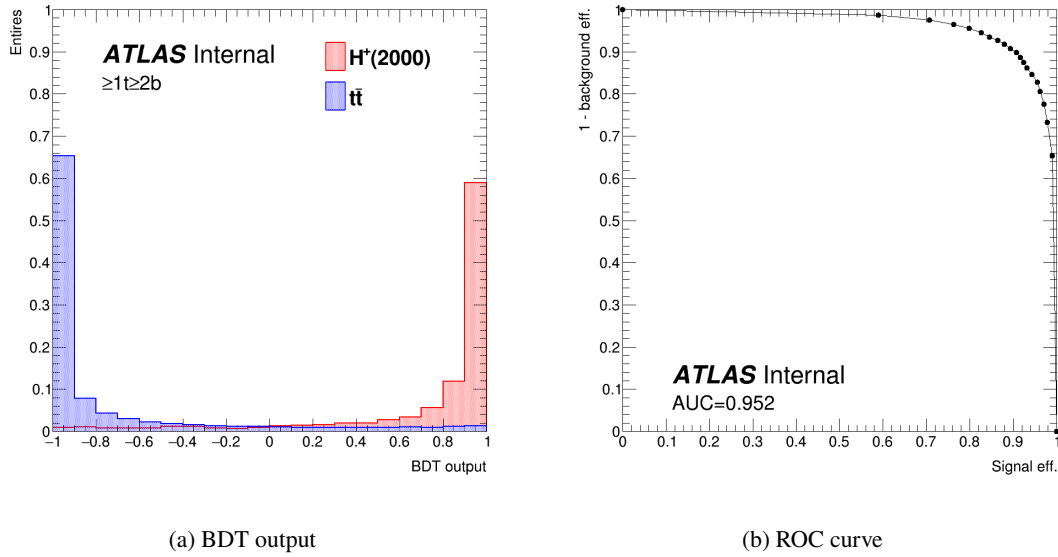


Figure 12: BDT distribution and ROC curve for the 2000 GeV H^+ mass hypothesis.

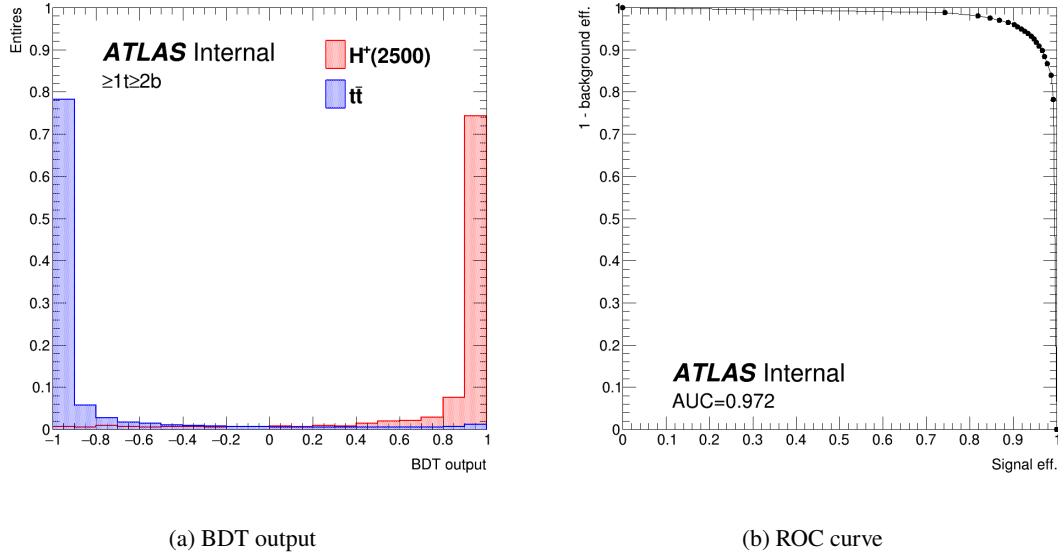


Figure 13: BDT distribution and ROC curve for the 2500 GeV H^+ mass hypothesis.

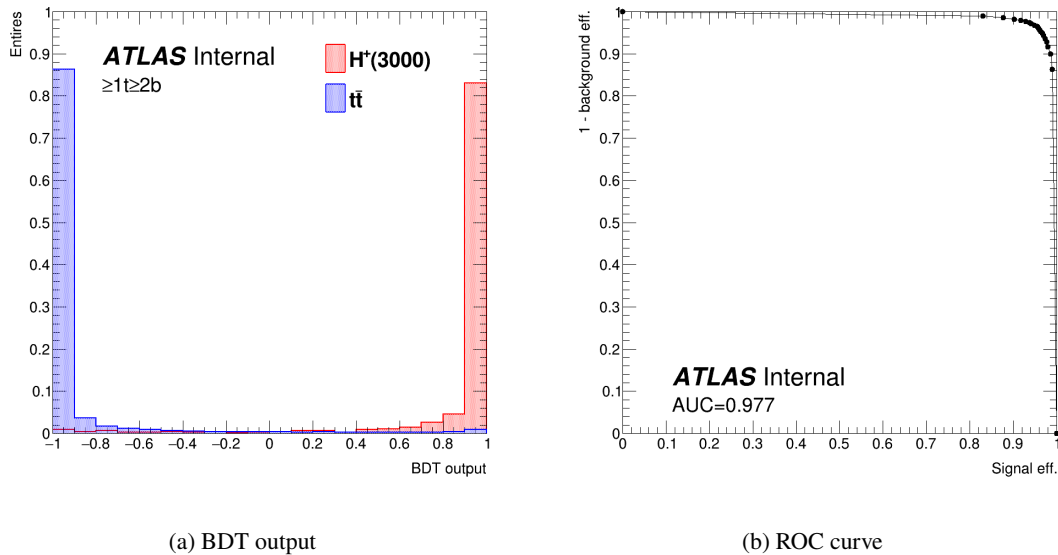
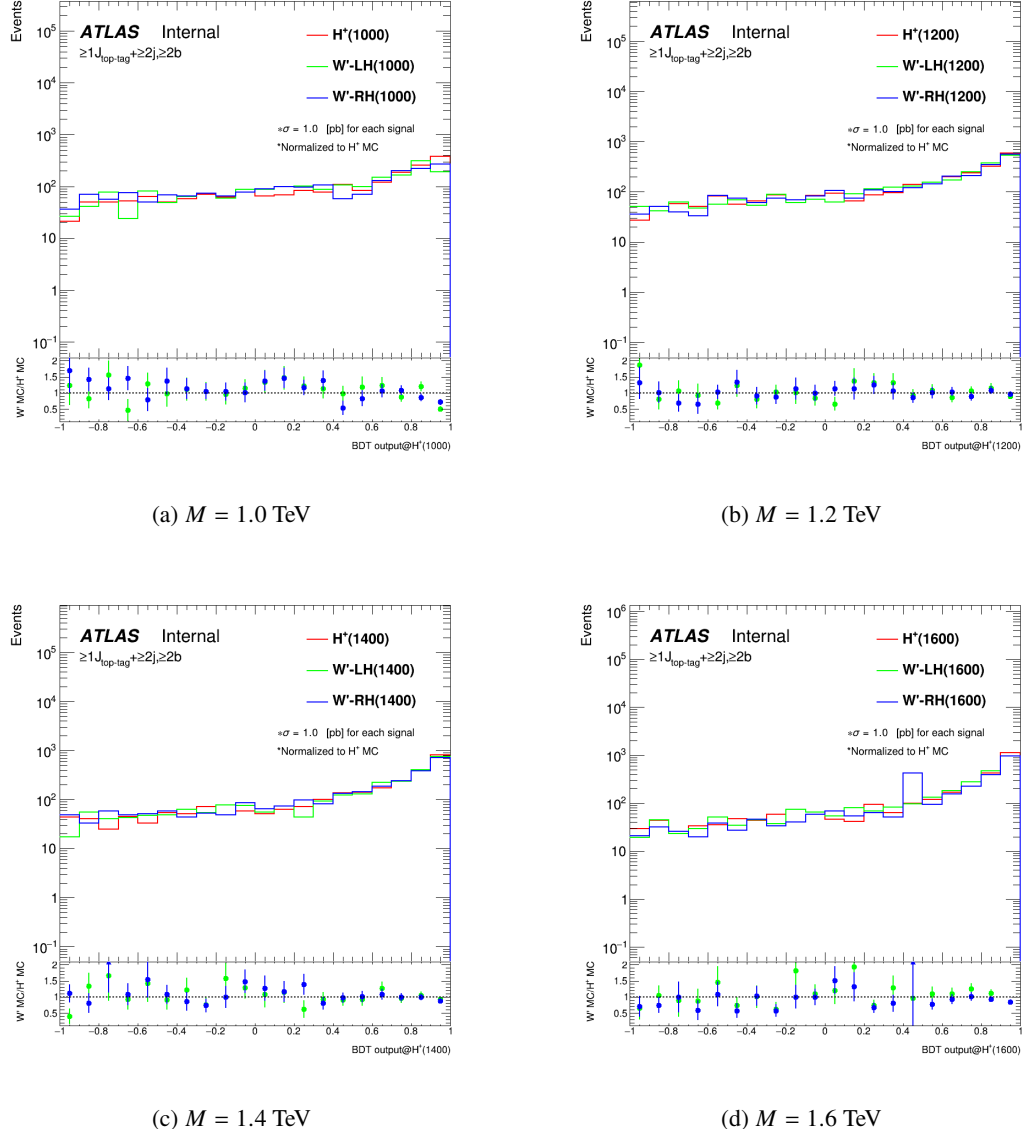


Figure 14: BDT distribution and ROC curve for the 3000 GeV H^+ mass hypothesis.

Comparison of BDT distributions between $H^+ \rightarrow tb$ and $W' \rightarrow tb$ events

BDT distributions for $W' \rightarrow tb$ events are compared with the ones for $H^+ \rightarrow tb$ events in Figure 15. The large differences above their statistic uncertainty are not observed. Therefore, it is expected to be able to obtain comparable sensitivity with $H^+ \rightarrow tb$ analysis without further optimization using $W' \rightarrow tb$ samples.



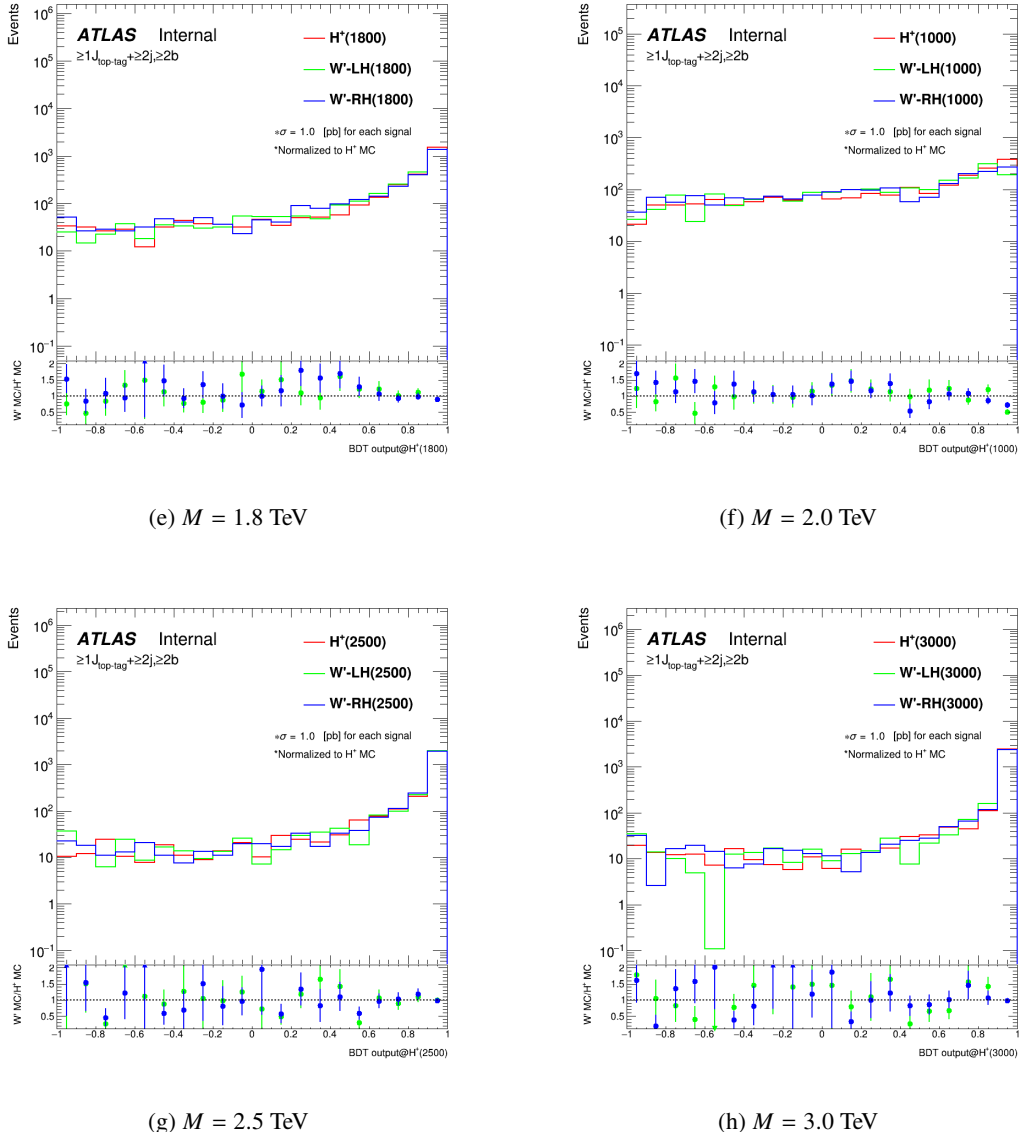


Figure 15: Comparison of BDT distributions between $H^+ \rightarrow tb$ and $W' \rightarrow tb$ events in the SR.

509 4.2 Analysis strategy above 3 TeV

510 For the mass point above 3 TeV, we adopt a different approach. Since it is difficult to estimate $t\bar{t} + \text{jets}$ events
 511 reliably in the very high H_T^{jets} region where most of the signal events distribute, we use a cut-and-counting
 512 method as detailed below, which avoids using the line shapes at the high H_T^{jets} region, and therefore is more
 513 robust against potential mis-modelling compared with the BDT method.

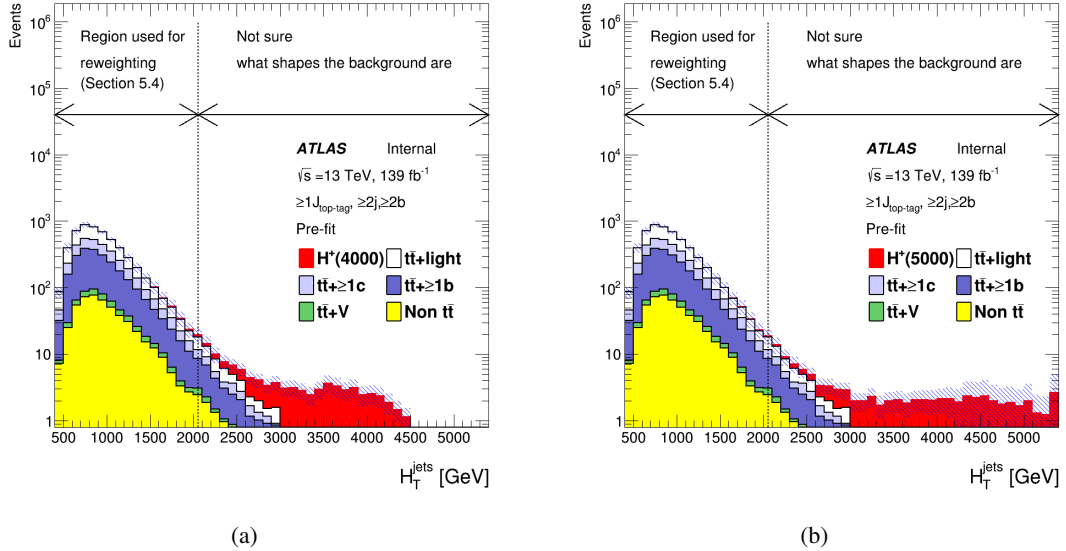


Figure 16: Signal and background comparison for 4000 (a) and 5000 (b) GeV mass hypotheses. These signal events distribute mostly in $H_T^{\text{jets}} > 2000$ GeV. These regions don't have enough shape information to perform reweighting in Section 5.4.

The event selection is essentially the same as the analysis below 3 TeV mass point as described in Subsection 4.1.1, with different region definitions. Events are required to have exactly one lepton (e or μ) matching the trigger lepton, at least one top tagged large- R jet. One signal region (SR) and two control regions (CR1, CR2) are defined according to the number of b -tagged small- R jets which satisfy $\Delta R(J_{\text{top-tag}}^{1\text{st}}, \text{jet}) > 1.0$ and H_T^{jets} . Events with exactly one b -tagged jet are categorized into CR2 region, which is exactly the same region as the CR region in Subsection 4.1.1. Events with two or more one b -tagged jet are categorized into SR if they have $H_T^{\text{jets}} > 2000$ GeV, and into CR1 if $H_T^{\text{jets}} \leq 2000$ GeV. The event selections in these regions are summarized in Table 14. Figure 17 to 19 show the H_T^{jets} distributions with the background compositions in each region. The number of bins of H_T^{jets} distribution in the SR is set to one, thus we only use the event count information, while we use the H_T^{jets} distribution of CR1 and CR2 in the final fit. The CR1 and CR2 are enriched in $t\bar{t}$ + HF and $t\bar{t}$ + light events, respectively. Therefore, these regions are used to control $t\bar{t}$ + jets events in the final fit. H_T^{jets} is used as final discriminates, as discussed in Section 7.

Cut	SR	CR1	CR2
leptons	Same requirements as Table 8		
Top-tagged large- R jets	Same requirements as Table 8		
Small- R jets	$N_{\text{jet}} \geq 2$ (Kinematic requirements are the same as Table 8)	$N_{\text{jet}} \geq 1$ (Kinematic requirements are the same as Table 8)	
b -tagged small- R jets	$N_{b-\text{jet}} \geq 2$	$N_{b-\text{jet}} = 1$	
H_T^{jets}	> 2000 GeV	≤ 2000 GeV	No cut

Table 14: Event selections in the SR, CR1, and CR2. After these selections, CR1 becomes enriched in $t\bar{t}$ + light, and CR2 becomes enriched in $t\bar{t}$ + HF.

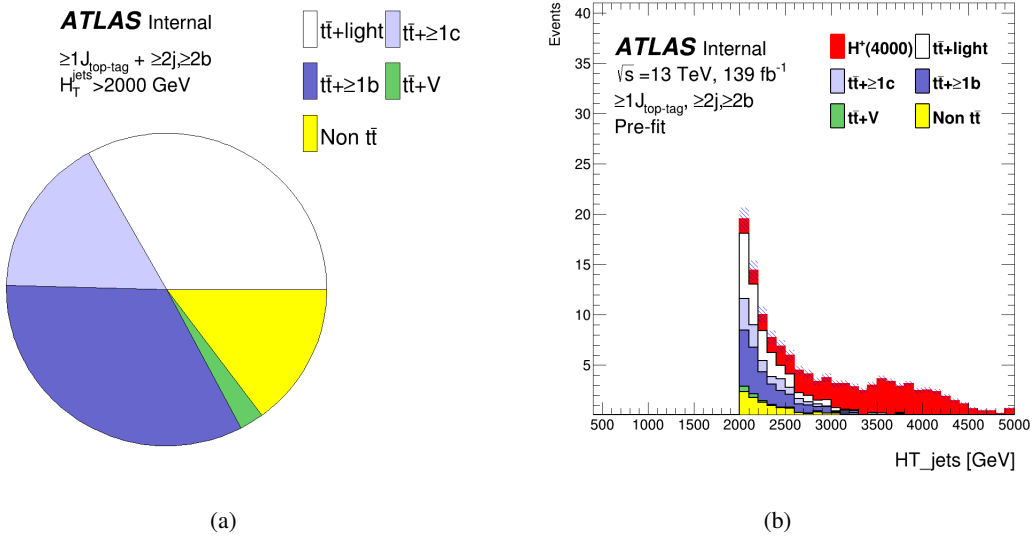


Figure 17: Background composition in the SR is shown in the pie chart (a) and the H_T^{jets} distributions (b). The number of bins of H_T^{jets} distribution is set to exactly one.

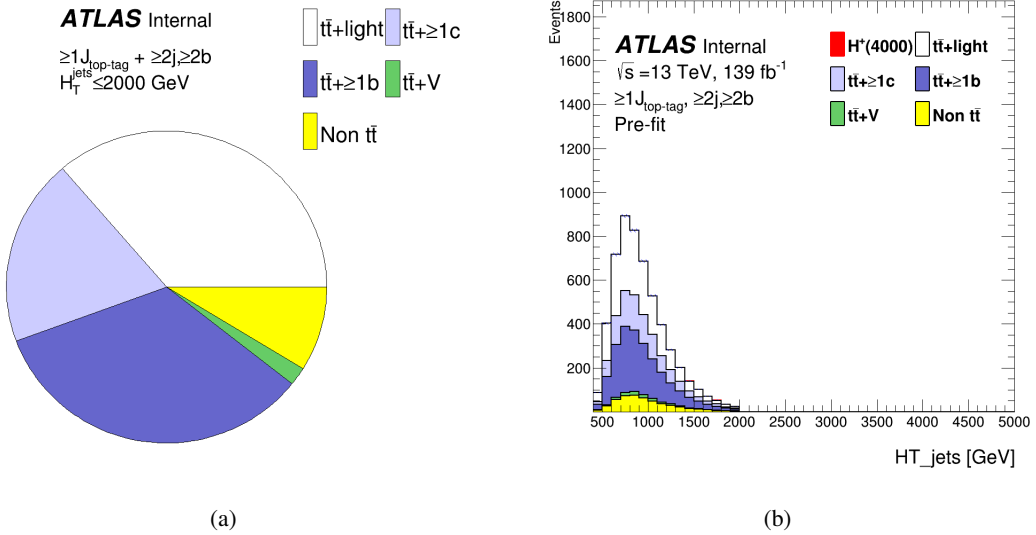


Figure 18: Background composition in the CR1 is shown in the pie chart (a) and the H_T^{jets} distributions (b).

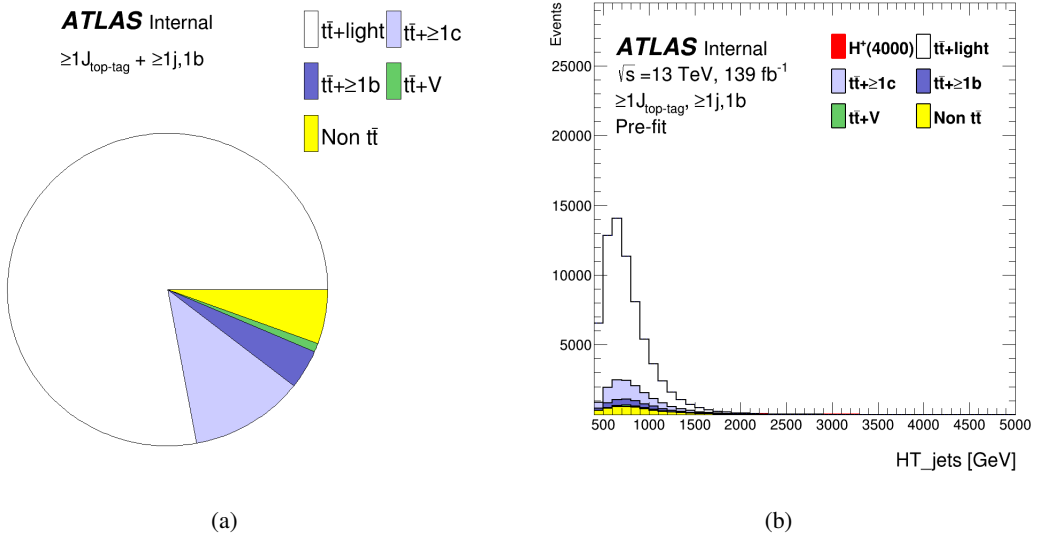


Figure 19: Background composition in the CR2 is shown in the pie chart (a) and the H_T^{jets} distributions (b). The CR2 is the same region as the CR of multivariate analysis defined in Section 4.1.1.

526 The number of expected signal and background events in the SR, CR1, and CR2 are shown in Table 15. The
 527 predicted number of H^+ and W' signal events for the 4000 and 5000 GeV mass hypothesis are estimated
 528 using $\sigma \times Br = 0.046 \text{ pb}$, as done in Table 9.

	SR	CR1	CR2
$t\bar{t} + \text{light}$	22 ± 6	1928 ± 94	54008 ± 2667
$t\bar{t} + \geq 1c$	11 ± 9	1052 ± 915	8011 ± 1450
$t\bar{t} + \geq 1b$	22 ± 11	1831 ± 920	2793 ± 1402
$t\bar{t} + W$	1 ± 0	37 ± 6	312 ± 41
$t\bar{t} + Z$	1 ± 0	67 ± 10	294 ± 38
Wt channel	3 ± 3	181 ± 104	1995 ± 825
t channel	1 ± 0	37 ± 24	172 ± 56
Other top sources	1 ± 0	8 ± 2	34 ± 5
$VV, V+\text{jets}$	5 ± 2	147 ± 54	1529 ± 530
$t\bar{t}H$	1 ± 0	103 ± 4	176 ± 5
Total	65 ± 6	5438 ± 264	69324 ± 3356
$H^+ 4000 \text{ GeV}$	57 ± 18	5 ± 2	100 ± 32
$H^+ 5000 \text{ GeV}$	56 ± 21	3 ± 1	98 ± 37

Table 15: Number of expected and selected events split according to the SR, CR1, and CR2. The quoted uncertainties include both statistical and systematic uncertainties before fitting.

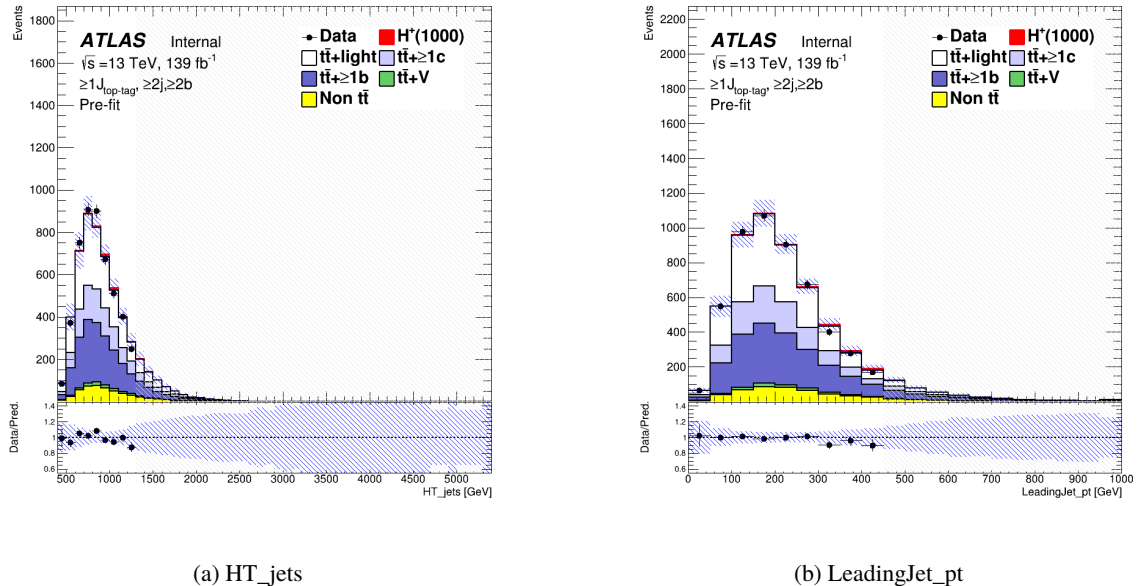
529 5 Background modeling

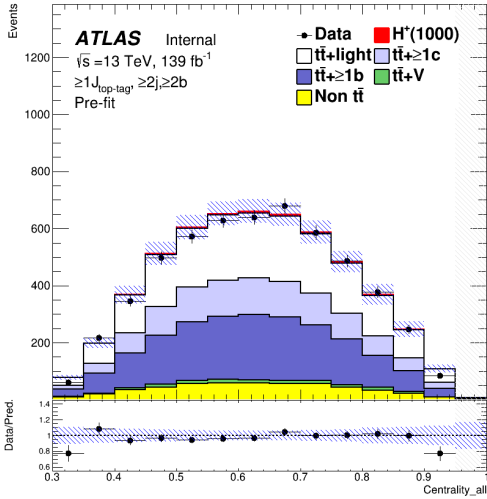
530 5.1 Blind strategy

531 In the following sections, the modelling of kinematic distributions, particularly those used for BDT training,
 532 of the $t\bar{t}$ + jets background is checked by comparing the data and MC. In order to avoid observing signals
 533 or any other biases before fixing the analysis procedure, the following blinding strategy is applied. The
 534 signal-to-noise ratio (S/B) is calculated in each bin of each distribution for all mass hypotheses (more
 535 details in Appendix B). The signal cross section (σ_{signal}) on each mass hypothesis is set to 0.046 pb, which
 536 is the upper limit at 1 TeV H^+ mass point obtained from the resolved $H^+ \rightarrow tb$ search [25]. Therefore, it can
 537 be considered the most conservative assumption. The data in bins with $S/B > 0.05$ in at least one mass
 538 hypothesis are blinded when the data is compared with MC.

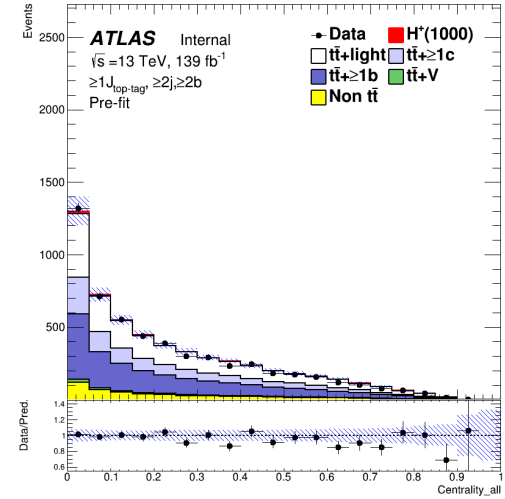
539 5.2 Data/MC comparison for BDT input variables

540 Figures 20 show the distributions of input variables for BDT training in the SR region with all systematic
 541 uncertainty sources, which are summarised in Table 18, except for $t\bar{t}$ + jets reweighting source. Data are
 542 blinded according to the blind strategy in Section 5.1. No significant difference between the data and MC
 543 is found in each variable.

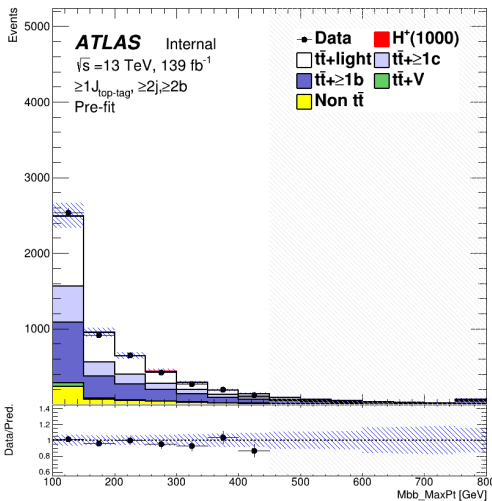




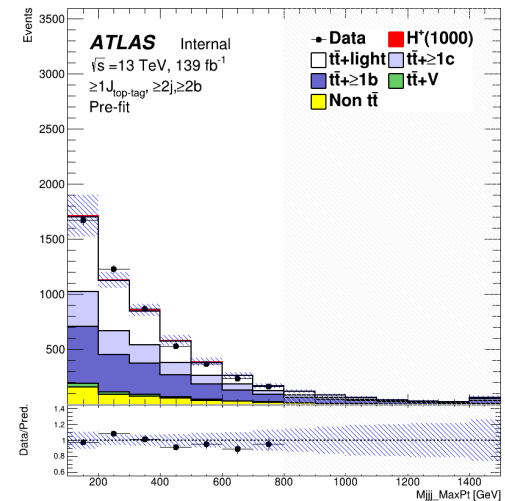
(c) Centrality_all



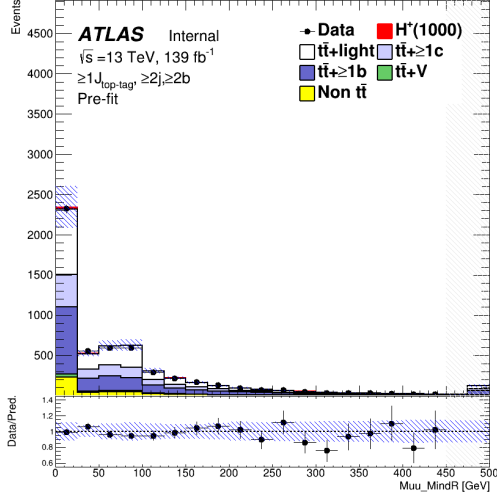
(d) H1_all



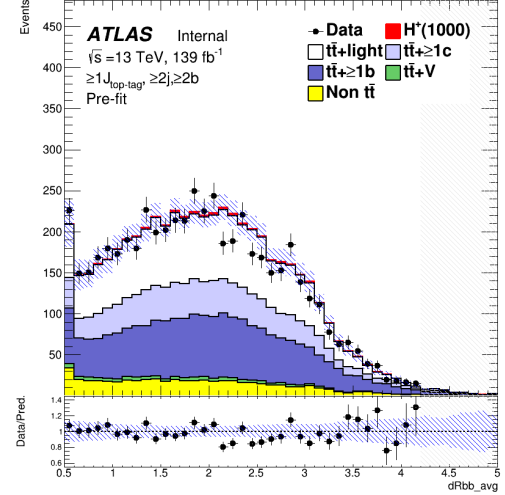
(e) Mbb_MaxPt



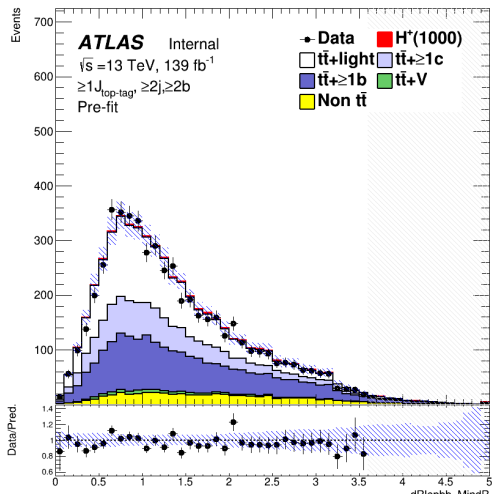
(f) Mjjj_MaxPt



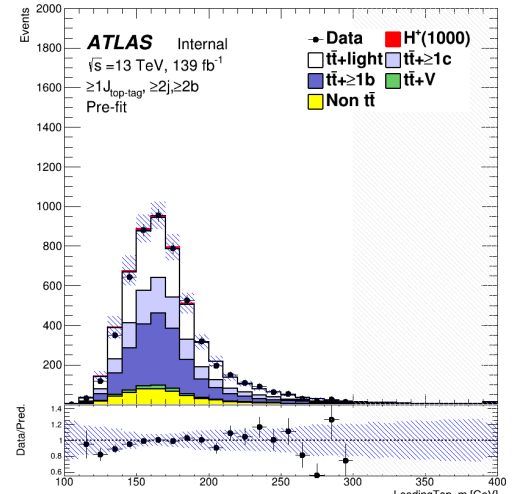
(g) Muu_MindR



(h) dRbb_avg



(i) dRlepb_MindR



(j) LeadingTop_m

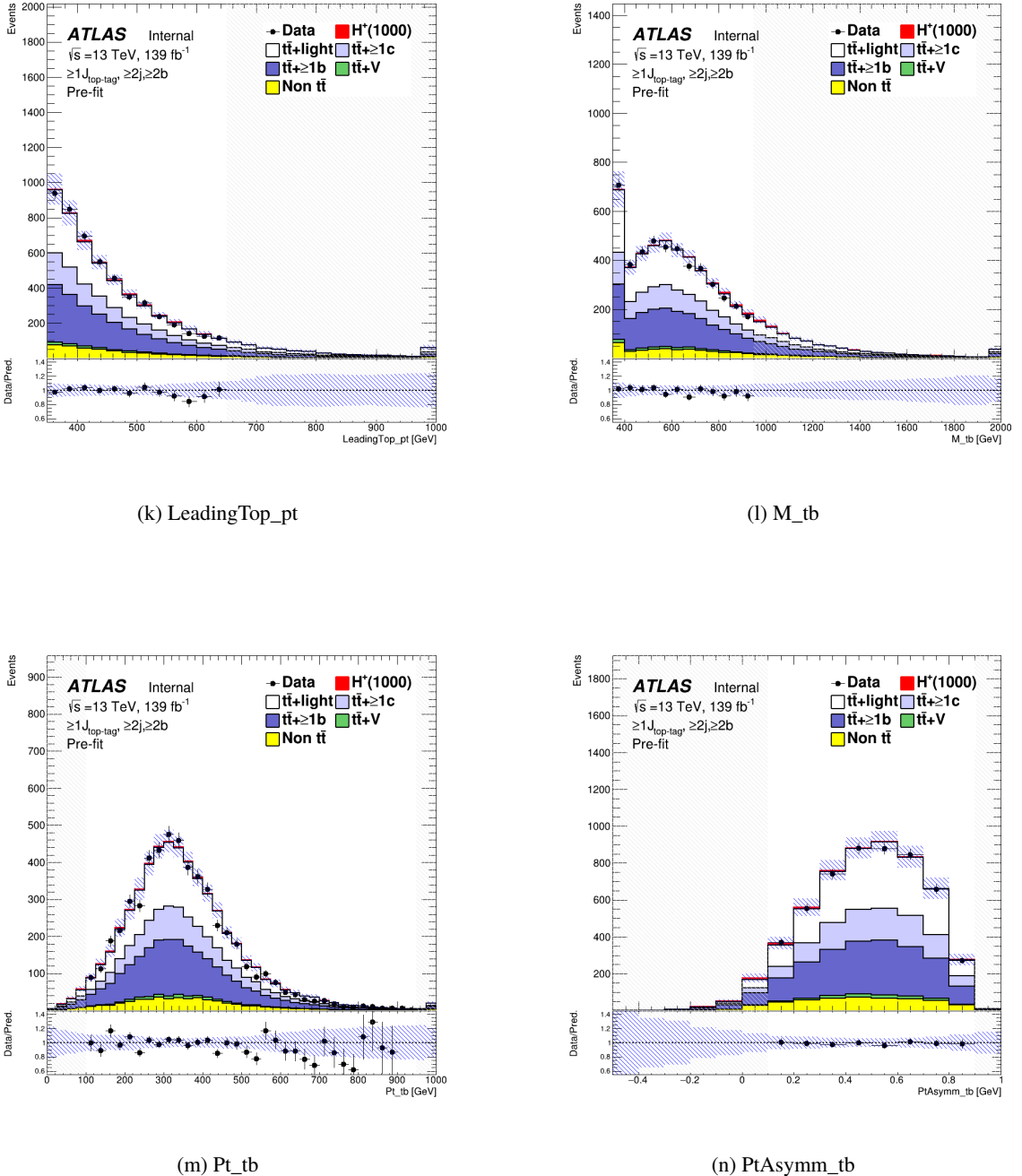
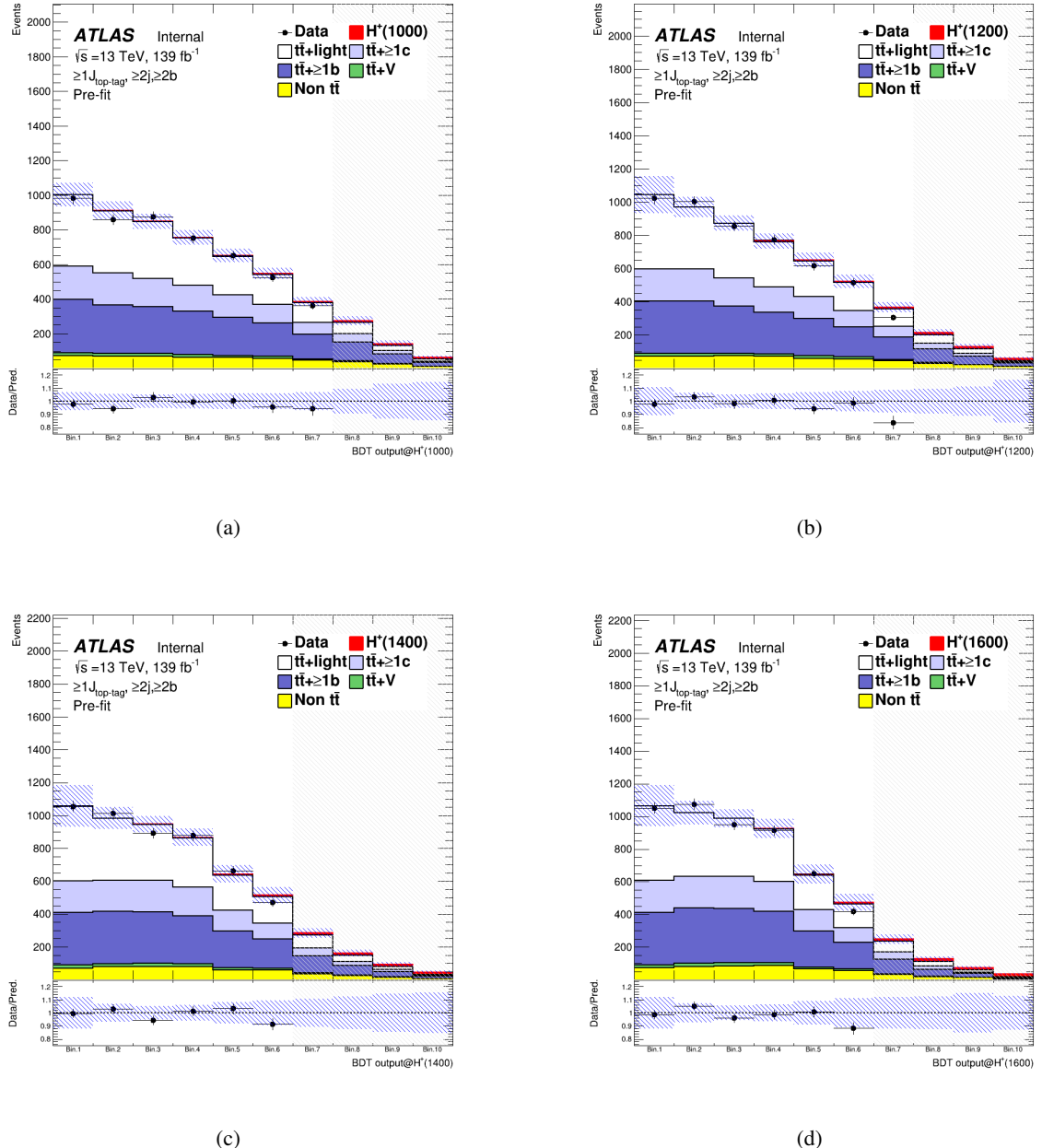


Figure 20: Comparison of the kinematic variables included in the BDT in the SR for the data and MC with all systematics uncertainties, which are summarised in Table 18, except for $t\bar{t}$ + jets reweighting source.

544 5.3 Data/MC comparison for BDT outputs

545 Figures 21(a) to 21(h) show the distributions of BDT output in the SR. The binning of each BDT output is
546 optimized for the search sensitivity by *TransfoD* algorithm [115]. Such binning results in extremely narrow

bins towards high BDT scored and makes the plot hard to see, as shown in Figure ?? in Appendix B.2 when plotted in a usual manner. We rather show the distribution with an equal interval for each bin. The distributions are input into the profile likelihood fit on each H^+ mass hypothesis as shown in Section 7. It is observed that the data/MC ratio tends to be lower for the high BDT score regions, which may bias the search for the signal in the highest BDT bins. The reweighting to correct for the slope is discussed in Section 5.4.



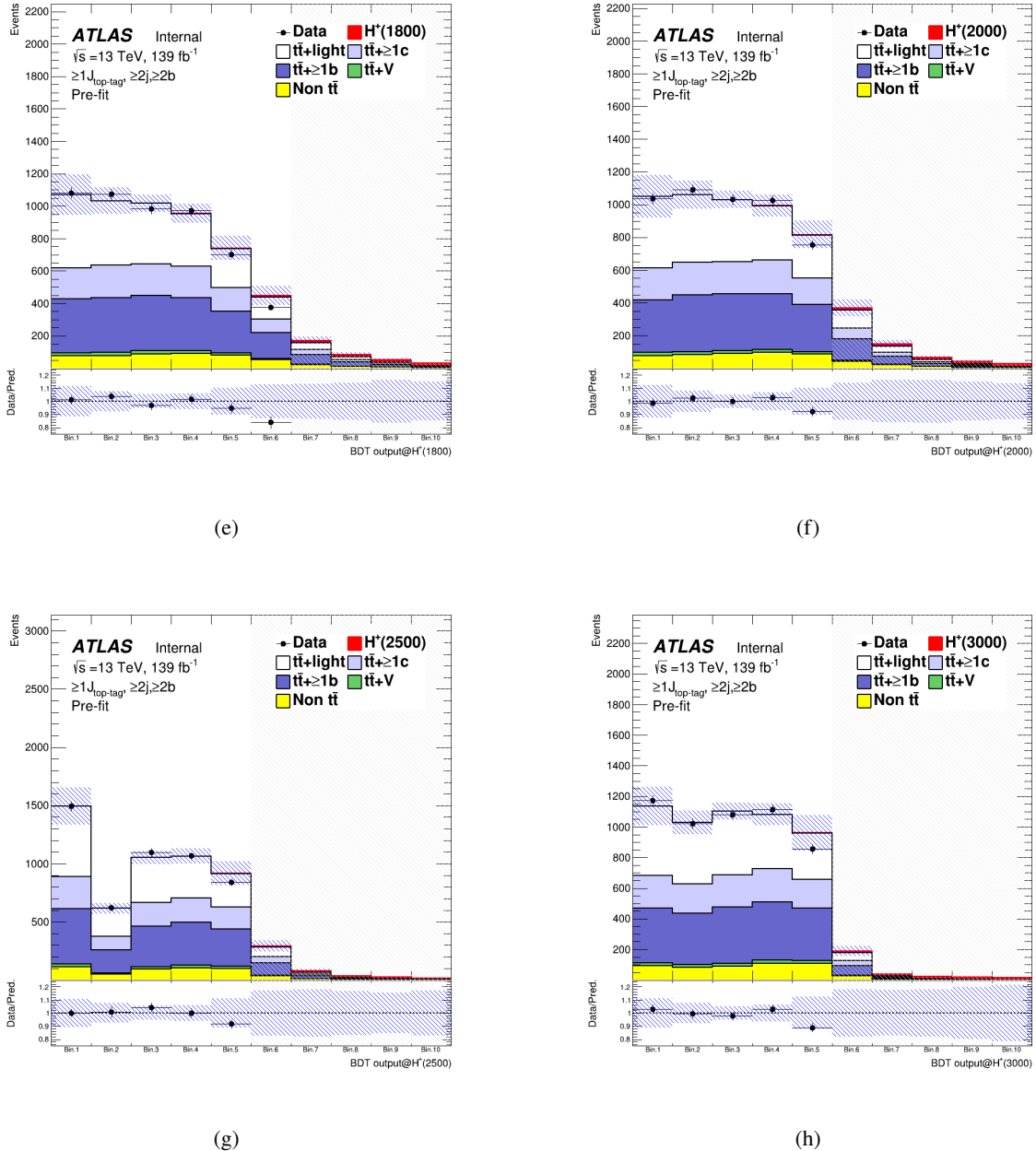


Figure 21: Pre-fit distribution of BDT output trained using from 1000 GeV (a) to 3000 GeV (h) H^+ samples in the SR.

5.4 Reweighting technique

Due to the mismodeling of the hard and soft jets, some extent of mis-modelling is expected in the $t\bar{t} + \text{jets}$ samples generated by Powheg + Phytia. These mis-modelings appear, for example, in the number of jets, p_T distribution of the leading top-tagged large-R jet (LeadingTop_pt) and the invariant mass distribution of small-R jet triplet with maximum p_T (Mjjj_MaxPt) (these small-R jets are mainly QCD jets) as shown in

558 Figure 22.

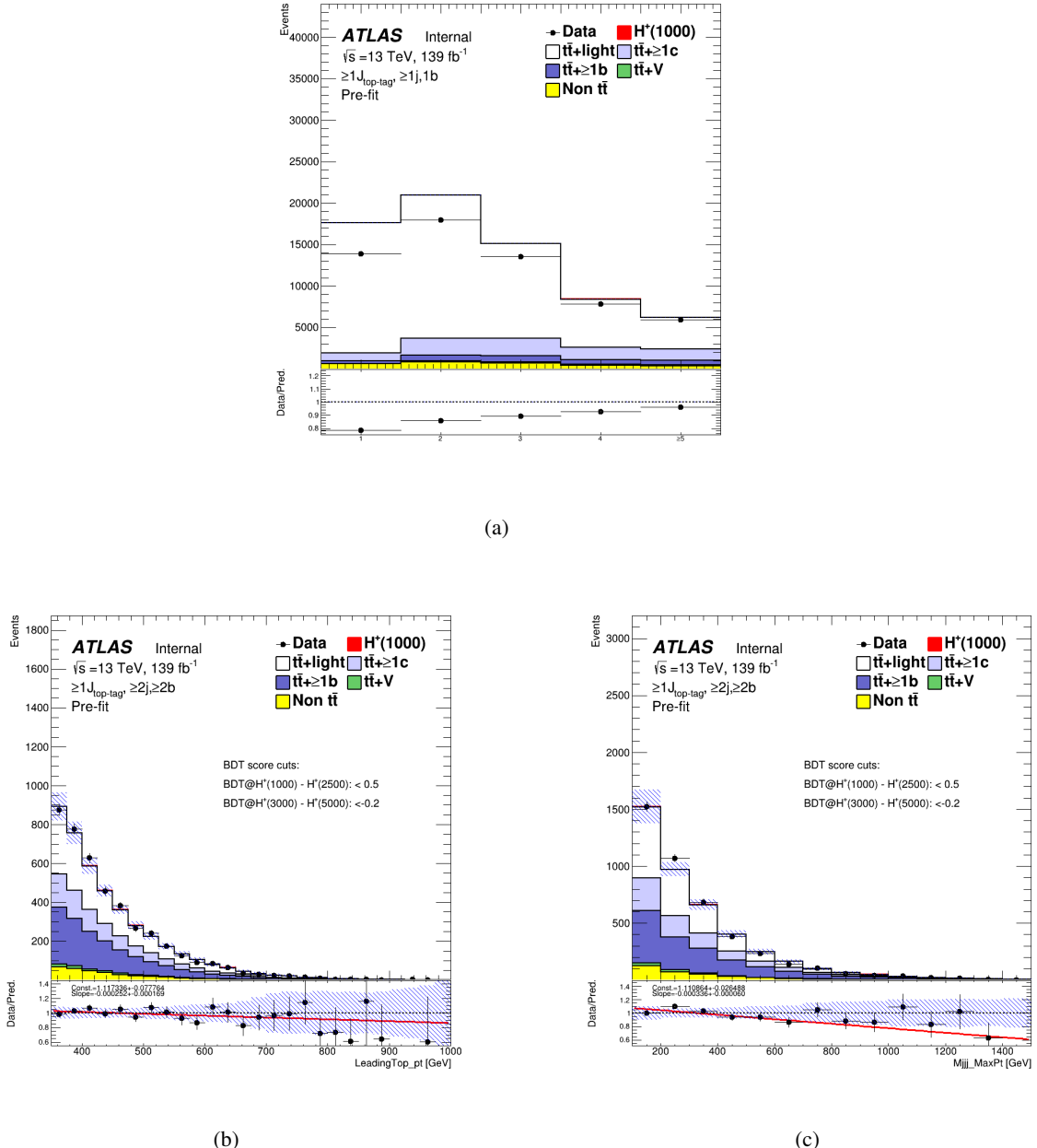


Figure 22: Number of jets in the CR (a), p_T distribution of the leading top-tagged large-R jet in the SR (b) and invariant mass distribution of small-R jet triplet with maximum p_T in the SR (c). These events in the SR are required to pass all BDT cuts shown in Table 16. Each data/MC ratio plot has a slope.

559 To improve the prediction of $t\bar{t} + \text{jets}$, data-based corrections are applied to the MC prediction. The
 560 reweighting factors are derived by comparing the number of jets (N_{jets}) and H_T^{jets} distributions between data
 561 and MC prediction. The reweighting factors for N_{jets} are derived in the CR. Since the modelling is assumed
 562 to be due mainly to the additional radiation in the parton shower, which is independent on the flavour of

associated jets, these reweighting factors are expected to improve the data/MC agreement in the SR as well, to the point that the remaining discrepancies would be well covered by the systematic model. The reweighting factors for H_T^{jets} are derived in the SR and CR, individually, after reweighting with N_{jets} . When the reweighting factors are derived in the SR, events in the only low BDT score region are selected to avoid being reweighted signal events. These events are required to pass all the cuts shown in Table 16.

Firstly, the data/MC ratios R are derived according to the following definition:

$$R = \frac{\text{Data} - \text{MC}^{\text{non-}t\bar{t}+\text{jets}}}{f \cdot \text{MC}^{t\bar{t}+\text{jets}}} \quad (1)$$

$t\bar{t} + \text{jets}$ includes the $t\bar{t} + \text{light}$, $t\bar{t}+ \geq 1c$ and $t\bar{t}+ \geq 1b$. The number of $t\bar{t} + \text{jets}$ MC events is scaled by f to the number of data subtracted non $t\bar{t} + \text{jets}$ MC events. Figure 23 shows the number of jets and data/MC ratio, R , distributions. The first reweighting is performed using the R in each N_{jets} bin, which is applied to $t\bar{t} + \text{light}$, $t\bar{t}+ \geq 1c$ and $t\bar{t}+ \geq 1b$. Figure 24 shows the H_T^{jets} and R distributions in each SR and CR after reweighting with N_{jets} . When the R is derived in the SR, events in the only low BDT score region are selected to avoid being reweighted signal events according to Table 16. These obtained R distributions are fitted with a quadratic function $(f(H_T^{\text{jets}}) = a + b \cdot H_T^{\text{jets}} + c \cdot (H_T^{\text{jets}})^2)$, where a , b , and c are free parameters determined in the fit), and the function is used for reweighting. The function is applied to $t\bar{t} + \text{light}$, $t\bar{t}+ \geq 1c$ and $t\bar{t}+ \geq 1b$ as well as N_{jets} reweighting. The obtained reweighting functions are also shown in Figure 24. Table 17 includes the fitted values for all the parameters. The statistical errors of fitted parameters are included as systematic uncertainties in the final fitting. The reweighting factors in $H_T^{\text{jets}} > 2072 \text{ GeV}$ region are used the value at $H_T^{\text{jets}} = 2072 \text{ GeV}$ because the weight value of -1σ become negative at the point.

Mass point [GeV]	BDT score cut
1000	< 0.5
1200	< 0.5
1400	< 0.5
1600	< 0.5
1800	< 0.5
2000	< 0.5
2500	< 0.5
3000	< -0.2
4000	< -0.2
5000	< -0.2

Table 16: Requirements on the events used for reweighting factor calculation in the SR. These cuts are defined so that events are derived from the regions with $S/B < 0.05$ for any mass points.

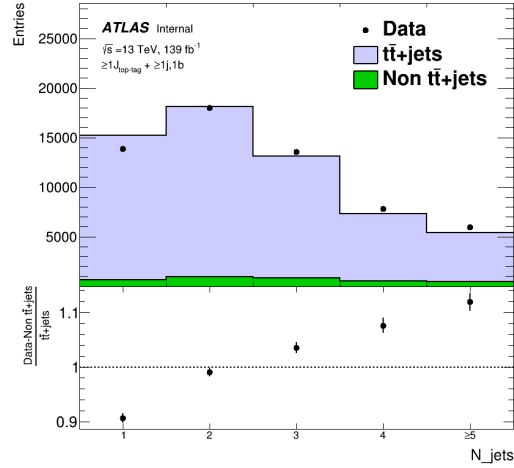


Figure 23: Number of jets (top canvas) and data/MC ratio, R , (bottom canvas) distributions. The first reweighting is performed using the R in each N_{jets} bin, , which is applied to $t\bar{t} + \text{light}$, $t\bar{t}+ \geq 1c$ and $t\bar{t}+ \geq 1b$.

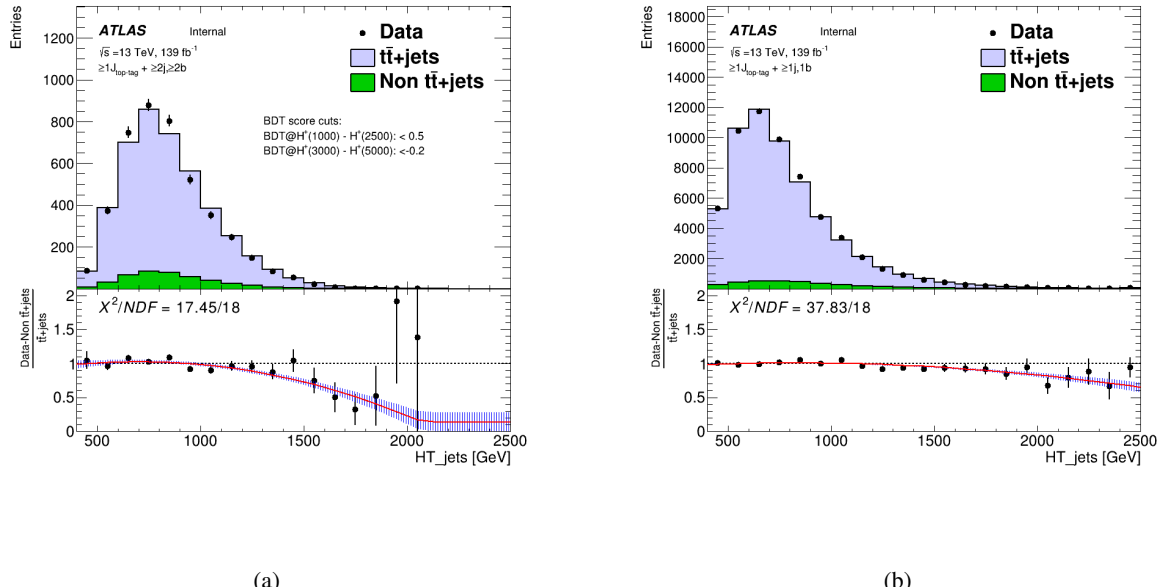
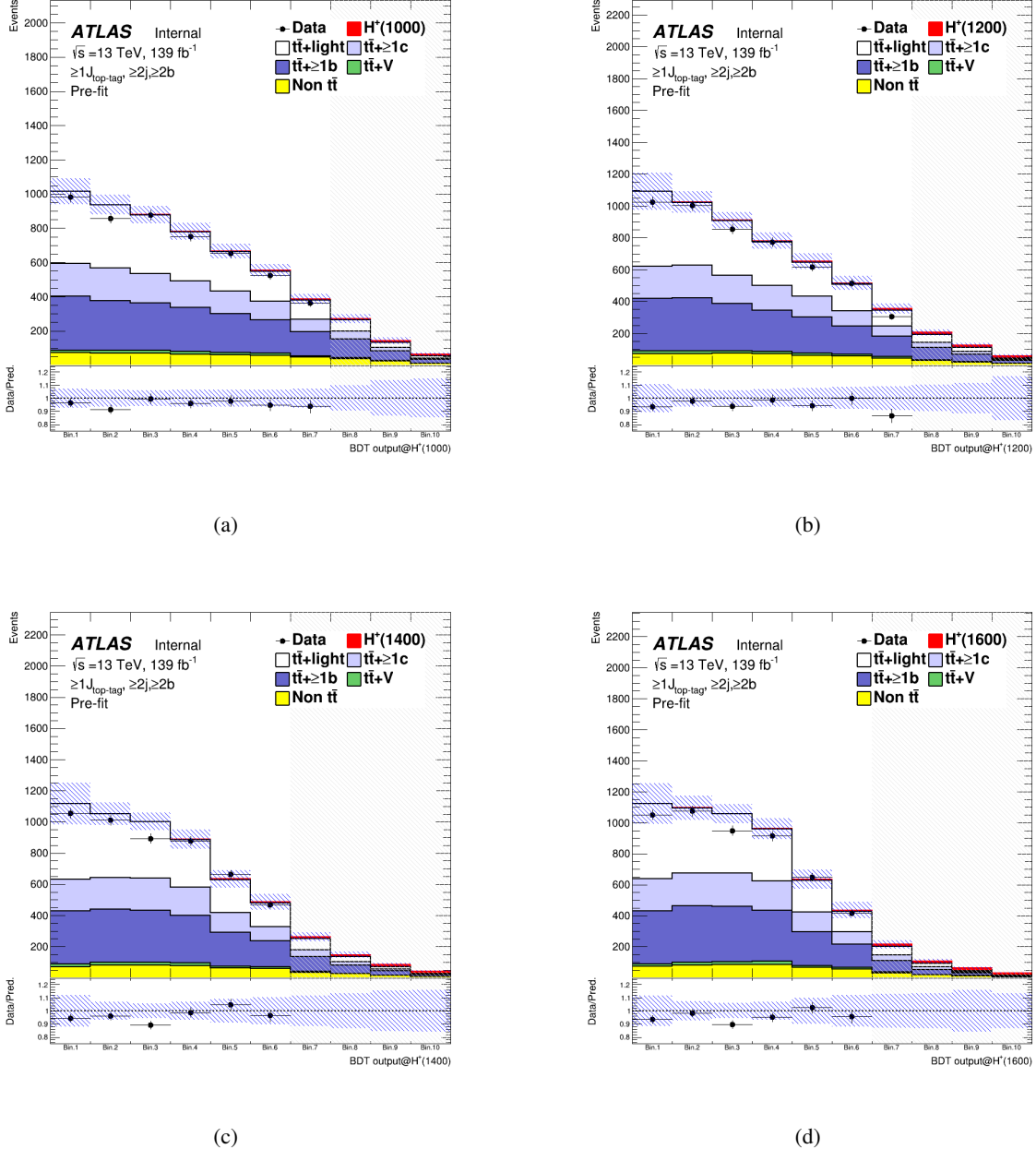


Figure 24: H_T^{jets} and data/MC ratio, R , distributions in the SR (a) and CR (b). The events in the SR are selected by BDT score. The red functions in the bottom canvases are the reweighting functions obtained by fitting to R distribution with a quadratic function. The blue bands are the statistical uncertainty ($\pm 1\sigma$) of the red function. They are included as systematic uncertainties in the final fitting. For events with $H_T^{\text{jets}} > 2072 \text{ GeV}$ in the SR, the same weight and its error as region $H_T^{\text{jets}} = 2072 \text{ GeV}$ is given.

Parameter	Value (SR)	Value (CR)
a	$(7.95 \pm 1.45) \times 10^{-1}$	$(9.20 \pm 0.32) \times 10^{-1}$
b	$(6.70 \pm 2.82) \times 10^{-4}$	$(2.14 \pm 0.67) \times 10^{-4}$
c	$(-4.75 \pm 1.29) \times 10^{-7}$	$(-1.29 \pm 0.32) \times 10^{-7}$

Table 17: Summary of parameters obtained by fitting of a quadratic function in the SR and CR ($f(H_T^{\text{jets}}) = a + b \cdot H_T^{\text{jets}} + c \cdot (H_T^{\text{jets}})^2$). The error of each parameter is from statistical uncertainty.

582 Figure 25(a) to Figure 25(h) show BDT output distributions applied to reweighting in the SR. The data/MC
 583 agreement in the high BDT score regions is improved.



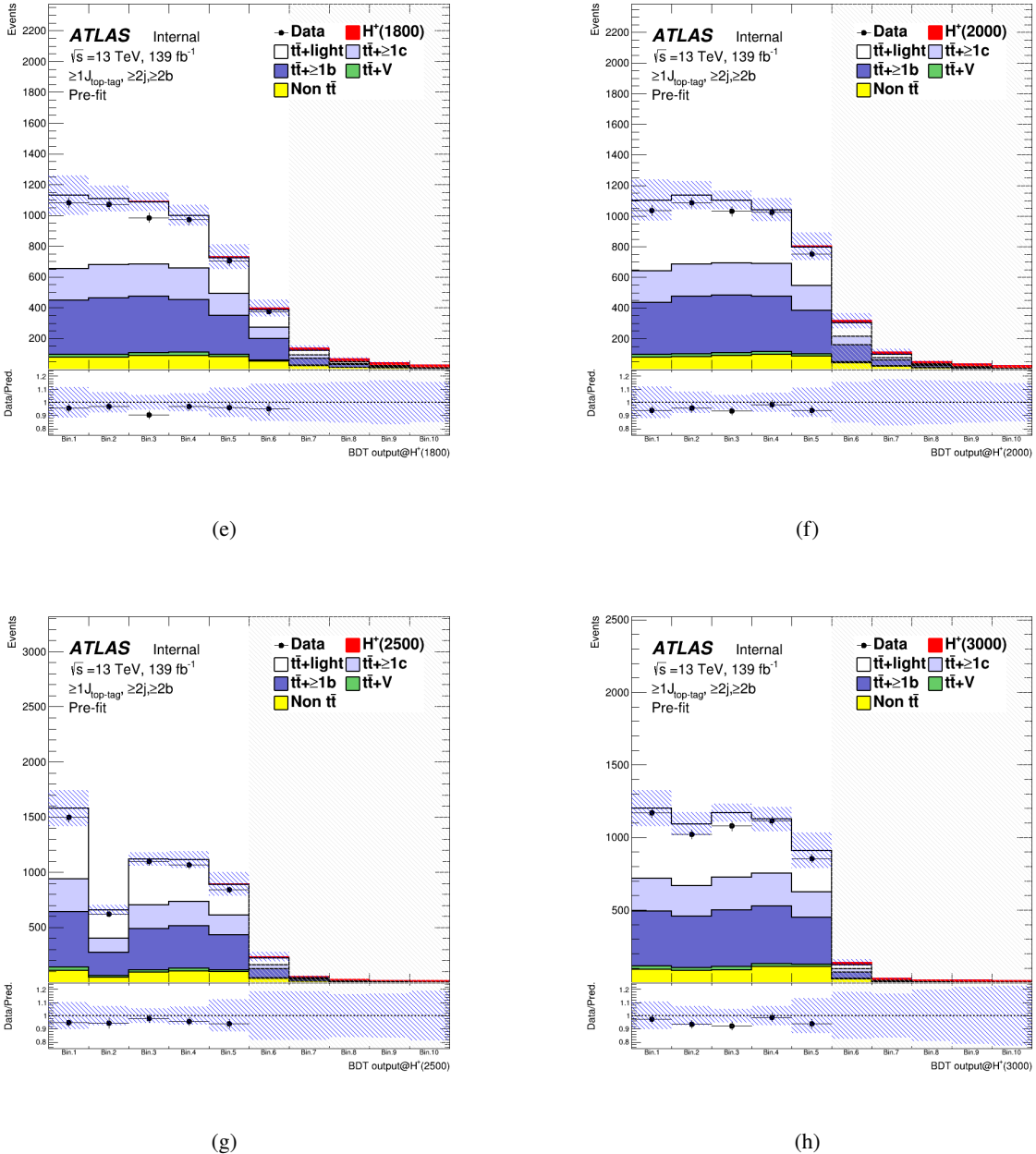


Figure 25: Pre-fit distributions of BDT output trained using from 1000 (a) to 3000 (h) GeV H^+ in the SR after reweighting.

584 6 Systematics Uncertainties

585 The uncertainties considered in the following may affect the overall normalization of the process, the
 586 shapes of the templates, or both. All the experimental uncertainties considered, with the exception of
 587 that in the luminosity, affect both normalization and shape in all the simulated samples. Uncertainties
 588 related to the modeling of the signal and background affect both normalization and shape, with the
 589 exception of cross-section and $t\bar{t}$ modeling uncertainties. The former only affects the normalization of the
 590 considered sample, while the latter only affects the shape of $t\bar{t}$ samples. Nevertheless, the normalization
 591 uncertainties modify the relative fractions of the different samples, leading to a shape uncertainty in the
 592 final distributions.

593 A single independent nuisance parameter is assigned to each source of systematic uncertainty in the
 594 statistical analysis. Some of the systematic uncertainties, in particular most of the experimental ones, are
 595 decomposed into several independent sources, as specified in the following. Each individual source then
 596 has a correlated effect across all analysis regions and signal and background samples. Table 18 presents a
 597 list of all systematic uncertainties considered and indicates for each category the number of independent
 598 components and whether they affect the normalization or shape.

Systematic uncertainty	Type	Components
Experimental uncertainties		
Luminosity	N	1
Pileup modeling	SN	1
<i>Physics objects</i>		
Electrons	SN	7
Muons	SN	15
Small-R jet energy scale	SN	31
Small-R jet energy resolution	SN	9
Small-R jet mass scale	SN	8
Large-R jet energy scale	SN	24
Large-R jet energy resolution	SN	12
Large-R jet mass scale	SN	18
Large-R jet mass resolution	SN	10
Jet vertex tagger	SN	1
<i>b-tagging</i>		
Efficiency	SN	9
Mis-tag rate (c)	SN	4
Mis-tag rate (light)	SN	4
p_T extrapolation efficiency	SN	2
<i>top-tagging</i>		
Signal efficiency	SN	9
p_T extrapolation signal efficiency	SN	1
background efficiency	SN	5
inefficiency	SN	3
Signal and background modeling		
<i>Signal</i>		
PDF variations	SN	30

Scales	SN	2
<i>t̄t background</i>		
PDF variations	SN	90
<i>t̄t + HF normalization</i>	N (free-floating)	1
<i>t̄t + light normalization</i>	N (free-floating)	1
<i>t̄t + light modeling</i>	S	6
<i>t̄t+ ≥ 1c modeling</i>	S	6
<i>t̄t+ ≥ 1b modeling</i>	S	7
<i>t̄t + jets reweighting</i>	SN	1
<i>t̄t+ ≥ 1b fraction</i>	N	1
<i>Other backgrounds</i>		
<i>t̄W cross-section</i>	N	2
<i>t̄Z cross-section</i>	N	2
<i>t̄W modeling</i>	SN	1
<i>t̄Z modeling</i>	SN	1
Single top cross-section	N	3
Single top modeling	SN	6
W+jets normalization	N	3
Z+jets normalization	N	1
Diboson normalization	N	1
<i>t̄t̄t̄ cross-section</i>	N	3

Table 18: List of systematic uncertainties included in the analysis. Each "S" and "N" of type means that the systematic source is considered the "Shape" and "Normalization" effect, respectively. When the type of systematic source is "SN", both "Shape" and "Normalization" effects are considered.

599 6.1 Luminosity and pile-up modeling

600 6.1.1 Luminosity

601 The uncertainty on the integrated luminosity for the full Run-2 dataset is 1.7% [51], obtained using
 602 LUCID-2 detector [116] for the primary luminosity measurement.

603 6.1.2 Pile-up modeling

604 A variation in the pile-up reweighting of the simulated events is included to cover the uncertainties in the
 605 ratio of the predicted and measured inelastic cross-sections in the fiducial volume defined by $M_X > 13$
 606 GeV, where M_X is the mass of the hadronic system [117]

607 **6.2 Reconstructed objects**

608 **6.2.1 Charged leptons**

609 Uncertainties associated with charged leptons arise from the trigger selection, the object reconstruction,
 610 identification and isolation criteria, as well as the lepton momentum scale and resolution. The reconstruction,
 611 identification, and isolation efficiency of electrons and muons, as well as the efficiency of the trigger used
 612 to record the events, differ slightly between data and simulation, which is compensated for by dedicated
 613 scale factors (SFs). Efficiency SFs are measured using tag-and-probe techniques on $Z \rightarrow l^+l^-$ data and
 614 simulated samples [94, 118], and are applied to the simulation to correct for the differences. The effect of
 615 these SFs as well as of their uncertainties are propagated as corrections to the MC event weight. In total,
 616 four independent components are considered for electrons and ten for muons.

617 Additional sources of uncertainty originate from the corrections applied to adjust the lepton momentum
 618 scale and resolution in the simulation to match those in data, measured using reconstructed distributions of
 619 the $Z \rightarrow l^+l^-$ and $J/\psi \rightarrow l^+l^-$ masses, as well as the E/p ratio measured in $W \rightarrow e\nu$ events, where E and p
 620 are the electron energy and momentum measured by the calorimeter and the tracker, respectively [94, 119].
 621 To evaluate the effect of momentum scale uncertainties, the event selection is redone with the lepton energy
 622 or momentum varied by $\pm 1\sigma$. For the momentum resolution uncertainties, the event selection is redone
 623 by smearing the lepton energy or momentum. In total, three independent components are considered for
 624 electrons and five for muons.

625 **6.2.2 Small- R jets, Large- R jets**

626 Uncertainties associated with jets arise from the efficiency of pile-up rejection by the JVT, from the jet
 627 energy scale (JES) and resolution (JER), from the jet mass scale (JMS) and resolution (JMR), and from b -
 628 and top-tagging.

629 **Jet vertex tagging:**

630 Scale factors are applied to correct discrepancies between data and MC for JVT efficiencies. These
 631 SFs are estimated using $Z \rightarrow \mu^+\mu^-$ with tag-and-probe techniques similar to those in Ref.[99], and
 632 the effect of these SFs as well as of their uncertainties are propagated as corrections to the MC event
 633 weight.

634 **Small- R jet:**

635 The *R4_CategoryReduction_FullJER.config* jet uncertainties configuration is used. The JES and
 636 its uncertainty for small- R jets are derived by combining information from test-beam data, LHC
 637 collision data and simulation [120]. The uncertainties from these measurements are factorized into
 638 several independent sources. Additional uncertainties are considered, related to jet flavor (using the
 639 conservative default value of $50 \pm 50\%$ for the quark/gluon fraction for all MC samples), pile-up
 640 corrections, η dependence, high- p_T jets, and differences between full and fast simulation, yielding a
 641 total of 31 independence sources.

642 The JER was measured in Run-2 data and simulation as a function of jet p_T and rapidity using dijet
 643 events, using a similar method as that in Ref. [121]. The combined uncertainty is propagated by
 644 smearing the jet p_T in MC, yielding to nine independent sources.

The JMS uncertainties for small- R jets are derived using the RTrk uncertainties that compare the ratio of the jet mass for calorimeter jets to the jet mass of track-based jets in data and MC simulation [122]. The six NPs are provided, which are related to baseline, modeling, tracking, and total statistics. The technique takes advantage of two independent measures of the jet's mass (in the calorimeter and using the ID), however, this assumption breaks in the case of particle flow jets which uses both calorimeter and tracking information. For PFlow jets, the uncertainties derived for EMTopo jets are used and two additional uncertainties are provided. These uncertainties are derived by comparing the jet mass of EMTopo and PFlow jets in data and MC. Two NPs are provided similarly to the RTrk uncertainties related to baseline and modeling. The JMS uncertainties are intentionally derived after the application of the JES and JER smearing. This is different compared to large- R jets where no nominal JER smearing is applied. The JES corrects the overall energy scale, which impacts the mass as it is applied to the full four-vector. The JMS correction and uncertainties are then a residual correction accounting for the distribution of energy within the jet. For this reason, the JES and JMS uncertainties are to first order uncorrelated effects.

Large- R jet:

The *R10_CategoryJES_FullJER_FullJMS.config* jet uncertainties configuration is used for JES, JER, and JMS variation. JES uncertainties for large- R jets are derived using a similar approach as for small- R jets [122]. The correlation between these two objects is taken into account in uncertainty evaluation. Additional uncertainties related to a topology of an event are included.

The JER uncertainties for large- R jets are derived in the same way as the small- R jets uncertainties. The dijet balance asymmetry is used to evaluate the JER, which is sufficient to cover the fully supported kinematic regime for large- R jet usage. The nominal data/MC difference is found to be consistent with 1 within uncertainty. For this reason, no nominal JER smearing is applied. Instead, the nominal data/MC difference from 1 is taken as an additional uncertainty on top of the uncertainties related to limited statistics, detector effects, or modeling. The FullJER model with 12 NPs is used. Both data and MC events are smeared to cover properly the correlations between jets in different regions of the detector.

The JMS uncertainties for large- R jets are derived from the forward folding technique (FF) in the limited region of $200 \text{ GeV} < p_T < 1000 \text{ GeV}$ around the W and top mass peaks [122, 123]. The RTrk technique is used to extend this region to $200 \text{ GeV} < p_T < 3000 \text{ GeV}$, $m < 600 \text{ GeV}$ and $|\eta| < 2.0$. The forward folding method is used to fit the W and top mass peaks in $t\bar{t}$ semileptonic events. The RTrk method uses the double ratio of data/MC for calorimeter-only quantities and track-only quantities. This technique can cover a wider range in p_T , η , and mass. However, the forward folding technique is more precise in the lower p_T region and the mass around the top and W masses. The uncertainties from the two approaches are combined and fitted as a function p_T in a given mass bin. Interpolation between mass bins is used to provide smooth uncertainties. The full set of JMS NPs is used in the analysis in order to allow possible combinations with other measurements. The NPs are related to limited statistics of measurements, detector effects, modeling, and selections. In addition, uncertainties related to interpolation between mass bins and uncertainties related to a difference between QCD and hadronic decay jet mass response are included.

Measurements of the JMR in the $t\bar{t}$ semileptonic events are also used to constrain the JMR uncertainties by using the forward folding method [122, 123]. Measurements are performed in two mass regions to cover W boson and top quark mass peaks. The W boson mass peak is fitted in a region of $50 \text{ GeV} < m_{\text{jet}} < 120 \text{ GeV}$ and $200 \text{ GeV} < p_{T,\text{jet}} < 350 \text{ GeV}$. The top mass peak is

689 fitted in a region of $120 \text{ GeV} < m_{\text{jet}} < 300 \text{ GeV}$ and $350 \text{ GeV} < p_{\text{T,jet}} < 1000 \text{ GeV}$. Relative JMR
 690 uncertainty of 20% is used outside these regions. FullJMR uncertainty model with 10 nuisance
 691 parameters is used to cover uncertainties related to the measurement of JMR using the FF method,
 692 interpolation between bins, and the comparison between different MC models for events outside the
 693 two regions. This measurement is within the top mass interval. However, $p_{\text{T,jet}}$ exceeds the p_{T} range
 694 provided by the FF method.

695 ***b*-tagging:**

696 *b*-tagging efficiencies in simulated samples are corrected to match efficiencies in data. Scale factors
 697 are derived as a function of p_{T} for jets containing *b*-jets, *c*-jets and for jets containing neither *b*- nor
 698 *c*-hadrons (light-jets) separately, in dedicated calibration analysis. For *b*-jets efficiencies, $t\bar{t}$ events in
 699 the dilepton topology are used, exploiting the very pure sample of *b*-jets arising from the decays of
 700 the top quarks [100]. For *c*-jet mistag rates, $t\bar{t}$ events in single-lepton topology are used, exploiting
 701 the *c*-jets from the hadronically decaying W bosons, using techniques similar to those in Ref. [124].
 702 For light-jets mistag rates, the so-called negative-tag method similar to that in Ref. [125] is used, but
 703 using $Z + \text{jets}$ events instead of di-jet events. In the three calibration analyses, a large number of
 704 uncertainty components are considered, and a principal component analysis is performed, yielding in
 705 45, 20, and 20 eigenvariations, respectively, for *b*-, *c*, and light-jets, which are taken as uncorrelated
 706 sources of uncertainties. The number of these eigenvariations corresponds to the number of p_{T} bins
 707 (9, 4, and 4, respectively, for *b*-, *c*- and light-jets). The calibration used in this analysis is stored in
 708 the following "CDI file":

709 `/cvmfs/atlas.cern.ch/repo/sw/database/GroupData/xAODTaggingEfficiency/13TeV/2020-21-13TeV-`
 710 `MC16-CDI-2021-04-16_v1.root.`

711 **Top-tagging:**

712 Uncertainties related to the top-tagging calibration are provided for the signal and the background
 713 jets [107, 126]. Jets are called signals if they pass contained top criteria. Otherwise, they are called
 714 background jets. Uncertainties for background jets are measured in two-phase spaces containing
 715 QCD multijet and gamma+jet processes. The signal jets uncertainties are measured in the boosted
 716 $t\bar{t}$ lepton+jets channel in the range of leading large- R jet $p_{\text{T}} \leq 1 \text{ TeV}$, because there are too few $t\bar{t}$
 717 events to extract scale factors for $p_{\text{T}} \geq 1 \text{ TeV}$. Therefore, additional uncertainties are assigned to
 718 cover signal modeling effects and extrapolation beyond the phase spaces. These uncertainties were
 719 released as part of the consolidated large- R jet uncertainties.

720

6.3 Signal modeling

721 The H^+ and W' signal uncertainty is modeled in two ways: by using the PDF uncertainties and through
 722 the variation of μ_f and μ_r . The uncertainties from the modeling of the PDF, which is done with the
 723 NNPDF2.3 or NNPDF3.0 PDF set for datasets simulated, are made using a symmetrized Hessian set,
 724 PDF4LHC15_nlo_30, following the PDF4LHC recommendations for LHC Run II [127]. The signal scale
 725 uncertainty is modeled by varying μ_f and μ_r up (and down) by a factor of 2 (or 0.5).

726 6.4 Background modeling
727 6.4.1 $t\bar{t}$ +jets
728 $t\bar{t}$ + heavy flavor classification

729 The $t\bar{t}$ + jets background is categorized according to the flavor of additional jets in the event, using the
 730 same procedure as described in Ref. [24]. Generator-level particle jets are reconstructed from stable
 731 particles (mean lifetime $\tau > 3 \times 10^{-11}$ seconds) using the anti- k_t algorithm with a radius parameter
 732 $R = 0.4$, and are required to have $p_T > 15$ GeV and $|\eta| < 2.5$. The flavor of a jet is determined by
 733 counting the number of b - or c -hadrons within $\Delta R < 0.4$ of the jet axis. Jets matched to exactly
 734 one b -hadron, with p_T above 5 GeV, are labeled single- b -jets, while those matched to two or more
 735 b -hadrons are labeled b -jets (with no p_T requirement on the second hadron); single- c - and c -jets are
 736 defined analogously, only considering jets not already defined as single- b - or b -jets. Events that have
 737 at least one single- b - or b -jet, not counting heavy-flavor jets from top-quark or W -boson decays, are
 738 labeled as $t\bar{t} + \geq 1b$; those with no single- b - or b -jet but at least one single- c - or c -jet are labeled
 739 as $t\bar{t} + \geq 1c$. Finally, events not containing any heavy-flavor jets aside from those from top-quark
 740 or W -boson decays are labeled as $t\bar{t}$ + light. This classification is used to define the background
 741 categories in the likelihood fit.

742 Systematic uncertainties

743 The systematic uncertainties affecting the $t\bar{t}$ + jets background modeling are summarized in Table
 744 19. The normalization of $t\bar{t}$ + light, $t\bar{t}$ + HF are allowed to vary freely in the fit. The normalization
 745 factors of $t\bar{t} + \geq 1c$ and $t\bar{t} + \geq 1b$ are estimated with a common parameter in the fit. However, since
 746 these distribution shapes are slightly different from each other in the high BDT score region as shown
 747 in Figure 26. Therefore uncertainty of the fraction between $t\bar{t} + \geq 1b$ and $t\bar{t} + \geq 1c$ can vary the
 748 overall template shape for $t\bar{t} + \geq (1b + 1c)$, and consequently affect the estimation of the number of
 749 observed signals. Referring to the post-fit results of the resolved analysis [25], the observed fraction
 750 (R_{ttb}^{Data}) differs from the expected one (R_{ttb}^{MC}) by about 12% as follows:

$$751 R_{ttb}^{\text{MC}} = \frac{N_{ttb}^{\text{MC}}}{N_{ttb}^{\text{MC}} + N_{ttc}^{\text{MC}}} \sim 0.64, \quad R_{ttb}^{\text{Data}} = \frac{N_{ttb}^{\text{Data}}}{N_{ttb}^{\text{Data}} + N_{ttc}^{\text{Data}}} \sim 0.72, \quad \frac{R_{ttb}^{\text{Data}}}{R_{ttb}^{\text{MC}}} \sim 0.88$$

752 In this analysis, the fraction uncertainty is conservatively assumed to be $\pm 50\%$, considering the
 753 different phase spaces with respect to the resolved analysis. The corresponding NP is introduced for
 754 the fit model.

Uncertainty source	Description	Components
$t\bar{t}$ + light normalization	Free-floating	$t\bar{t}$ + light
$t\bar{t}$ + HF normalization	Free-floating	$t\bar{t}+ \geq 1b$ and $t\bar{t}+ \geq 1c$
$t\bar{t}+ \geq 1b$ fraction	Fraction to the whole of $t\bar{t}$ + HF	$t\bar{t}+ \geq 1b$ and $t\bar{t}+ \geq 1c$
$t\bar{t}$ + jets reweighting	Statistical uncertainties of weights	All $t\bar{t}$ + jets
$t\bar{t}+ \geq 1b$ flavor scheme	5FS vs 4FS	$t\bar{t}+ \geq 1b$
NLO matching	MG5_aMC+Pythia	vs. Powheg+Pythia
PS & hadronisation	Powheg+Herwig	vs. Powheg+Pythia
α_S^{ISR}	<i>Var3cUp</i> (<i>Var3cDown</i>)	in Powheg+Pythia
μ_f	scaling by 0.5 (2.0)	in Powheg+Pythia
μ_r	scaling by 0.5 (2.0)	in Powheg+Pythia
FSR	Varying α_S^{FSR} (PS)	in Powheg+Pythia

Table 19: Summary of the sources of systematic uncertainty for $t\bar{t}$ + jets modeling. The systematic uncertainties listed in the second section of the table are evaluated in such a way to have no impact on the normalization of the three, $t\bar{t}$ + light, $t\bar{t}+ \geq 1c$ and $t\bar{t}+ \geq 1b$ components in the phase-space selected in the analysis. The last column of the table indicates the $t\bar{t}$ + jets components to which a systematic uncertainty is assigned. All systematic uncertainty sources are treated as uncorrelated across the three components.

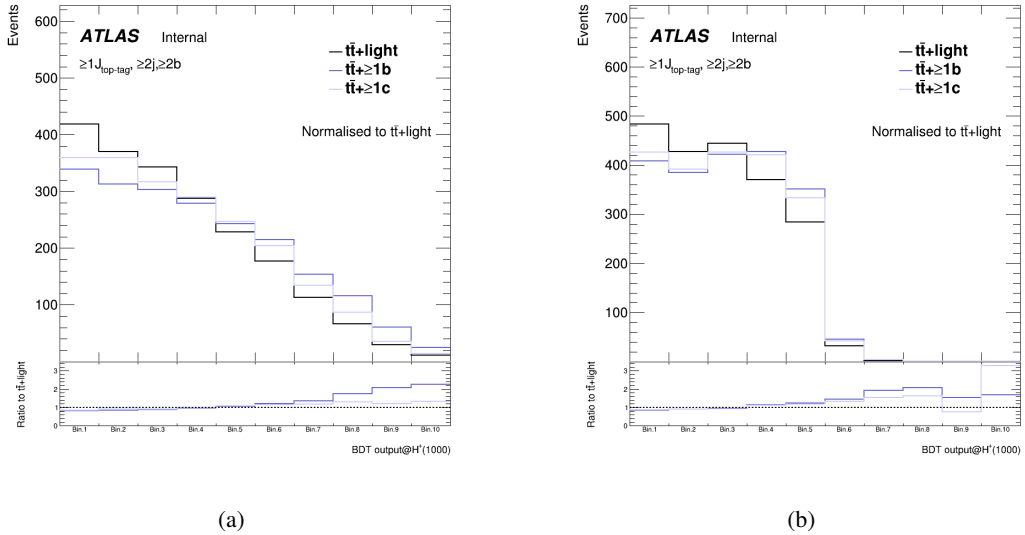


Figure 26: Comparison of the shape of BDT distributions in the SR among $t\bar{t}$ + jets events, where (a) is BDT output trained using 1000 GeV H^+ samples, and (b) is the one trained using 3000 GeV. $t\bar{t}+ \geq 1c$ and $t\bar{t}+ \geq 1b$ distributions are normalised to the distribution of $t\bar{t}$ + light. The ratios to $t\bar{t}$ + light distribution are shown at the bottom.

Besides normalization, the $t\bar{t}$ + light, $t\bar{t}+ \geq 1c$ and $t\bar{t}+ \geq 1b$ processes are affected by different types of uncertainties: $t\bar{t}$ + light has additional diagrams and profits from relatively precise measurements in data; $t\bar{t}+ \geq 1c$ and $t\bar{t}+ \geq 1b$ can have similar or different diagrams depending on the flavor scheme used for the PDF, and different mass of the c - and b -quark contribute to additional differences between these two processes. For these reasons, all uncertainties in the $t\bar{t}$ + jets background modeling are assigned independent nuisance parameters for the $t\bar{t}$ + light, $t\bar{t}+ \geq 1c$ and $t\bar{t}+ \geq 1b$ processes.

761 Systematic uncertainties on the reweighting are extracted according to the reweighting functions
 762 derived in Section 5.4. The differences between the BDT output distribution reweighted with the
 763 nominal reweighting function and the one reweighted with $\pm 1\sigma$ functions are included in the fit for
 764 each $t\bar{t} + \text{jets}$ as an NP.

765 Systematic uncertainties on the acceptance and shapes are extracted from the comparison between
 766 the nominal and different MC samples and settings. For ISR and FSR the settings of the nominal
 767 Powheg+Pythia sample are varied, resulting in different event weights; the uncertainty due to ISR is
 768 estimated by changing μ_r and μ_f in the ME and α_S^{ISR} in the PS, while the uncertainty due to FSR is
 769 estimated by changing α_S^{FSR} in the PS. For the ISR, the amount of radiation is increased (decreased)
 770 by scaling μ_r and μ_f by a factor 0.5 (2.0) and by using the Var3cUp (Var3cDown) variation from the
 771 A14 tune [59], corresponding to $\alpha_S^{\text{ISR}} = 0.140(0.115)$ instead of the nominal $\alpha_S^{\text{ISR}} = 0.127$. For the
 772 FSR, the amount of radiation is increased (decreased) varying μ_r for QCD emission in the FSR by a
 773 factor of 0.5 (2.0), corresponding to $\alpha_S^{\text{FSR}} = 0.1423(0.1147)$ instead of the nominal $\alpha_S^{\text{FSR}} = 0.127$.
 774 The nominal Powheg+Pythia sample is compared to the Powheg+Herwig sample to access the effect
 775 of the PS and hadronization models, and to the MG5_aMC sample to access the effect of the NLO
 776 matching technique.

777 The nominal prediction for the dominant $t\bar{t} + \geq 1b$ background, based on the Powheg+Phytia $t\bar{t}$ (5FS)
 778 sample in which all the additional partons are produced by the PS, is compared to the alternative
 779 Powheg+Phytia $t\bar{t}$ (4FS) sample, in which the $b\bar{b}$ pair is generated in addition to the $t\bar{t}$ pair at the
 780 ME level at NLO in QCD. The uncertainty resulting from comparing the shape of the two models is
 781 included.

782 6.4.2 Other backgrounds

783 The predicted $t\bar{t}H$ signal cross-section uncertainty is $^{+5.8\%}_{-9.2\%}$ (QCD scale) $\pm 3.6\%$ (PDF + α_S) [128–133].
 784 These two components are treated as uncorrelated in the fit. The effect of QCD scale and PDF variations
 785 on the shape of the distributions is found to be negligible. Uncertainties in the Higgs-boson branching
 786 fractions are also considered; these amount to 2.2% for the $b\bar{b}$ decay mode [128]. Uncertainties associated
 787 to the modeling of $t\bar{t}H$ by the Powheg+Phytia sample are also considered, for a total of four independent
 788 components. The uncertainty due to ISR is estimated by simultaneously changing μ_f and μ_r in the ME and
 789 α_S^{ISR} in the PS, while the uncertainty due to ISR is estimated by changing α_S^{FSR} in the PS. For the ISR and
 790 FSR, the amount of radiation is varied following the same procedure as for $t\bar{t}$. The nominal Powheg+Pythia
 791 sample is compared to the Powheg+Herwig sample to access the uncertainty due to PS and hadronization,
 792 and to the MG5_aMC+Phytia sample for the uncertainty due to the NLO matching.

793 A $\pm 5\%$ uncertainty is considered for the cross-sections of the three single-top production modes [134–138].
 794 Uncertainties associated with the PS and hadronisation model, and with the NLO matching scheme are
 795 evaluated by comparing, for each process, the nominal Powheg+Pythia sample to a sample produced using
 796 Powheg+Herwig and MG5_aMC+Pythia, respectively. The uncertainty associated to the interference
 797 between Wt and $t\bar{t}$ production at NLO [79] is assessed by comparing the nominal Powheg+Pythia sample
 798 produced using the "diagram removal" scheme to an alternative sample produced with the same generator
 799 but using the "diagram subtraction" scheme.

800 The uncertainty of the $t\bar{t}V$ NLO cross-section prediction is 15% [139, 140], split into PDF and scale
 801 uncertainties as for $t\bar{t}H$. An additional $t\bar{t}V$ modeling uncertainty, related to the choice of PS and

802 hadronisation model and NLO matching scheme is assessed by comparing the nominal MG5_aMC+Pythia
803 samples with alternative ones generated with Sherpa.

804 A total 50% normalization uncertainty is considered for the 4 tops background, covering effects from
805 varying μ_f and μ_r , PDFs and α_S [55, 141]. The small backgrounds from tZq and tWH are each assigned
806 cross-section uncertainties: $\pm 7.9\%$ and $\pm 0.9\%$ for tZq , accounting for μ_f and μ_r variations, and for PDFs,
807 respectively, and $\pm 50\%$ for tWZ [55].

808 An uncertainty of 40% is assumed for the $W +$ jets cross-section, with an additional 30% normalization
809 uncertainty used for $W +$ heavy-flavor jets, taken as uncorrelated between events with two and more than
810 two heavy-flavor jets. These uncertainties are based on variations of the μ_f and μ_r and of the matching
811 parameters in the Sherpa samples. An uncertainty of 35% is then applied to the $Z +$ jets normalization,
812 uncorrelated across jet bins, to account for both the variations of the scales and matching parameters in the
813 Sherpa samples and the uncertainty in the extraction from data of the correction factor for the heavy-flavor
814 component. Finally, a total 50% normalization uncertainty in the diboson background is assumed, which
815 includes uncertainties in the inclusive cross-section and additional jet production [142].

816 7 Profile Likelihood Fit

817 7.1 Method

818 In order to test for the presence of an $H^+ \rightarrow tb$ ($W' \rightarrow tb$) signal, a binned maximum-likelihood fitting to the
 819 data is performed simultaneously in all analysis regions, and each mass hypothesis is tested separately.
 820 The inputs to the fit are BDT distributions in the SR and H_T^{jets} distributions in the CR for the under 3 TeV
 821 mass hypothesis tests. On the other hand, they are only H_T^{jets} distributions in the SR, CR1, and CR2 on
 822 the above 3 TeV mass hypothesis tests. Two initially unconstrained fit parameters are used to model the
 823 normalization of the $t\bar{t}$ + light and $t\bar{t} + \geq 1$ HF jets background. The procedures used to quantify the level
 824 of agreement with the background-only or background-plus-signal hypothesis, and to determine exclusion
 825 limits, are based on the profile likelihood ratio test and the CL_s method. The parameter of interest is the
 826 signal strength, μ . The signal MC cross-sections are assumed to be 0.046 pb in the fittings.

827 To estimate the signal strength, a likelihood function, $\mathcal{L}(\mu, \theta)$, is constructed as the product of Poisson
 828 probability terms. One Poisson term is included for every bin of distributions in the analysis regions.
 829 The binning of each BDT output distribution is defined by an automatic binning algorithm, *TransfoD*,
 830 implemented in TRexFitter [115]. The expected number of events in the Poisson terms is a function of μ ,
 831 and a set of nuisance parameters, θ . The nuisance parameters encode effects from the normalization of
 832 backgrounds, including two free normalization factors for the $t\bar{t}$ + light and $t\bar{t} + \geq 1$ HF jets backgrounds,
 833 the systematic uncertainties, and one parameter per bin to model statistical uncertainties in the simulated
 834 samples. All nuisance parameters are constrained with Gaussian or log-normal terms. There are about
 835 340 nuisance parameters considered in the fit, the number varying slightly across the range of mass
 836 hypotheses.

837 To extract the exclusion limit on μ , the following test statistic is used:

$$\tilde{t}_\mu = \begin{cases} -2 \ln \frac{\mathcal{L}(\mu, \hat{\theta}(\mu))}{\mathcal{L}(0, \hat{\theta}(0))} & \mu < 0 \\ -2 \ln \frac{\mathcal{L}(\mu, \hat{\theta}(\mu))}{\mathcal{L}(\hat{\mu}, \hat{\theta})} & \mu \geq 0 \end{cases} \quad (2)$$

838 The values of the signal strength and nuisance parameters that maximize the likelihood function are
 839 represented by $\hat{\mu}$ and $\hat{\theta}$, respectively. For a given value of μ , the values of the nuisance parameters that
 840 maximize the likelihood function are represented by $\hat{\theta}(\mu)$.

841 7.2 Pruning and smoothing of systematic uncertainties

842 In the fits, pruning is applied at the threshold of 1%, meaning that if the effect of a nuisance parameter is
 843 smaller than 1% before fitting (separately for shape and normalization) it is excluded from the fit. This
 844 pruning procedure reduces the CPU time and helps the fit to converge. Appendix ?? shows the systematic
 845 uncertainties that are pruned in Asimov fits.

846 Smoothing is applied for systematic uncertainties on $t\bar{t}$ modelling by *MaxVariation* algorithm implemented
 847 in TRexFitter because these uncertainties are typically computed by comparing two different MC samples,
 848 or by applying MC generator weights on an MC sample, which dilutes the MC statistics and increases
 849 the fluctuations. No smoothing is applied for modelling systematic uncertainties on small backgrounds —
 850 given their small impact on the final result — or for experimental systematics — which are obtained either

851 by applying SFs typically close to unity (e.g. b -tagging), or by using the same simulated events but with
 852 different calibrations of the objects (e.g. JES).

853 7.3 Asimov fit

854 7.3.1 Pre-fit plots

855 The following section performs data fitting tests using Asimov datasets from nominal simulated samples.
 856 The signal events aren't injected into these Asimov datasets. Figure 27 to 36 show the pre-fit plots for each
 857 H^+ mass hypothesis. Similarly, Figure 37 to 45 and Figure 46 to 54 show the pre-fit plots for each W'_L and
 858 W'_R mass hypotheses, respectively.

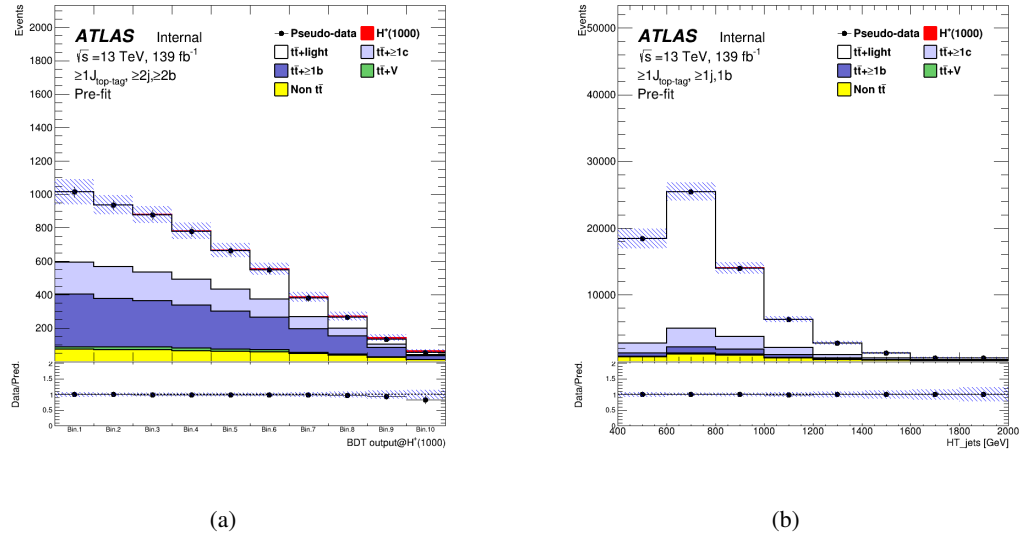


Figure 27: Pre-fit plots in the SR (left) and CR (right) for 1000 GeV mass hypothesis of H^+ signal.

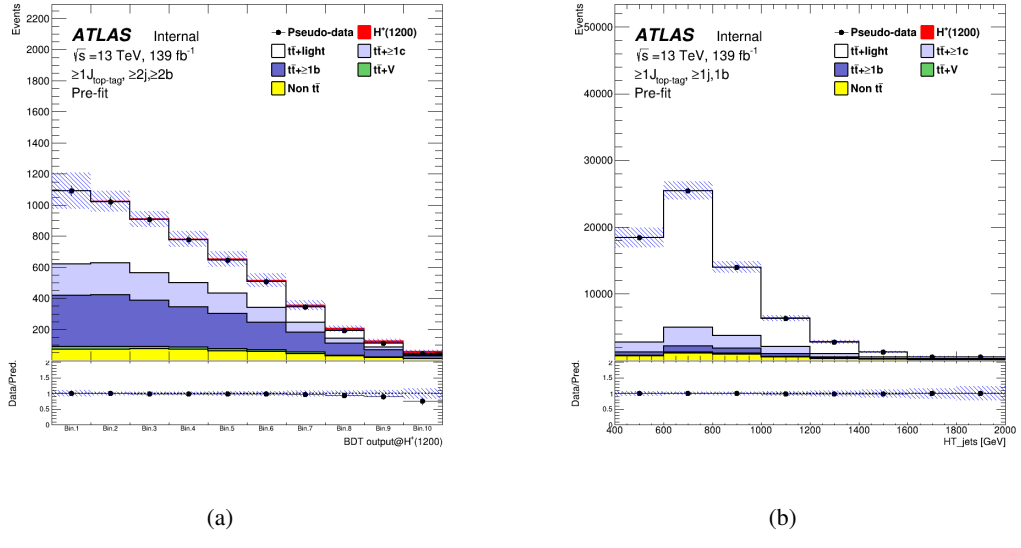


Figure 28: Pre-fit plots in the SR (left) and CR (right) for 1200 GeV mass hypothesis of H^+ signal.

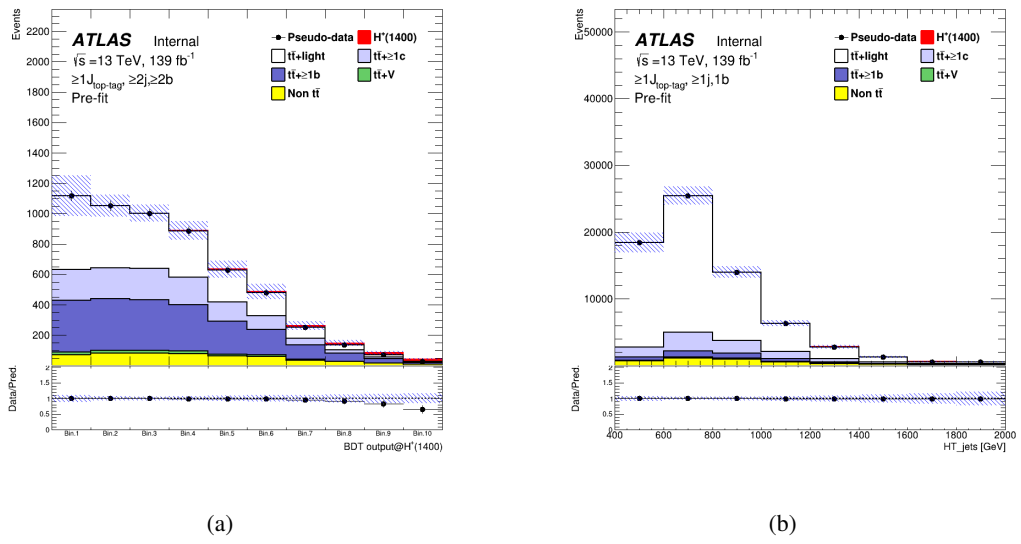


Figure 29: Pre-fit plots in the SR (left) and CR (right) for 1400 GeV mass hypothesis of H^+ signal.

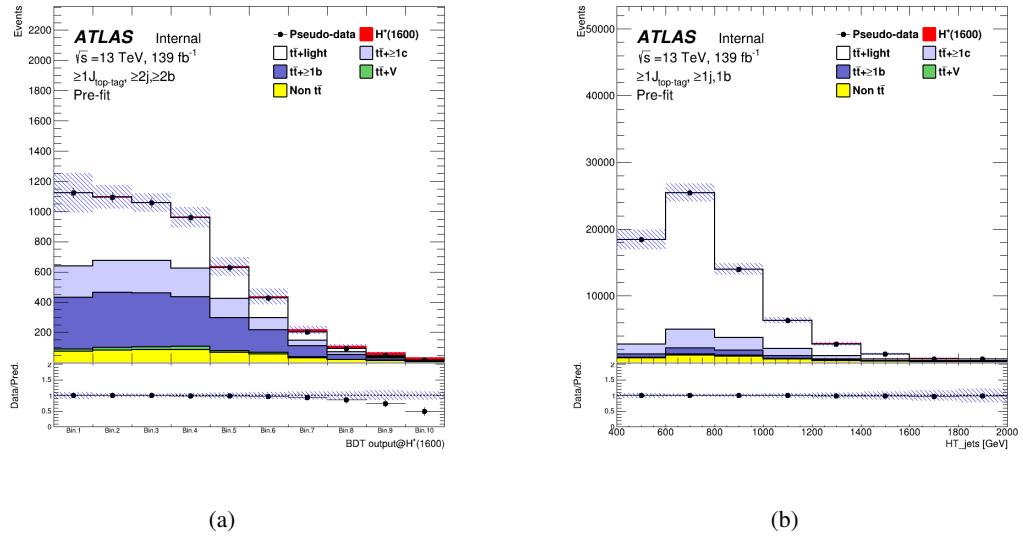


Figure 30: Pre-fit plots in the SR (left) and CR (right) for 1600 GeV mass hypothesis of H^+ signal.

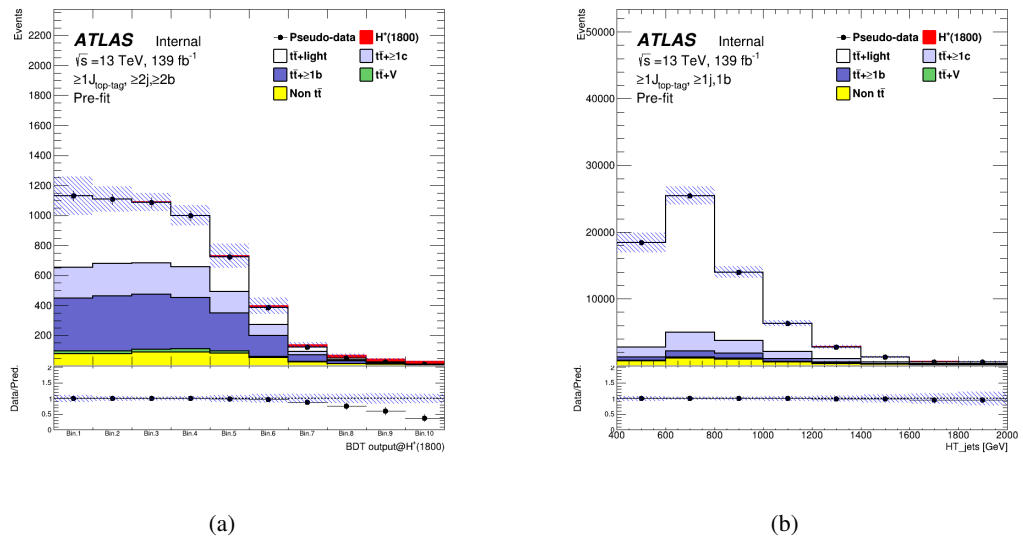


Figure 31: Pre-fit plots in the SR (left) and CR (right) for 1800 GeV mass hypothesis of H^+ signal.

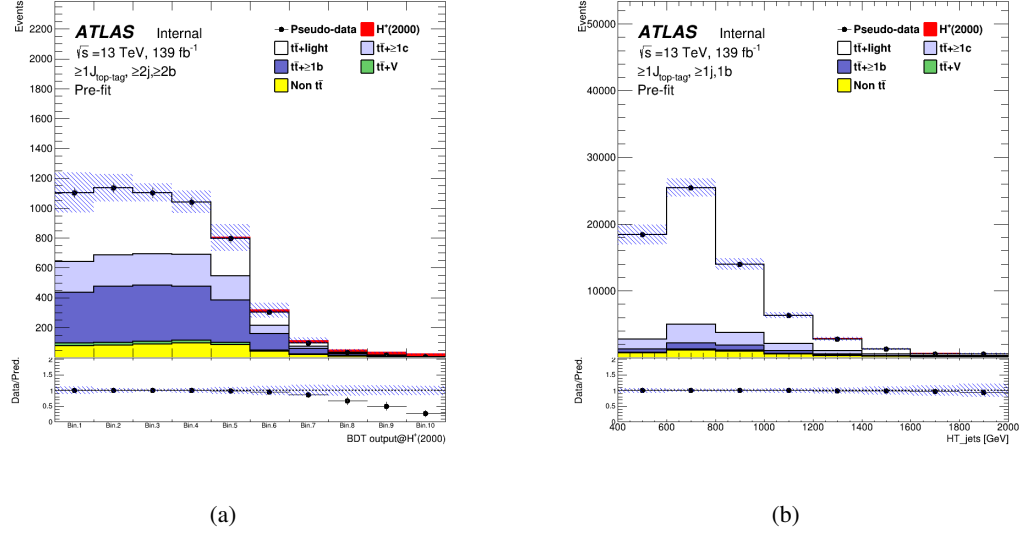


Figure 32: Pre-fit plots in the SR (left) and CR (right) for 2000 GeV mass hypothesis of H^+ signal.

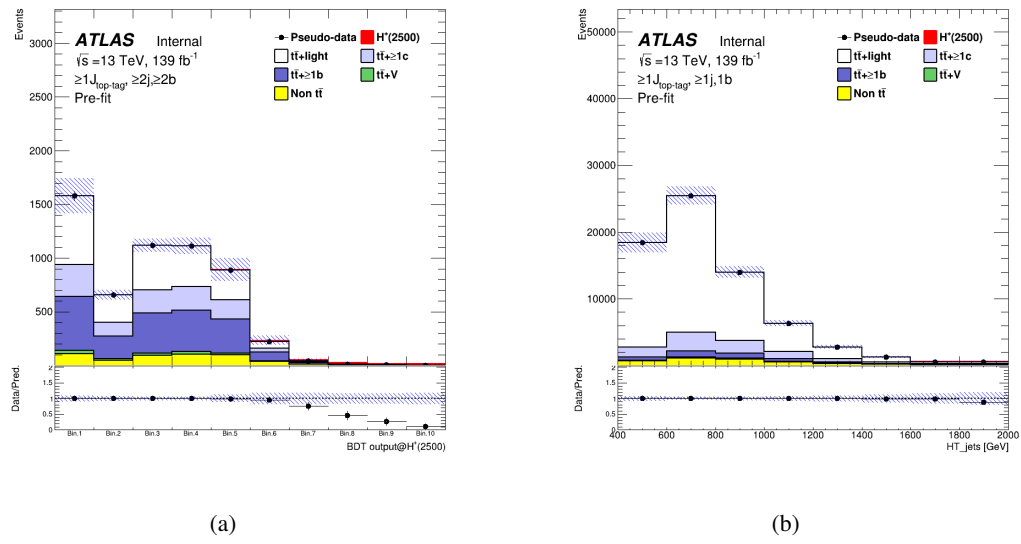


Figure 33: Pre-fit plots in the SR (left) and CR (right) for 2500 GeV mass hypothesis of H^+ signal.

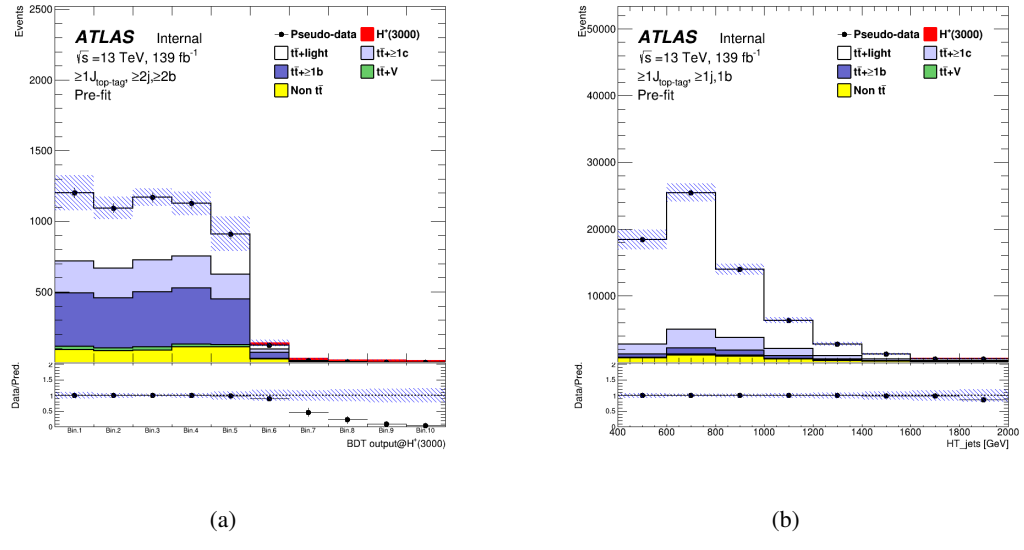


Figure 34: Pre-fit plots in the SR (left) and CR (right) for 3000 GeV mass hypothesis of H^+ signal.

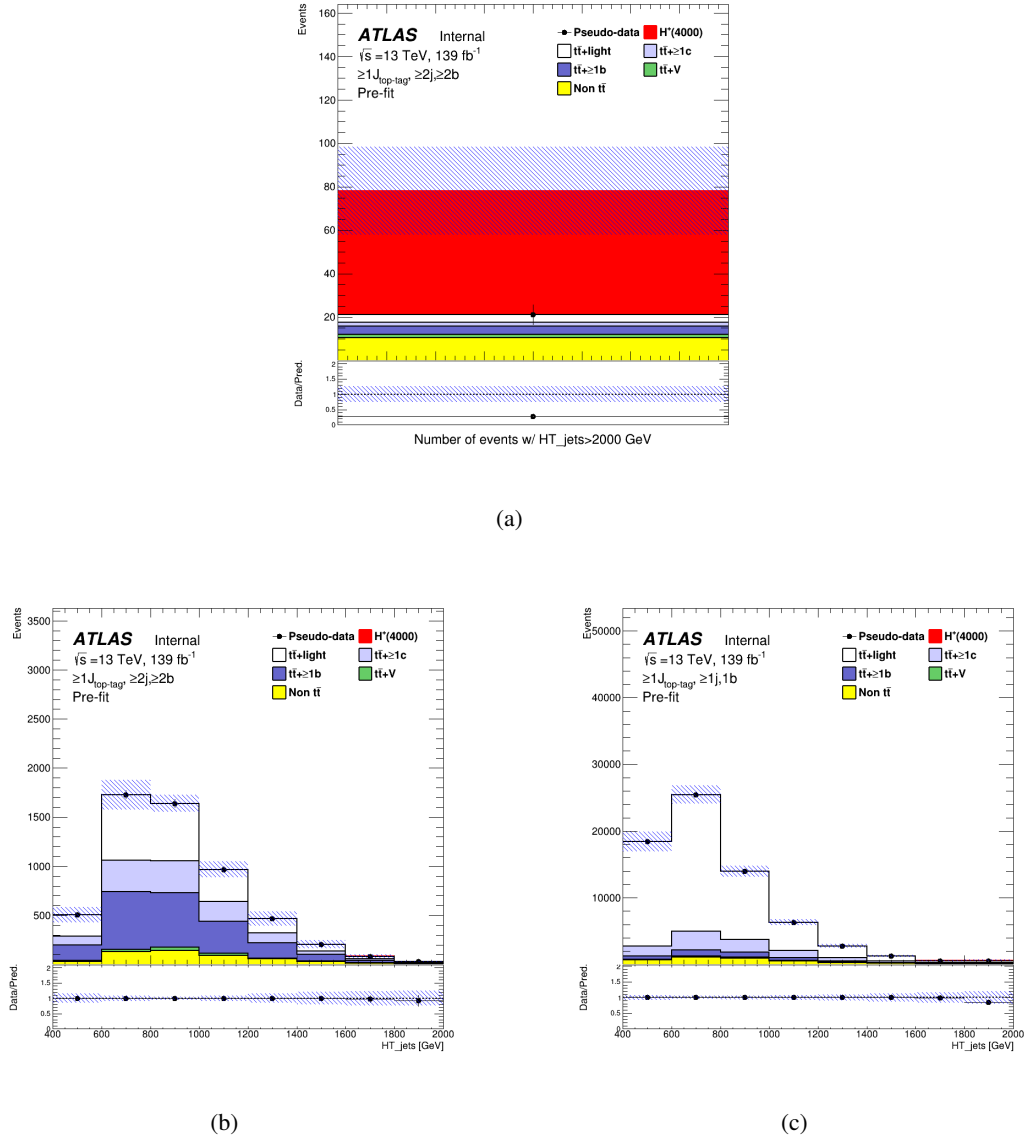


Figure 35: Pre-fit plots in the SR (top), CR1 (bottom-left), and CR2 (bottom-right) for 4000 GeV mass hypothesis of H^+ signal.

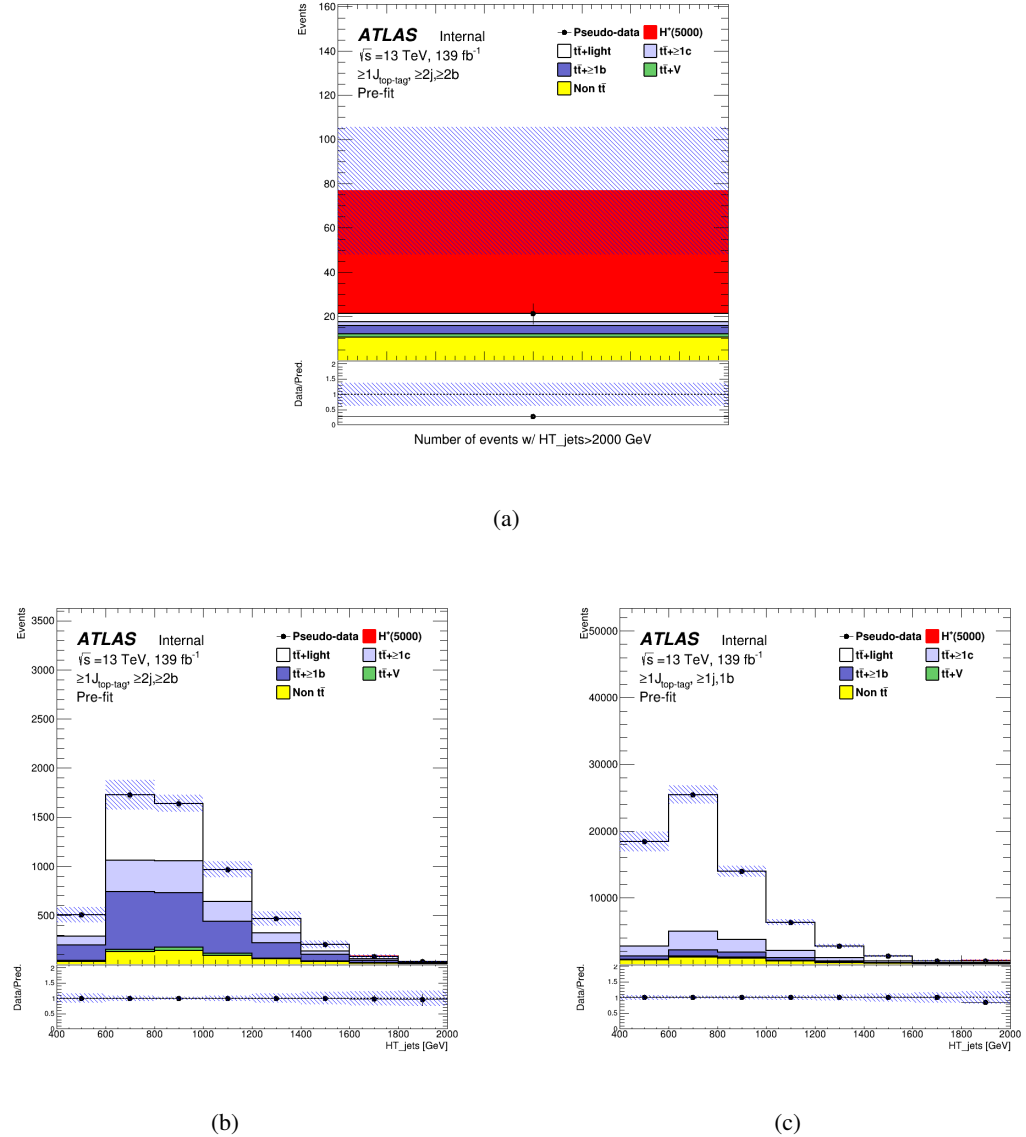


Figure 36: Pre-fit plots in the SR (top), CR1 (bottom-left), and CR2 (bottom-right) for 5000 GeV mass hypothesis of H^+ signal.

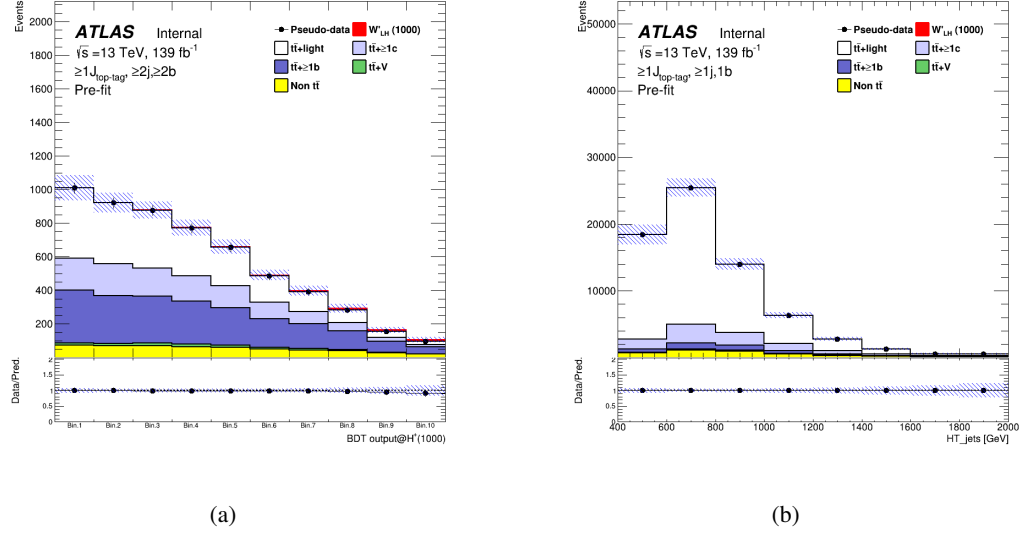


Figure 37: Pre-fit plots in the SR (left) and CR (right) for 1000 GeV mass hypothesis of W'_L signal.

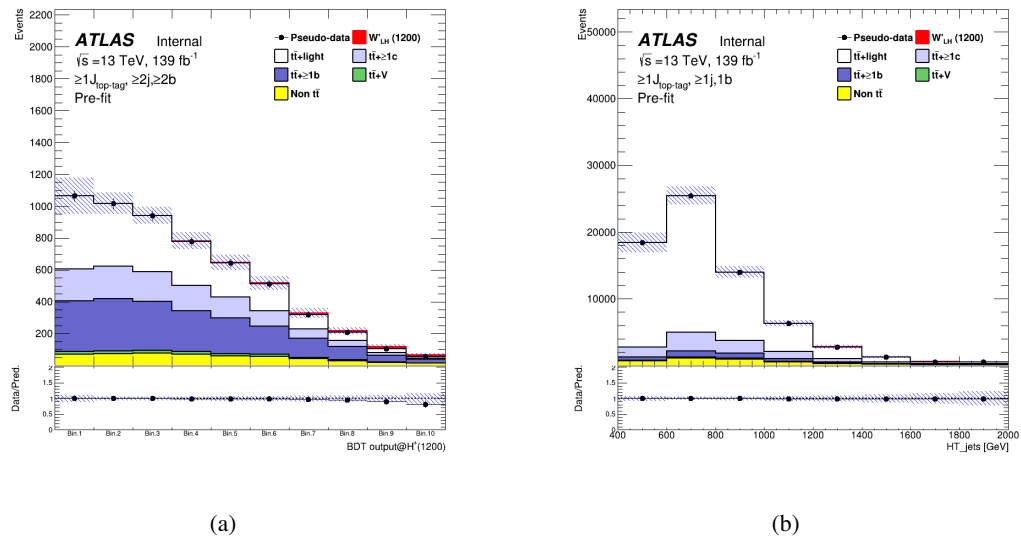


Figure 38: Pre-fit plots in the SR (left) and CR (right) for 1200 GeV mass hypothesis of W'_L signal.

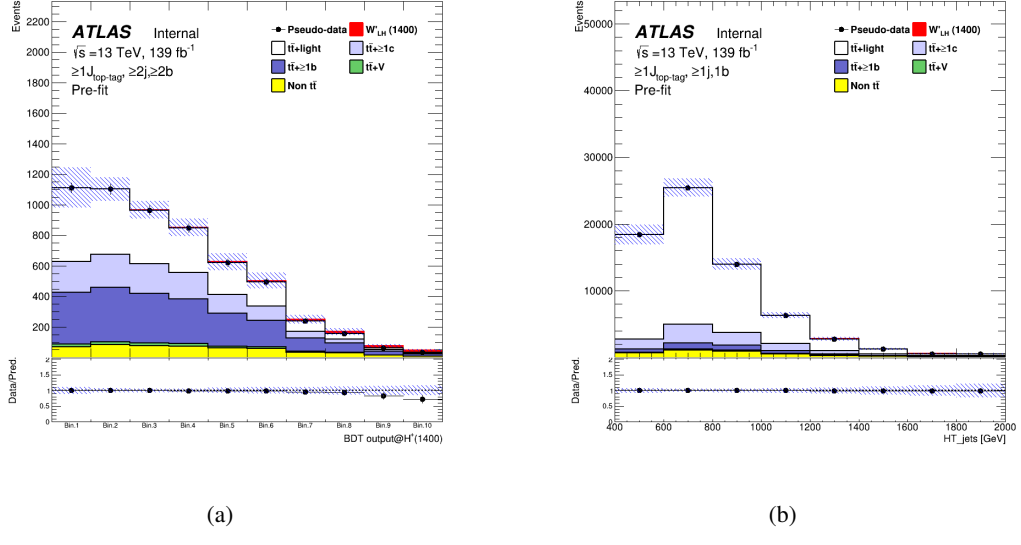


Figure 39: Pre-fit plots in the SR (left) and CR (right) for 1400 GeV mass hypothesis of W'_L signal.

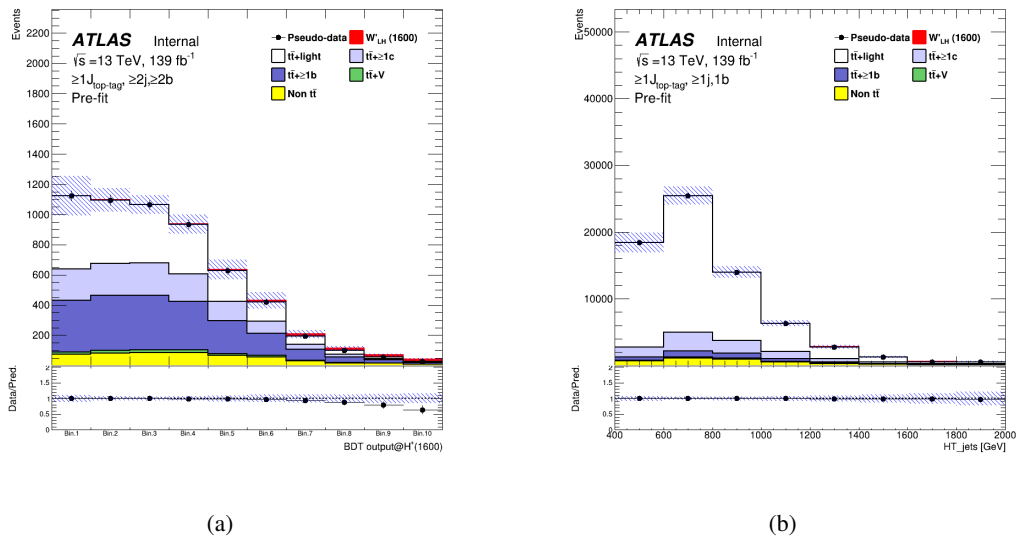


Figure 40: Pre-fit plots in the SR (left) and CR (right) for 1600 GeV mass hypothesis of W'_L signal.

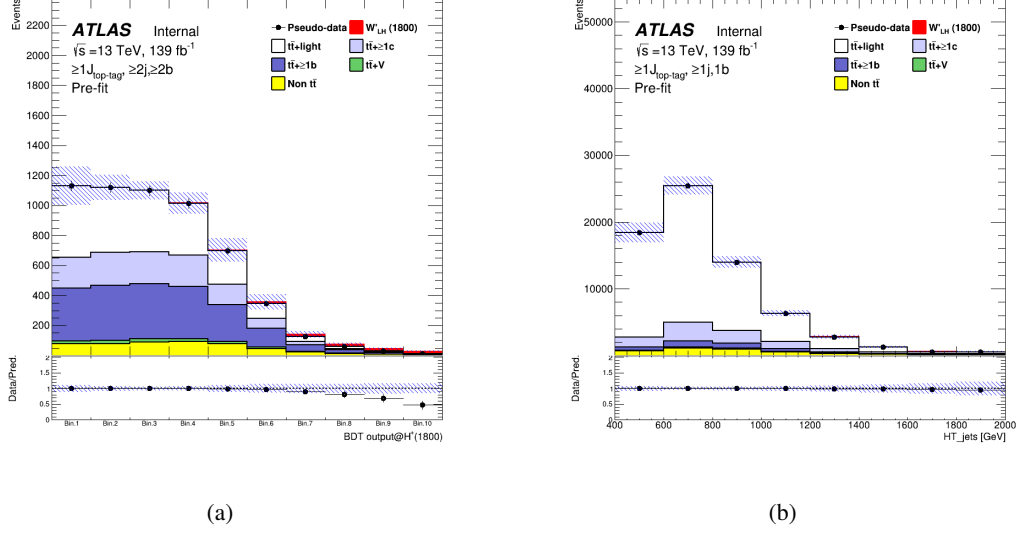


Figure 41: Pre-fit plots in the SR (left) and CR (right) for 1800 GeV mass hypothesis of W'_L signal.

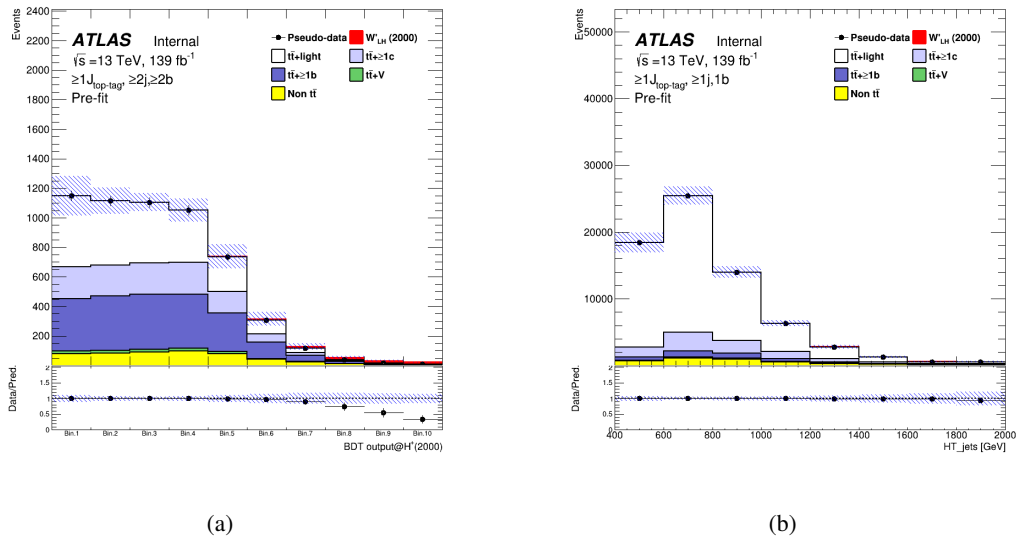


Figure 42: Pre-fit plots in the SR (left) and CR (right) for 2000 GeV mass hypothesis of W'_L signal.

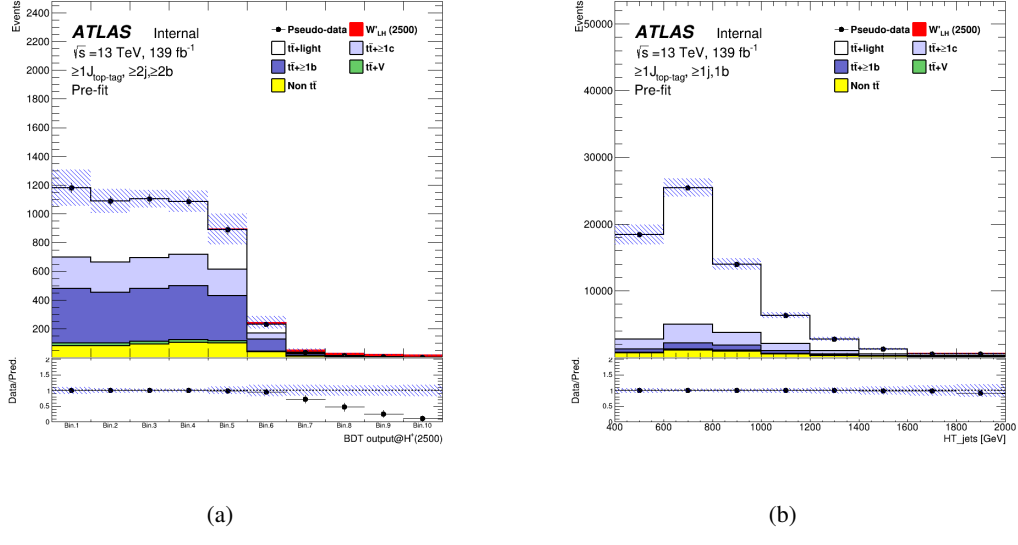


Figure 43: Pre-fit plots in the SR (left) and CR (right) for 2500 GeV mass hypothesis of W'_{L} signal.

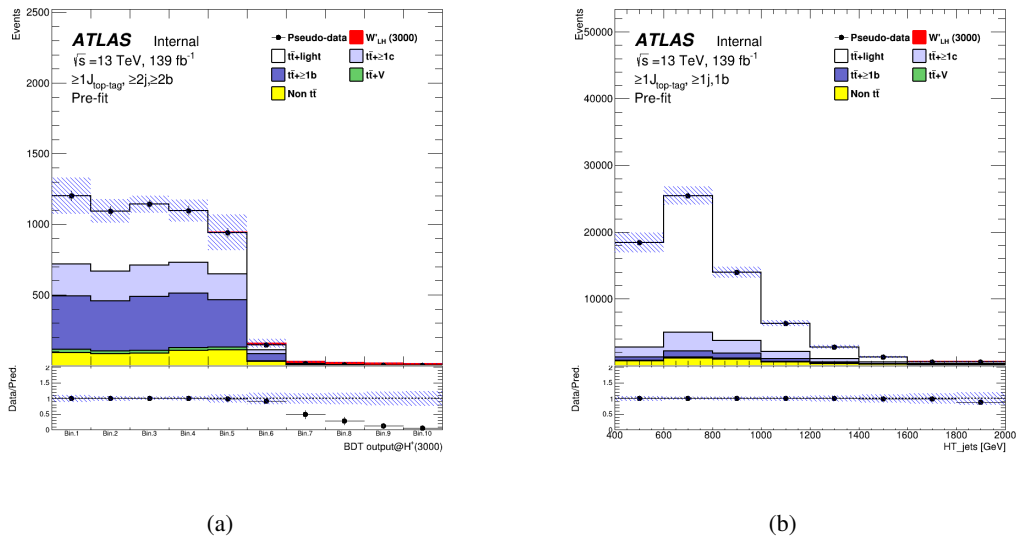


Figure 44: Pre-fit plots in the SR (left) and CR (right) for 3000 GeV mass hypothesis of W'_{L} signal.

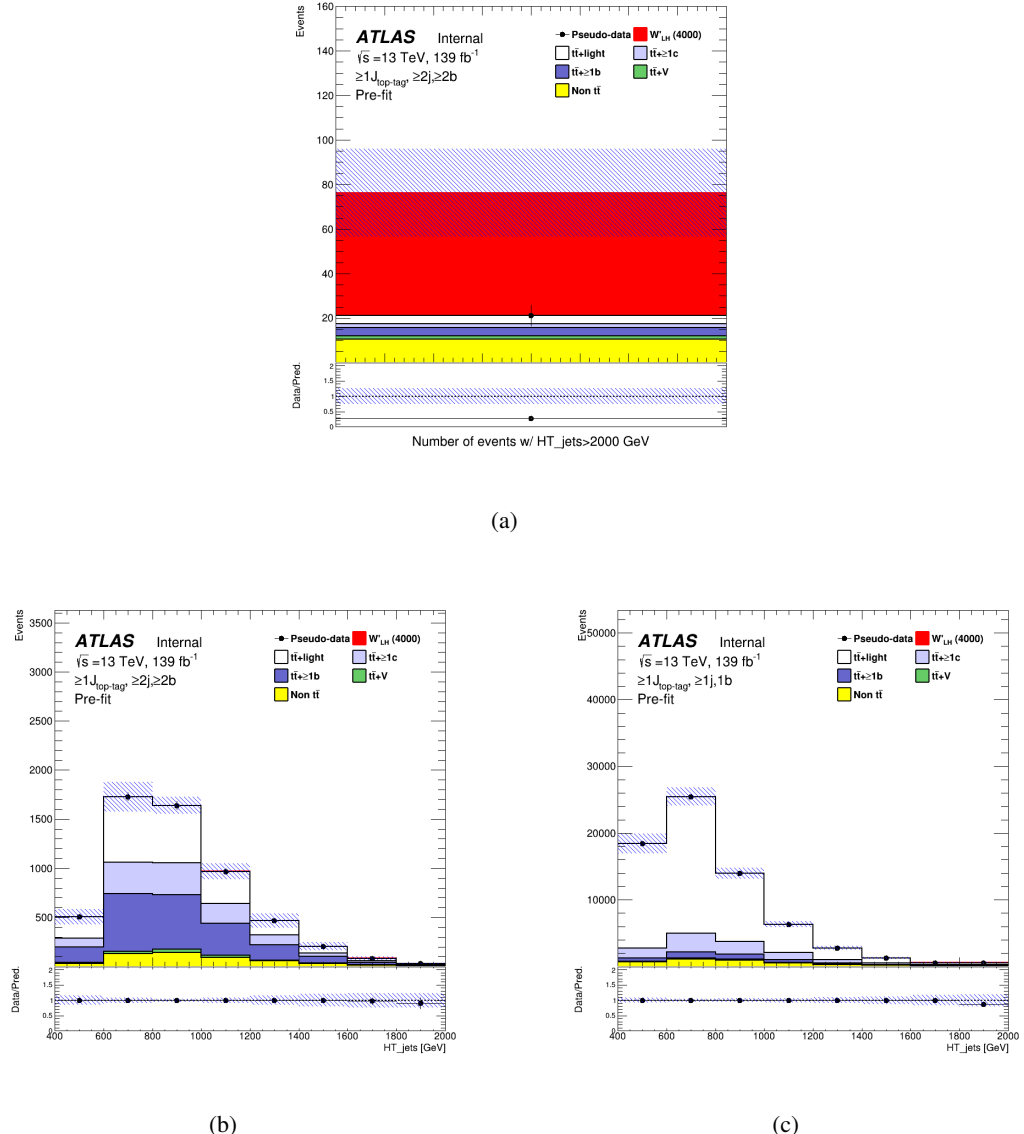


Figure 45: Pre-fit plots in the SR (top), CR1 (bottom-left), and CR2 (bottom-right) for 4000 GeV mass hypothesis of W'_L signal.

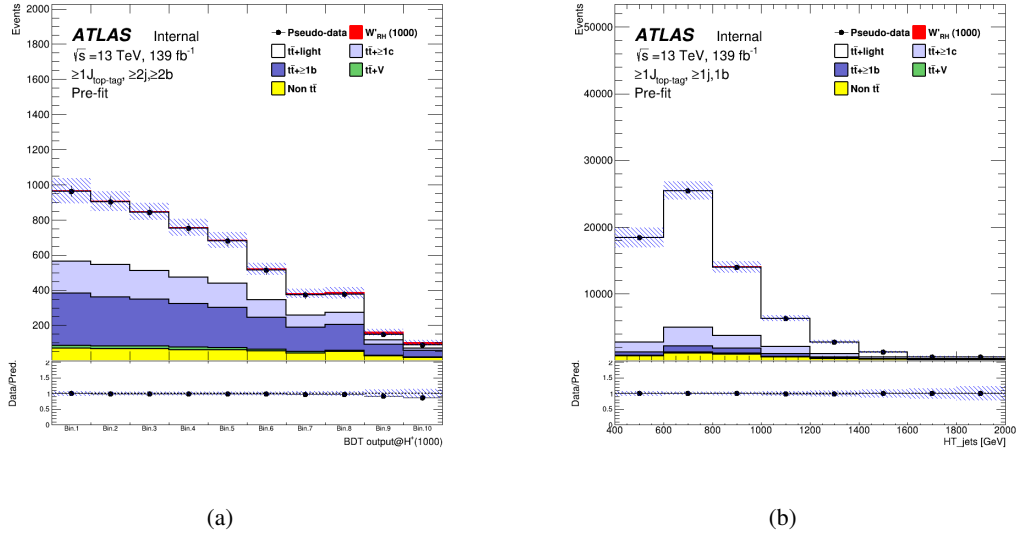


Figure 46: Pre-fit plots in the SR (left) and CR (right) for 1000 GeV mass hypothesis of W'_R signal.

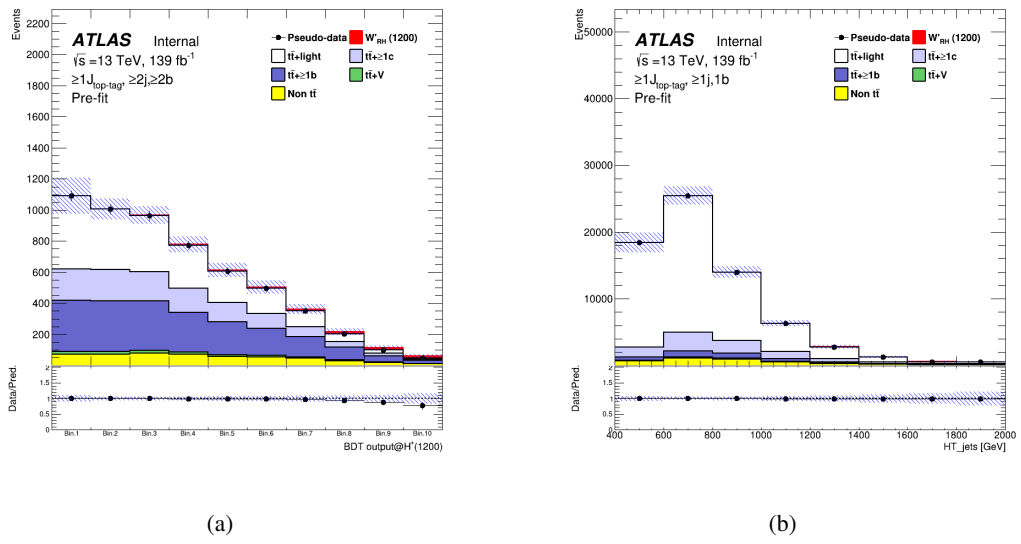


Figure 47: Pre-fit plots in the SR (left) and CR (right) for 1200 GeV mass hypothesis of W'_R signal.

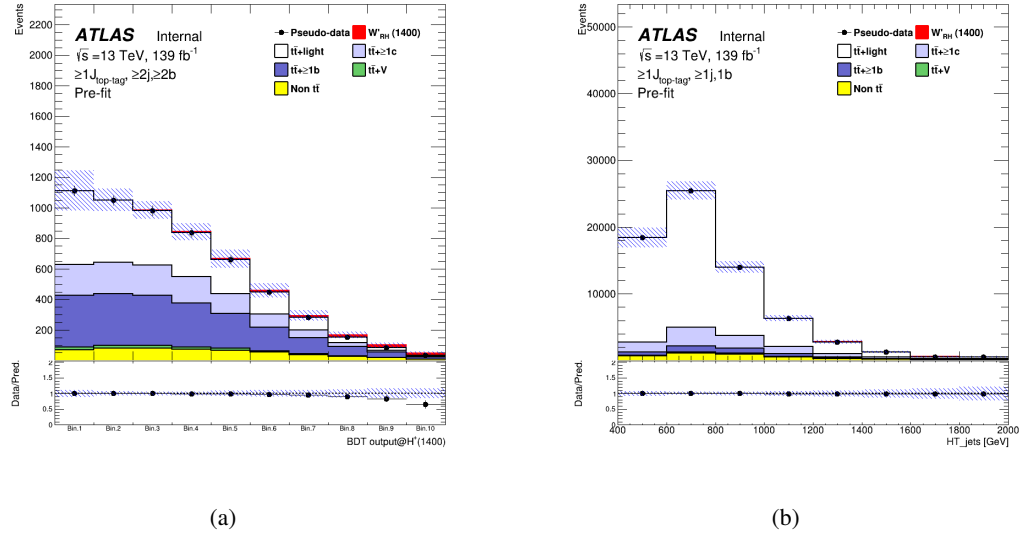


Figure 48: Pre-fit plots in the SR (left) and CR (right) for 1400 GeV mass hypothesis of W'_R signal.

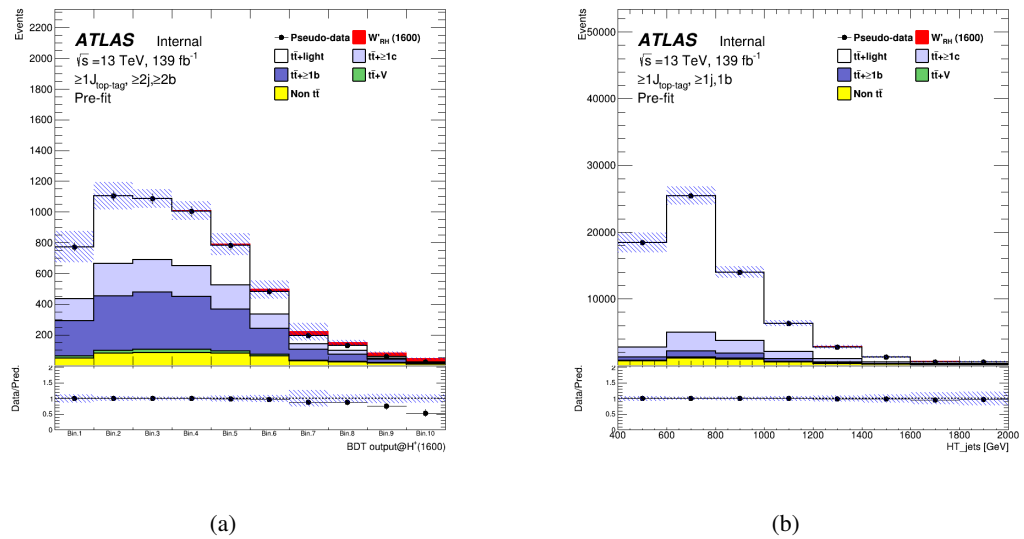


Figure 49: Pre-fit plots in the SR (left) and CR (right) for 1600 GeV mass hypothesis of W'_R signal.

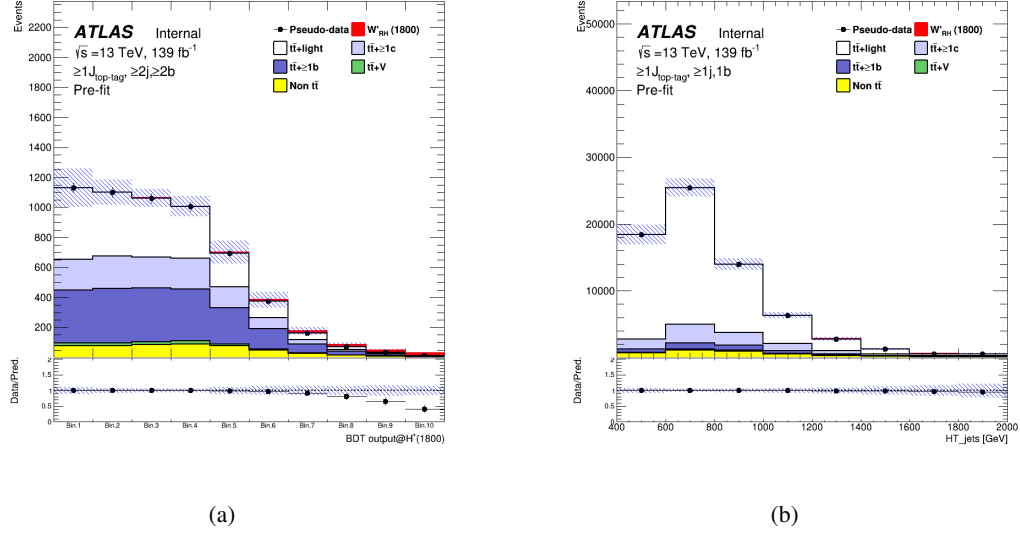


Figure 50: Pre-fit plots in the SR (left) and CR (right) for 1800 GeV mass hypothesis of W'_R signal.

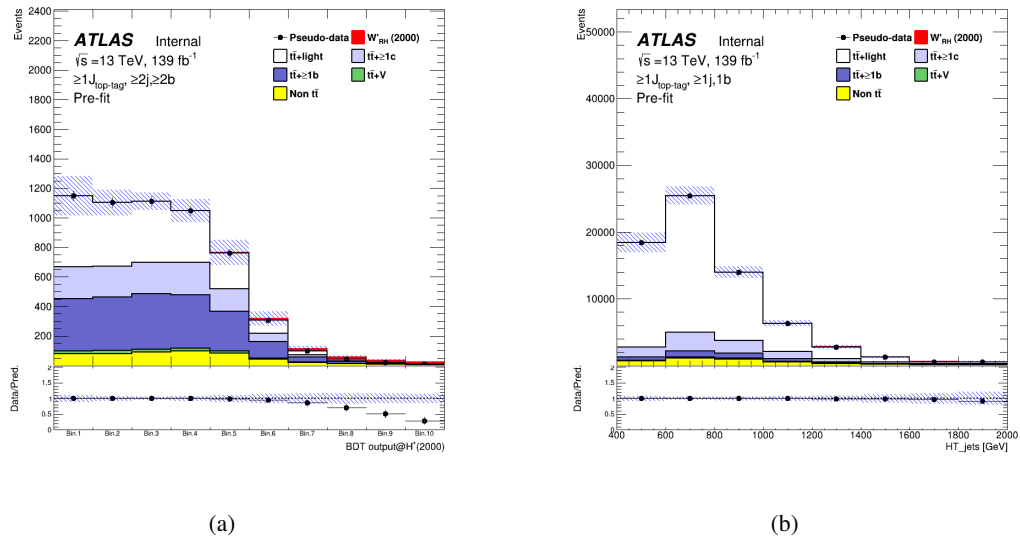


Figure 51: Pre-fit plots in the SR (left) and CR (right) for 2000 GeV mass hypothesis of W'_R signal.

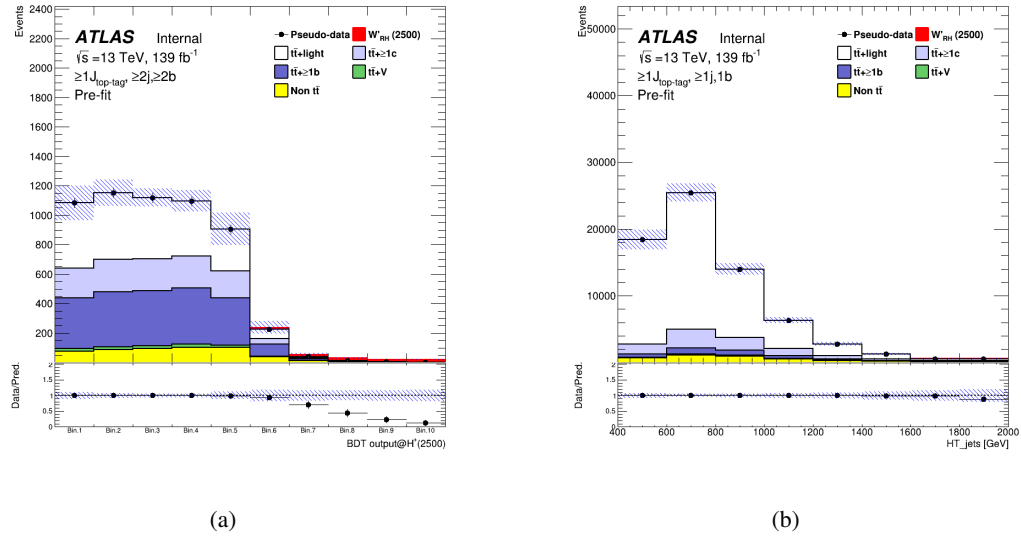


Figure 52: Pre-fit plots in the SR (left) and CR (right) for 2500 GeV mass hypothesis of W'_R signal.

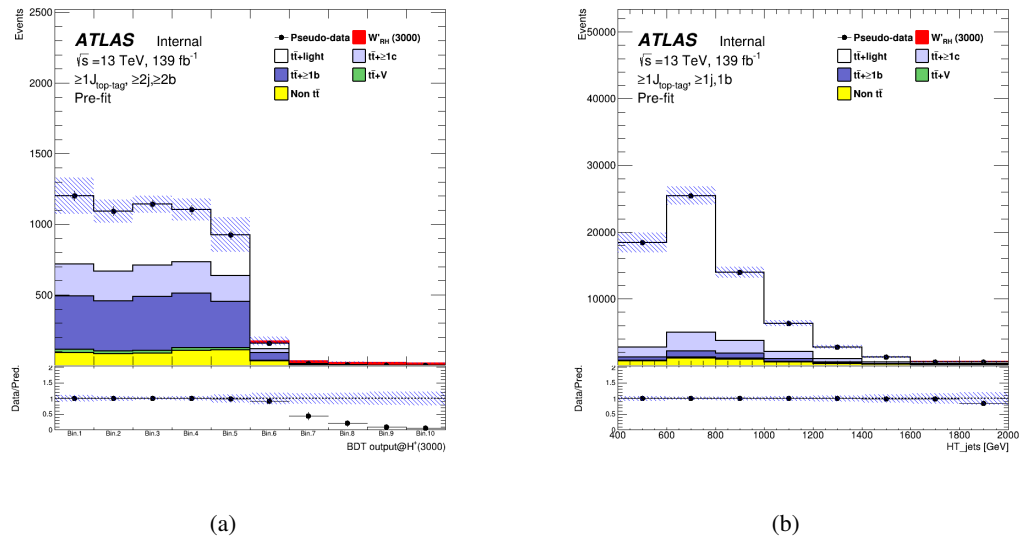


Figure 53: Pre-fit plots in the SR (left) and CR (right) for 3000 GeV mass hypothesis of W'_R signal.

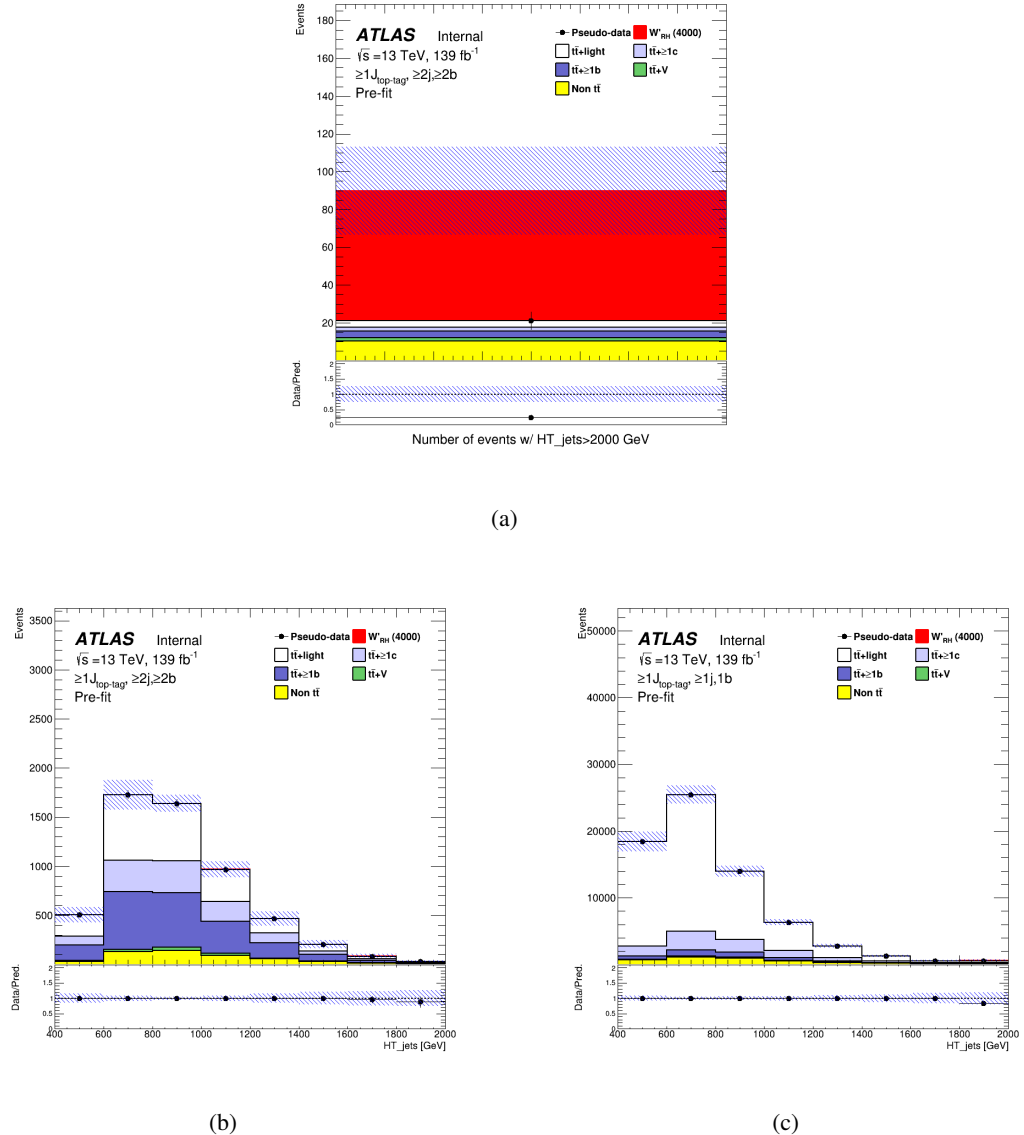


Figure 54: Pre-fit plots in the SR (top), CR1 (bottom-left), and CR2 (bottom-right) for 4000 GeV mass hypothesis of W'_R signal.

859 7.3.2 Asimov fit results

860 In the following, the results of the fitting to Asimov datasets are presented. Figures 55 to 74 show the
 861 nuisance parameters, normalization factors, correlation matrices, the effect of the different nuisance
 862 parameters before and after the fit and post-fit plots from the fits under each H^+ mass hypotheses. Similarly,
 863 Figure 75 to 92 and Figure 93 to 110 show the results from the fits under each W'_L and W'_R mass hypotheses,
 864 respectively.

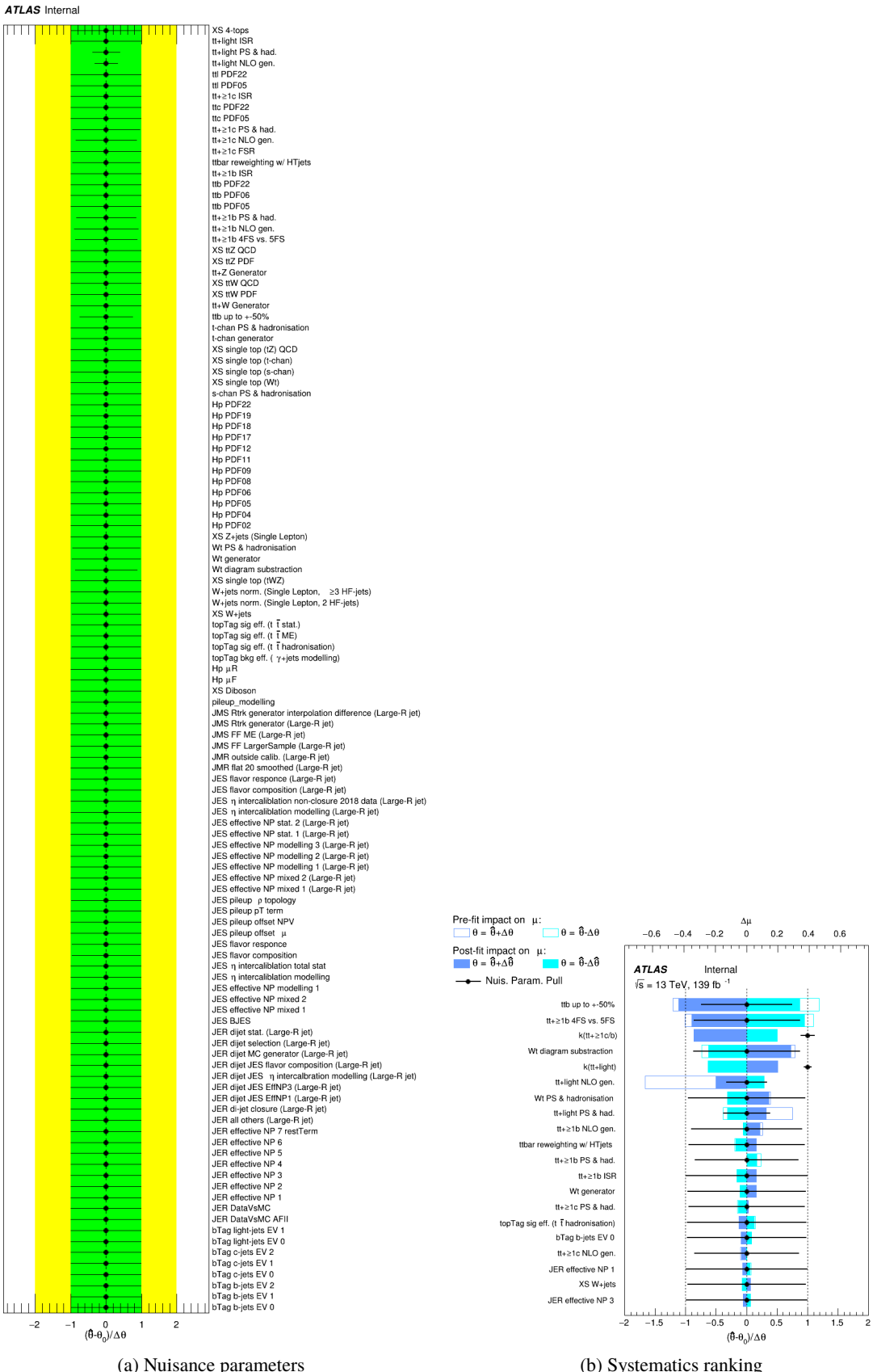
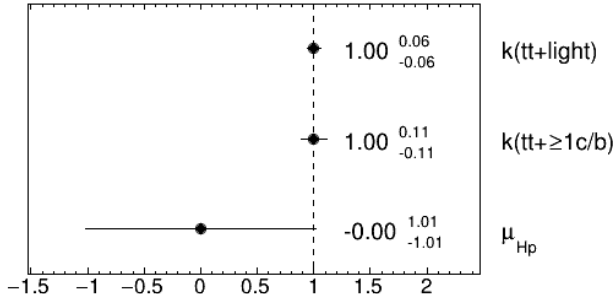


Figure 55: Nuisance parameters (left) and ranking plot (right) of the effect of various nuisance parameters before and after the fit for the 1000 GeV H^+ mass hypotheses.
22nd March 2023 – 00:45

ATLAS Internal

(a) Norm. factors

ATLAS Internal

	bTag b-jets EV 0	-0.6	-1.4	-2.9	2.8	-1.1	-0.4	-0.8	-0.0	-0.9	-1.1	0.5	3.7	-8.2	7.9	3.1	4.0	2.4	1.3	0.3	-1.3	-7.7	-3.1	43.2	-14.7
bTag b-jets EV 1	-0.6	100.0	-0.5	-1.2	1.2	-0.6	-0.1	-0.2	0.5	-0.2	-0.1	-0.6	-0.1	1.2	1.0	1.2	-0.0	-0.4	0.2	4.0	-6.6	1.8	21.6	-8.5	
JES effective NP modelling 1	-1.4	-0.5	100.0	-3.1	2.4	-1.8	-0.1	-0.4	1.5	-0.4	-0.5	-0.0	0.5	-2.3	3.6	3.2	1.8	1.9	-0.1	0.5	-6.4	-22.1	-0.7	-2.1	0.3
JES flavor composition	-2.9	-1.2	-3.1	100.0	5.5	-3.5	-0.3	-0.8	2.7	-0.8	-1.0	-0.1	-0.4	-4.9	6.0	4.7	5.0	1.1	-1.5	0.9	-2.5	-43.7	-0.7	-9.9	2.8
JES flavor response	2.8	1.2	2.4	5.5	100.0	2.7	0.3	0.8	-2.1	0.8	1.0	-0.4	1.2	5.7	-5.1	-2.6	-5.7	0.3	2.0	-0.7	-7.3	31.8	0.8	6.5	-1.7
JES pileup p topology	-1.1	-0.6	-1.8	-3.5	2.7	100.0	-0.1	-0.3	1.6	-0.3	0.0	-1.5	-0.7	2.3	3.6	2.0	-0.1	-0.9	0.4	-6.9	-27.5	-0.1	-30.6	10.3	
tive NP modelling 1 (Large-R jet)	-0.4	-0.1	-0.1	-0.3	0.3	-0.1	100.0	-0.1	0.2	-0.1	-0.1	-0.3	0.7	-1.2	0.7	0.1	0.4	0.3	-0.0	0.0	1.9	-2.0	-0.3	-15.0	-38.4
calibration modelling (Large-R jet)	-0.8	-0.2	-0.4	-0.8	0.8	-0.3	-0.1	100.0	0.1	-0.2	-0.3	0.1	0.8	-2.1	1.8	0.5	1.1	0.6	0.1	0.1	0.3	-3.0	-1.0	7.5	-23.0
topTag sig eff. ($t\bar{t}$ hadronisation)	-0.0	0.5	1.5	2.7	-2.1	1.6	0.2	0.1	100.0	0.1	0.1	1.8	-0.2	-1.5	0.8	0.4	0.8	-5.7	1.6	-1.1	19.2	28.0	4.9	-12.5	-64.8
topTag sig eff. ($t\bar{t}$ ME)	-0.9	-0.2	-0.4	-0.8	0.8	-0.3	-0.1	-0.2	0.1	100.0	-0.3	-0.0	1.3	-2.9	1.9	0.3	1.2	0.6	0.1	0.1	0.6	-2.8	-1.2	1.7	-25.2
topTag sig eff. ($t\bar{t}$ stat.)	-1.1	-0.2	-0.5	-1.0	1.0	-0.3	-0.1	-0.3	0.1	-0.3	100.0	0.0	1.8	-4.0	2.5	0.3	1.5	0.8	0.2	0.1	0.4	-3.2	-2.0	0.7	-31.2
XS W+jets	0.5	-0.1	-0.0	-0.1	-0.4	0.0	-0.3	0.1	1.8	-0.0	0.0	100.0	7.1	-2.0	-1.9	-1.4	-4.0	3.9	-0.9	0.7	22.5	-18.3	2.6	-7.0	-11.8
Wt diagram subtraction	3.7	-0.6	0.5	-0.4	1.2	-1.5	0.7	0.8	-0.2	1.3	1.8	7.1	100.0	33.1	-11.6	4.7	3.6	-17.3	-5.3	-1.1	-14.0	7.8	29.9	27.8	2.7
ttb up to ±50%	8.2	-0.1	-2.3	-4.9	5.7	-0.7	-1.2	-2.1	-1.5	-2.9	-4.0	-2.0	33.1	100.0	13.1	-14.6	9.9	5.6	-1.4	0.9	-12.1	2.7	-38.7	38.1	-2.3
tt+≥1b 4FS vs. 5FS	7.9	1.2	3.6	6.0	-5.1	2.3	0.7	1.8	0.8	1.9	2.5	-1.9	-11.6	13.1	100.0	-21.2	-8.3	-12.0	-11.3	-0.6	2.2	-6.1	-37.6	18.0	-9.9
tt+≥1b PS & had.	3.1	1.0	3.2	4.7	-2.6	3.6	0.1	0.5	0.4	0.3	0.3	-1.4	4.7	-14.6	-21.2	100.0	-2.2	-3.1	-11.6	0.1	-17.4	10.5	-2.1	-0.4	3.0
ttbar reweighting w/ HT jets	4.0	1.2	1.8	5.0	-5.7	2.0	0.4	1.1	0.8	1.2	1.5	-4.0	3.6	9.9	-8.3	-2.2	100.0	5.4	1.5	0.0	7.0	5.9	6.3	-44.2	16.5
tt+≥1c NLO gen.	2.4	-0.0	1.9	1.1	0.3	-0.1	0.3	0.6	-5.7	0.6	0.8	3.9	-17.3	5.6	-12.0	-3.1	5.4	100.0	-8.9	-2.3	-52.3	10.1	-1.9	-2.9	-0.9
tt+≥1c PS & had.	1.3	-0.4	-0.1	-1.5	2.0	-0.9	-0.0	0.1	1.6	0.1	0.2	-0.9	-5.3	-1.4	-11.3	-11.6	1.5	-8.9	100.0	0.2	-4.3	-26.9	3.2	-2.1	-0.8
tt PDF05	0.3	0.2	0.5	0.9	-0.7	0.4	0.0	0.1	-1.1	0.1	0.1	0.7	-1.1	0.9	-0.6	0.1	0.0	-2.3	0.2	100.0	-5.5	8.3	-0.7	-0.9	27.6
tt+light NLO gen.	-1.3	4.0	-6.4	-2.5	-7.3	-6.9	1.9	0.3	-19.2	0.6	0.4	22.5	-14.0	-12.1	2.2	-17.4	7.0	-52.3	-4.3	-5.5	100.0	-34.0	-16.1	-7.0	3.7
tt+light PS & had.	-7.7	-6.6	-22.1	-43.7	31.8	-27.5	-2.0	-3.0	28.0	-2.8	-3.2	-18.3	7.8	2.7	-6.1	10.5	5.9	10.1	-26.9	8.3	-34.0	100.0	13.2	-1.6	-7.1
μ_{H_p}	-3.1	1.8	-0.7	-0.7	0.8	-0.1	-0.3	-1.0	-4.9	-1.2	-2.0	2.6	29.9	-38.7	-37.6	-2.1	6.3	-1.9	3.2	-0.7	-16.1	13.2	100.0	-27.8	20.8
$k(t\bar{t}+c/b)$	43.2	21.6	-2.1	-9.9	6.5	-30.6	-15.0	7.5	-12.5	1.7	0.7	-7.0	27.8	38.1	18.0	-0.4	-44.2	-2.9	-2.1	-0.9	-7.0	-1.6	-27.8	100.0	-17.2
$k(t\bar{t}+light)$	-14.7	-8.5	0.3	2.8	-1.7	10.3	-38.4	-23.0	-64.6	-25.2	-31.2	-11.8	2.7	-2.3	-9.9	3.0	16.5	-0.9	-0.8	27.6	3.7	-7.1	20.8	-17.2	100.0

(b) Correlation matrix

Figure 56: Signal strength and normalization factors (top) and correlation matrix (bottom) for the 1000 GeV H^+ mass hypotheses.

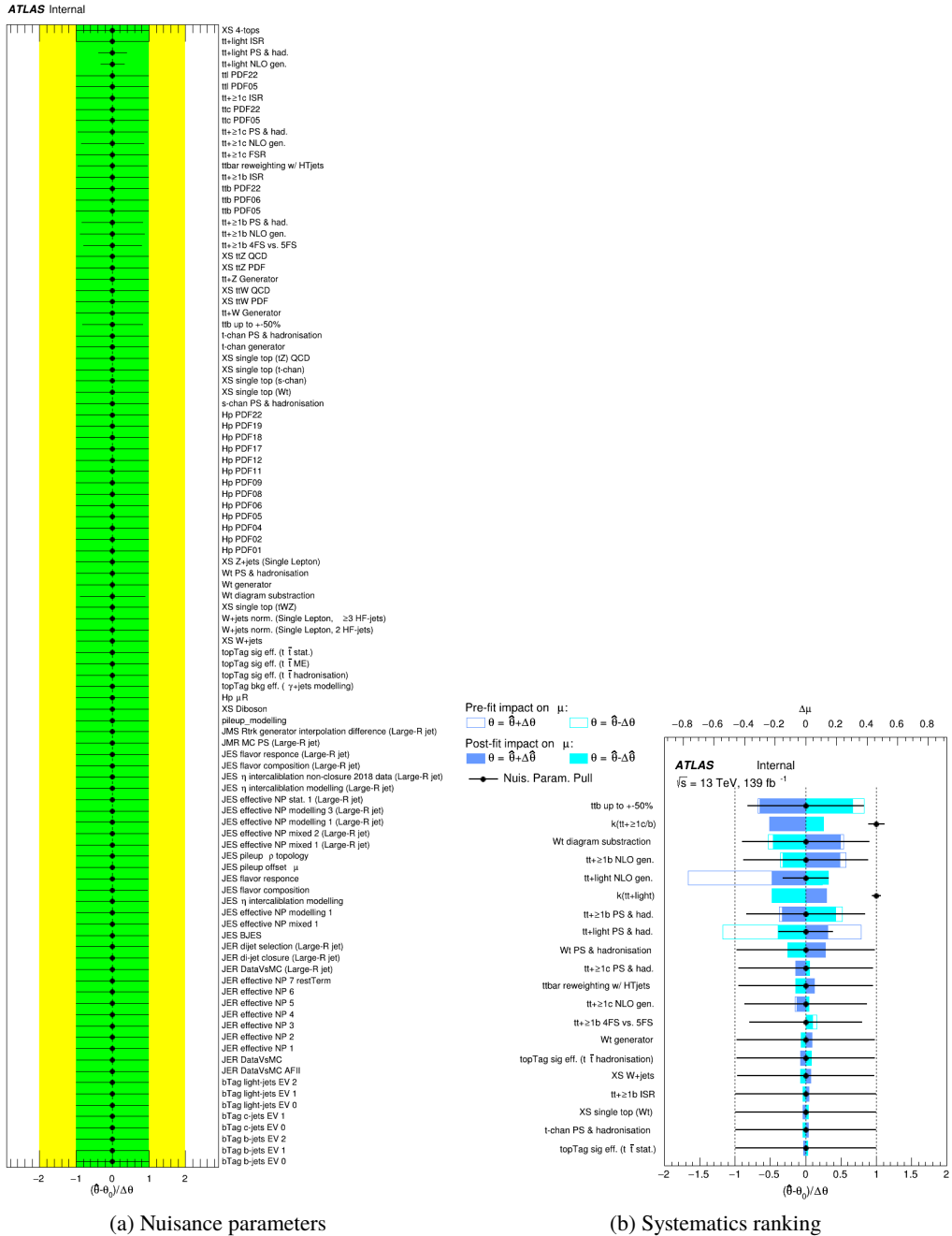
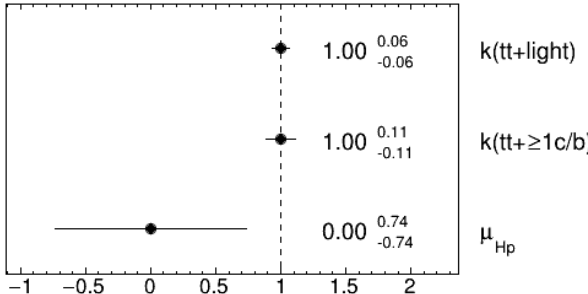
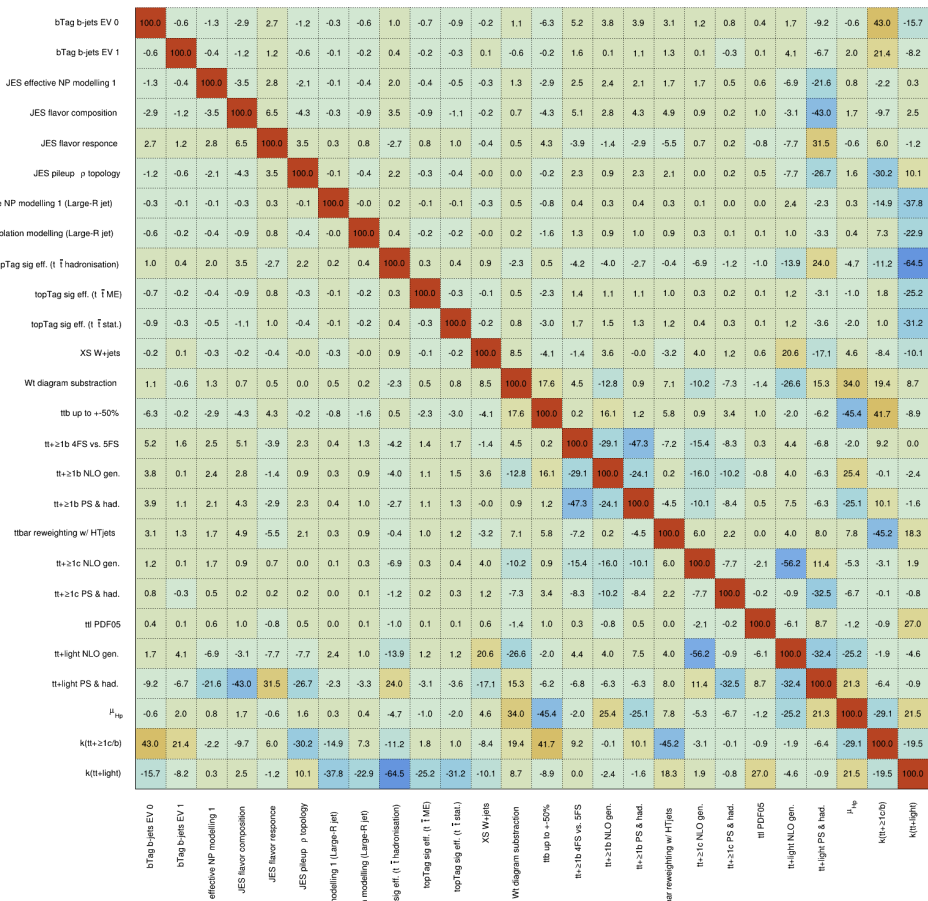


Figure 57: Nuisance parameters (left) and ranking plot (right) of the effect of various nuisance parameters before and after the fit for the 1200 GeV H^+ mass hypotheses.

ATLAS Internal**ATLAS Internal**

(b) Correlation matrix

Figure 58: Signal strength and normalization factors (top) and correlation matrix (bottom) for the 1200 GeV H^+ mass hypotheses.

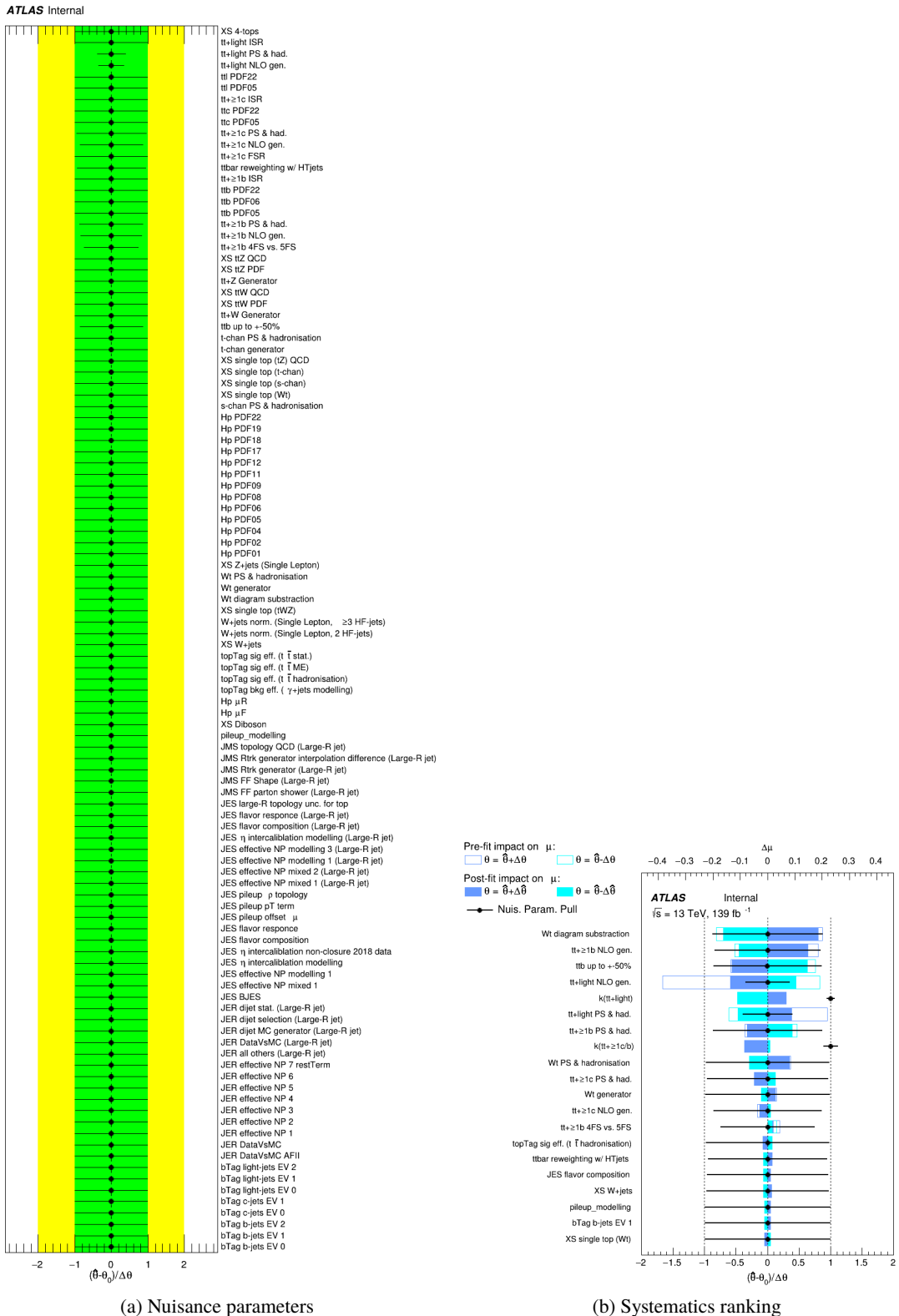
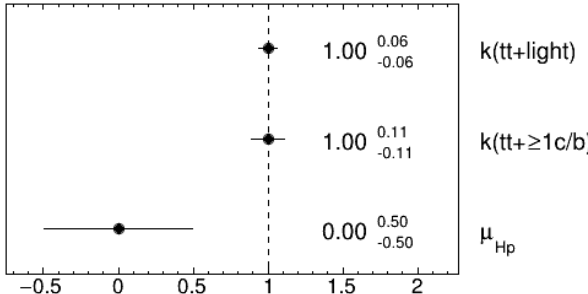


Figure 59: Nuisance parameters (left) and ranking plot (right) of the effect of various nuisance parameters before and after the fit for the 1400 GeV H^+ mass hypotheses.

ATLAS Internal

(a) Norm. factors

ATLAS Internal

	bTag b-jets EV 0	bTag b-jets EV 1	JES effective NP modeling 1	JES flavor composition	JES flavor response	JES pileup topology	utive NP modelling 1 (Large-R jet)	abilitation modelling (Large-R jet)	topTag sig eff. ($t \bar{t}$ hadronisation)	topTag sig eff. ($t \bar{t}$ ME)	topTag sig eff. ($t \bar{t}$ stat.)	XS W+jets	W diagram subtraction	ttb up to +50%	tt+>1b 4FS vs. 5FS	tt+>1b NLO gen.	tt+>1b PS & had.	ttbar reweighting w/ H+jets	tt+>1c NLO gen.	tt+>1c PS & had.	tt PDF05	tt+light NLO gen.	tt+light PS & had.	μ_{H_p}	k($t(t+1c/b)$)	k($t(t+light)$)
100.0	-0.5	-1.2	2.8	2.5	-1.4	-0.3	-0.4	1.2	-0.5	-0.7	0.1	0.2	-4.2	5.3	3.7	3.3	1.9	-0.3	0.1	0.2	4.5	-10.7	1.1	44.5	-16.7	
-0.5	100.0	-0.4	-1.0	1.0	-0.4	-0.1	-0.2	0.4	-0.2	-0.2	0.1	-1.1	0.1	1.6	-0.2	1.0	1.4	0.3	-0.4	0.1	4.3	-7.2	2.1	21.6	-8.4	
-1.2	-0.4	100.0	-3.8	2.9	-2.4	-0.2	-0.2	2.4	-0.4	-0.4	-0.4	0.2	-3.5	1.5	3.0	1.8	0.2	0.6	0.3	0.5	-4.8	-21.4	1.3	-1.8	-0.3	
-2.8	-1.0	-3.8	100.0	6.4	-4.7	-0.4	-0.6	4.2	-0.9	-1.0	-0.4	-0.5	-7.7	2.8	4.6	3.3	2.4	-1.1	-0.3	0.9	-1.1	-41.9	2.6	-9.8	2.0	
2.5	1.0	2.9	6.4	100.0	3.6	0.4	0.6	-3.0	0.8	1.0	-0.3	1.6	6.6	-2.2	-2.2	-2.0	-3.9	2.2	1.2	-0.7	-9.0	31.3	-0.8	6.0	-0.9	
-1.4	-0.4	-2.4	-4.7	3.6	100.0	-0.2	-0.2	2.7	-0.4	-0.5	-0.3	-0.4	-4.2	1.0	2.9	2.0	0.6	-1.0	0.3	0.5	-7.7	-24.7	1.6	-31.1	10.3	
-0.3	-0.1	-0.2	-0.4	0.4	-0.2	100.0	-0.0	0.3	-0.1	-0.1	-0.3	0.9	-1.5	0.6	1.1	0.5	0.0	-0.2	0.1	0.0	1.6	-1.7	-0.9	-14.7	37.8	
-0.4	-0.2	-0.2	-0.6	0.6	-0.2	-0.0	100.0	0.2	-0.1	-0.1	0.1	-0.2	-0.5	0.9	0.0	0.4	0.9	0.1	-0.4	0.1	2.3	-4.6	-0.0	7.9	-23.1	
1.2	0.4	2.4	4.2	-3.0	2.7	0.3	0.2	100.0	0.4	0.4	1.1	-0.8	1.8	-5.1	-6.2	-4.2	1.1	-6.3	-2.0	-1.0	-12.6	22.2	-3.3	-11.6	-63.9	
-0.5	-0.2	-0.4	-0.9	0.8	-0.4	-0.1	-0.1	0.4	100.0	-0.2	-0.0	0.4	-1.7	1.5	1.2	0.9	0.6	-0.2	-0.1	0.1	1.9	-3.5	-0.3	2.2	-25.4	
-0.7	-0.2	-0.4	-1.0	1.0	-0.5	-0.1	-0.1	0.4	-0.2	100.0	-0.0	0.7	-2.3	1.9	1.7	1.1	0.7	-0.3	-0.1	0.1	2.1	-4.0	-1.1	1.4	-31.4	
0.1	0.1	-0.4	-0.4	-0.3	-0.3	-0.3	0.1	1.1	-0.0	-0.0	100.0	7.6	-2.4	-2.3	2.9	0.4	-4.0	3.5	1.1	0.6	21.3	-17.8	3.1	-7.0	-11.1	
0.2	-1.1	0.2	-0.5	1.6	-0.4	0.9	-0.2	-0.8	0.4	0.7	7.6	100.0	19.4	3.6	-16.1	2.8	10.2	-4.6	-0.7	-0.8	-26.8	16.8	41.2	18.6	7.4	
-4.2	0.1	-3.5	-7.7	6.6	-4.2	-1.5	-0.5	1.8	-1.7	-2.3	-2.4	-19.4	100.0	-3.4	15.7	-1.9	-2.1	-9.3	0.1	0.5	9.7	-7.2	-30.3	45.4	-12.0	
5.3	1.6	1.5	2.8	-2.2	1.0	0.6	0.9	-5.1	1.5	1.9	-2.3	3.6	-3.4	100.0	-39.5	-47.2	-7.3	-15.5	-10.7	0.9	9.3	-5.8	-0.1	7.8	0.8	
3.7	-0.2	3.0	4.6	-2.2	2.9	1.1	0.0	-6.2	1.2	1.7	2.9	-16.1	15.7	-39.5	100.0	-25.3	6.5	-7.5	-10.0	-0.3	4.1	-10.0	25.4	3.2	-0.6	
3.3	1.0	1.8	3.3	-2.0	2.0	0.5	0.4	-4.2	0.9	1.1	0.4	2.8	-1.9	-47.2	-25.3	100.0	-1.5	-8.3	-9.3	0.5	2.7	-1.3	-17.4	5.2	1.2	
1.9	1.4	0.2	2.4	-3.9	0.6	0.0	0.9	1.1	0.6	0.7	-4.0	10.2	-2.1	-7.3	6.5	-1.5	100.0	5.3	5.0	0.2	-3.2	16.2	3.2	-46.3	19.0	
-0.3	0.3	0.6	-1.1	2.2	-1.0	-0.2	0.1	-6.3	-0.2	-0.3	3.5	-4.6	-9.3	-15.5	-7.5	-8.3	5.3	100.0	-6.3	-1.9	-62.6	21.1	-3.9	-6.0	4.6	
0.1	-0.4	0.3	-0.3	1.2	0.3	0.1	-0.4	-2.0	-0.1	-0.1	1.1	-0.7	0.1	-10.7	-10.0	-9.3	5.0	-6.3	100.0	0.1	-7.2	-39.4	-8.3	-1.8	2.0	
0.2	0.1	0.5	0.9	-0.7	0.5	0.0	0.1	-1.0	0.1	0.1	0.6	-0.8	0.5	0.9	-0.3	0.5	0.2	-1.9	0.1	100.0	-6.7	9.1	-0.3	-1.3	27.3	
4.5	4.3	-4.8	-1.1	-9.0	-7.7	1.6	2.3	-12.6	1.9	2.1	21.3	-26.8	9.7	9.3	4.1	2.7	-3.2	-62.6	-7.2	-6.7	100.0	-39.4	-23.9	6.4	-8.9	
-10.7	-7.2	-21.4	-41.9	31.3	-24.7	-1.7	-4.6	22.2	-3.5	-4.0	-17.8	16.8	-7.2	-5.8	-10.0	-1.3	16.2	21.1	-27.6	9.1	-39.4	100.0	19.0	-10.9	2.3	
1.1	2.1	1.3	2.6	-0.8	1.6	-0.9	-0.0	-3.3	-0.3	-1.1	3.1	41.2	-30.3	-0.1	17.4	3.2	-3.9	-8.3	-0.3	-23.9	19.0	100.0	-13.5	16.4		
44.5	21.6	-1.8	-9.8	6.0	-31.1	-14.7	7.9	-11.6	2.2	1.4	-7.0	18.6	45.4	7.8	-3.2	5.2	-46.3	-6.0	-1.8	-1.3	6.4	-10.9	-13.5	100.0	-20.4	
-16.7	-8.4	-0.3	2.0	-0.9	10.3	-37.8	-23.1	-63.9	-25.4	-31.4	-11.1	7.4	-12.0	0.8	-0.6	1.2	19.0	4.6	2.0	27.3	-8.9	2.3	16.4	-20.4	100.0	

(b) Correlation matrix

Figure 60: Signal strength and normalization factors (top) and correlation matrix (bottom) for the 1400 GeV H^+ mass hypotheses.

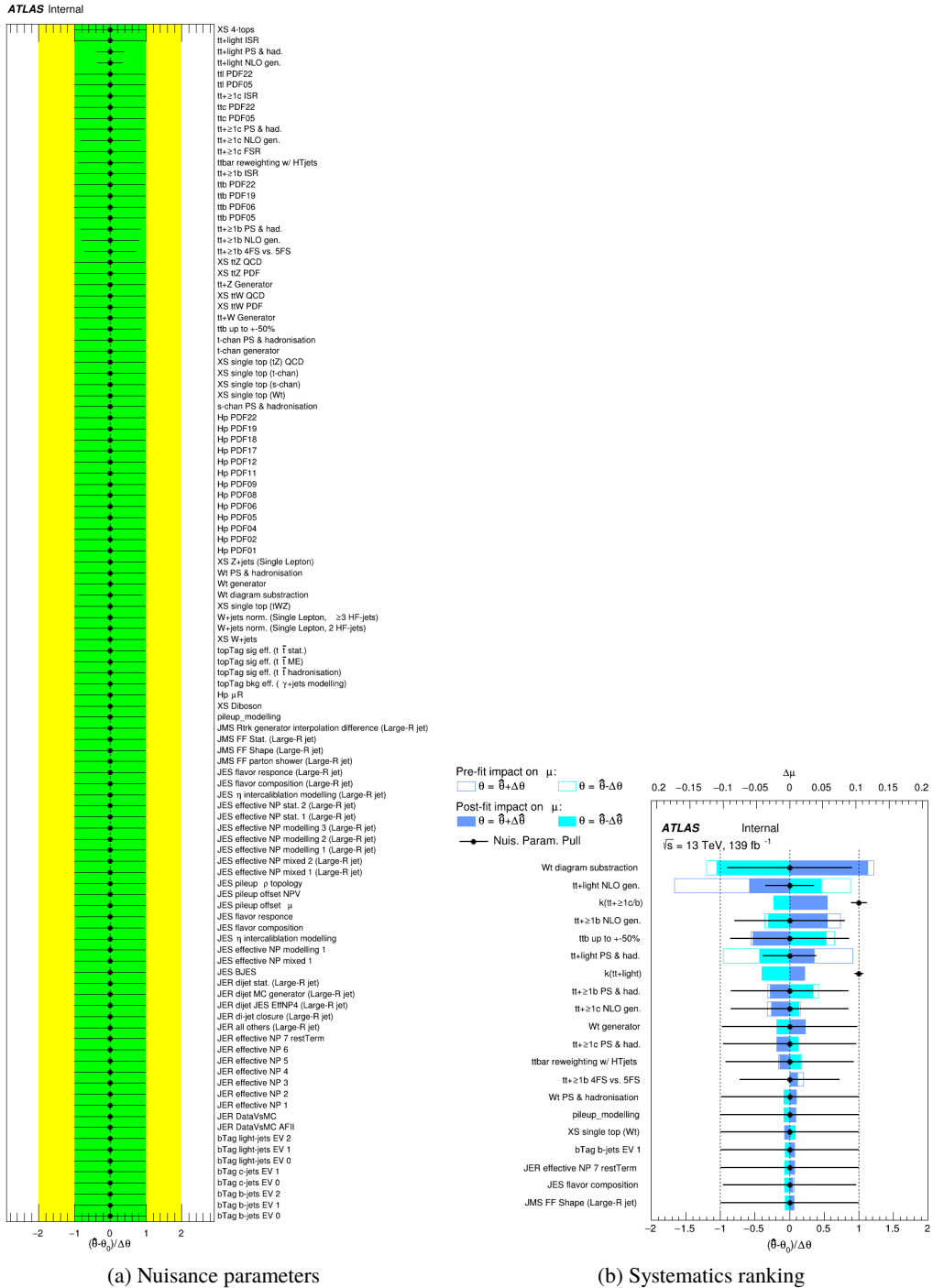
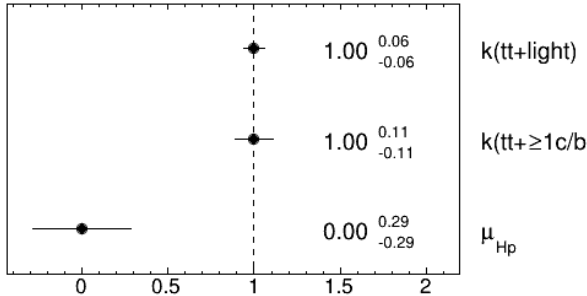
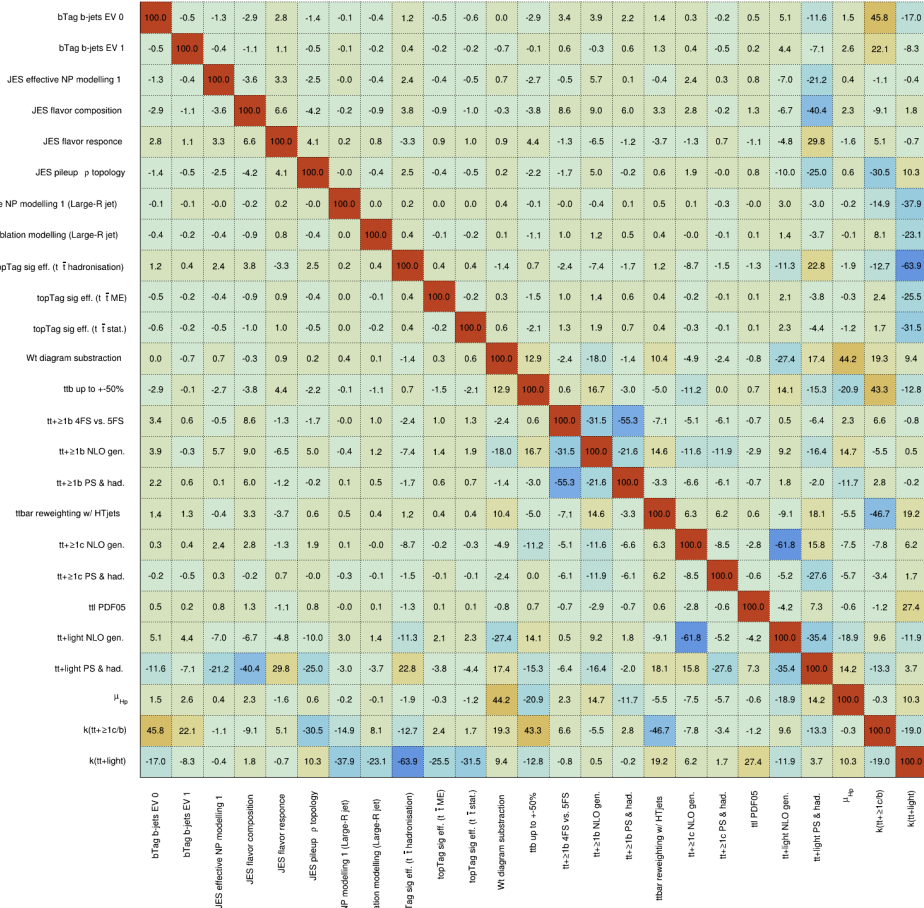


Figure 61: Nuisance parameters (left) and ranking plot (right) of the effect of various nuisance parameters before and after the fit for the 1600 GeV H^+ mass hypotheses.

ATLAS Internal

(a) Norm. factors

ATLAS Internal

(b) Correlation matrix

Figure 62: Signal strength and normalization factors (top) and correlation matrix (bottom) for the 1600 GeV H^+ mass hypotheses.

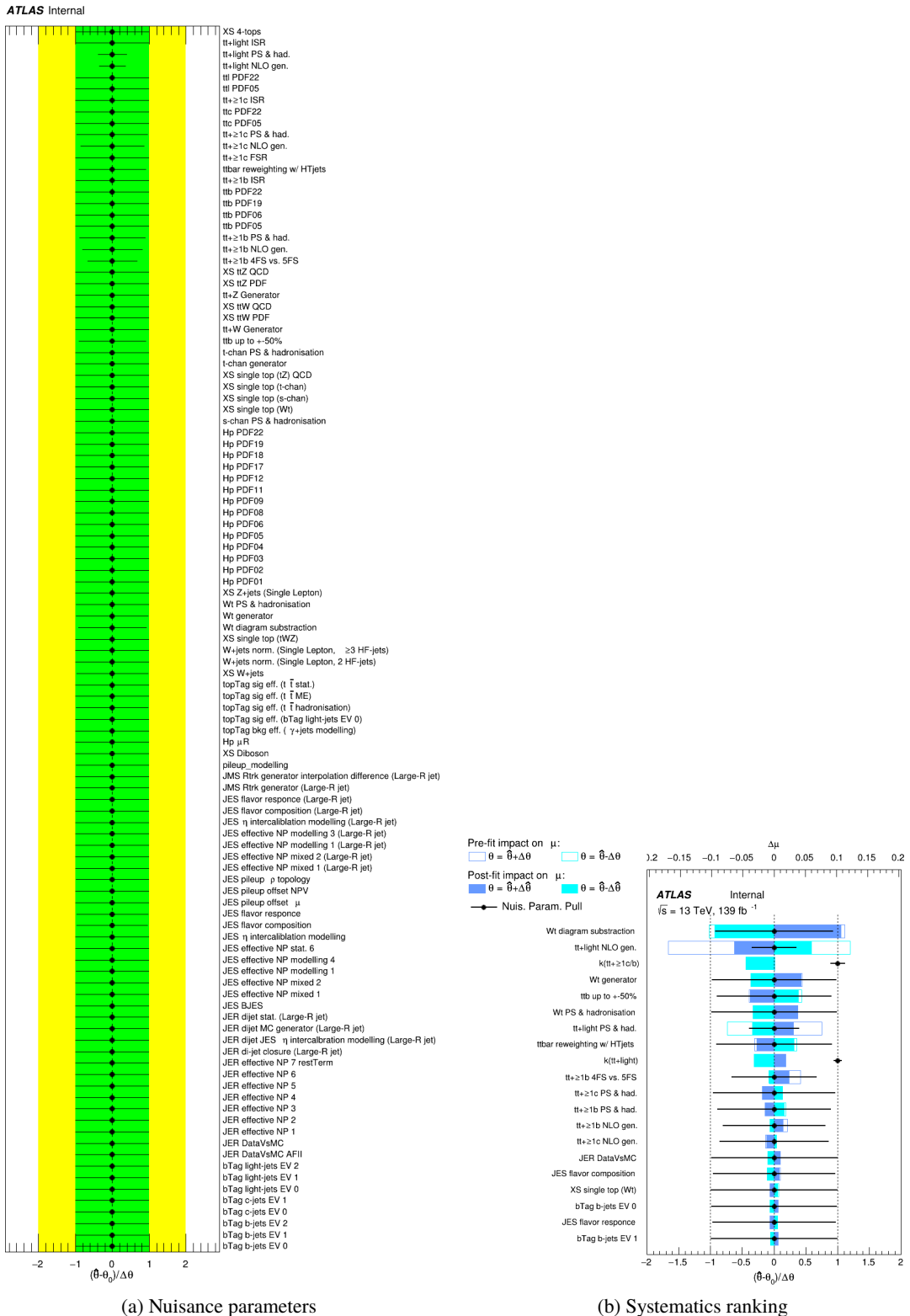
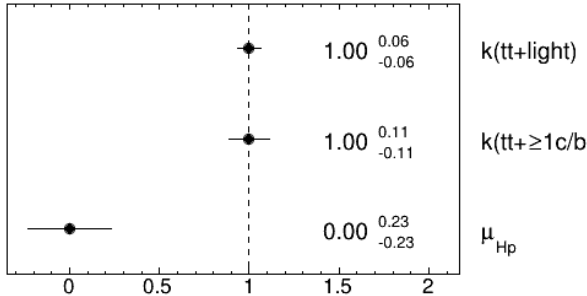


Figure 63: Nuisance parameters (left) and ranking plot (right) of the effect of various nuisance parameters before and after the fit for the 1800 GeV H^+ mass hypotheses.

ATLAS Internal

(a) Norm. factors

ATLAS Internal

	bTag b-jets EV 0	-0.5	-1.0	-2.6	2.5	-1.2	-0.2	-0.4	0.9	-0.5	-0.6	-0.0	0.5	-3.0	4.1	3.1	2.1	1.0	0.4	-0.3	0.4	4.9	-11.7	2.9	45.9	-16.6	
bTag b-jets EV 1	-0.5	100.0	-0.4	-1.1	1.0	-0.5	-0.1	-0.2	0.4	-0.2	-0.2	0.0	-0.3	-0.4	0.9	-0.1	0.5	1.4	0.2	-0.4	0.2	4.2	-6.9	2.7	22.0	-8.1	
JES effective NP modeling 1	-1.0	-0.4	100.0	-3.0	2.5	-1.9	-0.1	-0.4	1.8	-0.3	-0.4	-0.3	1.0	-2.3	1.0	4.0	1.6	0.3	1.2	-0.2	0.6	-5.5	-22.2	2.1	-1.3	0.1	
JES flavor composition	-2.6	-1.1	-3.0	100.0	5.6	-3.6	-0.3	-1.0	3.1	-0.8	-1.0	0.1	0.2	-4.7	11.3	8.5	6.7	3.9	0.7	-0.5	1.0	-5.6	-40.6	4.3	-9.5	2.7	
JES flavor response	2.5	1.0	2.5	5.6	100.0	3.2	0.3	0.8	-2.3	0.8	1.1	-0.4	-0.9	6.6	-2.3	-5.5	-2.4	-2.8	1.5	1.5	-0.8	-5.5	30.6	-2.7	5.2	-1.7	
JES pileup p topology	-1.2	-0.5	-1.9	-3.6	3.2	100.0	-0.1	-0.4	1.8	-0.4	-0.5	-0.2	1.2	-3.4	0.3	4.6	1.9	0.7	-0.5	-0.5	0.6	-9.1	-25.4	1.7	-30.6	10.9	
tive NP modelling 1 (Large-R jet)	-0.2	-0.1	-0.1	-0.3	0.3	-0.1	100.0	-0.0	0.2	-0.0	-0.0	-0.2	0.2	-0.3	0.4	0.2	0.4	0.4	-0.1	-0.1	0.0	2.7	-2.6	-0.7	-14.9	37.7	
ablation modelling (Large-R jet)	-0.4	-0.2	-0.4	-1.0	0.8	-0.4	-0.0	-0.1	100.0	0.4	-0.1	-0.1	0.1	-0.2	-0.2	2.0	1.5	1.5	1.1	-0.0	0.2	0.1	1.4	-3.4	0.7	7.9	-23.1
topTag sig eff. (t T hadronisation)	0.9	0.4	1.8	3.1	-2.3	1.8	0.2	0.4	100.0	0.3	0.4	1.0	-1.9	1.2	-4.5	-5.8	-2.5	0.5	-6.9	-0.7	-1.1	-12.7	23.9	-2.6	-12.2	-64.0	
topTag sig eff. (t T ME)	-0.5	-0.2	-0.3	-0.8	0.8	-0.4	-0.0	-0.1	0.3	100.0	-0.2	-0.1	0.2	-1.2	1.4	1.0	0.7	0.3	0.0	-0.1	0.1	2.0	-3.8	0.2	2.5	-25.3	
topTag sig eff. (t T stat.)	-0.6	-0.2	-0.4	-1.0	1.1	-0.5	-0.0	-0.1	0.4	-0.2	100.0	-0.1	0.4	-1.6	1.7	1.4	0.9	0.2	-0.0	-0.1	0.1	2.3	-4.4	-0.7	1.8	-31.3	
XW+jets	-0.0	0.0	-0.3	0.1	-0.4	-0.2	-0.2	0.1	1.0	-0.1	-0.1	100.0	6.6	-1.6	-2.4	3.8	1.4	-4.7	3.7	0.7	0.5	20.8	-18.2	-0.9	-6.4	-11.3	
Wt diagram subtraction	0.5	-0.3	1.0	0.2	-0.9	1.2	0.2	-0.2	-1.9	0.2	0.4	6.6	100.0	11.3	8.0	-14.0	-2.0	-13.0	-4.3	-2.4	-0.9	-31.1	19.2	50.6	18.8	10.6	
ttb up to +50%	-3.0	-0.4	-2.3	-4.7	6.6	-3.4	-0.3	-0.2	1.2	-1.2	-1.6	-1.6	11.3	100.0	-0.2	12.4	0.6	-7.3	-5.0	-0.6	0.6	11.4	-13.5	-17.4	46.1	-14.5	
tt+≥1b 4FS vs. 5FS	4.1	0.9	1.0	11.3	-2.3	0.3	0.4	2.0	-4.5	1.4	1.7	-2.4	8.0	-0.2	100.0	-33.2	-44.0	-8.6	-17.5	-9.7	-1.4	8.2	-12.3	7.7	8.9	0.3	
tt+≥1b NLO gen.	3.1	-0.1	4.0	8.5	-5.5	4.6	0.2	1.5	-5.8	1.0	1.4	3.8	-14.0	12.4	-33.2	100.0	-28.6	14.6	-7.2	-12.3	-2.3	3.8	-12.4	3.6	-5.8	-0.0	
tt+≥1b PS & had.	2.1	0.5	1.6	6.7	-2.4	1.9	0.4	1.5	-2.5	0.7	0.9	1.4	-2.0	0.6	-44.0	-28.6	100.0	-0.5	-3.8	-7.4	-1.1	2.1	-3.4	-6.9	1.2	-0.6	
ttbar reweighting w/ H+jets	1.0	1.4	0.3	3.9	-2.8	0.7	0.4	1.1	0.5	0.3	0.2	-4.7	13.0	-7.3	-8.6	14.6	-0.5	100.0	6.5	4.6	0.2	-13.0	19.1	-12.9	-45.0	19.9	
tt+≥1c NLO gen.	0.4	0.2	1.2	0.7	1.5	-0.5	-0.1	-0.0	-6.9	0.0	-0.0	3.7	-4.3	-5.0	-17.5	-7.2	-3.8	6.5	100.0	-7.6	-2.3	-0.1	-0.9	18.5	-3.6	-5.1	4.3
tt+≥1c PS & had.	-0.3	-0.4	-0.2	-0.5	1.5	-0.5	-0.1	0.2	-0.7	-0.1	-0.1	0.7	-2.4	-0.6	-9.7	-12.3	-7.4	4.6	-7.6	100.0	-0.4	-5.6	-26.7	-7.5	-2.9	0.9	
tt PDF05	0.4	0.2	0.6	1.0	-0.8	0.6	0.0	0.1	-1.1	0.1	0.1	0.5	-0.9	0.6	-1.4	-2.3	-1.1	0.2	-2.3	-0.4	100.0	-4.7	7.7	-1.2	-1.1	27.0	
tt+light NLO gen.	4.9	4.2	-5.5	-5.6	-5.5	-9.1	2.7	1.4	-12.7	2.0	2.3	20.8	-31.1	11.4	8.2	3.8	2.1	-13.0	-61.9	-5.6	-4.7	100.0	-37.5	-27.6	10.2	-11.2	
tt+light PS & had.	-11.7	-6.9	-22.2	-40.6	30.6	-25.4	-2.6	-3.4	23.9	-3.8	-4.4	-18.2	19.2	-13.5	-12.3	-12.4	-3.4	19.1	18.5	-26.7	7.7	-37.5	100.0	14.5	-13.0	2.7	
μ_{H_p}	2.9	2.7	2.1	4.3	-2.7	1.7	-0.7	0.7	-2.6	0.2	-0.7	-0.9	50.6	-17.4	7.7	3.6	-6.9	-12.9	-3.6	-7.5	-1.2	-27.6	14.5	100.0	9.7	10.7	
k(tt+≥1b)	45.9	22.0	-1.3	-9.5	5.2	-30.6	-14.9	7.9	-12.2	2.5	1.8	-6.4	18.8	46.1	8.9	-5.8	1.2	-45.0	-5.1	-2.9	-1.1	10.2	-13.0	9.7	100.0	-19.6	
k(tt+light)	-16.6	-8.1	0.1	2.7	-1.7	10.9	-37.7	-23.1	-64.0	-25.3	-31.3	-11.3	10.6	-14.5	0.3	-0.0	-0.6	19.9	4.3	0.9	27.0	-11.2	2.7	10.7	-19.6	100.0	

(b) Correlation matrix

Figure 64: Signal strength and normalization factors (top) and correlation matrix (bottom) for the 1800 GeV H^+ mass hypotheses.

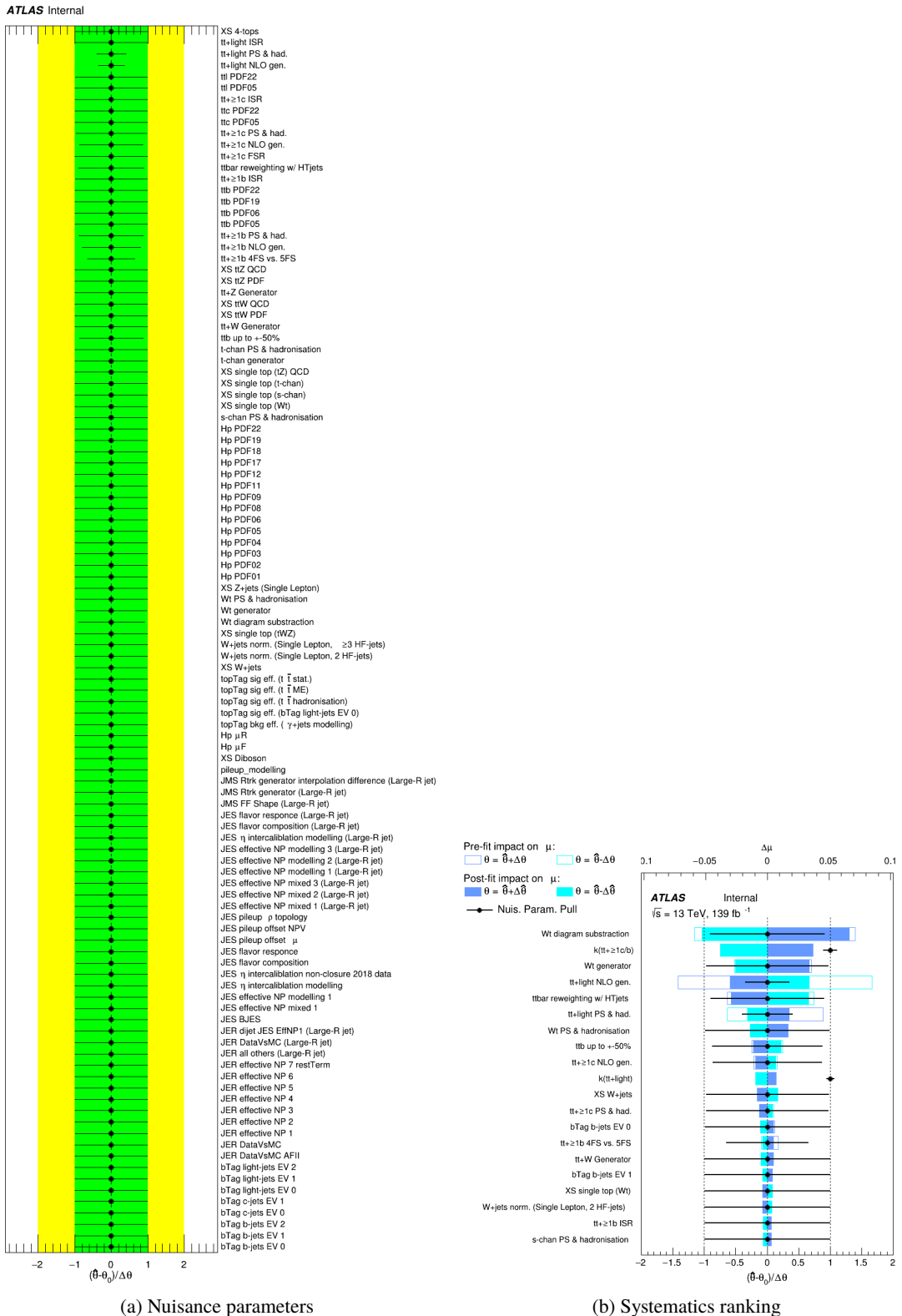
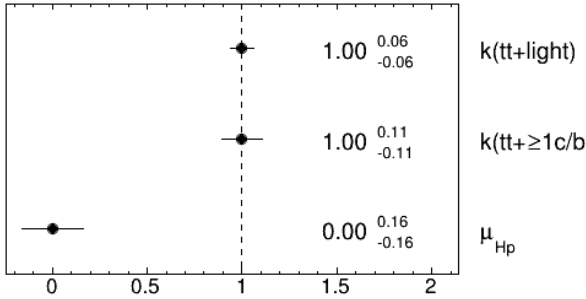


Figure 65: Nuisance parameters (left) and ranking plot (right) of the effect of various nuisance parameters before and after the fit for the 2000 GeV H^+ mass hypotheses.

ATLAS Internal

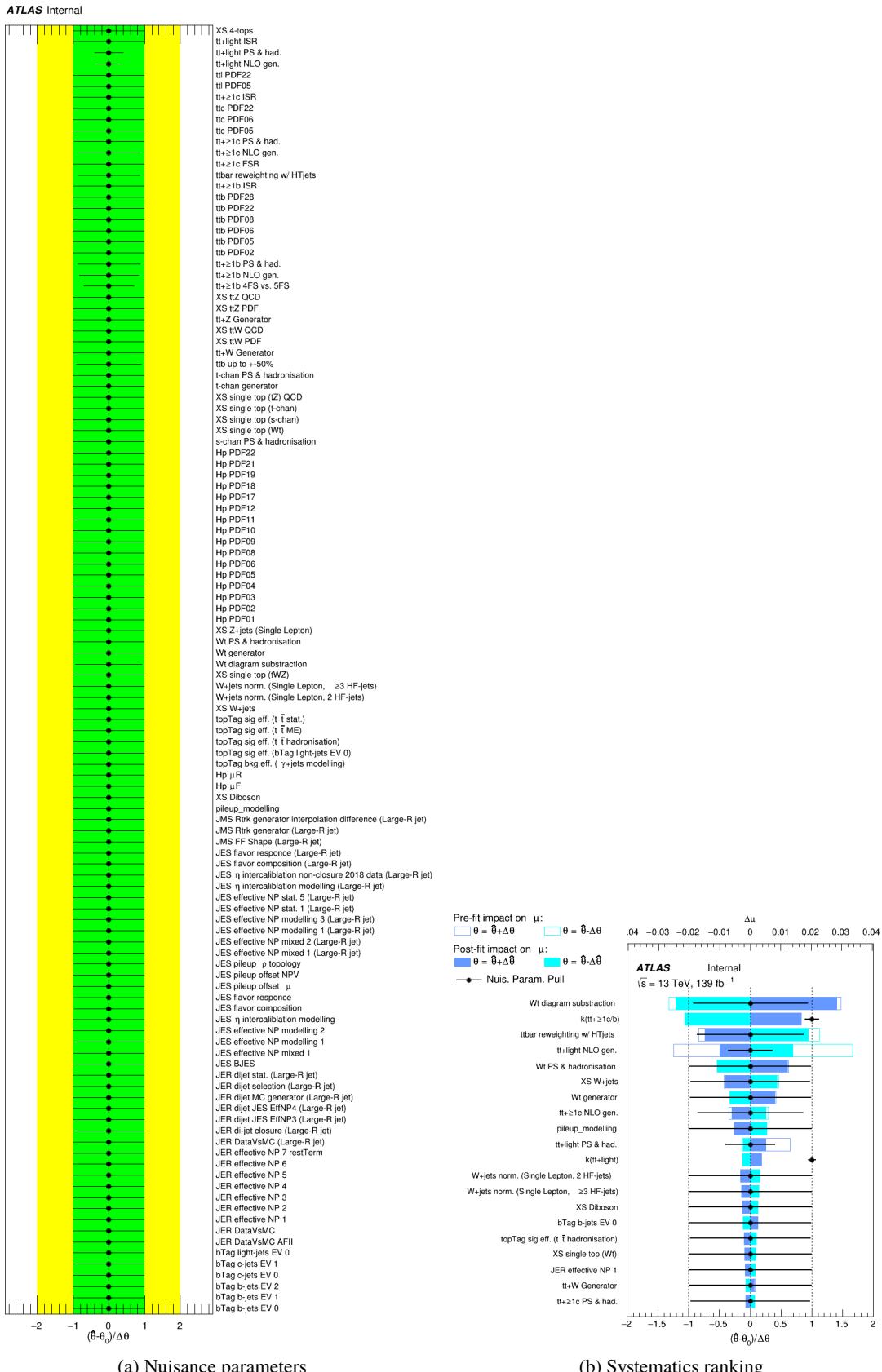
(a) Norm. factors

ATLAS Internal

	bTag b-jets EV 0	bTag b-jets EV 1	JES effective NP modelling 1	JES flavor composition	JES flavor response	JES pileup p topology	tive NP modelling 1 (Large-R jet)	calibration modelling (Large-R jet)	topTag sig eff. ($t\bar{t}$ hadronisation)	topTag sig eff. ($t\bar{t}$ ME)	topTag sig eff. ($t\bar{t}$ stat.)	Wt diagram subtraction	ttb up to +50%	tt+>1b 4FS vs. 5FS	tt+>1b NLO gen.	tt+>1b PS & had.	ttbar reweighting w/ HT jets	tt+>1c NLO gen.	tt+>1c PS & had.	tt PDF05	tt+light NLO gen.	tt+light PS & had.	μ_{H_p}	$k(t\bar{t}+\geq 1 c/b)$	$k(t\bar{t}+\text{light})$
bTag b-jets EV 0	100.0	-0.5	-0.9	-2.2	2.3	-1.1	-0.2	-0.4	0.7	-0.4	-0.5	0.1	-2.0	1.5	1.2	1.1	1.8	0.2	-0.7	0.3	7.3	-13.3	3.5	46.6	-16.7
bTag b-jets EV 1	-0.5	100.0	-0.4	-1.0	0.9	-0.4	-0.1	-0.2	0.3	-0.2	-0.2	-0.4	-0.4	0.9	-0.4	0.5	1.5	-0.0	-0.5	0.1	4.5	-7.0	2.5	22.3	-8.2
JES effective NP modelling 1	-0.9	-0.4	100.0	-2.8	2.5	-1.9	-0.1	-0.3	1.6	-0.3	-0.4	0.5	-1.5	0.1	3.4	0.9	0.2	1.9	-0.4	0.6	-4.9	-22.7	1.1	-0.9	-0.1
JES flavor composition	-2.2	-1.0	-2.8	100.0	5.5	-3.4	-0.3	-0.8	2.7	-0.8	-1.0	-0.7	-3.7	13.3	7.5	6.7	3.6	0.5	-1.2	1.0	-4.4	-40.9	0.7	-8.9	2.3
JES flavor response	2.3	0.9	2.5	5.5	100.0	3.2	0.4	0.8	-1.9	0.8	1.0	-0.2	4.9	-2.0	-5.0	-2.0	-2.8	0.3	1.5	-0.8	-6.1	31.0	-1.4	4.3	-1.4
JES pileup p topology	-1.1	-0.4	-1.9	-3.4	3.2	100.0	-0.1	-0.4	1.5	-0.4	-0.5	0.5	-2.2	-0.2	4.2	1.1	0.3	0.7	-0.6	0.6	-8.8	-25.7	-0.3	-30.4	10.7
tive NP modelling 1 (Large-R jet)	-0.2	-0.1	-0.1	-0.3	0.4	-0.1	100.0	-0.1	0.1	-0.1	-0.1	0.7	-0.9	0.1	0.8	0.2	-0.3	0.1	-0.1	0.0	1.8	-2.2	-1.0	-14.8	-37.6
calibration modelling (Large-R jet)	-0.4	-0.2	-0.3	-0.8	0.8	-0.4	-0.1	100.0	0.2	-0.1	-0.2	0.2	-0.7	0.8	1.0	0.5	0.3	0.1	-0.2	0.1	1.5	-3.8	0.4	8.4	-23.0
topTag sig eff. ($t\bar{t}$ hadronisation)	0.7	0.3	1.6	2.7	-1.9	1.5	0.1	0.2	100.0	0.2	0.3	-1.1	2.0	4.9	-3.0	-1.6	0.1	-6.7	-0.2	-1.0	-14.2	24.6	-1.3	11.7	-64.0
topTag sig eff. ($t\bar{t}$ ME)	-0.4	-0.2	-0.3	-0.8	0.8	-0.4	-0.1	-0.1	0.2	100.0	-0.2	0.3	-1.1	0.9	1.0	0.6	0.3	0.0	-0.2	0.1	2.2	-3.9	0.3	2.7	-25.4
topTag sig eff. ($t\bar{t}$ stat.)	-0.5	-0.2	-0.4	-1.0	1.0	-0.5	-0.1	-0.2	0.3	-0.2	100.0	0.6	-1.4	1.1	1.5	0.7	0.2	0.0	-0.3	0.1	2.4	-4.5	-0.4	2.1	-31.4
Wt diagram subtraction	0.1	-0.4	0.5	-0.7	-0.2	0.5	0.7	0.2	-1.1	0.3	0.6	100.0	8.4	7.8	-12.7	1.9	15.4	-9.5	-0.9	-0.6	-27.7	19.4	42.3	17.3	9.8
ttb up to +50%	-2.0	-0.4	-1.5	-3.7	4.9	-2.2	-0.9	-0.7	2.0	-1.1	-1.4	8.4	100.0	6.1	5.4	-1.1	-8.9	-1.7	-2.9	0.5	10.9	-14.1	-6.7	44.7	-14.7
tt+>1b 4FS vs. 5FS	1.5	0.9	0.1	13.3	-2.0	-0.2	0.1	0.8	-4.9	0.9	1.1	7.8	6.1	100.0	-38.1	-54.1	-8.3	0.8	-4.3	-1.0	-1.2	-12.3	2.9	10.2	0.9
tt+>1b NLO gen.	1.2	-0.4	3.4	7.5	-5.0	4.2	0.8	1.0	-3.0	1.0	1.5	-12.7	5.4	-38.1	100.0	-25.4	21.0	-13.8	-10.6	-2.2	4.8	-8.7	-1.3	-12.4	1.1
tt+>1b PS & had.	1.1	0.5	0.9	6.7	-2.0	1.1	0.2	0.5	-1.6	0.6	0.7	1.9	-1.1	-54.1	-25.4	100.0	-1.0	-1.4	-5.4	-0.9	-2.8	-0.4	1.2	1.0	0.5
ttbar reweighting w/ HT jets	1.8	1.5	0.2	3.6	-2.8	0.3	-0.3	0.3	-0.1	0.3	0.2	15.4	-8.9	-8.3	21.0	-1.0	100.0	10.5	5.2	0.3	-20.1	22.2	-19.3	-44.5	20.8
tt+>1c NLO gen.	0.2	-0.0	1.9	0.5	0.3	0.7	0.1	0.1	-6.7	0.0	0.0	-9.5	-1.7	0.8	-13.8	-1.4	10.5	100.0	-7.3	-2.5	-60.6	17.7	-5.4	-7.8	3.5
tt+>1c PS & had.	-0.7	-0.5	-0.4	-1.2	1.5	-0.6	-0.1	-0.2	-0.2	-0.2	-0.3	-0.9	-2.9	-4.3	-10.6	-5.4	5.2	-7.3	100.0	-0.4	-9.6	-22.7	-3.5	-4.2	1.5
tt PDF05	0.3	0.1	0.6	1.0	-0.8	0.6	0.0	0.1	-1.0	0.1	0.1	-0.6	0.5	-1.0	-2.2	-0.9	0.3	-2.5	-0.4	100.0	-5.0	7.9	-0.8	-1.2	27.2
tt+light NLO gen.	7.3	4.5	-4.9	-4.4	-6.1	-8.8	1.8	1.5	-14.2	2.2	2.4	-27.7	10.9	-1.2	4.8	-2.8	-20.1	-60.6	-9.6	-5.0	100.0	-39.6	-20.6	15.5	-10.8
tt+light PS & had.	-13.3	-7.0	-22.7	-40.9	31.0	-25.7	-2.2	-3.8	24.6	-3.9	-4.5	19.4	-14.1	-12.3	-8.7	-0.4	22.2	17.7	-22.7	7.9	-39.6	100.0	11.0	-15.2	2.9
μ_{H_p}	3.5	2.5	1.1	0.7	-1.4	-0.3	-1.0	0.4	-1.3	0.3	-0.4	42.3	-6.7	2.9	-1.3	1.2	-19.3	-5.4	-3.5	-0.8	-20.6	11.0	100.0	18.0	5.4
$k(t\bar{t}+\geq 1 c/b)$	46.6	22.3	-0.9	-8.9	4.3	-30.4	-14.8	8.4	-11.7	2.7	2.1	17.3	44.7	10.2	-12.4	1.0	-44.5	-7.8	-4.2	-1.2	15.5	-15.2	18.0	100.0	-20.0
$k(t\bar{t}+\text{light})$	-16.7	-8.2	-0.1	2.3	-1.4	10.7	-37.6	-23.0	-64.0	25.4	-31.4	9.8	-14.7	0.9	1.1	0.5	20.8	3.5	1.5	27.2	-10.8	2.9	5.4	-20.0	100.0

(b) Correlation matrix

Figure 66: Signal strength and normalization factors (top) and correlation matrix (bottom) for the 2000 GeV H^+ mass hypotheses.

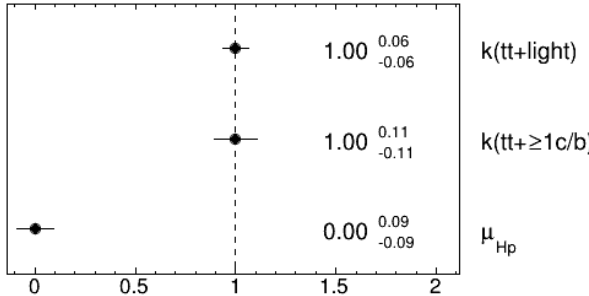


(a) Nuisance parameters

(b) Systematics ranking

Figure 67: Nuisance parameters (left) and ranking plot (right) of the effect of various nuisance parameters before and after the fit for the 2500 GeV H^+ mass hypotheses.
22nd March 2023 – 00:45

ATLAS Internal



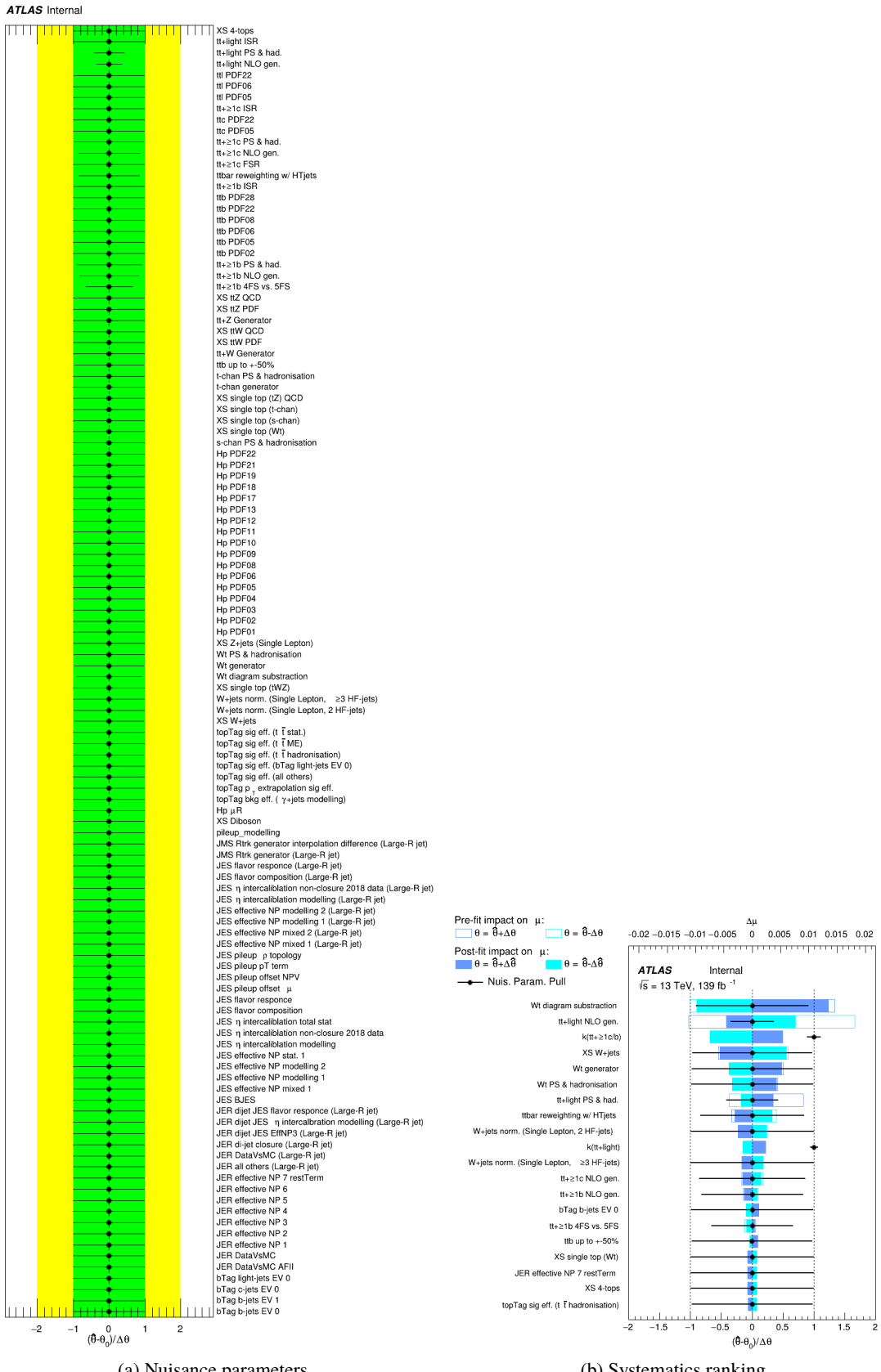
(a) Norm. factors

ATLAS Internal

	bTag b-jets EV 0	bTag b-jets EV 1	JES effective NP modelling 1	JES flavor composition	JES flavor response	JES pileup p topology	tive NP modelling 1 (Large-R jet)	calibration modelling (Large-R jet)	topTag sig eff. ($t\bar{t}$ hadronisation)	topTag sig eff. ($t\bar{t}$ ME)	topTag sig eff. ($t\bar{t}$ stat.)	Wt diagram subtraction	tbt up to +50%	tbt+>1b 4FS vs. 5FS	tbt+>1b NLO gen.	tbt+>1b PS & had.	tbt reweighting w/ HT jets	tbt+>1c NLO gen.	tbt+>1c PS & had.	tt PDF05	tt+light NLO gen.	tt+light PS & had.	μ_{H_p}	k($t\bar{t} + \geq 1 c/b$)	k($t\bar{t}$ +light)
bTag b-jets EV 0	100.0	-0.6	-1.1	-2.6	2.4	-1.3	-0.2	-0.4	0.7	-0.4	-0.5	-0.3	-2.0	2.8	1.3	1.3	1.9	0.8	-0.4	0.4	6.4	-12.4	2.6	46.5	-16.7
bTag b-jets EV 1	-0.6	100.0	-0.5	-1.2	1.1	-0.6	-0.1	-0.2	0.4	-0.2	-0.2	-0.2	-0.9	0.8	0.2	0.3	1.1	0.3	-0.3	0.2	3.5	-6.3	1.4	22.5	-8.1
JES effective NP modelling 1	-1.1	-0.5	100.0	-3.1	2.5	-2.0	-0.1	-0.4	1.6	-0.3	-0.4	0.4	-2.1	0.6	1.8	-0.0	0.0	2.4	-0.3	0.6	-4.9	-22.2	1.1	-1.2	0.1
JES flavor composition	-2.6	-1.2	-3.1	100.0	5.7	-3.7	-0.3	-0.9	2.6	-0.9	-1.0	-0.1	-4.6	8.0	5.1	3.5	2.5	1.9	-1.4	1.0	-4.2	-41.1	1.1	-8.6	2.7
JES flavor response	2.4	1.1	2.5	5.7	100.0	3.2	0.3	0.8	-1.9	0.8	1.0	0.5	5.3	-3.4	-2.6	-1.0	-2.9	-0.2	1.7	-0.8	-6.3	30.6	-1.6	4.7	-1.5
JES pileup p topology	-1.3	-0.6	-2.0	-3.7	3.2	100.0	-0.1	-0.4	1.5	-0.4	-0.5	0.4	-3.3	0.2	2.4	-0.2	-0.4	1.3	-0.6	0.6	-8.9	-25.2	-0.2	-30.6	10.9
tive NP modelling 1 (Large-R jet)	-0.2	-0.1	-0.1	-0.3	0.3	-0.1	100.0	-0.0	0.2	-0.0	-0.0	0.6	-0.8	-0.5	0.1	-0.1	-0.3	-0.1	-0.2	-0.0	2.5	-2.6	-1.0	-14.8	-37.7
calibration modelling (Large-R jet)	-0.4	-0.2	-0.4	-0.9	0.8	-0.4	-0.0	100.0	0.3	-0.1	-0.2	0.1	-0.8	1.0	0.7	0.4	0.3	0.2	-0.1	0.1	1.5	-3.7	0.2	8.4	-23.0
topTag sig eff. ($t\bar{t}$ hadronisation)	0.7	0.4	1.6	2.6	-1.9	1.5	0.2	0.3	100.0	0.3	0.3	-1.5	0.2	2.7	-2.2	-0.8	-0.9	-6.9	-0.0	-1.0	-15.1	25.3	-2.2	-12.1	64.0
topTag sig eff. ($t\bar{t}$ ME)	-0.4	-0.2	-0.3	-0.9	0.8	-0.4	-0.0	-0.1	0.3	100.0	-0.2	0.2	-1.0	0.9	0.7	0.4	0.3	0.1	-0.2	0.1	2.3	-3.9	0.1	2.6	-25.4
topTag sig eff. ($t\bar{t}$ stat.)	-0.5	-0.2	-0.4	-1.0	1.0	-0.5	-0.0	-0.2	0.3	-0.2	100.0	0.3	-1.4	1.1	1.0	0.5	0.1	0.1	-0.2	0.1	2.6	-4.5	-0.5	2.0	-31.4
Wt diagram subtraction	-0.3	-0.2	0.4	-0.1	0.5	0.4	0.6	0.1	-1.5	0.2	0.3	100.0	5.4	3.3	-8.8	0.0	14.1	-8.2	-1.7	-0.7	-32.3	20.3	33.0	18.6	10.5
tbt up to +50%	-2.0	-0.9	-2.1	-4.6	5.3	-3.3	-0.8	-0.8	0.2	-1.0	-1.4	5.4	100.0	-4.0	10.6	-1.6	-10.9	-2.0	-1.7	0.5	15.7	-16.0	0.8	46.4	-14.7
tbt+>1b 4FS vs. 5FS	2.8	0.8	0.6	8.0	-3.4	0.2	-0.5	1.0	-2.7	0.9	1.1	3.3	-4.0	100.0	-45.1	-50.5	-6.3	-5.7	-2.9	-1.3	2.7	-7.8	-0.9	4.3	0.5
tbt+>1b NLO gen.	1.3	0.2	1.8	5.1	-2.6	2.4	0.1	0.7	-2.2	0.7	1.0	-8.8	10.6	-45.1	100.0	-25.3	22.9	-13.7	-6.1	-1.4	3.9	-6.1	-0.3	-9.9	0.7
tbt+>1b PS & had.	1.3	0.3	-0.0	3.5	-1.0	-0.2	-0.1	0.4	-0.8	0.4	0.5	0.0	-1.6	-50.5	-25.3	100.0	-0.9	-3.0	-2.0	-0.6	-1.1	2.2	-1.4	0.6	-0.0
tbt reweighting w/ HT jets	1.9	1.1	0.0	2.5	-2.9	-0.4	-0.3	0.3	-0.9	0.3	0.1	14.1	-10.9	-6.3	22.9	-0.9	100.0	11.0	5.9	0.2	-22.0	24.1	-18.3	-42.9	21.1
tbt+>1c NLO gen.	0.8	0.3	2.4	1.9	-0.2	1.3	-0.1	0.2	-6.9	0.1	0.1	-8.2	-2.0	-5.7	-13.7	-3.0	11.0	100.0	-8.6	-2.7	-57.4	14.5	-6.5	-7.5	3.8
tbt+>1c PS & had.	-0.4	-0.3	-0.3	-1.4	1.7	-0.6	-0.2	-0.1	-0.0	-0.2	-0.2	-1.7	-2.9	-6.1	-2.0	5.9	-8.6	100.0	-0.3	-9.7	-21.7	-1.6	-4.1	1.1	
tt PDF05	0.4	0.2	0.6	1.0	-0.8	0.6	-0.0	0.1	-1.0	0.1	0.1	-0.7	0.5	-1.3	-1.4	-0.6	0.2	-2.7	-0.3	100.0	-4.9	7.7	-0.7	-1.1	27.1
tt+light NLO gen.	6.4	3.5	-4.9	-4.2	-6.3	-8.9	2.5	1.5	-15.1	2.3	2.6	-32.3	15.7	2.7	3.9	-1.1	-22.0	-57.4	-9.7	-4.9	100.0	-40.6	-14.3	16.0	-11.4
tt+light PS & had.	-12.4	-6.3	-22.2	-41.1	30.6	-25.2	-2.6	-3.7	25.3	-3.9	-4.5	20.3	-16.0	-7.8	-6.1	2.2	24.1	14.5	-21.7	7.7	-40.6	100.0	5.0	-15.8	2.6
μ_{H_p}	2.6	1.4	1.1	1.1	-1.6	-0.2	-1.0	0.2	-2.2	0.1	-0.5	33.0	0.8	-0.9	-0.3	-1.4	-18.3	-6.5	-1.6	-0.7	-14.3	5.0	100.0	20.4	4.4
k($t\bar{t} + \geq 1 c/b$)	46.5	22.5	-1.2	-8.6	4.7	-30.6	-14.8	8.4	-12.1	2.6	2.0	18.6	46.4	4.3	-9.9	0.6	-42.9	-7.5	-4.1	-1.1	16.0	-15.8	20.4	100.0	-19.7
k($t\bar{t}$ +light)	-16.7	-8.1	0.1	2.7	-1.5	10.9	-37.7	-23.0	-64.0	25.4	-31.4	10.5	-14.7	0.5	0.7	-0.0	21.1	3.8	1.1	27.1	-11.4	2.6	4.4	-19.7	100.0

(b) Correlation matrix

Figure 68: Signal strength and normalization factors (top) and correlation matrix (bottom) for the 2500 GeV H^+ mass hypotheses.

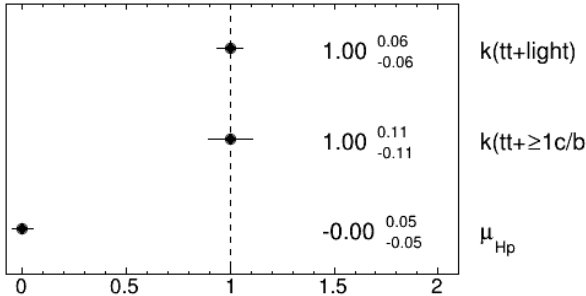


(a) Nuisance parameters

(b) Systematics ranking

Figure 69: Nuisance parameters (left) and ranking plot (right) of the effect of various nuisance parameters before and after the fit for the 3000 GeV H^+ mass hypotheses.
22nd March 2023 – 00:45

ATLAS Internal



(a) Norm. factors

ATLAS Internal

	bTag b-jets EV 0	bTag b-jets EV 1	JES effective NP modelling 1	JES flavor composition	JES flavor response	JES pileup p topology	tive NP modelling 1 (Large-R jet)	calibration modelling (Large-R jet)	topTag sig eff. ($t\bar{t}$ hadronisation)	topTag sig eff. ($t\bar{t}$ ME)	topTag sig eff. ($t\bar{t}$ stat.)	Wt diagram subtraction	tbt up to +50%	tbt up to 4FS vs. 5FS	tbt ≥ 1b NLO gen.	tbt ≥ 1b PS & had.	tbt reweighting w/ HT jets	tbt ≥ 1c NLO gen.	tbt ≥ 1c PS & had.	tbt PDF05	tbt-light NLO gen.	tbt-light PS & had.	μ_{H_p}	$k(t\bar{t}+\geq 1c/b)$	$k(t\bar{t}+\text{light})$
bTag b-jets EV 0	100.0	-0.6	-0.9	-2.1	2.3	-1.0	-0.2	-0.5	0.7	-0.5	-0.5	-0.3	-2.0	0.9	1.5	1.1	1.7	0.4	-0.6	0.3	7.0	-13.0	2.2	47.0	-16.7
bTag b-jets EV 1	-0.6	100.0	-0.4	-1.0	1.1	-0.5	-0.1	-0.2	0.3	-0.2	-0.2	-0.3	-0.9	0.3	0.3	0.4	1.2	0.1	-0.4	0.2	3.9	-6.5	1.1	22.6	-8.1
JES effective NP modelling 1	-0.9	-0.4	100.0	-2.5	2.1	-1.5	-0.1	-0.3	1.6	-0.3	-0.3	-0.2	-1.0	0.7	1.2	0.6	1.3	1.6	-0.8	0.5	-3.3	-22.9	1.2	-1.6	-0.1
JES flavor composition	-2.1	-1.0	-2.5	100.0	5.0	-3.0	-0.3	-0.8	2.4	-0.7	-0.8	-1.2	-3.8	12.1	3.9	4.2	3.5	0.4	-2.2	0.8	-2.2	-41.4	0.2	-9.1	2.4
JES flavor response	2.3	1.1	2.1	5.0	100.0	2.8	0.4	0.9	-2.0	0.8	1.0	0.7	4.3	-2.7	-3.5	-1.4	-2.2	-0.3	1.9	-0.7	-6.0	30.7	-1.0	4.2	-1.2
JES pileup p topology	-1.0	-0.5	-1.5	-3.0	2.8	100.0	-0.1	-0.4	1.6	-0.3	-0.4	-0.2	-1.8	0.1	1.3	-0.1	0.3	0.8	-1.4	0.4	-7.6	-26.0	-0.7	-30.6	10.6
tive NP modelling 1 (Large-R jet)	-0.2	-0.1	-0.1	-0.3	0.4	-0.1	100.0	-0.1	0.1	-0.1	-0.1	-0.8	-0.7	-0.2	0.6	0.1	-0.5	0.2	-0.1	0.0	1.8	-2.2	-1.1	-14.8	-37.7
calibration modelling (Large-R jet)	-0.5	-0.2	-0.3	-0.8	0.9	-0.4	-0.1	100.0	0.2	-0.2	-0.2	0.2	-1.0	2.1	2.2	1.1	-0.9	0.5	0.1	0.1	-0.1	-3.0	-0.2	9.0	-23.0
topTag sig eff. ($t\bar{t}$ hadronisation)	0.7	0.3	1.6	2.4	-2.0	1.6	0.1	0.2	100.0	0.2	0.2	1.7	0.5	0.3	-1.9	0.5	0.3	-7.1	0.3	-1.0	-16.7	25.2	-1.5	-12.8	63.9
topTag sig eff. ($t\bar{t}$ ME)	-0.5	-0.2	-0.3	-0.7	0.8	-0.3	-0.1	-0.2	0.2	100.0	-0.2	0.2	-0.8	0.6	0.7	0.5	0.3	0.1	-0.2	0.1	2.4	-4.0	-0.0	2.7	-25.4
topTag sig eff. ($t\bar{t}$ stat.)	-0.5	-0.2	-0.3	-0.8	1.0	-0.4	-0.1	-0.2	0.2	-0.2	100.0	0.5	-1.1	0.7	1.0	0.6	0.2	0.1	-0.2	0.1	2.6	-4.7	-0.5	2.1	-31.4
Wt diagram subtraction	-0.3	-0.3	-0.2	-1.2	0.7	0.2	0.8	0.2	-1.7	0.2	0.5	100.0	3.7	8.6	-6.5	0.3	12.4	-9.7	-2.1	-0.7	-31.8	20.4	25.6	18.7	9.5
tbt up to +50%	-2.0	-0.9	-1.0	-3.8	4.3	-1.8	-0.7	-1.0	0.5	-0.8	-1.1	3.7	100.0	6.0	4.4	2.7	-2.0	-1.2	-1.2	0.4	18.4	-17.7	2.0	44.2	-15.0
tbt up to 4FS vs. 5FS	0.9	0.3	0.7	12.1	-2.7	0.1	-0.2	2.1	0.3	0.6	0.7	8.6	6.0	100.0	-40.0	-45.1	2.5	-0.1	-4.3	-0.9	-5.3	-6.7	1.8	4.8	0.0
tbt ≥ 1b NLO gen.	1.5	0.3	1.2	3.9	-3.5	1.3	0.6	2.2	-1.9	0.7	1.0	-6.5	4.4	-40.0	100.0	-22.4	28.1	-17.5	-9.6	-1.5	3.9	-1.4	-2.7	-12.7	1.9
tbt ≥ 1b PS & had.	1.1	0.4	0.6	4.2	-1.4	-0.1	0.1	1.1	0.5	0.5	0.6	0.3	2.7	-45.1	-22.4	100.0	1.9	-1.4	-4.5	-0.5	-4.9	3.9	-1.0	1.2	-1.2
tbt reweighting w/ HT jets	1.7	1.2	1.3	3.5	-2.2	0.3	-0.5	-0.9	0.3	0.3	0.2	12.4	-2.0	2.5	28.1	1.9	100.0	18.7	7.3	0.4	-30.9	24.6	-6.6	-39.9	19.3
tbt ≥ 1c NLO gen.	0.4	0.1	1.6	0.4	-0.3	0.8	0.2	0.5	-7.1	0.1	0.1	-9.7	-1.2	-0.1	-17.5	-1.4	18.7	100.0	-7.2	-2.4	-55.3	15.9	-3.4	-11.6	4.6
tbt ≥ 1c PS & had.	-0.6	-0.4	-0.8	-2.2	1.9	-1.4	-0.1	0.1	0.3	-0.2	-0.2	-2.1	-1.2	-4.3	-9.6	-4.5	7.3	-7.2	100.0	-0.2	-8.5	-20.6	-0.8	-4.6	1.0
tbt PDF05	0.3	0.2	0.5	0.8	-0.7	0.4	0.0	0.1	-1.0	0.1	0.1	-0.7	0.4	-0.9	-1.5	-0.5	0.4	-2.4	-0.2	100.0	0.5	8.0	-0.5	-1.2	27.2
tbt-light NLO gen.	7.0	3.9	-3.3	-2.2	-6.0	-7.6	1.8	-0.1	-15.7	2.4	2.6	-31.8	18.4	-5.3	3.9	-4.9	-30.9	-55.3	-8.5	-5.2	100.0	-44.5	-13.5	21.8	-12.2
tbt-light PS & had.	-13.0	-6.5	-22.9	-41.4	30.7	-26.0	-2.2	-3.0	25.2	-4.0	-4.7	20.4	-17.7	-6.7	-1.4	3.9	24.6	15.9	-20.6	8.0	-44.5	100.0	6.5	-17.1	3.0
μ_{H_p}	2.2	1.1	1.2	0.2	-1.0	-0.7	-1.1	-0.2	-1.5	-0.0	-0.5	25.6	2.0	1.8	-2.7	-1.0	-6.6	-3.4	-0.8	-0.5	-13.5	6.5	100.0	13.9	4.9
$k(t\bar{t}+\geq 1c/b)$	47.0	22.6	-1.6	-9.1	4.2	-30.6	-14.8	9.0	-12.8	2.7	2.1	18.7	44.2	4.8	-12.7	1.2	-39.9	-11.6	-4.6	-1.2	21.6	-17.1	13.9	100.0	-19.5
$k(t\bar{t}+\text{light})$	-16.7	-8.1	-0.1	2.4	-1.2	10.6	-37.7	-23.0	-63.9	25.4	-31.4	9.5	-15.0	0.0	1.9	-1.2	19.3	4.6	1.0	27.2	-12.2	3.0	4.9	-19.5	100.0

(b) Correlation matrix

Figure 70: Signal strength and normalization factors (top) and correlation matrix (bottom) for the 3000 GeV H^+ mass hypotheses.

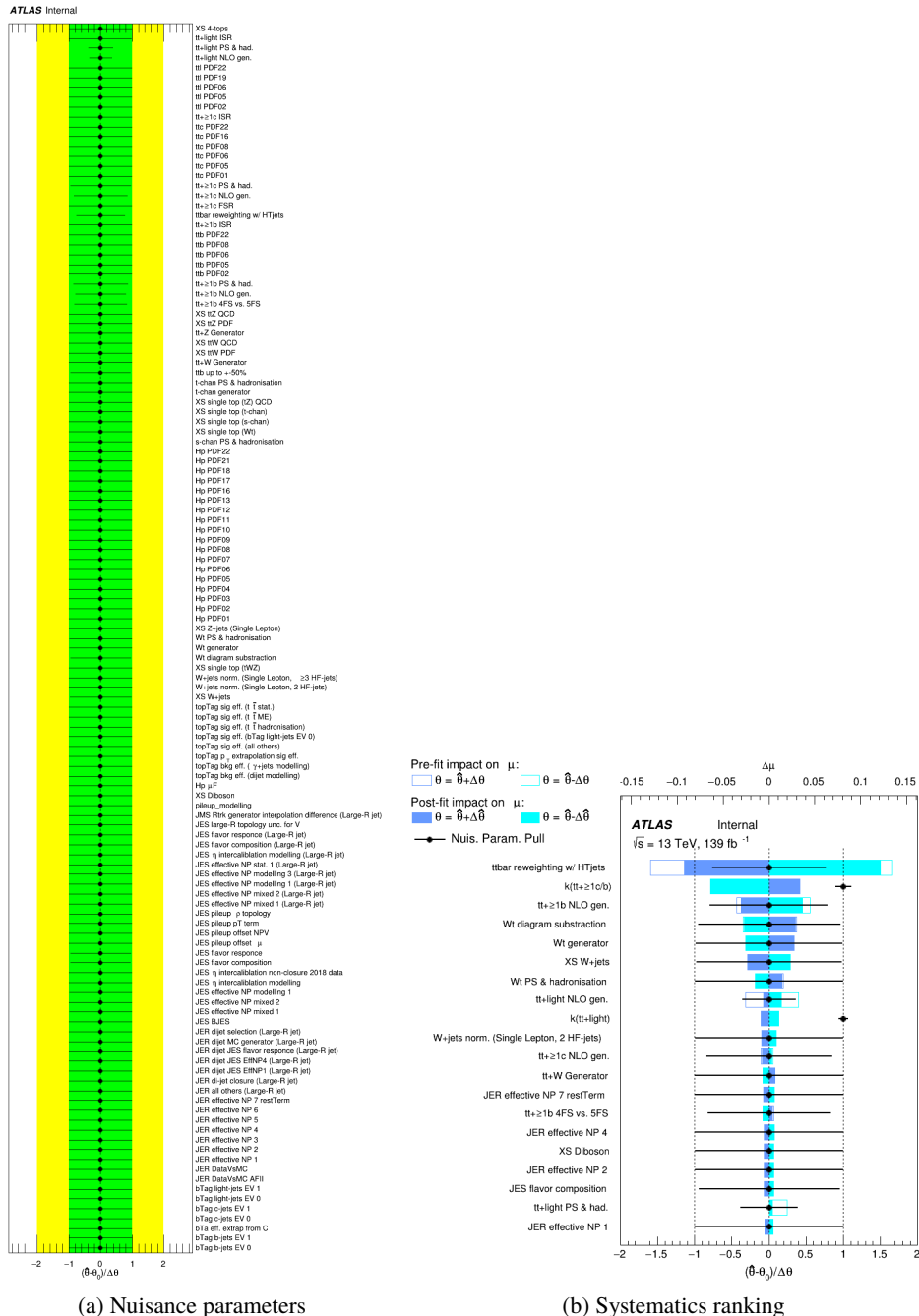
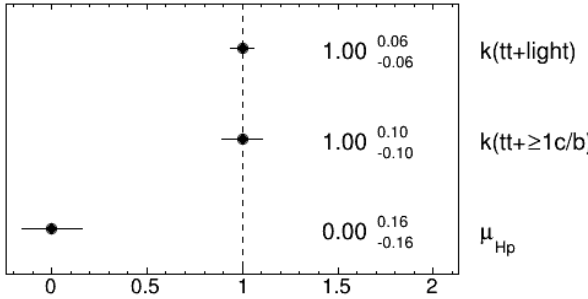


Figure 71: Nuisance parameters (left) and ranking plot (right) of the effect of various nuisance parameters before and after the fit for the 4000 GeV H^+ mass hypotheses.

ATLAS Internal

(a) Norm. factors

ATLAS Internal

	bTag b-jets EV 0	bTag b-jets EV 1	JES flavor composition	JES flavor response	JES pileup p topology	ive NP modelling 1 (Large-R jet)	alibration modelling (Large-R jet)	topTag sig eff. ($t\bar{t}$ hadronisation)	topTag sig eff. ($t\bar{t}$ TME)	topTag sig eff. ($t\bar{t}$ stat.)	XS W+jets	Wt diagram subtraction	t \bar{t} up to +50%	t \bar{t} + ≥ 1 b 4FS vs. 5FS	t \bar{t} + ≥ 1 b NLO gen.	t \bar{t} + ≥ 1 b PS & had.	t \bar{t} reweighting w/ HT jets	t \bar{t} + ≥ 1 c NLO gen.	t \bar{t} + ≥ 1 c PS & had.	t \bar{t} PDF05	t \bar{t} +light NLO gen.	t \bar{t} +light PS & had.	μ_{H_p}	k($t\bar{t} + \geq 1 c/b$)	k($t\bar{t} + \text{light}$)
bTag b-jets EV 0	100.0	-0.7	-4.5	3.4	-1.7	-0.2	-0.5	1.7	-0.6	-0.7	0.5	-1.4	-1.5	7.3	-0.9	5.0	5.0	2.9	0.1	0.3	3.3	-9.0	-2.2	46.5	-17.1
bTag b-jets EV 1	-0.7	100.0	-1.2	1.1	-0.5	-0.1	-0.2	0.4	-0.2	-0.2	-0.1	0.0	-0.6	1.1	-0.2	0.8	1.4	0.2	-0.3	0.1	3.4	-6.6	2.0	23.4	-8.2
JES flavor composition	-4.5	-1.2	100.0	8.4	-5.3	-0.4	-1.0	4.2	-1.0	-1.3	1.0	-1.5	-1.6	14.3	7.1	11.1	2.8	4.0	0.5	0.9	-9.4	-36.6	-3.0	-9.1	1.3
JES flavor response	3.4	1.1	8.4	100.0	4.3	0.3	0.9	-2.9	0.9	1.2	-0.8	1.3	2.0	-10.6	-6.5	-8.2	0.7	-0.3	0.2	-0.7	-1.7	27.2	-0.7	2.6	0.1
JES pileup p topology	-1.7	-0.5	-5.3	4.3	100.0	-0.1	-0.5	2.0	-0.4	-0.5	0.5	-0.2	-0.2	6.2	6.3	5.4	-1.1	0.8	0.3	0.5	-11.3	-23.2	-0.5	-30.7	9.9
ive NP modelling 1 (Large-R jet)	-0.2	-0.1	-0.4	0.3	-0.1	100.0	-0.0	0.2	-0.0	-0.0	-0.2	0.2	-0.4	0.5	0.4	0.5	-0.1	0.1	-0.1	-0.0	2.2	-2.5	-0.5	-15.5	-37.9
alibration modelling (Large-R jet)	-0.5	-0.2	-1.0	0.9	-0.5	-0.0	100.0	0.4	-0.1	-0.2	0.1	-0.2	-0.4	1.0	0.0	0.7	0.2	0.2	-0.2	0.1	1.7	-3.9	-0.4	8.8	-23.3
topTag sig eff. ($t\bar{t}$ hadronisation)	1.7	0.4	4.2	-2.9	2.0	0.2	0.4	100.0	0.4	0.5	0.7	-1.0	0.2	-7.0	-3.3	-4.3	-1.8	-8.5	-1.0	-1.0	-10.7	22.5	2.2	-1.7	-64.3
topTag sig eff. ($t\bar{t}$ TME)	-0.6	0.2	-1.0	0.9	-0.4	0.0	-0.1	0.4	100.0	0.2	-0.0	-0.0	0.5	1.1	0.0	0.8	0.5	0.1	-0.2	0.1	2.5	-4.1	0.1	2.7	-25.6
topTag sig eff. ($t\bar{t}$ stat.)	-0.7	-0.2	-1.3	1.2	-0.5	-0.0	-0.2	0.5	-0.2	100.0	0.0	-0.2	-0.7	1.4	0.1	1.0	0.1	0.2	-0.3	0.1	2.9	-4.8	-1.3	2.1	-31.8
XS W+jets	0.5	-0.1	1.0	-0.8	0.5	-0.2	0.1	0.7	-0.0	0.0	100.0	4.6	-1.8	-0.2	2.9	0.4	-1.2	3.4	0.2	0.5	20.6	-20.3	-14.6	-8.8	-11.0
Wt diagram subtraction	-1.4	0.0	-1.5	1.3	-0.2	0.2	-0.2	-1.0	-0.0	-0.2	4.6	100.0	-0.3	1.6	-10.9	-1.4	3.7	-7.3	-2.0	-0.9	-37.5	25.6	19.0	23.5	10.8
t \bar{t} up to +50%	-1.5	-0.6	-1.6	2.0	-0.2	-0.4	0.2	0.5	-0.7	-1.8	-0.3	100.0	-6.0	-10.2	-6.2	-2.8	-2.4	-5.6	0.1	31.7	-30.3	-0.1	43.2	-15.7	
t \bar{t} + ≥ 1 b 4FS vs. 5FS	7.3	1.1	14.3	-10.6	6.2	0.5	1.0	-7.0	1.1	1.4	-0.2	1.6	-6.0	100.0	-26.4	-36.3	-6.1	-16.2	-12.5	-1.0	5.2	-15.4	3.6	3.8	2.5
t \bar{t} + ≥ 1 b NLO gen.	-0.9	-0.2	7.1	-6.5	6.3	0.4	0.0	-3.3	0.0	0.1	2.9	-10.9	-10.2	26.4	100.0	-29.7	24.9	-9.5	-14.1	-1.6	-6.6	-2.3	-23.5	-20.5	6.0
t \bar{t} + ≥ 1 b PS & had.	5.0	0.8	11.1	-8.2	5.4	0.5	0.7	-4.3	0.8	1.0	0.4	-1.4	-6.2	-36.3	-29.7	100.0	-2.2	-11.8	-12.1	-0.7	9.6	-12.3	1.4	-0.5	1.8
t \bar{t} reweighting w/ HT jets	5.0	1.4	2.8	0.7	-1.1	-0.1	0.2	-1.8	0.5	0.1	-1.2	3.7	-2.8	-6.1	24.9	-2.2	100.0	1.1	1.3	0.4	-11.3	16.3	-77.2	-36.0	15.6
t \bar{t} + ≥ 1 c NLO gen.	2.9	0.2	4.0	-0.3	0.8	0.1	0.2	-8.5	0.1	0.2	3.4	-7.3	-2.4	-16.2	-9.5	-11.8	1.1	100.0	-9.0	-2.1	-52.8	9.0	-3.9	-1.3	3.1
t \bar{t} + ≥ 1 c PS & had.	0.1	-0.3	0.5	0.2	0.3	-0.1	-0.2	-1.0	-0.2	-0.3	0.2	-2.0	-5.6	-12.5	-14.1	-12.1	1.3	-9.0	100.0	-0.2	-2.8	-30.5	-0.7	-3.7	1.8
t \bar{t} PDF05	0.3	0.1	0.9	-0.7	0.5	-0.0	0.1	-1.0	0.1	0.1	0.5	-0.9	0.1	-1.0	-1.6	-0.7	0.4	-2.1	-0.2	100.0	-5.1	8.6	-0.0	-1.6	27.3
t \bar{t} +light NLO gen.	3.3	3.4	-9.4	-1.7	-11.3	2.2	1.7	-10.7	2.5	2.9	20.6	-37.5	31.7	5.2	-6.6	9.6	-11.3	-52.8	-2.8	-5.1	100.0	-38.3	-7.7	13.6	-16.2
t \bar{t} +light PS & had.	-9.0	-6.6	-36.6	27.2	-23.2	-2.5	-3.9	22.5	-4.1	-4.8	-20.3	25.6	-30.3	-15.4	-2.3	-12.3	16.3	9.0	-30.5	8.6	-38.3	100.0	0.8	-13.9	6.8
μ_{H_p}	-2.2	2.0	-3.0	-0.7	-0.5	-0.5	-0.4	2.2	0.1	-1.3	-14.6	19.0	-0.1	3.6	-23.5	1.4	-77.2	-3.9	-0.7	-0.0	-7.7	0.8	100.0	37.6	-5.8
k($t\bar{t} + \geq 1 c/b$)	46.5	23.4	-9.1	2.6	-30.7	-15.5	8.8	-11.7	2.7	2.1	-8.8	23.5	43.2	3.8	-20.5	-0.5	-36.0	-1.3	-3.7	-1.6	13.6	-13.9	37.6	100.0	-16.8
k($t\bar{t} + \text{light}$)	-17.1	-8.2	1.3	0.1	9.9	-37.9	-23.3	-64.3	-25.6	-31.8	-11.0	10.8	-15.7	2.5	6.0	1.8	15.6	3.1	1.8	27.3	-16.2	6.8	-5.8	-16.8	100.0

(b) Correlation matrix

Figure 72: Signal strength and normalization factors (top) and correlation matrix (bottom) for the 4000 GeV H^+ mass hypotheses.

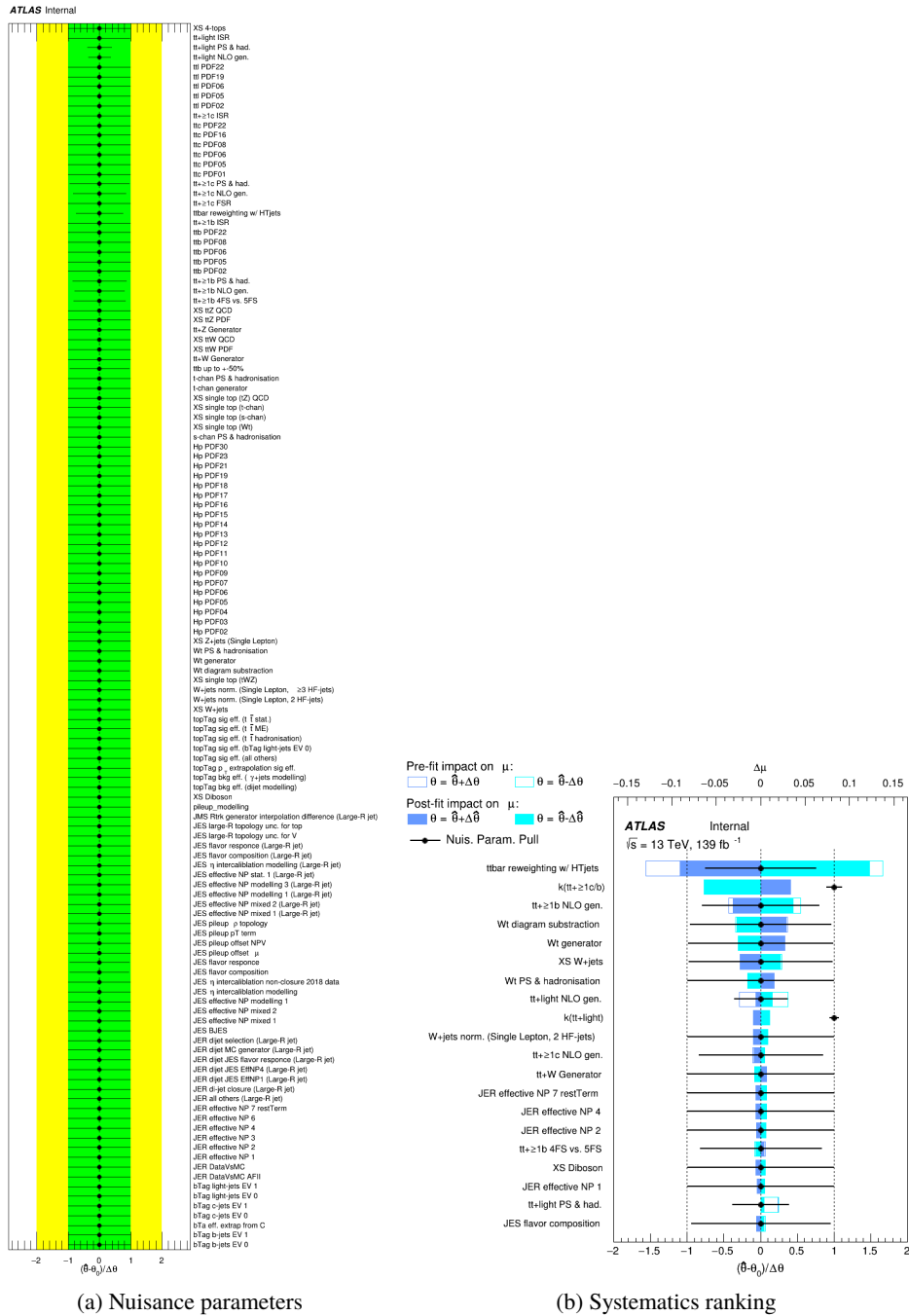
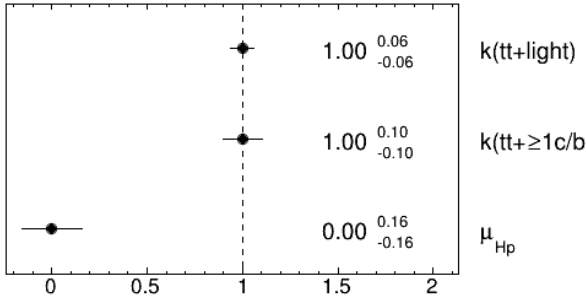


Figure 73: Nuisance parameters (left) and ranking plot (right) of the effect of various nuisance parameters before and after the fit for the 5000 GeV H^+ mass hypotheses.

ATLAS Internal

(a) Norm. factors

ATLAS Internal

	bTag b-jets EV 0	bTag b-jets EV 1	JES flavor composition	JES flavor response	JES pileup p topology	ative NP modelling 1 (Large-R jet)	calibration modelling (Large-R jet)	topTag sig eff. ($t\bar{t}$ hadronisation)	topTag sig eff. ($t\bar{t}$ TME)	topTag sig eff. ($t\bar{t}$ stat.)	XS W+jets	Wt diagram subtraction	tbt up to +50%	tt+>1b 4FS vs. 5FS	tt+>1b NLO gen.	tt+>1b PS & had.	ttbar reweighting w/ HT jets	tt+>1c NLO gen.	tt+>1c PS & had.	tt PDF05	tt+light NLO gen.	tt+light PS & had.	μ_{H_p}	k(tt+ge1c/b)	k(tt+light)
bTag b-jets EV 0	100.0	-0.7	-4.5	3.4	-1.7	-0.2	-0.5	1.7	-0.6	-0.7	0.5	-1.4	-1.5	7.3	-0.9	5.0	5.1	2.9	0.1	0.3	3.3	-8.9	-2.2	46.5	-17.1
bTag b-jets EV 1	-0.7	100.0	-1.2	1.1	-0.5	-0.1	-0.2	0.4	-0.2	-0.2	-0.1	0.0	-0.6	1.1	-0.2	0.8	1.5	0.2	-0.3	0.1	3.5	-6.6	2.0	23.3	-8.1
JES flavor composition	-4.5	-1.2	100.0	8.4	-5.3	-0.4	-1.0	4.2	-1.0	-1.3	1.0	-1.5	-1.7	14.3	7.1	11.1	2.7	4.0	0.5	0.9	-9.5	-36.6	-2.9	-9.1	1.3
JES flavor response	3.4	1.1	8.4	100.0	4.3	0.3	0.9	-2.9	0.9	1.2	-0.8	1.2	2.0	-10.6	-6.5	-8.2	0.8	-0.3	0.2	-0.7	-1.6	27.1	-0.8	2.6	0.2
JES pileup p topology	-1.7	-0.5	-5.3	4.3	100.0	-0.1	-0.5	2.0	-0.4	-0.5	0.4	-0.2	-0.2	6.2	6.3	5.4	-1.2	0.8	0.3	0.5	-11.3	-23.2	-0.5	-30.6	9.8
ative NP modelling 1 (Large-R jet)	-0.2	-0.1	-0.4	0.3	-0.1	100.0	-0.0	0.2	-0.0	-0.0	-0.2	0.2	-0.5	0.5	0.4	0.5	-0.1	0.1	-0.1	-0.0	2.2	-2.5	-0.5	-15.6	-37.9
calibration modelling (Large-R jet)	-0.5	-0.2	-1.0	0.9	-0.5	-0.0	100.0	0.4	-0.1	-0.2	0.1	-0.2	-0.4	1.0	0.0	0.7	0.2	0.2	-0.2	0.1	1.7	-3.9	-0.4	8.7	-23.3
topTag sig eff. ($t\bar{t}$ hadronisation)	1.7	0.4	4.2	-2.9	2.0	0.2	0.4	100.0	0.4	0.5	0.7	-1.1	0.2	-7.1	-3.2	-4.3	-1.7	-8.5	-1.0	-1.0	-10.7	22.4	2.1	-11.8	-64.3
topTag sig eff. ($t\bar{t}$ TME)	-0.6	0.2	-1.0	0.9	-0.4	0.0	-0.1	0.4	100.0	0.2	-0.1	-0.1	-0.6	1.1	0.0	0.8	0.5	0.2	-0.2	0.1	2.5	4.1	0.2	2.7	-25.6
topTag sig eff. ($t\bar{t}$ stat.)	-0.7	-0.2	-1.3	1.2	-0.5	-0.0	-0.2	0.5	-0.2	100.0	0.0	-0.2	-0.7	1.4	0.1	1.0	0.1	0.2	-0.3	0.1	2.9	-4.8	-1.2	2.1	-31.8
XS W+jets	0.5	-0.1	1.0	-0.8	0.4	-0.2	0.1	0.7	-0.1	0.0	100.0	4.6	-1.8	-0.2	2.9	0.4	-1.5	3.4	0.2	0.5	20.5	-20.3	-14.6	-8.8	-11.0
Wt diagram subtraction	-1.4	0.0	-1.5	1.2	-0.2	0.2	-0.2	-1.1	-0.1	-0.2	4.6	100.0	-0.3	1.6	-11.0	-1.4	4.0	-7.4	-2.0	-0.9	-37.7	25.7	19.5	23.7	11.0
tbt up to +50%	-1.5	-0.6	-1.7	2.0	-0.2	-0.5	-0.4	0.2	-0.6	-0.7	-1.8	-0.3	100.0	-6.0	-10.4	-6.2	-3.1	-2.3	-5.6	0.1	31.7	-30.4	0.2	43.6	-15.8
tt+>1b 4FS vs. 5FS	7.3	1.1	14.3	-10.6	6.2	0.5	1.0	-7.1	1.1	1.4	-0.2	1.6	-6.0	100.0	-26.3	-36.3	-6.0	-16.2	-12.5	-1.0	5.2	-15.4	3.5	3.7	2.5
tt+>1b NLO gen.	-0.9	-0.2	7.1	-6.5	6.3	0.4	0.0	-3.2	0.0	0.1	2.9	-11.0	-10.4	26.3	100.0	-29.7	25.0	-9.5	-14.1	-1.6	-6.7	-2.3	-23.7	-20.6	5.9
tt+>1b PS & had.	5.0	0.8	11.1	-8.2	5.4	0.5	0.7	-4.3	0.8	1.0	0.4	-1.4	-6.2	-36.3	-29.7	100.0	-2.2	-11.8	-12.1	-0.7	9.6	-12.2	1.5	-0.5	1.9
ttbar reweighting w/ HT jets	5.1	1.5	2.7	0.8	-1.2	-0.1	0.2	-1.7	0.5	0.1	-1.5	4.0	-3.1	-6.0	25.0	-2.2	100.0	1.1	1.2	0.4	-11.9	16.6	-76.3	-35.4	15.5
tt+>1c NLO gen.	2.9	0.2	4.0	-0.3	0.8	0.1	0.2	-8.5	0.2	0.2	3.4	-7.4	-2.3	-16.2	-9.5	-11.8	1.1	100.0	-9.0	-2.1	52.7	8.9	-4.1	-1.3	3.1
tt+>1c PS & had.	0.1	-0.3	0.5	0.2	0.3	-0.1	-0.2	-1.0	-0.2	-0.3	0.2	-2.0	-5.6	-12.5	-14.1	-12.1	1.2	-9.0	100.0	-0.2	-2.7	-30.5	-0.7	-3.7	1.8
tt PDF05	0.3	0.1	0.9	-0.7	0.5	-0.0	0.1	-1.0	0.1	0.1	0.5	-0.9	0.1	-1.0	-1.6	-0.7	0.4	-2.1	-0.2	100.0	-5.1	8.5	-0.0	-1.5	27.3
tt+light NLO gen.	3.3	3.5	-9.5	-1.6	-11.3	2.2	1.7	-10.7	2.5	2.9	20.5	-37.7	31.7	5.2	-6.7	9.6	-11.9	52.7	-2.7	-5.1	100.0	-38.4	-7.5	13.8	-16.4
tt+light PS & had.	-8.9	-6.6	-36.6	27.1	-23.2	-2.5	-3.9	22.4	-4.1	-4.8	-20.3	25.7	-30.4	-15.4	-2.3	-12.2	16.6	8.9	-30.5	8.5	-38.4	100.0	0.8	-14.0	6.9
μ_{H_p}	-2.2	2.0	-2.9	-0.8	-0.5	-0.5	-0.4	2.1	0.2	-1.2	-14.6	19.5	0.2	3.5	-23.7	1.5	-76.3	-4.1	-0.7	-0.0	-7.5	0.8	100.0	37.2	-5.5
k(tt+ge1c/b)	46.5	23.3	-9.1	2.6	-30.6	-15.6	8.7	-11.8	2.7	2.1	-8.8	23.7	43.6	3.7	-20.6	-0.5	-35.4	-1.3	-3.7	-1.5	13.8	-14.0	37.2	100.0	-16.7
k(tt+light)	-17.1	-8.1	1.3	0.2	9.8	-37.9	-23.3	-64.3	-25.6	-31.8	-11.0	11.0	-15.8	2.5	5.9	1.9	15.5	3.1	1.8	27.3	-16.4	6.9	-5.5	-16.7	100.0

(b) Correlation matrix

Figure 74: Signal strength and normalization factors (top) and correlation matrix (bottom) for the 5000 GeV H^+ mass hypotheses.

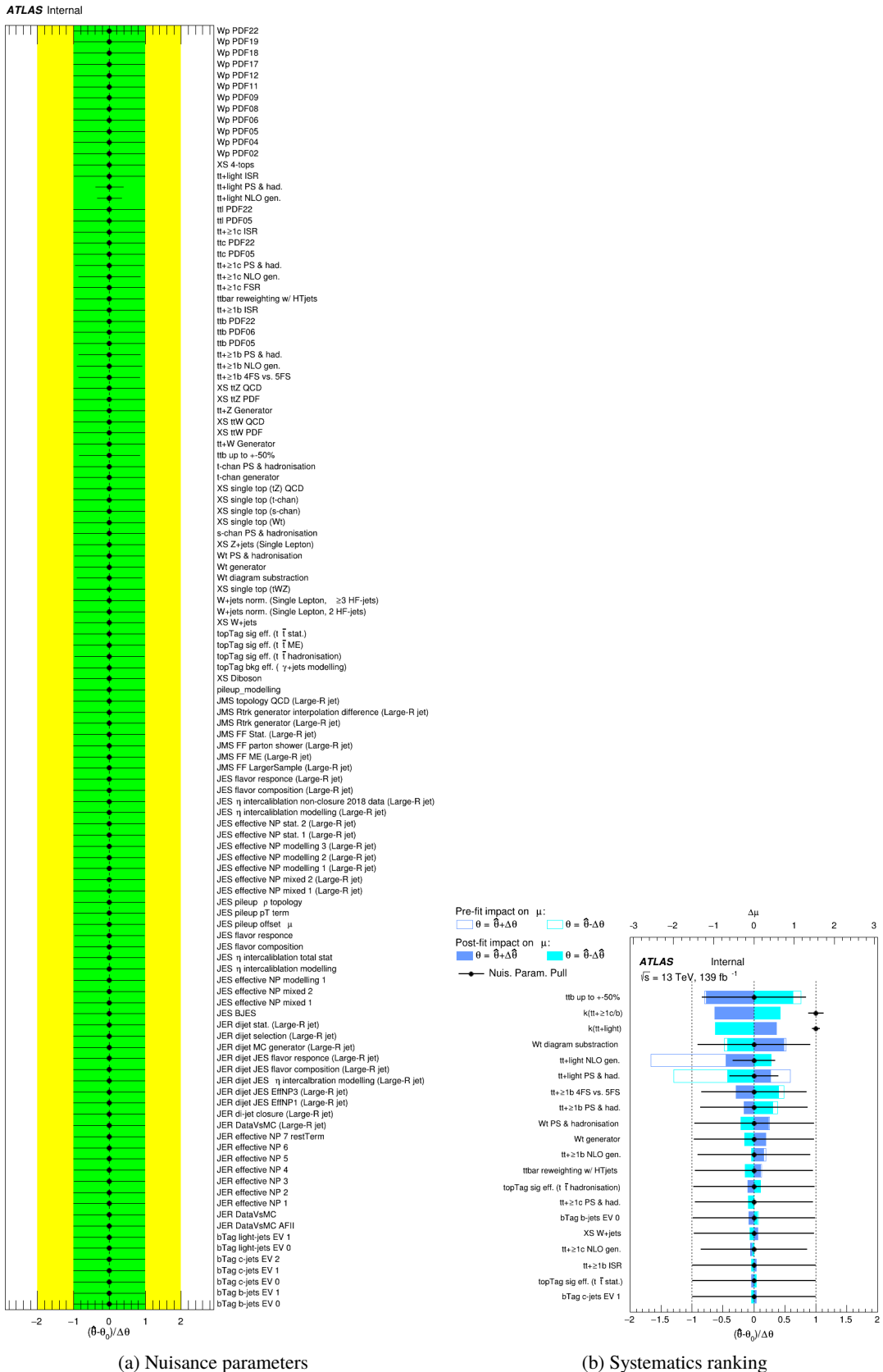
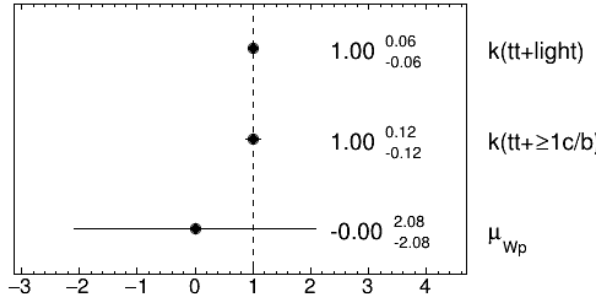


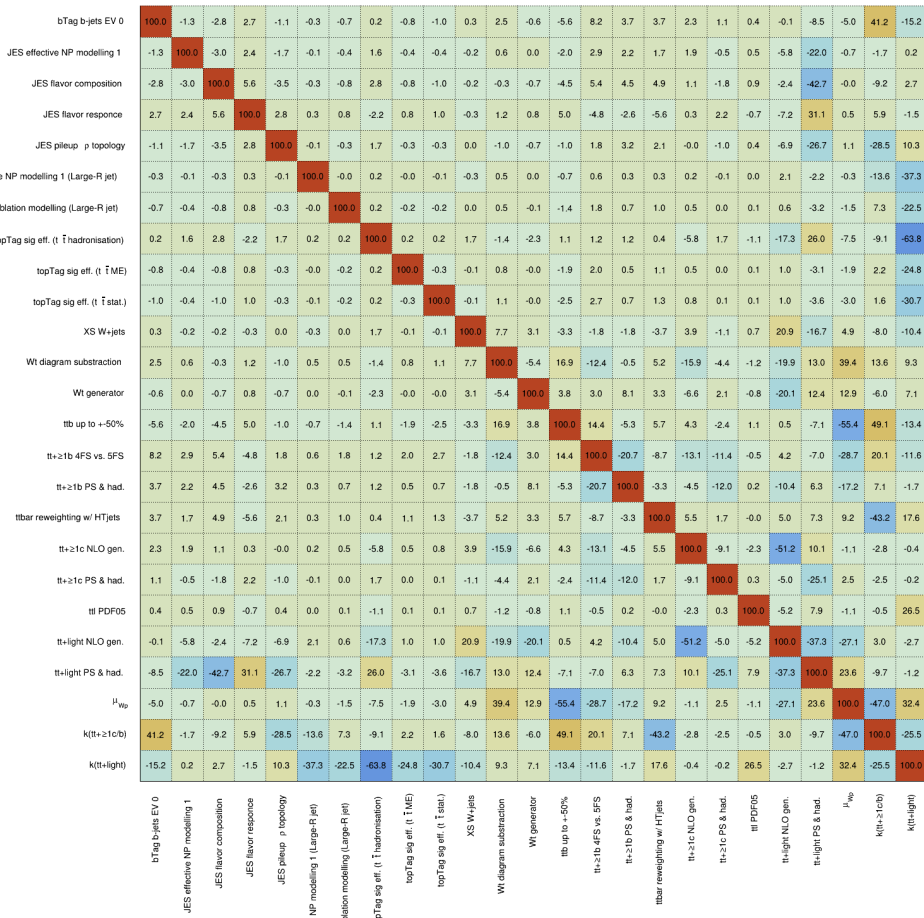
Figure 75: Nuisance parameters (left) and ranking plot (right) of the effect of various nuisance parameters before and after the fit for the 1000 GeV W'_L mass hypotheses.

ATLAS Internal



(a) Norm. factors

ATLAS Internal



(b) Correlation matrix

Figure 76: Signal strength and normalization factors (top) and correlation matrix (bottom) for the 1000 GeV W'_L mass hypotheses.

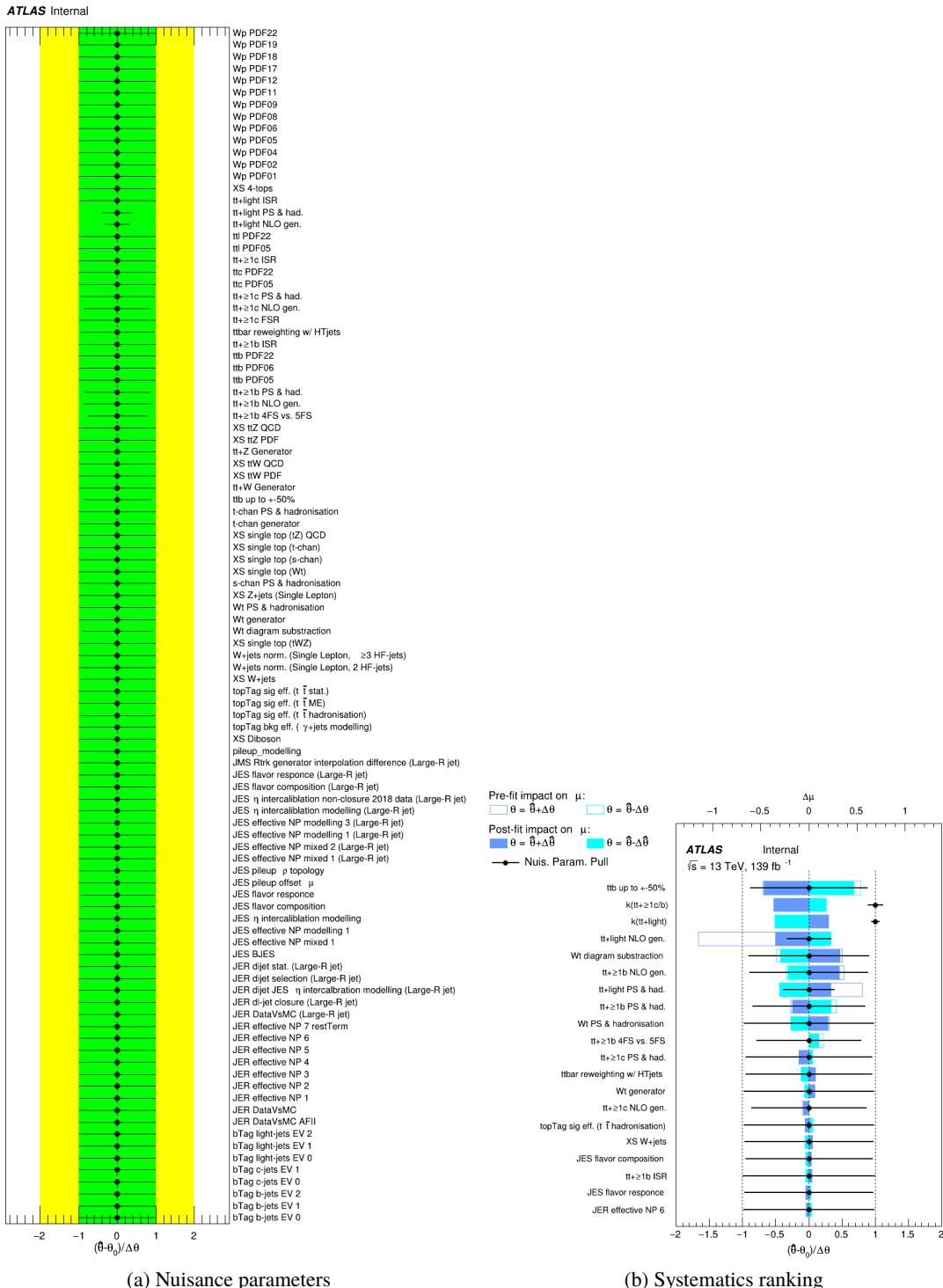
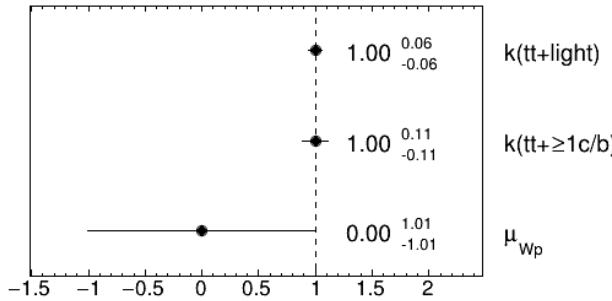
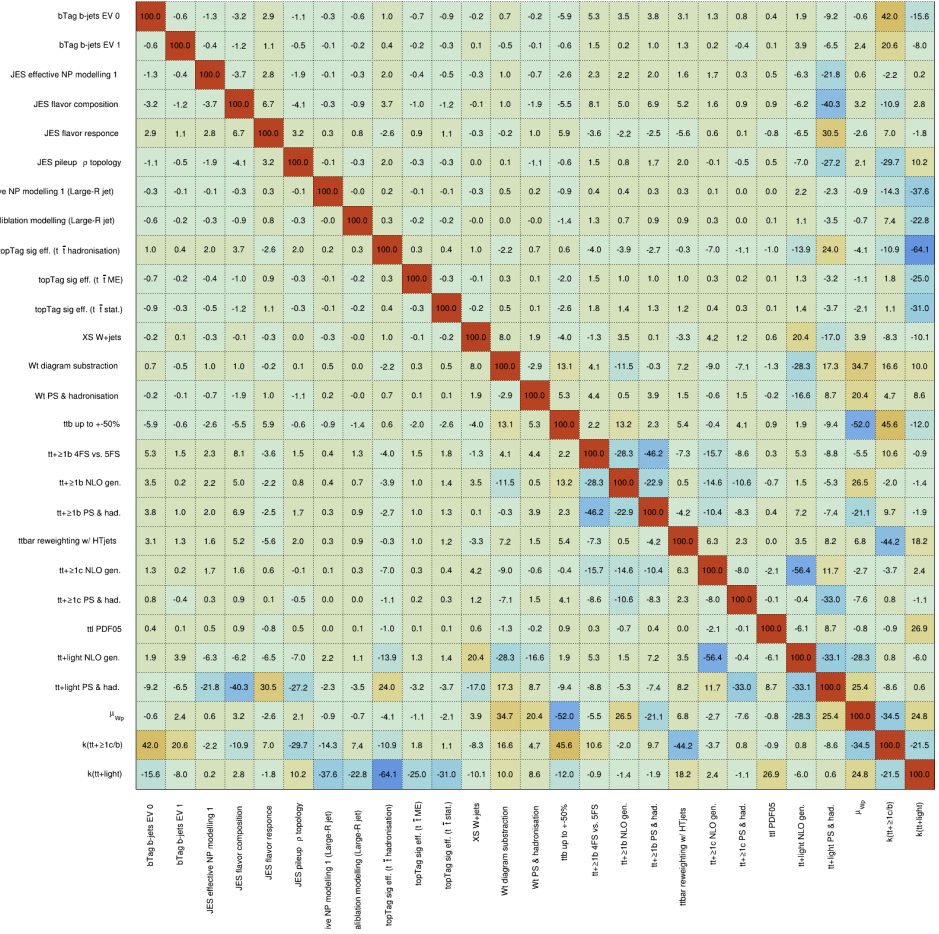


Figure 77: Nuisance parameters (left) and ranking plot (right) of the effect of various nuisance parameters before and after the fit for the 1200 GeV W' mass hypotheses.

ATLAS Internal

(a) Norm. factors

ATLAS Internal

(b) Correlation matrix

Figure 78: Signal strength and normalization factors (top) and correlation matrix (bottom) for the 1200 GeV W'_L mass hypotheses.

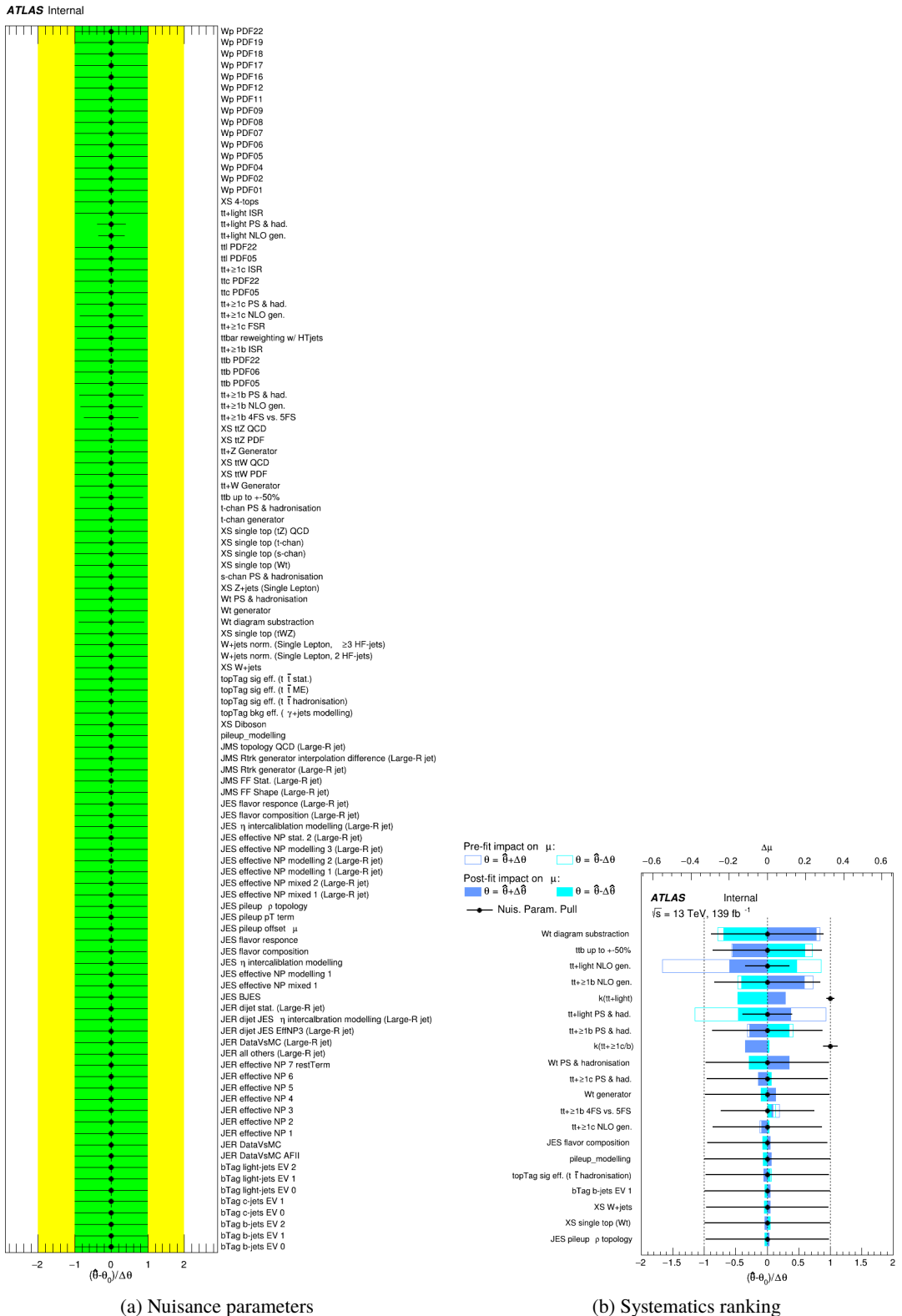
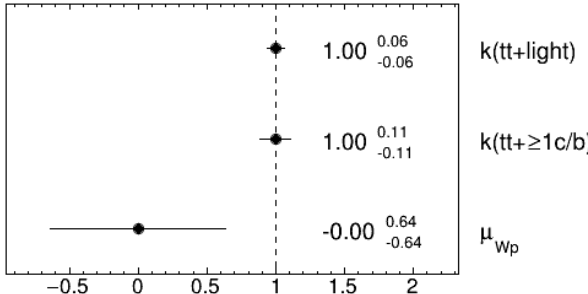


Figure 79: Nuisance parameters (left) and ranking plot (right) of the effect of various nuisance parameters before and after the fit for the 1400 GeV W'_L mass hypotheses.

ATLAS Internal**ATLAS Internal**

	bTag b-jets EV 0	-0.5	-1.2	-2.9	2.6	-1.5	-0.3	-0.5	1.2	-0.5	-0.7	0.1	0.4	-4.3	5.1	3.7	3.2	1.9	-0.2	0.0	0.2	4.4	-10.6	0.9	44.3	-16.6	
bTag b-jets EV 1	-0.5	100.0	-0.4	-1.0	1.0	-0.4	-0.1	-0.2	0.4	-0.2	-0.2	0.1	-0.7	-0.1	1.4	-0.1	0.8	1.3	0.2	-0.5	0.1	4.2	-7.1	2.3	21.5	-8.3	
JES effective NP modeling 1	-1.2	-0.4	100.0	-4.2	3.1	-2.6	-0.2	-0.4	2.6	-0.4	-0.4	-0.5	0.5	-3.7	0.9	3.0	1.6	0.1	0.3	0.1	0.6	-4.7	-20.9	1.4	-1.8	-0.3	
JES flavor composition	-2.9	-1.0	-4.2	100.0	6.9	-5.1	-0.5	-0.9	4.5	-0.9	-1.1	-0.5	0.3	-8.4	2.2	5.0	3.2	2.1	-1.5	-0.6	1.0	-1.4	-40.7	3.1	-9.8	2.1	
JES flavor response	2.6	1.0	3.1	6.9	100.0	3.9	0.4	0.8	-3.2	0.8	1.0	-0.2	0.7	7.4	-1.3	-2.5	-1.5	-0.7	2.5	1.6	-0.8	-8.6	30.4	-1.4	6.1	-1.2	
JES pileup topology	-1.5	-0.4	-2.6	-5.1	3.9	100.0	-0.2	-0.4	2.8	-0.4	-0.5	-0.4	0.0	-4.6	0.1	2.8	1.6	0.3	-1.3	-0.1	0.6	-7.5	-24.1	1.9	-31.0	10.4	
tree NP modelling 1 (Large-R jet)	-0.3	-0.1	-0.2	-0.5	0.4	-0.2	100.0	-0.1	0.3	-0.1	-0.1	-0.3	0.9	-1.5	0.5	1.0	0.5	0.0	-0.2	0.1	0.0	1.7	-1.7	-0.9	-14.7	37.7	
ablation modelling (Large-R jet)	-0.5	-0.2	-0.4	-0.9	0.8	-0.4	-0.1	100.0	0.4	-0.1	-0.2	0.1	0.2	-1.3	1.3	1.0	0.8	0.6	-0.1	-0.1	0.1	1.3	-3.5	-0.2	7.8	23.0	
topTag sig eff. (t t hadronisation)	1.2	0.4	2.6	4.5	-3.2	2.8	0.3	0.4	100.0	0.4	0.5	1.2	-1.1	1.9	-4.5	-6.0	-3.9	1.2	-6.0	-1.7	-1.1	-12.8	21.8	-3.1	-11.7	63.9	
topTag sig eff. (t t ME)	-0.5	-0.2	-0.4	-0.9	0.8	-0.4	-0.1	-0.1	0.4	100.0	-0.2	-0.0	0.4	-1.7	1.4	1.2	0.9	0.6	-0.2	-0.1	0.0	1.9	-3.5	-0.5	2.2	25.4	
topTag sig eff. (t t stat.)	-0.7	-0.2	-0.4	-1.1	1.0	-0.5	-0.1	-0.2	0.5	-0.2	100.0	-0.0	0.7	-2.3	1.8	1.6	1.1	0.7	-0.3	-0.1	0.1	2.1	-4.0	-1.2	1.5	-31.4	
XStW+jets	0.1	0.1	-0.5	-0.5	-0.2	-0.4	-0.3	0.1	1.2	-0.0	-0.0	100.0	7.2	-2.4	-2.7	2.5	0.5	-4.1	3.6	0.9	0.6	21.3	-17.7	2.5	-6.9	-11.2	
Wt diagram subtraction	0.4	-0.7	0.5	0.3	0.7	0.0	0.9	0.2	-1.1	0.4	0.7	7.2	100.0	17.0	4.0	-13.9	1.9	9.0	-5.3	-0.9	-0.9	-27.8	17.6	45.0	17.7	8.4	
tbt up to +50%	-4.3	-0.1	-3.7	-8.4	7.4	-4.6	-1.5	-1.3	1.9	-1.7	-2.3	-2.4	17.0	100.0	-3.4	15.3	-1.3	-1.3	-8.9	-0.4	0.6	10.4	-7.5	-32.5	46.0	-12.5	
t t+geq 1 b4FS vs. 5FS	5.1	1.4	0.9	2.2	-1.3	0.1	0.5	1.3	-4.5	1.4	1.8	-2.7	4.0	-3.4	100.0	-39.8	-46.7	-6.8	-14.4	-12.6	1.2	7.6	-3.1	0.2	7.9	1.0	
t t+geq 1 b NLO gen.	3.7	-0.1	3.0	5.0	-2.5	2.8	1.0	1.0	-4.0	1.2	1.6	2.5	-13.9	15.3	-39.8	100.0	-25.3	5.6	-8.6	-9.7	-0.2	3.5	-9.4	25.9	2.8	-0.4	
t t+geq 1 b PS & had.	3.2	0.8	1.6	3.2	-1.5	1.6	0.5	0.8	-3.9	0.9	1.1	0.5	1.9	-1.3	-46.7	-25.3	100.0	-0.7	-7.2	-10.0	0.6	1.9	-0.7	-17.2	5.1	1.0	
t tbar reweighting w/ Ht jets	1.9	1.3	0.1	2.1	-3.7	0.3	0.0	0.6	1.2	0.6	0.7	-4.1	9.0	-1.3	-6.8	5.6	-0.7	100.0	5.8	4.9	0.3	-3.0	16.4	1.2	-45.9	18.6	
t t+geq 1 c NLO gen.	-0.2	0.2	0.3	-1.5	2.5	-1.3	-0.2	-0.1	-6.0	-0.2	-0.3	3.6	-5.3	-8.9	-14.4	-8.6	-7.2	5.8	100.0	-6.6	-1.9	-0.1	-0.7	21.8	-2.9	-6.3	4.4
t t+geq 1 c PS & had.	-0.0	-0.5	0.1	-0.6	1.6	-0.1	0.1	-0.1	-1.7	-0.1	-0.1	0.9	-0.9	-0.4	-12.6	-9.7	-10.0	4.9	-6.6	100.0	0.3	-6.6	-27.3	-5.7	-2.1	1.9	
tt PDF05	0.2	0.1	0.6	1.0	-0.8	0.6	0.0	0.1	-1.1	0.0	0.1	0.6	-0.9	0.6	1.2	-0.2	0.6	0.3	-1.9	0.3	100.0	-6.7	9.0	-0.4	-1.3	27.3	
tt+light NLO gen.	4.4	4.2	-4.7	-1.4	-8.6	-7.5	1.7	1.3	-12.8	1.9	2.1	21.3	-27.8	10.4	7.6	3.5	1.9	-3.0	-61.7	-6.6	-6.7	100.0	-41.1	-27.4	7.0	-9.3	
tt+light PS & had.	-10.6	-7.1	-20.9	-40.7	30.4	-24.1	-1.7	-3.5	21.8	-3.5	-4.0	-17.7	17.6	-7.5	-3.1	-9.4	-0.7	16.4	21.8	-27.3	9.0	-41.1	100.0	20.8	-11.5	2.9	
μ_{Wp}	0.9	2.3	1.4	3.1	-1.4	1.9	-0.9	-0.2	-3.1	-0.5	-1.2	2.5	45.0	-32.5	0.2	25.9	-17.2	1.2	-2.9	-5.7	-0.4	-27.4	20.8	100.0	-14.3	17.9	
$k(t t+geq 1 b)$	44.3	21.5	-1.8	-9.8	6.1	-31.0	-14.7	7.8	-11.7	2.2	1.5	-6.9	17.7	46.0	7.9	-2.8	5.1	-45.9	-6.3	-2.1	-1.3	7.0	-11.5	-14.3	100.0	-20.6	
$k(t t+light)$	-16.6	-8.3	-0.3	2.1	-1.2	10.4	-37.7	-23.0	-63.9	-25.4	-31.4	-11.2	8.4	-12.5	1.0	-0.4	1.0	18.6	4.4	1.9	27.3	-9.3	2.9	17.9	-20.6	100.0	

(b) Correlation matrix

Figure 80: Signal strength and normalization factors (top) and correlation matrix (bottom) for the 1400 GeV W'_L mass hypotheses.

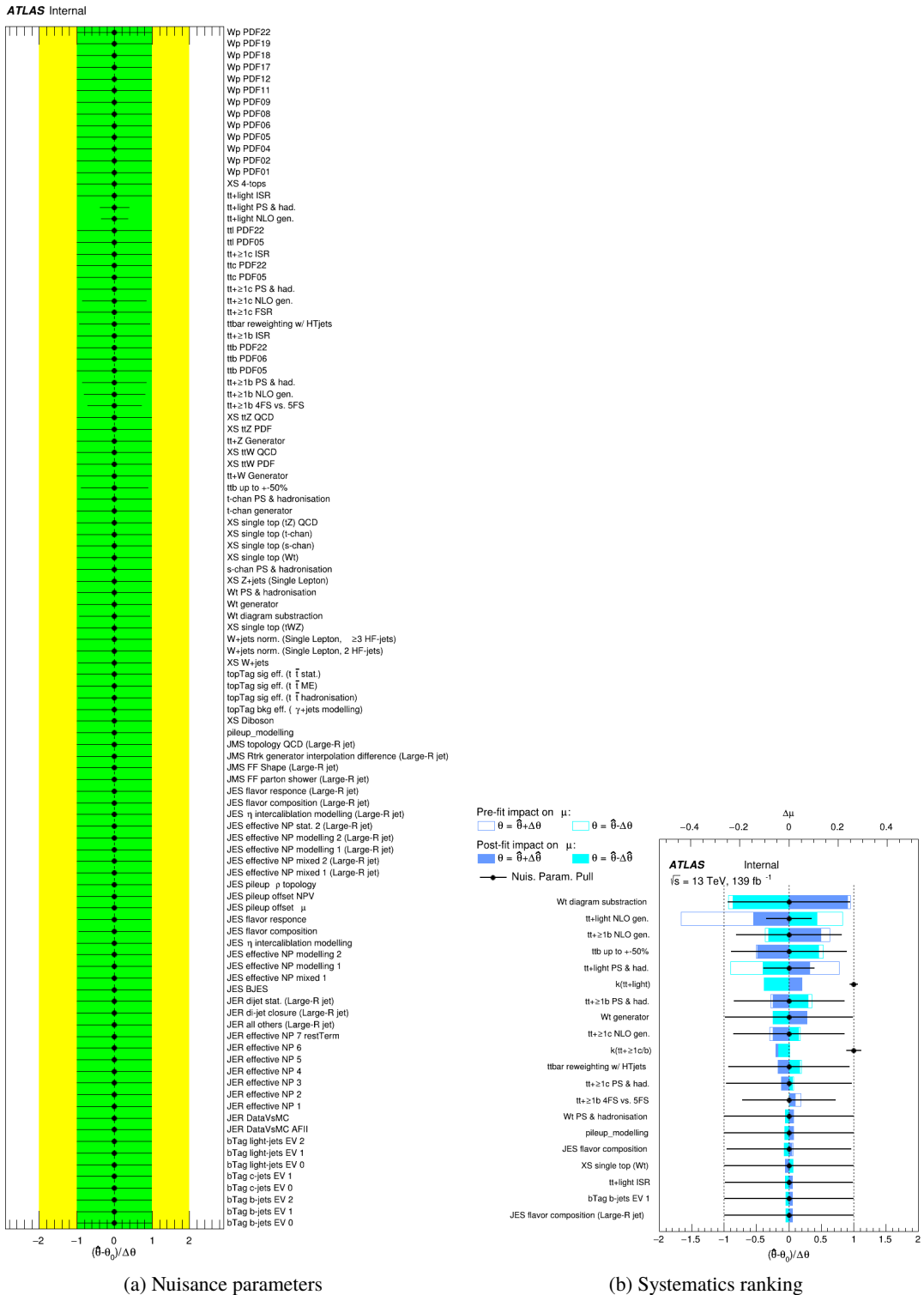
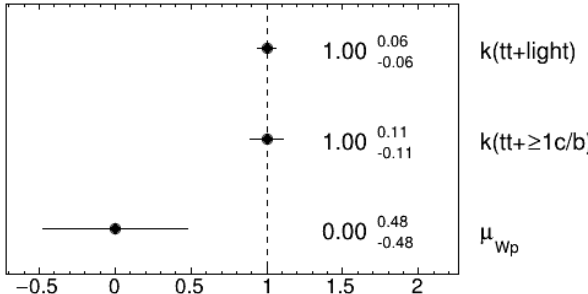


Figure 81: Nuisance parameters (left) and ranking plot (right) of the effect of various nuisance parameters before and after the fit for the 1600 GeV W'_L mass hypotheses.

ATLAS Internal



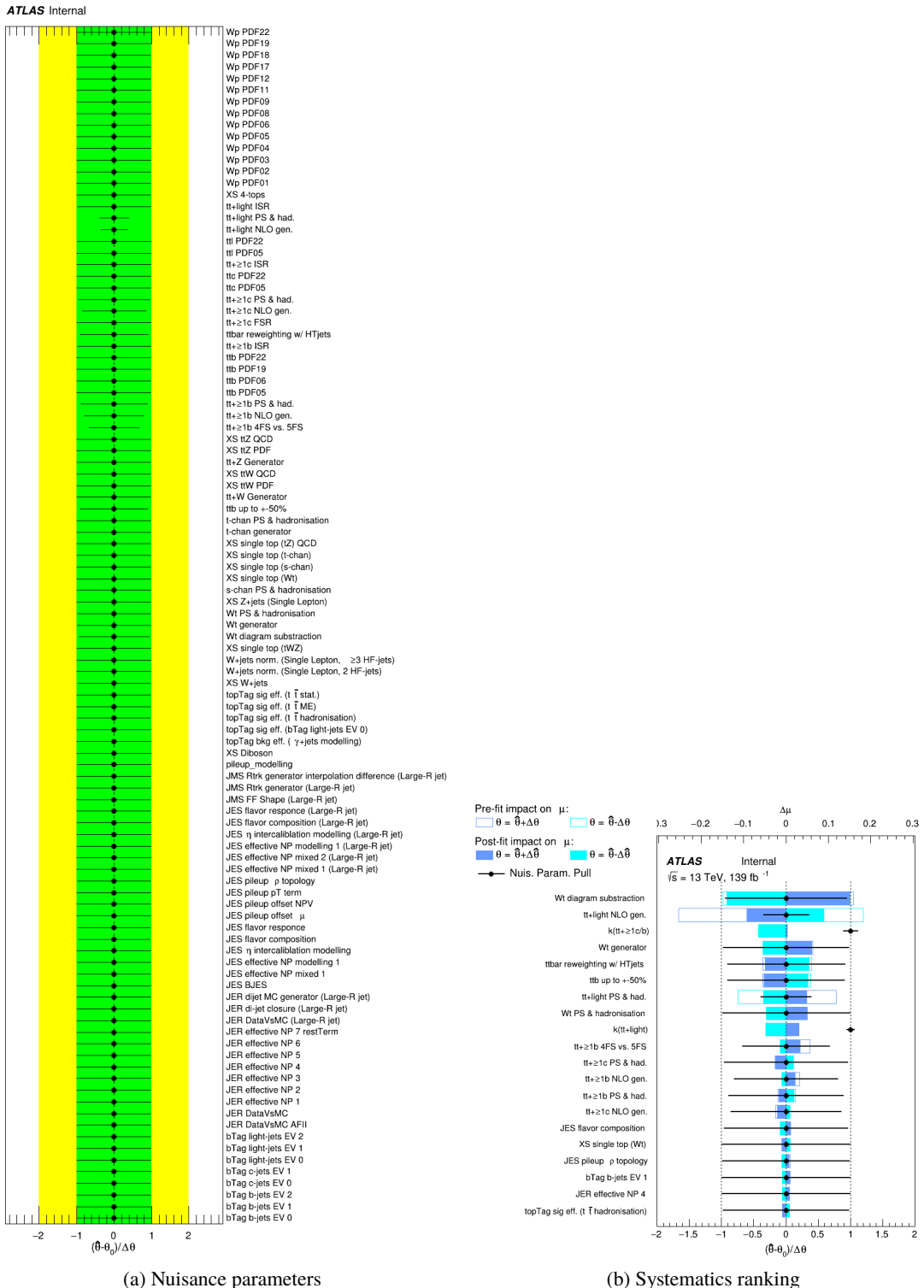
(a) Norm. factors

ATLAS Internal

	bTag b-jets EV 0	bTag b-jets EV 1	JES effective NP modelling 1	JES flavor composition	JES flavor response	JES pileup p topology	tive NP modelling 1 (Large-R jet)	calibration modelling (Large-R jet)	topTag sig eff. (t T hadronisation)	topTag sig eff. (t T ME)	topTag sig eff. (t T stat.)	Wt diagram subtraction	tbt up to +50%	tbt up to 4FS vs. 5FS	tbt >= 1b NLO gen.	tbt >= 1b PS & had.	tbt reweighting w/ HT jets	tbt >= 1c NLO gen.	tbt >= 1c PS & had.	tbt PDF05	tbt-light NLO gen.	tbt-light PS & had.	μ_{W_p}	k(tt+geq1c/b)	k(tt+light)
bTag b-jets EV 0	100.0	-0.5	-1.1	-2.5	2.6	-1.3	-0.2	-0.4	1.0	-0.5	-0.6	0.2	3.1	1.7	2.7	0.9	1.4	-0.0	-0.6	0.4	6.1	-12.4	1.4	45.6	-16.7
bTag b-jets EV 1	-0.5	100.0	-0.4	-1.0	1.0	-0.5	-0.1	-0.2	0.4	-0.2	-0.2	-0.1	-0.7	0.7	0.1	0.3	1.1	0.1	-0.5	0.2	4.1	-6.8	3.0	21.9	-8.1
JES effective NP modelling 1	-1.1	-0.4	100.0	-3.4	3.3	-2.5	-0.1	-0.4	2.3	-0.4	-0.4	0.7	-2.0	-0.8	4.9	0.1	0.1	2.6	0.1	0.8	-6.3	-21.4	1.3	-1.1	-0.3
JES flavor composition	-2.5	-1.0	-3.4	100.0	6.0	-4.1	-0.3	-0.9	3.7	-0.9	-1.1	0.8	-4.0	11.6	9.9	7.6	3.5	2.5	-0.2	1.2	-7.8	-39.2	3.6	-9.1	2.2
JES flavor response	2.6	1.0	3.3	6.0	100.0	4.2	0.3	0.8	-3.2	0.9	1.1	-0.2	6.0	2.6	-6.2	1.4	-2.9	-0.6	1.1	-1.1	-5.7	30.3	-1.9	5.1	-1.1
JES pileup p topology	-1.3	-0.5	-2.5	-4.1	4.2	100.0	-0.2	-0.4	2.5	-0.4	-0.5	0.7	-2.3	-2.0	5.3	-0.2	0.6	1.9	-0.0	0.8	-10.0	-24.6	1.7	-30.4	10.4
tive NP modelling 1 (Large-R jet)	-0.2	-0.1	-0.1	-0.3	0.3	-0.2	100.0	-0.0	0.3	-0.0	-0.0	0.5	-0.3	0.1	0.2	0.2	0.3	0.1	-0.1	0.0	2.5	-2.5	-0.9	-14.7	-37.7
calibration modelling (Large-R jet)	-0.4	-0.2	-0.4	-0.9	0.8	-0.4	-0.0	100.0	0.4	-0.1	-0.2	0.1	-1.1	1.0	1.2	0.5	0.4	-0.0	-0.1	0.1	1.4	-3.7	-0.2	8.1	-23.0
topTag sig eff. (t T hadronisation)	1.0	0.4	2.3	3.7	-3.2	2.5	0.3	0.4	100.0	0.4	0.5	-1.9	1.4	2.4	-7.7	-1.6	1.3	8.4	-1.2	-1.3	-10.9	22.4	-1.9	-12.5	63.8
topTag sig eff. (t T ME)	-0.5	-0.2	-0.4	-0.9	0.9	-0.4	-0.0	-0.1	0.4	100.0	-0.2	0.2	-1.4	1.0	1.3	0.6	0.4	-0.2	-0.1	0.1	2.1	-3.7	-0.4	2.4	-25.4
topTag sig eff. (t T stat.)	-0.6	-0.2	-0.4	-1.1	1.1	-0.5	-0.0	-0.2	0.5	-0.2	100.0	0.3	-1.8	1.3	1.8	0.8	0.4	-0.2	-0.1	0.1	2.4	-4.4	-1.5	1.7	-31.4
Wt diagram subtraction	0.2	-0.1	0.7	0.8	-0.2	0.7	0.5	0.1	-1.9	0.2	0.3	100.0	4.6	-2.1	-10.9	-4.2	6.6	-7.1	-3.4	-0.9	-30.1	19.7	55.8	16.4	12.0
tbt up to +50%	-3.1	-0.7	-2.0	-4.0	6.0	-2.3	-0.3	-1.1	1.4	-1.4	-1.8	4.6	100.0	0.0	13.0	-0.3	-3.2	-6.6	-0.4	0.9	14.5	-16.1	-28.7	43.2	-14.7
tbt up to 4FS vs. 5FS	1.7	0.7	-0.8	11.6	2.6	-2.0	0.1	1.0	-2.4	1.0	1.3	-2.1	0.0	100.0	-29.6	-54.7	-7.4	-4.9	-5.9	-0.7	-0.8	-4.6	2.6	5.7	-0.5
tbt >= 1b NLO gen.	2.7	0.1	4.9	9.9	-6.2	5.3	0.2	1.2	-7.7	1.3	1.8	-10.9	13.0	-29.6	100.0	-23.4	12.7	-14.0	-12.1	-3.0	6.7	-14.1	22.1	-6.1	2.2
tbt >= 1b PS & had.	0.9	0.3	0.1	7.6	1.4	-0.2	0.2	0.5	-1.6	0.6	0.8	-4.2	-0.3	-54.7	-23.4	100.0	-2.0	-5.5	-6.1	-0.7	2.4	-2.4	-15.8	2.6	-0.9
tbt reweighting w/ HT jets	1.4	1.1	0.1	3.5	-2.9	0.6	0.3	0.4	1.3	0.4	0.4	6.6	-3.2	-7.4	12.7	-2.0	100.0	8.1	5.8	0.6	-8.4	17.1	-9.2	-46.5	18.4
tbt >= 1c NLO gen.	-0.0	0.1	2.6	2.5	-0.6	1.9	0.1	-0.0	-8.4	-0.2	-0.2	-7.1	-6.6	-4.9	-14.0	-5.5	8.1	100.0	-8.8	-2.8	-59.8	14.7	-11.7	-7.2	5.2
tbt >= 1c PS & had.	-0.6	-0.5	0.1	-0.2	1.1	-0.0	-0.1	-0.1	-1.2	-0.1	-0.1	-3.4	-0.4	-5.9	-12.1	-6.1	5.8	-8.8	100.0	-0.5	-4.9	-27.3	-5.4	-3.8	1.4
tbt PDF05	0.4	0.2	0.8	1.2	-1.1	0.8	0.0	0.1	-1.3	0.1	0.1	-0.9	0.9	-0.7	-3.0	-0.7	0.6	-2.8	-0.5	100.0	-4.1	7.2	-0.6	-1.2	27.2
tbt-light NLO gen.	6.1	4.1	-6.3	-7.8	-5.7	-10.0	2.5	1.4	-10.9	2.1	2.4	-30.1	14.5	-0.8	6.7	2.4	-8.4	-59.8	-4.9	-4.1	100.0	-36.8	-27.3	10.9	-13.0
tbt-light PS & had.	-12.4	-6.8	-21.4	-39.2	30.3	-24.6	-2.5	-3.7	22.4	-3.7	-4.4	19.7	-16.1	-4.6	-14.1	-2.4	17.1	14.7	-27.3	7.2	-36.8	100.0	19.8	-14.3	4.7
μ_{W_p}	1.4	3.0	1.3	3.6	-1.9	1.7	-0.9	-0.2	-1.9	-0.4	-1.5	55.8	-28.7	2.6	22.1	-15.8	-9.2	-11.7	-5.4	-0.6	-27.3	19.8	100.0	-2.5	14.9
k(tt+geq1c/b)	45.6	21.9	-1.1	-9.1	5.1	-30.4	-14.7	8.1	-12.5	2.4	1.7	16.4	43.2	5.7	-6.1	2.6	-46.5	-7.2	-3.8	-1.2	10.9	-14.3	-2.5	100.0	-19.6
k(tt+light)	-16.7	-8.1	-0.3	2.2	-1.1	10.4	-37.7	-23.0	-63.8	25.4	-31.4	12.0	-14.7	-0.5	2.2	-0.9	18.4	5.2	1.4	27.2	-13.0	4.7	14.9	-19.6	100.0

(b) Correlation matrix

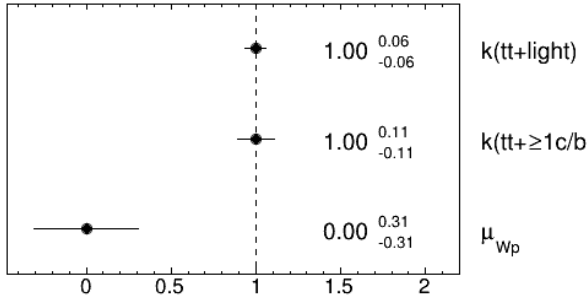
Figure 82: Signal strength and normalization factors (top) and correlation matrix (bottom) for the 1600 GeV W'_L mass hypotheses.



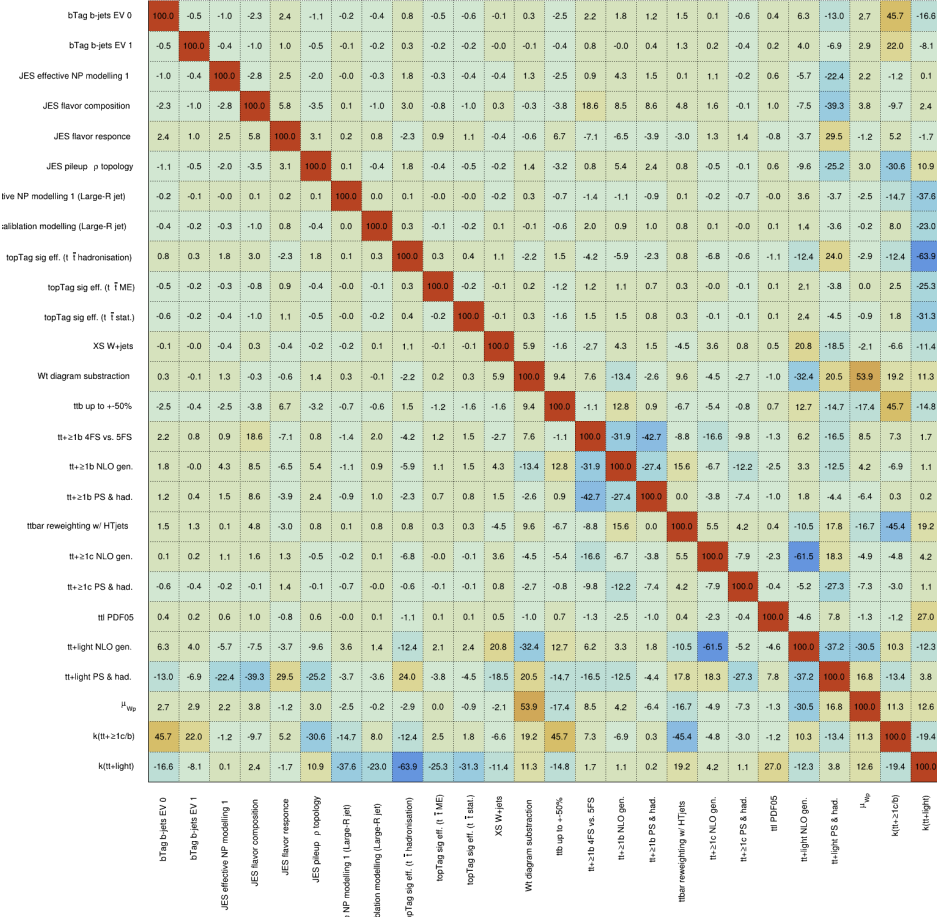
(a) Nuisance parameters

(b) Systematics ranking

Figure 83: Nuisance parameters (left) and ranking plot (right) of the effect of various nuisance parameters before and after the fit for the 1800 GeV W'_L mass hypotheses.

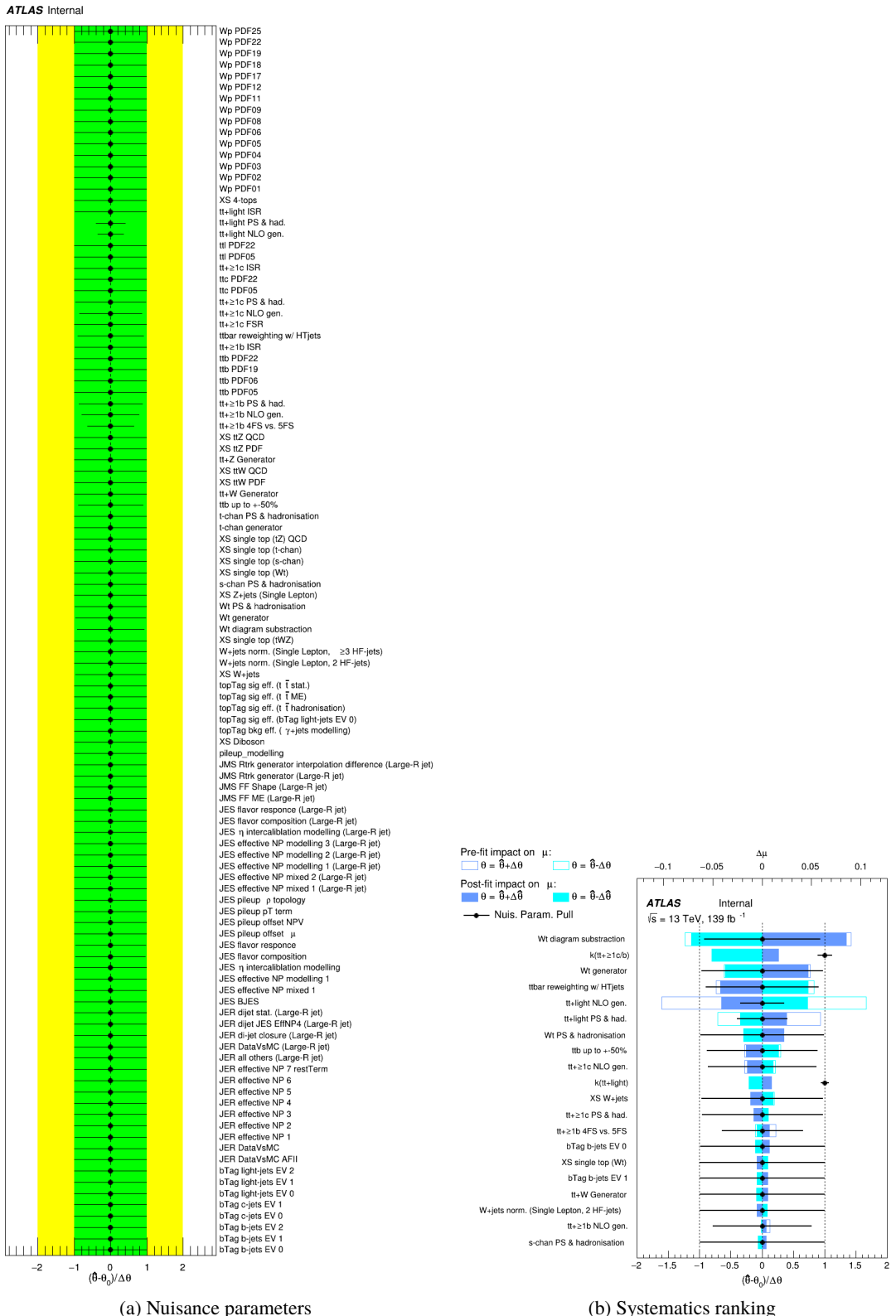
ATLAS Internal

(a) Norm. factors

ATLAS Internal

(b) Correlation matrix

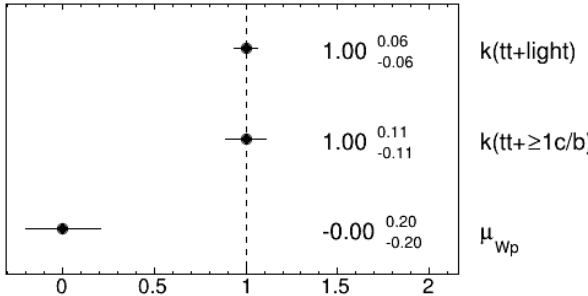
Figure 84: Signal strength and normalization factors (top) and correlation matrix (bottom) for the 1800 GeV W'_L mass hypotheses.



(a) Nuisance parameters

(b) Systematics ranking

Figure 85: Nuisance parameters (left) and ranking plot (right) of the effect of various nuisance parameters before and after the fit for the 2000 GeV W'_L mass hypotheses.

ATLAS Internal

(a) Norm. factors

ATLAS Internal

	bTag b-jets EV 0	-0.5	-0.9	2.2	2.2	-1.1	-0.2	-0.4	0.7	-0.4	-0.5	0.1	0.2	2.1	1.8	1.2	1.2	1.7	0.2	-0.7	0.3	7.2	-13.2	3.5	46.2	-16.7
bTag b-jets EV 1	-0.5	100.0	-0.4	-1.0	0.9	-0.4	-0.1	-0.2	0.3	-0.2	-0.3	-0.2	-0.5	1.0	-0.4	0.5	1.4	-0.1	-0.5	0.1	4.4	-6.9	2.6	22.2	-8.2	
JES effective NP modeling 1	-0.9	-0.4	100.0	-2.8	2.3	-1.9	-0.1	-0.3	1.5	-0.3	-0.4	0.4	0.8	-1.4	0.2	3.2	1.0	0.2	1.9	-0.3	0.6	-4.7	-22.7	0.9	-0.9	-0.1
JES flavor composition	-2.2	-1.0	-2.8	100.0	5.1	-3.4	-0.3	-0.8	2.7	-0.8	-0.9	-0.9	0.1	-3.5	13.4	7.0	6.9	3.9	0.5	-1.2	1.0	-4.0	-41.0	1.5	-9.0	2.3
JES flavor response	2.2	0.9	2.3	5.1	100.0	3.0	0.4	0.7	-1.9	0.8	1.0	-0.1	-1.0	5.5	-1.4	-3.2	-1.1	-3.0	0.5	2.0	-0.7	-7.0	31.7	-0.9	4.7	-1.6
JES pileup topology	-1.1	-0.4	-1.9	-3.4	3.0	100.0	-0.2	-0.4	1.4	-0.4	-0.5	0.4	0.8	-2.3	-0.6	4.3	1.2	0.2	0.8	-0.4	0.6	-8.7	-25.8	-0.7	-30.1	10.7
utive NP modelling 1 (Large-R jet)	-0.2	-0.1	-0.1	-0.3	0.4	-0.2	100.0	-0.0	0.2	-0.0	-0.1	0.6	0.3	-0.9	0.1	0.8	0.2	-0.2	0.1	-0.1	0.0	1.9	-2.2	-1.1	-14.8	-37.6
ablation modelling (Large-R jet)	-0.4	-0.2	-0.3	-0.8	0.7	-0.4	-0.0	100.0	0.3	-0.1	-0.2	0.1	0.2	-0.8	0.9	1.0	0.6	0.3	0.1	-0.2	0.1	1.5	-3.8	0.4	8.3	-23.0
topTag sig eff. ($t \bar{t}$ hadronisation)	0.7	0.3	1.5	2.7	-1.9	1.4	0.2	0.3	100.0	0.3	0.3	-1.3	-1.6	1.9	-5.5	-2.9	-1.7	-0.2	-6.7	-0.1	-1.0	-13.9	24.4	-1.4	-11.7	-64.1
topTag sig eff. ($t \bar{t}$ ME)	-0.4	-0.2	-0.3	-0.8	0.8	-0.4	-0.0	-0.1	0.3	100.0	-0.2	0.3	0.2	-1.1	1.0	1.1	0.6	0.3	0.0	-0.2	0.1	2.2	-3.9	0.2	2.6	-25.4
topTag sig eff. ($t \bar{t}$ stat.)	-0.5	-0.2	-0.4	-0.9	1.0	-0.5	-0.1	-0.2	0.3	-0.2	100.0	0.5	0.4	-1.5	1.2	1.5	0.7	0.2	0.0	-0.2	0.1	2.4	-4.5	-0.5	2.0	-31.4
Wt diagram subtraction	0.1	-0.3	0.4	-0.9	-0.1	0.4	0.6	0.1	-1.3	0.3	0.5	100.0	-7.1	7.8	6.4	-10.8	1.5	11.6	-8.9	-1.0	-0.6	-30.7	20.4	43.5	19.3	10.0
Wt generator	0.2	-0.2	0.8	0.1	-1.0	0.8	0.3	0.2	-1.6	0.2	0.4	-7.1	100.0	5.9	3.8	-8.0	2.2	7.4	-6.8	-0.5	-0.6	-11.7	7.1	21.3	-4.4	6.0
ttb up to +50%	-2.1	-0.5	-1.4	-3.5	5.5	-2.3	-0.9	-0.8	1.9	-1.1	-1.5	7.8	5.9	100.0	4.4	8.3	-2.0	-6.8	-1.1	-2.1	0.5	10.1	-14.2	-8.0	44.9	-14.8
tt+ ≥ 1 b 4FS vs. 5FS	1.8	1.0	0.2	13.4	-1.4	-0.6	0.1	0.9	-5.5	1.0	1.2	6.4	3.8	4.4	100.0	-38.1	-53.7	-9.6	1.3	-2.9	-1.2	-0.9	-12.8	3.4	10.2	0.8
tt+ ≥ 1 b NLO gen.	1.2	-0.4	3.2	7.0	-3.2	4.3	0.8	1.0	-2.9	1.1	1.5	-10.6	-8.0	8.3	-38.1	100.0	-25.9	21.9	-14.4	-10.8	-2.1	5.2	-7.9	0.4	-11.2	1.0
tt+ ≥ 1 b PS & had.	1.2	0.5	1.0	6.9	-1.1	1.2	0.2	0.6	-1.7	0.6	0.7	1.5	2.2	-2.0	-53.7	-25.9	100.0	-1.5	-1.8	-5.6	-1.0	-2.7	-0.2	0.2	0.9	0.5
ttbar reweighting w/ H7jets	1.7	1.4	0.2	3.9	-3.0	0.2	-0.2	0.3	-0.2	0.3	0.2	11.6	7.4	-6.8	-9.6	21.9	-1.5	100.0	11.0	5.7	0.3	-18.2	20.6	-21.6	-45.3	20.4
tt+ ≥ 1 c NLO gen.	0.2	-0.1	1.9	0.5	0.5	0.8	0.1	0.1	-6.7	0.0	0.0	-8.9	-6.8	-1.1	1.3	-14.4	-1.8	11.0	100.0	-7.9	-2.5	-59.9	17.6	-6.8	-7.6	3.6
tt+ ≥ 1 c PS & had.	-0.7	-0.5	-0.3	-1.2	2.0	-0.4	-0.1	-0.2	-0.1	-0.2	-0.2	-1.0	-0.5	-2.1	-2.9	-10.8	-5.6	5.7	-7.9	100.0	-0.5	-9.1	-22.4	-3.6	-4.2	1.4
tt PDF05	0.3	0.1	0.6	1.0	-0.7	0.6	0.0	0.1	-1.0	0.1	0.1	-0.6	-0.6	0.5	-1.2	-2.1	-1.0	0.3	-2.5	-0.5	100.0	-4.9	7.9	-0.8	-1.2	27.2
tt+light NLO gen.	7.2	4.4	-4.7	-4.0	-7.0	-8.7	1.9	1.5	-13.9	2.2	2.4	-30.7	-11.7	10.1	-0.9	5.2	-2.7	-18.2	-59.9	-9.1	-4.9	100.0	-40.4	-22.2	13.1	-10.9
tt+light PS & had.	-13.2	-6.9	-22.7	-41.0	31.7	-25.8	-2.2	-3.8	24.4	-3.9	-4.5	20.4	7.1	-14.2	-12.8	-7.9	-0.2	20.6	17.6	-22.4	7.9	-40.4	100.0	12.1	-14.0	3.0
μ_{W_p}	3.5	2.6	0.9	1.5	-0.9	-0.7	-1.1	0.4	-1.4	0.2	-0.5	43.5	21.3	-8.0	3.4	0.4	0.2	-21.6	-6.8	-3.6	-0.8	-22.2	12.1	100.0	18.6	6.0
$k(t t+1c/b)$	46.2	22.2	-0.9	-9.0	4.7	-30.1	-14.8	8.3	-11.7	2.6	2.0	19.3	-4.4	44.9	10.2	-11.2	0.9	45.3	-7.6	-4.2	-1.2	13.1	-14.0	18.6	100.0	-19.7
$k(t t+light)$	-16.7	-8.2	-0.1	2.3	-1.6	10.7	-37.6	-23.0	-64.1	25.4	-31.4	10.0	6.0	-14.8	0.8	1.0	0.5	20.4	3.6	1.4	27.2	-10.9	3.0	6.0	-19.7	100.0

(b) Correlation matrix

Figure 86: Signal strength and normalization factors (top) and correlation matrix (bottom) for the 2000 GeV W'_L mass hypotheses.

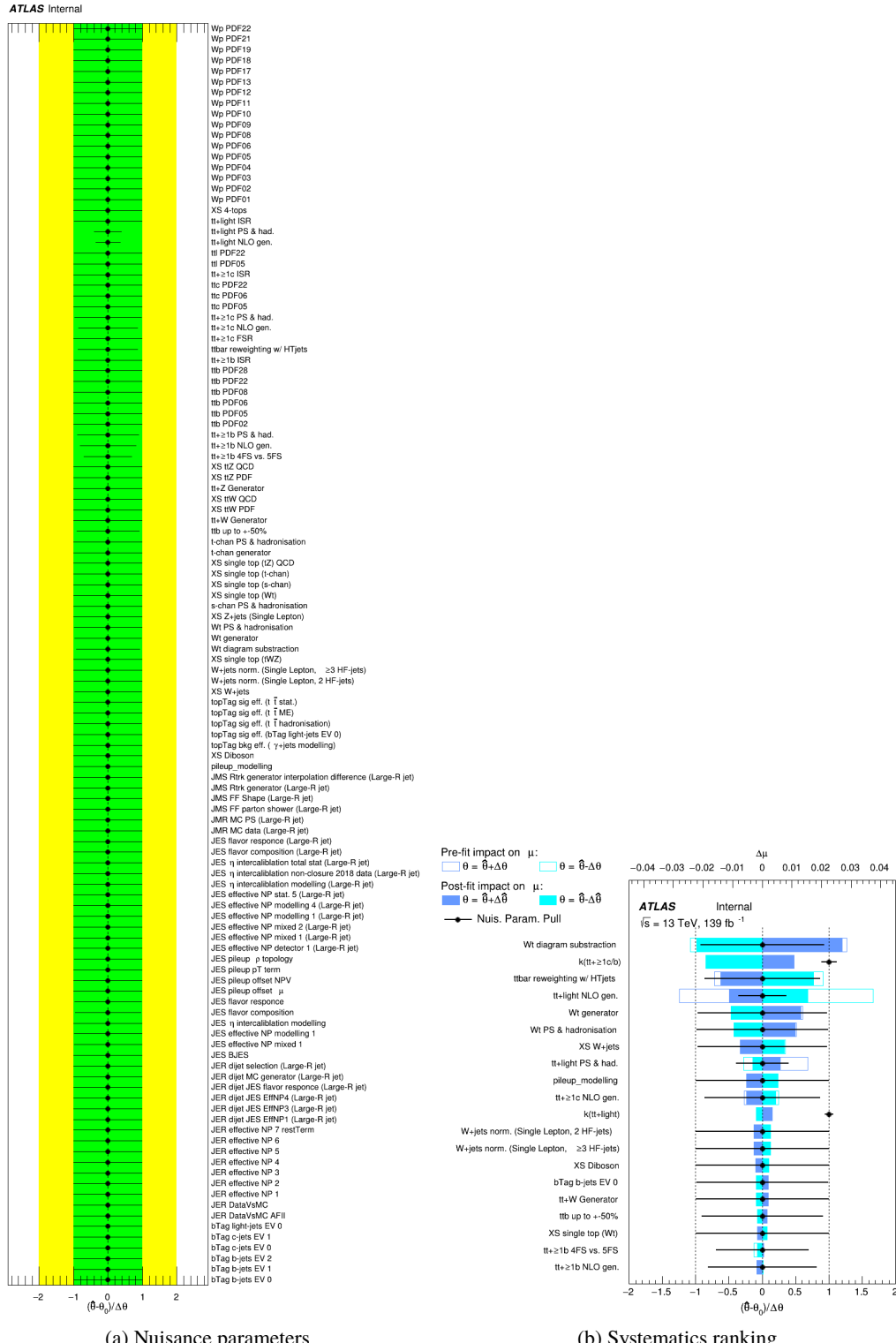
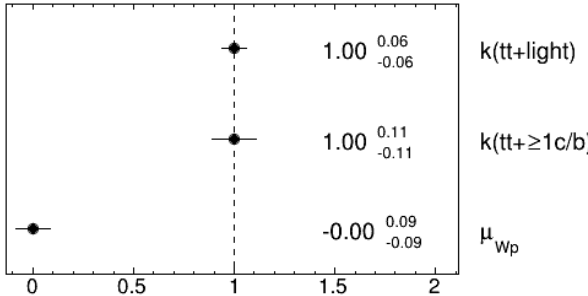


Figure 87: Nuisance parameters (left) and ranking plot (right) of the effect of various nuisance parameters before and after the fit for the 2500 GeV W' mass hypotheses.

ATLAS Internal

(a) Norm. factors

ATLAS Internal

	bTag b-jets EV 0	bTag b-jets EV 1	JES effective NP modelling 1	JES flavor composition	JES flavor response	JES pileup p topology	tive NP modelling 1 (Large-R jet)	calibration modelling (Large-R jet)	topTag sig eff. ($t\bar{t}$ hadronisation)	topTag sig eff. ($t\bar{t}$ ME)	topTag sig eff. ($t\bar{t}$ stat.)	Wt diagram subtraction	tbt up to +50%	tbt+>1b 4FS vs. 5FS	tbt+>1b NLO gen.	tbt+>1b PS & had.	tbt reweighting w/ HT jets	tbt+>1c NLO gen.	tbt+>1c PS & had.	tbt PDF05	tbt-light NLO gen.	tbt-light PS & had.	μ_{W_p}	k($t\bar{t}+\geq 1\text{c}/b$)	k($t\bar{t}+\text{light}$)
bTag b-jets EV 0	100.0	-0.6	-1.1	-2.7	2.6	-1.3	-0.2	-0.4	0.8	-0.5	-0.6	-0.4	-2.1	2.1	1.9	1.1	2.0	0.5	-0.9	0.4	6.6	-12.4	2.3	46.3	-16.7
bTag b-jets EV 1	-0.6	100.0	-0.5	-1.2	1.2	-0.6	-0.1	-0.2	0.4	-0.2	-0.3	-0.2	-0.9	0.4	0.5	0.2	1.2	0.2	-0.5	0.2	3.6	-6.3	1.2	22.4	-8.1
JES effective NP modelling 1	-1.1	-0.5	100.0	-3.1	2.7	-2.1	-0.1	-0.4	1.7	-0.4	-0.4	0.2	-2.0	-0.4	3.0	-0.3	0.2	1.9	-1.2	0.7	-4.5	-22.3	1.1	-1.3	0.1
JES flavor composition	-2.7	-1.2	-3.1	100.0	5.7	-3.6	-0.3	-0.9	2.9	-0.9	-1.0	-1.0	-3.2	15.5	8.4	7.2	4.3	1.6	-1.7	1.1	-6.0	-39.3	0.5	-9.4	2.4
JES flavor response	2.6	1.2	2.7	5.7	100.0	3.3	0.4	0.8	-2.2	0.9	1.0	0.6	5.5	-1.3	-4.0	-0.3	-2.8	0.4	2.7	-0.8	-6.8	30.9	-0.9	4.9	-1.5
JES pileup p topology	-1.3	-0.6	-2.1	-3.6	3.3	100.0	-0.2	-0.4	1.7	-0.4	-0.5	0.2	-3.0	-0.7	3.5	-0.3	0.0	0.6	-1.6	0.6	-8.2	-25.5	0.0	-30.8	10.9
tive NP modelling 1 (Large-R jet)	-0.2	-0.1	-0.1	-0.3	0.4	-0.2	100.0	-0.1	0.2	-0.1	-0.1	0.6	-0.9	0.1	0.7	0.2	-0.4	0.0	-0.2	0.0	2.0	-2.2	-1.1	-14.8	-37.6
calibration modelling (Large-R jet)	-0.4	-0.2	-0.4	-0.9	0.8	-0.4	-0.1	100.0	0.3	-0.1	-0.2	0.0	-0.8	0.8	0.9	0.4	0.3	0.1	-0.3	0.1	1.6	-3.7	0.1	8.3	-23.0
topTag sig eff. ($t\bar{t}$ hadronisation)	0.8	0.4	1.7	2.9	-2.2	1.7	0.2	0.3	100.0	0.2	0.3	1.7	0.5	2.3	-3.0	-0.5	-0.5	-6.9	0.2	-1.0	-14.6	25.1	-1.5	12.2	-64.0
topTag sig eff. ($t\bar{t}$ ME)	-0.5	-0.2	-0.4	-0.9	0.9	-0.4	-0.1	-0.1	0.2	100.0	-0.2	0.1	-1.0	0.7	0.9	0.4	0.4	0.0	-0.3	0.1	2.4	-3.9	-0.0	2.6	-25.3
topTag sig eff. ($t\bar{t}$ stat.)	-0.6	-0.3	-0.4	-1.0	1.0	-0.5	-0.1	-0.2	0.3	-0.2	100.0	0.3	-1.4	0.9	1.2	0.5	0.2	-0.0	-0.4	0.1	2.7	-4.6	-0.6	1.9	-31.4
Wt diagram subtraction	-0.4	-0.2	0.2	-1.0	0.6	0.2	0.6	0.0	-1.7	0.1	0.3	100.0	5.7	2.5	-9.6	-1.0	13.6	-7.1	-1.2	-0.7	-31.9	20.8	32.3	18.7	10.3
tbt up to +50%	-2.1	-0.9	-2.0	-3.2	5.5	-3.0	-0.9	-0.8	0.5	-1.0	-1.4	5.7	100.0	-4.5	13.2	-0.8	-9.2	-4.3	-3.6	0.5	16.4	-16.5	2.6	45.8	-14.5
tbt+>1b 4FS vs. 5FS	2.1	0.4	-0.4	15.5	-1.3	-0.7	0.1	0.8	-2.3	0.7	0.9	2.5	-4.5	100.0	-39.1	-51.4	-5.6	-8.6	-7.7	-0.9	3.3	-9.5	1.1	3.2	1.5
tbt+>1b NLO gen.	1.9	0.5	3.0	8.4	-4.0	3.5	0.7	0.9	-3.0	0.9	1.2	-9.6	13.2	-39.1	100.0	-22.3	25.0	-13.8	-5.3	-1.8	4.6	-10.4	-1.5	-10.1	0.5
tbt+>1b PS & had.	1.1	0.2	-0.3	7.2	-0.3	-0.3	0.2	0.4	-0.5	0.4	0.5	-1.0	-0.8	-51.4	-22.3	100.0	0.8	-4.9	-4.7	-0.4	0.0	0.9	-0.6	-0.5	0.2
tbt reweighting w/ HT jets	2.0	1.2	0.2	4.3	-2.8	0.0	-0.4	0.3	-0.5	0.4	0.2	13.6	-9.2	-5.6	25.0	0.8	100.0	8.6	4.1	0.1	-20.4	23.2	-17.8	-42.9	20.9
tbt+>1c NLO gen.	0.5	0.2	1.9	1.6	0.4	0.6	-0.0	0.1	-6.9	0.0	-0.0	-7.1	-4.3	-8.6	-13.8	-4.9	8.6	100.0	-7.1	-2.5	-58.7	16.1	-6.0	-6.9	4.1
tbt+>1c PS & had.	-0.9	-0.5	-1.2	-1.7	2.7	-1.6	-0.2	-0.3	0.2	-0.3	-0.4	-1.2	-3.6	-7.7	-5.3	-4.7	4.1	-7.1	100.0	-0.0	-10.9	-20.5	-1.0	-4.0	1.5
tbt PDF05	0.4	0.2	0.7	1.1	-0.8	0.6	0.0	0.1	-1.0	0.1	0.1	-0.7	0.5	-0.9	-1.8	-0.4	0.1	-2.5	-0.0	100.0	-5.1	7.8	-0.8	-1.1	27.1
tbt-light NLO gen.	6.6	3.6	-4.5	-6.0	-6.8	-8.2	2.0	1.6	-14.6	2.4	2.7	-31.9	16.4	3.3	4.6	0.0	-20.4	-58.7	-10.9	-5.1	100.0	-40.4	-16.6	15.8	-11.6
tbt-light PS & had.	-12.4	-6.3	-22.3	-39.3	30.9	-25.5	-2.2	-3.7	25.1	-3.9	-4.6	20.8	-16.5	-9.5	-10.4	0.9	23.2	16.1	-20.5	7.8	-40.4	100.0	6.4	-15.7	2.9
μ_{W_p}	2.3	1.2	1.1	0.5	-0.9	0.0	-1.1	0.1	-1.5	-0.0	-0.6	32.3	2.6	1.1	-1.5	-0.6	-17.8	-6.0	-1.0	-0.8	-16.6	6.4	100.0	19.9	4.1
k($t\bar{t}+\geq 1\text{c}/b$)	46.3	22.4	-1.3	-9.4	4.9	-30.8	-14.8	8.3	-12.2	2.6	1.9	18.7	45.8	3.2	-10.1	-0.5	-42.9	-6.9	-4.0	-1.1	15.6	-15.7	19.9	100.0	-19.6
k($t\bar{t}+\text{light}$)	-16.7	-8.1	0.1	2.4	-1.5	10.9	-37.6	-23.0	-64.0	25.3	-31.4	10.3	-14.5	1.5	0.5	0.2	20.9	4.1	1.5	27.1	-11.6	2.9	4.1	-19.6	100.0

(b) Correlation matrix

Figure 88: Signal strength and normalization factors (top) and correlation matrix (bottom) for the 2500 GeV W'_L mass hypotheses.

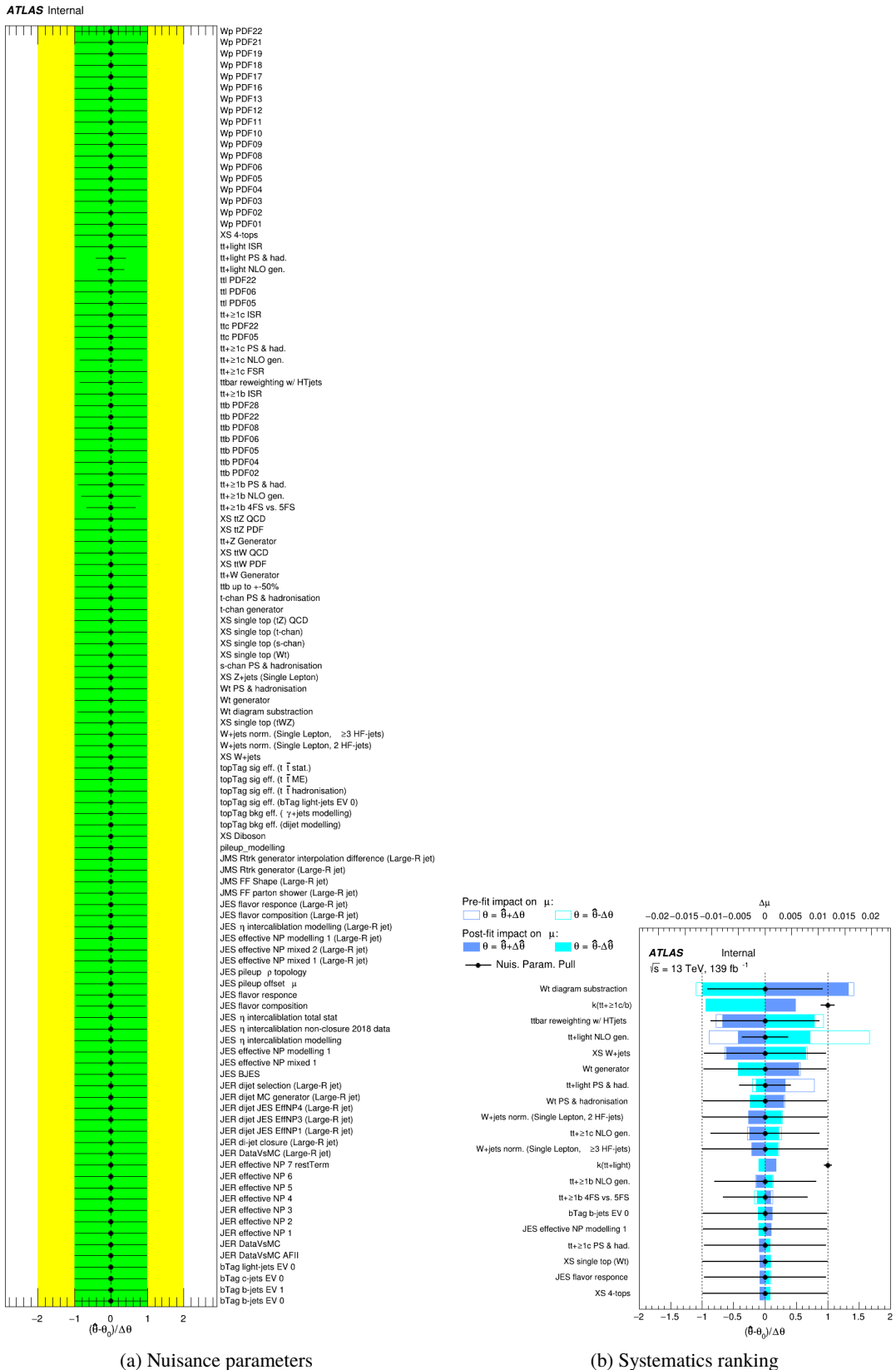
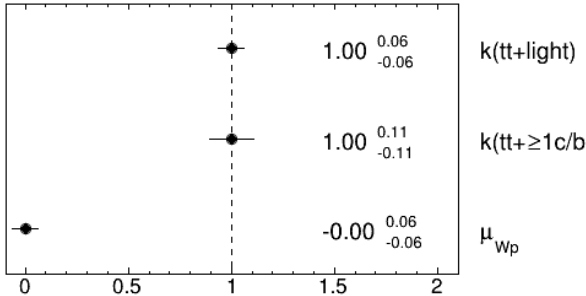


Figure 89: Nuisance parameters (left) and ranking plot (right) of the effect of various nuisance parameters before and after the fit for the 3000 GeV W'_L mass hypotheses.

ATLAS Internal

(a) Norm. factors

ATLAS Internal

	bTag b-jets EV 0	-0.5	-0.9	-2.2	2.3	-1.0	-0.2	-0.4	0.7	-0.4	-0.5	-0.4	-1.9	1.2	1.3	1.1	1.9	0.2	-0.6	0.3	7.0	-13.1	2.2	46.9	-16.8
bTag b-jets EV 1	-0.5	100.0	-0.4	-1.0	1.1	-0.5	-0.1	-0.2	0.4	-0.2	-0.2	-0.3	-0.8	0.4	0.1	0.4	1.3	-0.0	-0.4	0.2	3.8	-6.6	1.1	22.6	-8.1
JES effective NP modelling 1	-0.9	-0.4	100.0	-2.8	2.1	-1.5	-0.1	-0.3	1.5	-0.3	-0.3	-0.4	-1.0	2.9	2.1	1.5	1.4	1.6	-0.6	0.5	-3.9	-22.4	1.9	-1.7	-0.1
JES flavor composition	-2.2	-1.0	-2.8	100.0	4.7	-2.9	-0.2	-0.7	2.3	-0.7	-0.9	-1.8	-3.7	17.7	5.7	6.9	4.9	-0.1	-1.8	0.8	-3.1	-40.1	0.5	-10.1	2.4
JES flavor response	2.3	1.1	2.1	4.7	100.0	2.7	0.4	0.7	-1.9	0.8	0.9	0.9	3.9	-1.0	-2.8	-1.0	-3.2	0.1	2.1	-0.6	-7.3	31.8	-1.6	4.6	-1.3
JES pileup p topology	-1.0	-0.5	-1.5	-2.9	2.7	100.0	-0.2	-0.3	1.5	-0.3	-0.4	0.1	-1.8	1.0	2.0	0.3	0.0	0.6	-1.6	0.4	-7.6	-26.0	-0.9	-30.4	10.6
tive NP modelling 1 (Large-R jet)	-0.2	-0.1	-0.1	-0.2	0.4	-0.2	100.0	-0.0	0.2	-0.0	-0.0	0.7	-0.6	-0.2	0.5	0.1	-0.4	0.1	-0.1	0.0	2.0	-2.3	-1.0	-14.8	-37.7
calibration modelling (Large-R jet)	-0.4	-0.2	-0.3	-0.7	0.7	-0.3	-0.0	100.0	0.3	-0.1	-0.1	0.0	-0.6	0.7	0.6	0.4	0.4	0.1	-0.2	0.1	1.7	-4.0	0.1	8.5	-23.1
topTag sig eff. ($t\bar{t}$ hadronisation)	0.7	0.4	1.5	2.3	-1.9	1.5	0.2	0.3	100.0	0.3	0.3	1.7	0.4	0.5	-1.6	0.3	-0.5	-6.8	0.3	-1.0	-15.4	25.5	-1.3	12.4	-64.0
topTag sig eff. ($t\bar{t}$ ME)	-0.4	-0.2	-0.3	-0.7	0.8	-0.3	-0.0	-0.1	0.3	100.0	-0.2	0.2	-0.8	0.7	0.6	0.5	0.4	-0.0	-0.2	0.1	2.5	-4.1	-0.0	2.7	-25.4
topTag sig eff. ($t\bar{t}$ stat.)	-0.5	-0.2	-0.3	-0.9	0.9	-0.4	-0.0	-0.1	0.3	-0.2	100.0	0.4	-1.0	0.8	1.0	0.6	0.2	-0.0	-0.3	0.1	2.7	-4.8	-0.5	2.1	-31.4
Wt diagram subtraction	-0.4	-0.3	-0.4	-1.8	0.9	0.1	0.7	0.0	-1.7	0.2	0.4	100.0	3.6	7.2	-6.6	-0.4	12.8	-8.8	-1.5	-0.7	-32.2	21.6	25.1	18.6	10.0
tt up to +50%	-1.9	-0.8	-1.0	-3.7	3.9	-1.8	-0.6	-0.6	0.4	-0.8	-1.0	3.6	100.0	6.2	4.4	3.0	-0.9	-2.0	-1.6	0.3	18.7	-18.1	0.1	43.4	-15.0
tt+>1b 4FS vs. 5FS	1.2	0.4	2.9	17.7	-1.0	1.0	-0.2	0.7	-0.5	0.7	0.8	7.2	6.2	100.0	-39.7	-43.7	-1.7	-0.6	-3.7	-1.1	-6.4	-10.5	2.4	6.8	0.6
tt+>1b NLO gen.	1.3	0.1	2.1	5.7	-2.8	2.0	0.5	0.6	-1.6	0.6	1.0	-6.6	4.4	-39.7	100.0	-23.6	26.6	-16.5	-8.7	-1.4	2.9	-3.0	-3.2	-13.0	2.1
tt+>1b PS & had.	1.1	0.4	1.5	6.9	-1.0	0.3	0.1	0.4	0.3	0.5	0.6	-0.4	3.0	-43.7	-23.6	100.0	2.2	-2.1	-4.3	-0.6	-3.6	1.6	-0.7	0.8	-0.8
ttbar reweighting w/ HT jets	1.9	1.3	1.4	4.9	-3.2	0.0	-0.4	0.4	-0.5	0.4	0.2	12.8	-0.9	-1.7	26.6	2.2	100.0	14.4	5.2	0.1	-23.6	21.6	-14.3	-40.2	19.3
tt+>1c NLO gen.	0.2	-0.0	1.6	-0.1	0.1	0.6	0.1	0.1	-6.8	-0.0	-0.0	-8.8	-2.0	-0.6	-16.5	-2.1	14.4	100.0	-6.8	-2.3	-56.1	17.1	-4.8	-9.9	4.3
tt+>1c PS & had.	-0.6	-0.4	-0.6	-1.8	2.1	-1.6	-0.1	-0.2	0.3	-0.2	-0.3	-1.5	-1.6	-3.7	-8.7	-4.3	5.2	-6.8	100.0	-0.2	-9.7	-20.4	-1.7	-3.7	1.0
tt PDF05	0.3	0.2	0.5	0.8	-0.6	0.4	0.0	0.1	-1.0	0.1	0.1	-0.7	0.3	-1.1	-1.4	-0.6	0.1	-2.3	-0.2	100.0	5.2	8.0	-0.5	-1.1	27.1
tt+light NLO gen.	7.0	3.8	-3.9	-3.1	-7.3	-7.6	2.0	1.7	-15.4	2.5	2.7	-32.2	18.7	-6.4	2.9	-3.6	-23.6	-56.1	-9.7	-5.2	100.0	-44.6	-12.4	18.5	-12.1
tt+light PS & had.	-13.1	-6.6	-22.4	-40.1	31.8	-26.0	-2.3	-4.0	25.5	-4.1	-4.8	21.6	-18.1	-10.5	-3.0	1.6	21.6	17.1	-20.4	8.0	-44.6	100.0	5.5	-15.8	3.3
μ_{W_p}	2.2	1.1	1.9	0.5	-1.6	-0.9	-1.0	0.1	-1.3	-0.0	-0.5	25.1	0.1	2.4	-3.2	-0.7	-14.3	-4.8	-1.7	-0.5	-12.4	5.5	100.0	16.4	3.5
$k(t\bar{t}+\geq 1 c/b)$	46.9	22.6	-1.7	-10.1	4.6	-30.4	-14.8	8.5	-12.4	2.7	2.1	18.6	43.4	6.8	-13.0	0.8	-40.2	-9.9	-3.7	-1.1	18.5	-15.8	16.4	100.0	-19.5
$k(t\bar{t}+\text{light})$	-16.8	-8.1	-0.1	2.4	-1.3	10.6	-37.7	-23.1	-64.0	25.4	-31.4	10.0	-15.0	0.6	2.1	-0.8	19.3	4.3	1.0	27.1	-12.1	3.3	3.5	-19.5	100.0

(b) Correlation matrix

Figure 90: Signal strength and normalization factors (top) and correlation matrix (bottom) for the 3000 GeV W'_L mass hypotheses.

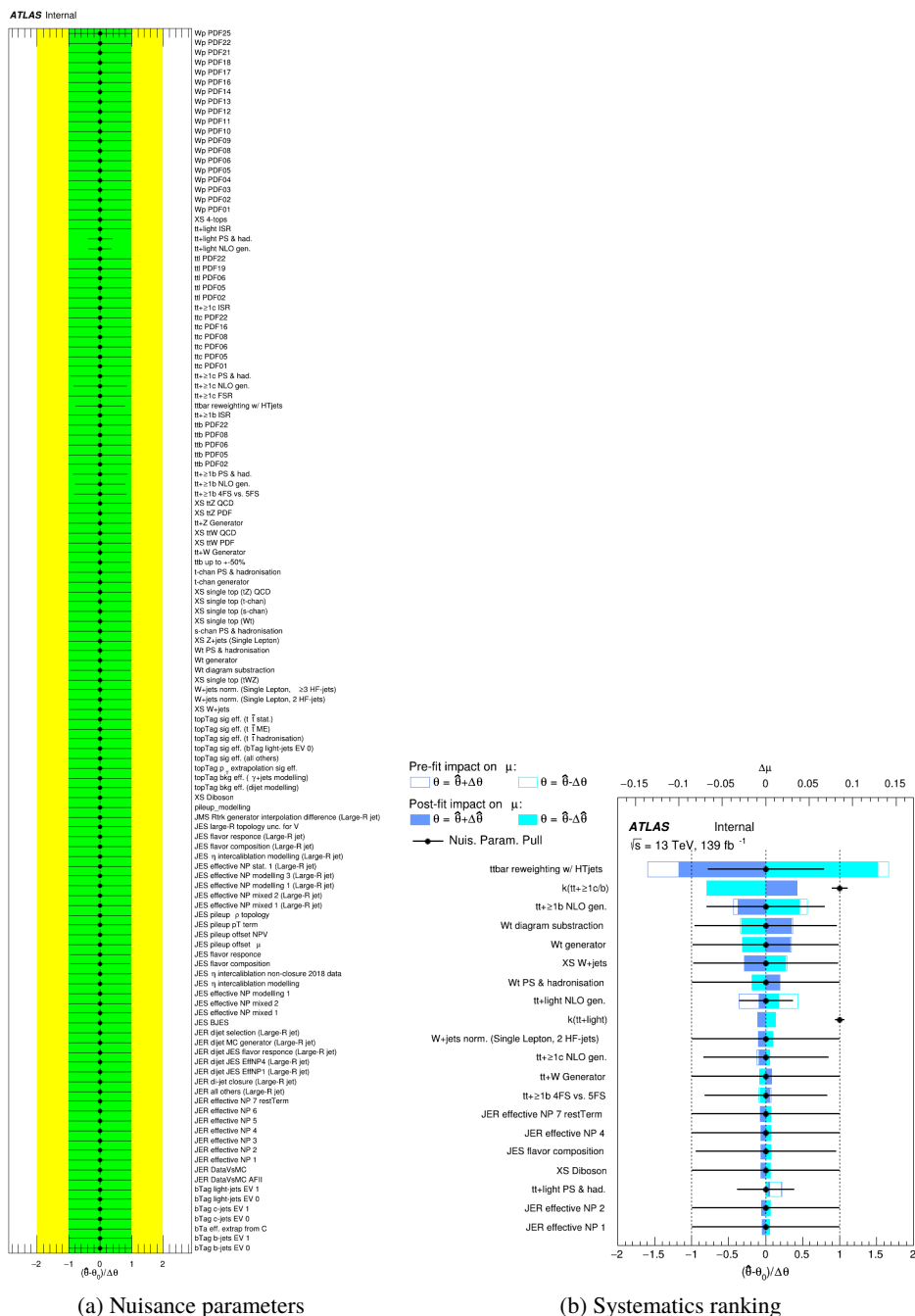
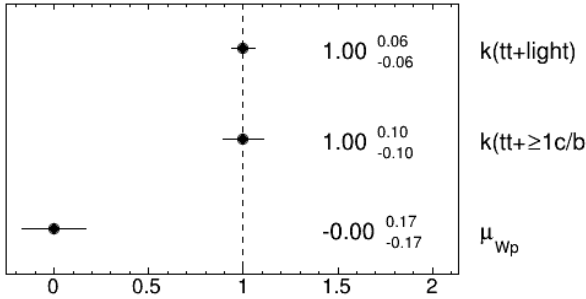


Figure 91: Nuisance parameters (left) and ranking plot (right) of the effect of various nuisance parameters before and after the fit for the 4000 GeV W'_1 mass hypotheses.

ATLAS Internal

(a) Norm. factors

ATLAS Internal

	bTag b-jets EV 0	bTag b-jets EV 1	JES flavor composition	JES flavor response	JES pileup p topology	ative NP modelling 1 (Large-R jet)	calibration modelling (Large-R jet)	topTag sig eff. ($t\bar{t}$ hadronisation)	topTag sig eff. ($t\bar{t}$ TME)	topTag sig eff. ($t\bar{t}$ stat.)	XS W+jets	Wt diagram subtraction	tbt up to +50%	tt+>1b 4FS vs. 5FS	tt+>1b NLO gen.	tt+>1b PS & had.	ttbar reweighting w/ HT jets	tt+>1c NLO gen.	tt+>1c PS & had.	tt PDF05	tt+light NLO gen.	tt+light PS & had.	μ_{W_p}	k($t\bar{t} + \geq 1 c/b$)	k($t\bar{t}$ +light)
bTag b-jets EV 0	100.0	-0.7	-4.5	3.4	-1.6	-0.2	-0.5	1.7	-0.6	-0.7	0.5	-1.4	-1.5	7.3	-0.8	5.0	5.2	2.9	0.1	0.3	3.3	-8.9	-2.4	46.2	-17.0
bTag b-jets EV 1	-0.7	100.0	-1.2	1.1	-0.5	-0.1	-0.2	0.4	-0.2	-0.3	-0.1	0.0	-0.6	1.2	-0.2	0.8	1.4	0.2	-0.3	0.1	3.4	-6.6	1.9	23.3	-8.1
JES flavor composition	-4.5	-1.2	100.0	8.3	-5.3	-0.3	-1.0	4.2	-1.0	-1.3	1.0	-1.5	-1.6	14.2	7.2	11.1	3.1	4.0	0.5	0.9	-9.4	-36.6	-3.4	-9.3	1.3
JES flavor response	3.4	1.1	8.3	100.0	4.3	0.3	0.9	-2.9	0.9	1.2	-0.9	1.4	2.0	-10.6	-6.7	-8.2	0.3	-0.4	0.1	-0.7	-1.7	27.1	-0.2	2.8	0.1
JES pileup p topology	-1.6	-0.5	-5.3	4.3	100.0	-0.1	-0.4	2.0	-0.4	-0.5	0.5	-0.3	-0.2	6.2	6.4	5.4	-1.0	0.8	0.3	0.5	-11.3	-23.2	-0.7	-30.6	9.8
ative NP modelling 1 (Large-R jet)	-0.2	-0.1	-0.3	0.3	-0.1	100.0	-0.0	0.2	-0.0	-0.1	-0.2	0.2	-0.5	0.5	0.4	0.5	-0.0	0.1	-0.1	0.0	2.2	-2.5	-0.5	-15.5	-37.9
calibration modelling (Large-R jet)	-0.5	-0.2	-1.0	0.9	-0.4	-0.0	100.0	0.4	-0.1	-0.2	0.1	-0.2	-0.4	1.0	0.0	0.7	0.3	0.2	-0.2	0.1	1.7	-3.9	-0.5	8.7	-23.2
topTag sig eff. ($t\bar{t}$ hadronisation)	1.7	0.4	4.2	-2.9	2.0	0.2	0.4	100.0	0.3	0.4	0.7	-1.0	0.2	-7.0	-3.3	-4.3	-1.9	-8.5	-1.0	-1.0	-10.7	22.4	2.3	-1.7	-64.2
topTag sig eff. ($t\bar{t}$ TME)	-0.6	0.2	-1.0	0.9	-0.4	0.0	-0.1	0.3	100.0	0.2	-0.0	-0.1	-0.6	1.1	0.1	0.8	0.5	0.2	-0.2	0.1	2.5	4.1	0.1	2.7	-25.6
topTag sig eff. ($t\bar{t}$ stat.)	-0.7	-0.3	-1.3	1.2	-0.5	-0.1	-0.2	0.4	-0.2	100.0	0.0	-0.2	-0.7	1.4	0.2	1.0	0.3	0.2	-0.3	0.1	2.9	-4.8	-1.4	2.0	-31.7
XS W+jets	0.5	-0.1	1.0	-0.9	0.5	-0.2	0.1	0.7	-0.0	0.0	100.0	4.7	-1.7	-0.3	2.8	0.4	-1.1	3.4	0.2	0.5	20.6	-20.4	-14.2	-8.7	-11.0
Wt diagram subtraction	-1.4	0.0	-1.5	1.4	-0.3	0.2	-0.2	-1.0	-0.1	-0.2	4.7	100.0	-0.4	1.6	-10.8	-1.4	3.8	-7.4	-2.1	-0.9	-37.9	25.8	18.4	23.4	11.0
tbt up to +50%	-1.5	-0.6	-1.6	2.0	-0.2	-0.5	-0.4	0.2	-0.6	-0.7	-1.7	-0.4	100.0	-6.0	-10.2	-6.2	-2.5	-2.4	-5.6	0.1	31.7	-30.4	-0.4	43.2	-15.7
tt+>1b 4FS vs. 5FS	7.3	1.2	14.2	-10.6	6.2	0.5	1.0	-7.0	1.1	1.4	-0.3	1.6	-6.0	100.0	-26.5	-36.3	-6.4	-16.2	-12.5	-1.0	5.1	-15.4	4.0	3.9	2.4
tt+>1b NLO gen.	-0.8	-0.2	7.2	-6.7	6.4	0.4	0.0	-3.3	0.1	0.2	2.8	-10.8	-10.2	26.5	100.0	-29.6	25.3	-9.5	-14.0	-1.6	-6.5	-2.4	-23.8	-20.8	6.1
tt+>1b PS & had.	5.0	0.8	11.1	-8.2	5.4	0.5	0.7	-4.3	0.8	1.0	0.4	-1.4	-6.2	-36.3	-29.6	100.0	-21	-11.8	-12.1	-0.7	9.6	-12.2	1.3	-0.5	1.8
ttbar reweighting w/ HT jets	5.2	1.4	3.1	0.3	-1.0	-0.0	0.3	-1.9	0.5	0.3	-1.1	3.8	-2.5	-6.4	25.3	-2.1	100.0	1.2	1.5	0.3	-10.6	15.6	-78.2	-36.5	15.8
tt+>1c NLO gen.	2.9	0.2	4.0	-0.4	0.8	0.1	0.2	-8.5	0.2	0.2	3.4	-7.4	-2.4	-16.2	-9.5	-11.8	1.2	100.0	-9.0	-2.1	52.6	8.9	-4.0	-1.4	3.1
tt+>1c PS & had.	0.1	-0.3	0.5	0.1	0.3	-0.1	-0.2	-1.0	-0.2	-0.3	0.2	-2.1	-5.6	-12.5	-14.0	-12.1	1.5	-9.0	100.0	-0.2	-2.7	-30.5	-1.0	-3.8	1.8
tt PDF05	0.3	0.1	0.9	-0.7	0.5	0.0	0.1	-1.0	0.1	0.1	0.5	-0.9	0.1	-1.0	-1.6	-0.7	0.3	-2.1	-0.2	100.0	-5.1	8.5	0.0	-1.5	27.3
tt+light NLO gen.	3.3	3.4	-9.4	-1.7	-11.3	2.2	1.7	-10.7	2.5	2.9	20.6	-37.9	31.7	5.1	-6.5	9.6	-10.6	-52.6	-2.7	-5.1	100.0	-38.5	-8.2	13.3	-16.3
tt+light PS & had.	-8.9	-6.6	-36.6	27.1	-23.2	-2.5	-3.9	22.4	-4.1	-4.8	-20.4	25.8	-30.4	-15.4	-2.4	-12.2	15.6	8.9	-30.5	8.5	-38.5	100.0	1.2	-13.8	6.9
μ_{W_p}	-2.4	1.9	-3.4	-0.2	-0.7	-0.5	-0.5	2.3	0.1	-1.4	-14.2	18.4	-0.4	4.0	-23.8	1.3	-78.2	-4.0	-1.0	0.0	-8.2	1.2	100.0	38.0	-6.1
k($t\bar{t} + \geq 1 c/b$)	46.2	23.3	-9.3	2.8	-30.6	-15.5	8.7	-11.7	2.7	2.0	-8.7	23.4	43.2	3.9	-20.8	-0.5	-36.5	-1.4	-3.8	-1.5	13.3	-13.8	38.0	100.0	-16.9
k($t\bar{t}$ +light)	-17.0	-8.1	1.3	0.1	9.8	-37.9	-23.2	-64.2	-25.6	31.7	-11.0	11.0	-15.7	2.4	6.1	1.8	15.8	3.1	1.8	27.3	-16.3	6.9	-6.1	-16.9	100.0

(b) Correlation matrix

Figure 92: Signal strength and normalization factors (top) and correlation matrix (bottom) for the 4000 GeV W'_L mass hypotheses.

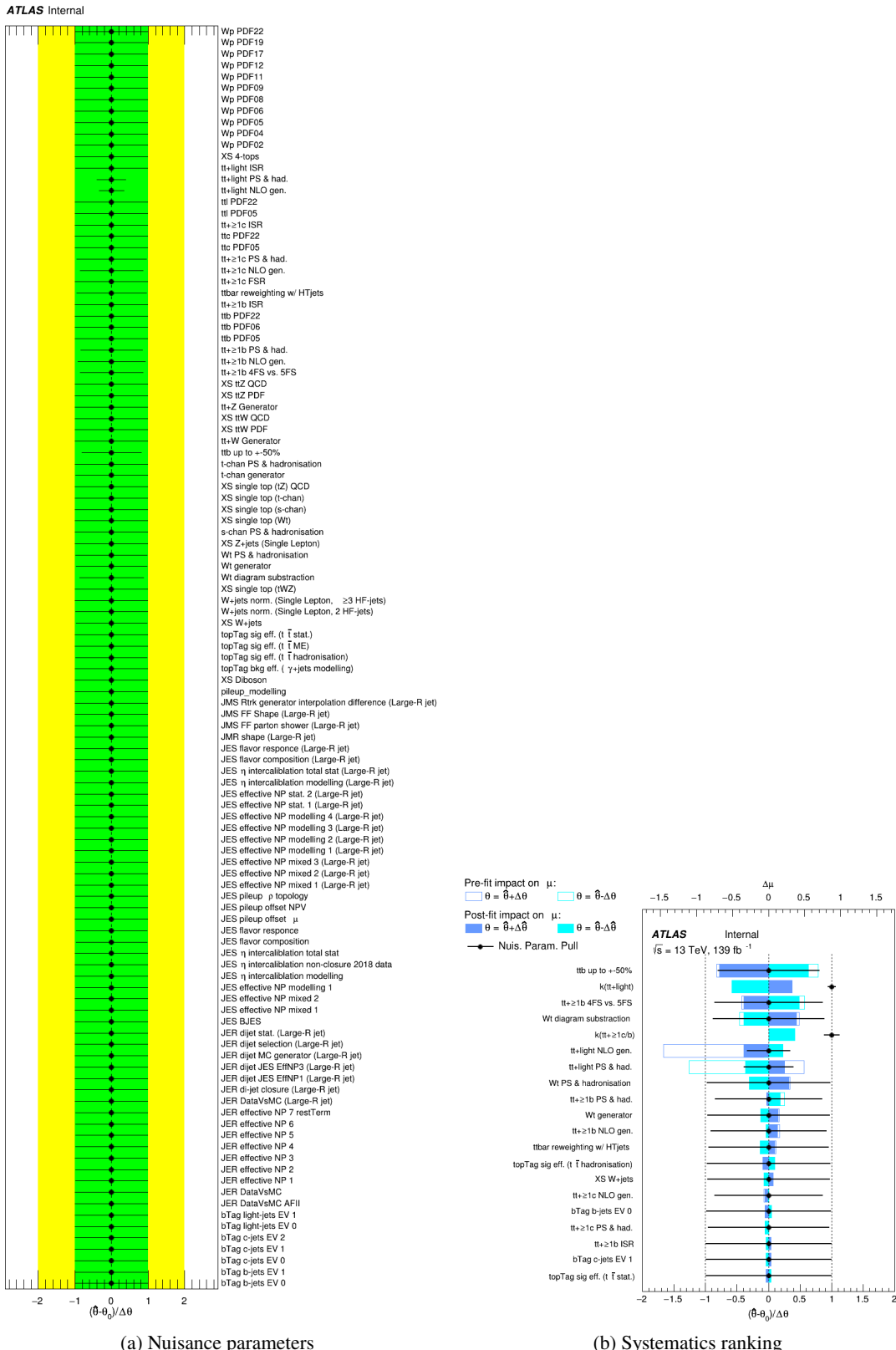
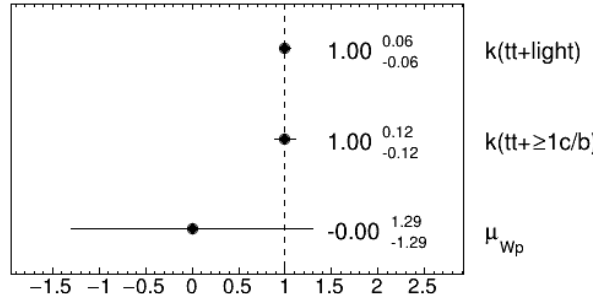


Figure 93: Nuisance parameters (left) and ranking plot (right) of the effect of various nuisance parameters before and after the fit for the 1000 GeV W'_P mass hypotheses.

ATLAS Internal**ATLAS Internal**

	bTag b-jets EV 0	-0.6	-1.3	-2.9	2.7	-1.1	-0.4	-0.7	0.1	-0.8	-1.0	0.5	3.3	-0.7	-6.7	7.4	3.0	3.8	1.8	0.8	0.3	0.4	-8.4	-3.3	41.6	-14.9
bTag b-jets EV 1	-0.6	100.0	-0.5	-1.2	1.2	-0.6	-0.1	-0.2	0.4	-0.2	-0.2	-0.1	-0.3	-0.2	-0.5	0.9	0.8	1.2	-0.2	-0.4	0.2	3.9	-6.4	2.3	20.1	-8.1
JES effective NP modeling 1	-1.3	-0.5	100.0	-3.2	2.4	-1.9	-0.0	-0.4	1.5	-0.3	-0.4	-0.1	0.2	-0.7	-1.7	2.9	2.9	1.7	1.2	-0.4	0.5	-4.9	-21.9	-0.4	-1.8	0.1
JES flavor composition	-2.9	-1.2	-3.2	100.0	5.6	-3.7	-0.2	-0.8	2.7	-0.8	-1.0	0.0	-0.4	-1.2	-4.4	5.6	5.0	5.0	0.2	-1.6	0.9	-1.4	-42.6	-0.3	-9.4	2.7
JES flavor response	2.7	1.2	2.4	5.6	100.0	2.9	0.3	0.8	-2.1	0.8	1.0	-0.5	1.1	0.9	5.1	-4.8	-2.6	-5.7	0.8	1.9	-0.7	-7.8	31.2	-0.6	6.4	-1.7
JES pileup p topology	-1.1	-0.6	-1.9	-3.7	2.9	100.0	0.1	-0.3	1.6	-0.3	-0.3	0.1	-1.6	-1.0	-0.5	2.2	3.9	2.2	-0.7	-0.9	0.4	-6.2	-26.6	0.5	-29.1	10.2
tive NP modelling 1 (Large-R jet)	-0.4	-0.1	-0.0	-0.2	0.3	0.1	100.0	-0.1	0.2	-0.1	-0.1	-0.4	1.5	0.2	-2.0	0.6	-1.1	0.4	0.6	-0.1	0.0	1.2	-1.9	-0.4	-14.3	37.3
abilitation modelling (Large-R jet)	-0.7	-0.2	-0.4	-0.8	0.8	-0.3	-0.1	100.0	0.2	-0.2	0.1	0.8	-0.1	-1.8	1.6	0.4	1.1	0.4	-0.0	0.1	0.7	-3.2	-1.1	7.3	22.7	
topTag sig eff. ($t\bar{t}$ hadronisation)	0.1	0.4	1.5	2.7	-2.1	1.6	0.2	0.2	100.0	0.2	0.2	1.7	-0.9	-0.5	-0.3	1.1	1.0	0.6	-5.5	1.2	-1.1	-18.0	26.9	-6.3	-10.6	-64.1
topTag sig eff. ($t\bar{t}$ ME)	-0.8	-0.2	-0.3	-0.8	0.8	-0.3	-0.1	-0.2	0.2	100.0	-0.3	-0.0	1.2	-0.1	-2.4	1.8	0.3	1.1	0.4	0.0	0.1	1.0	-3.0	-1.4	1.9	-24.9
topTag sig eff. ($t\bar{t}$ stat.)	-1.0	-0.2	-0.4	-1.0	1.0	-0.3	-0.1	-0.2	0.2	-0.3	100.0	-0.0	1.6	-0.1	-3.2	2.4	0.3	1.4	0.6	0.1	0.1	1.0	-3.5	-2.4	1.2	-30.9
XStW+jets	0.5	-0.1	-0.1	0.0	-0.5	0.1	-0.4	0.1	1.7	-0.0	-0.0	100.0	8.0	2.2	-3.2	-2.6	-2.5	-3.8	3.5	-0.5	0.7	21.6	-17.8	5.0	-7.8	-10.7
Wt diagram subtraction	3.3	-0.3	0.2	-0.4	1.1	-1.6	1.5	0.8	-0.9	1.2	1.6	8.0	100.0	-1.5	24.8	-12.5	4.4	4.3	-17.6	-5.3	-1.3	-15.4	10.2	32.9	20.5	5.7
Wt PS & hadronisation	-0.7	-0.2	-0.7	-1.2	0.9	-1.0	0.2	-0.1	-0.5	-0.1	-0.1	-0.1	100.0	3.0	6.1	6.7	1.9	-1.4	2.9	-0.2	-19.8	10.0	22.6	1.2	10.8	
ttb up to +50%	-6.7	-0.5	-1.7	4.4	5.1	-0.5	-2.0	-1.8	-0.3	-2.4	-3.2	-3.2	24.8	3.0	100.0	14.8	-12.4	7.7	4.8	-1.3	1.0	-3.4	-4.9	-50.5	45.5	-8.9
tt+>1b 4FS vs. SFS	7.4	0.9	2.9	5.6	-4.8	2.2	0.6	1.6	1.1	1.8	2.4	-2.6	-12.5	6.1	14.8	100.0	-21.1	-8.3	-11.8	-10.9	-0.4	1.2	-5.9	-33.0	20.1	-10.8
tt+>1b PS & had.	3.0	0.8	2.9	5.0	-2.6	3.9	-1.1	0.4	1.0	0.3	0.3	-2.5	4.4	6.7	-12.4	-21.1	100.0	-2.5	-2.1	-10.1	0.3	-17.8	9.9	-6.4	1.2	2.1
ttbar reweighting w/ H7jets	3.8	1.2	1.7	5.0	-5.7	2.2	0.4	1.1	0.6	1.1	1.4	-3.8	4.3	1.9	7.7	-8.3	-2.5	100.0	5.9	1.9	0.0	5.2	6.7	7.7	-43.3	17.1
tt+>1c NLO gen.	1.8	-0.2	1.2	0.2	0.8	-0.7	0.6	0.4	-5.5	0.4	0.6	3.5	-17.6	-1.4	4.8	-11.8	-2.1	5.9	100.0	-9.0	-2.2	-51.4	12.2	-2.2	-3.0	-0.7
tt+>1c PS & had.	0.8	-0.4	-0.4	-1.6	1.9	-0.9	-0.1	-0.0	1.2	0.0	0.1	-0.5	-5.3	2.9	-1.3	-10.9	-10.1	1.9	-9.0	100.0	0.1	-4.7	-25.7	0.8	-2.0	-0.3
tt PDF05	0.3	0.2	0.5	0.9	-0.7	0.4	0.0	0.1	-1.1	0.1	0.1	0.7	-1.3	-0.2	1.0	-0.4	0.3	0.0	-2.2	0.1	100.0	-5.4	8.1	-1.0	-0.7	27.0
tt+light NLO gen.	0.4	3.9	-4.9	-1.4	-7.8	-6.2	1.2	0.7	-18.0	1.0	1.0	21.6	-15.4	-19.8	-3.4	1.2	-17.8	5.2	-51.4	4.7	-5.4	100.0	-39.3	-21.4	0.1	-0.3
tt+light PS & had.	-8.4	-6.4	-21.9	-42.6	31.2	-26.6	-1.9	-3.2	26.9	-3.0	-3.5	-17.8	10.2	10.0	-4.9	-5.9	9.9	6.7	12.2	-25.7	8.1	-39.3	100.0	20.1	-7.4	-3.1
μ_{Wp}	-3.3	2.3	-0.4	-0.3	-0.6	0.5	-0.4	-1.1	-6.3	-1.4	-2.4	5.0	32.9	22.6	-50.5	-33.0	-6.4	7.7	-2.2	0.8	-1.0	-21.4	20.1	100.0	-41.2	28.5
k(t+>1b)	41.6	20.1	-1.8	-9.4	6.4	-29.1	-14.3	7.3	-10.6	1.9	1.2	-7.8	20.5	1.2	45.5	20.1	1.2	43.3	-3.0	-2.0	-0.7	0.1	-7.4	-41.2	100.0	-22.4
k(t+light)	-14.9	-8.1	0.1	2.7	-1.7	10.2	-37.3	-22.7	-64.1	-24.9	-30.9	-10.7	5.7	10.8	-8.9	-10.8	2.1	17.1	-0.7	-0.3	27.0	-0.3	-3.1	28.5	-22.4	100.0

(b) Correlation matrix

Figure 94: Signal strength and normalization factors (top) and correlation matrix (bottom) for the 1000 GeV W'_R mass hypotheses.

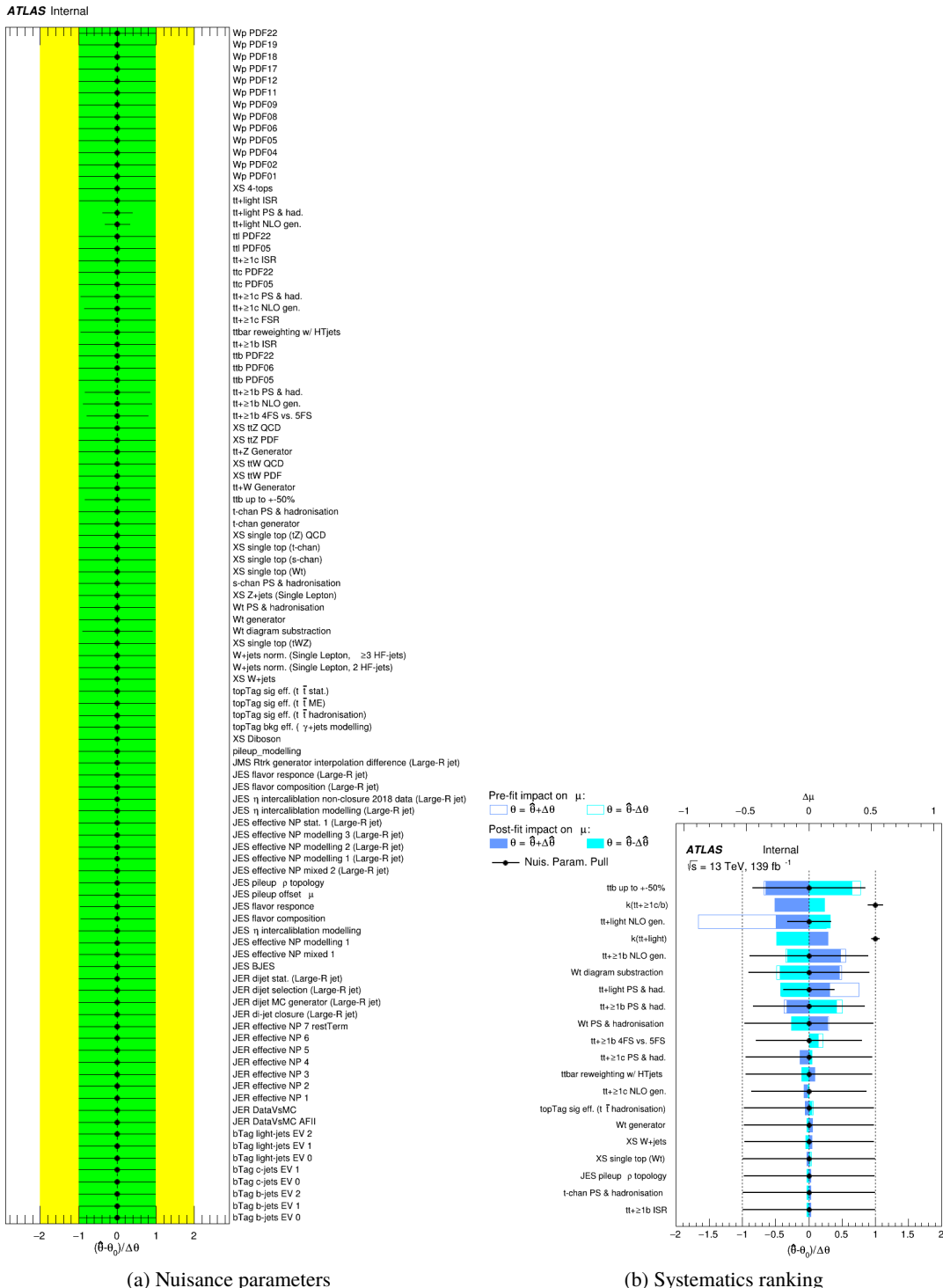
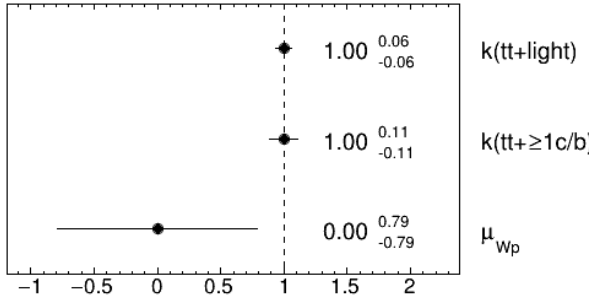


Figure 95: Nuisance parameters (left) and ranking plot (right) of the effect of various nuisance parameters before and after the fit for the 1200 GeV W'_R mass hypotheses.

ATLAS Internal

(a) Norm. factors

ATLAS Internal

	bTag b-jets EV 0	-0.6	-1.4	-2.9	2.7	-1.2	-0.3	-0.6	1.0	-0.7	-0.9	-0.2	1.1	-5.9	5.3	3.6	4.1	3.2	1.3	0.9	0.4	1.7	-9.2	-0.7	42.8	-15.7
bTag b-jets EV 1	-0.6	100.0	-0.5	-1.2	1.2	-0.6	-0.1	-0.2	0.4	-0.2	-0.3	0.1	-0.5	-0.4	1.6	0.2	1.1	1.3	0.2	-0.3	0.1	4.0	-6.6	2.1	21.1	8.2
JES effective NP modeling 1	-1.4	-0.5	100.0	-3.5	2.8	-2.1	-0.1	-0.4	2.0	-0.4	-0.5	-0.4	1.3	-2.8	2.5	2.3	2.0	1.7	1.9	0.5	0.6	-6.8	-21.4	0.7	-2.3	0.3
JES flavor composition	-2.9	-1.2	-3.5	100.0	6.3	-4.2	-0.3	-0.8	3.5	-0.9	-1.0	-0.2	0.7	-4.3	5.0	2.6	4.0	4.8	1.2	-0.2	1.0	-2.6	-42.9	1.2	-9.6	2.4
JES flavor response	2.7	1.2	2.8	6.3	100.0	3.5	0.3	0.8	-2.7	0.8	1.0	-0.4	0.7	4.2	-3.8	-1.1	-2.6	-5.5	0.5	0.6	-0.7	-8.2	31.6	-0.8	6.0	-1.1
JES pileup topology	-1.2	-0.6	-2.1	-4.2	3.5	100.0	-0.1	-0.3	2.2	-0.3	-0.4	-0.1	0.4	-0.9	2.1	1.1	2.0	2.1	0.2	-0.0	0.5	-7.9	-26.2	2.2	-30.3	10.3
tive NP modelling 1 (Large-R jet)	-0.3	-0.1	-0.1	-0.3	0.3	-0.1	100.0	-0.1	0.2	-0.1	-0.1	-0.3	0.6	-1.1	0.4	0.5	0.4	0.3	0.1	0.1	0.0	2.0	-2.2	-0.9	-14.6	37.7
ablation modelling (Large-R jet)	-0.6	-0.2	-0.4	-0.8	0.8	-0.3	-0.1	100.0	0.3	-0.2	-0.2	-0.0	0.2	-1.6	1.3	0.9	1.0	0.9	0.4	0.2	0.1	0.8	-3.3	-0.9	7.5	22.9
topTag sig eff. ($t\bar{t}$ hadronisation)	1.0	0.4	2.0	3.5	-2.7	2.2	0.2	0.3	100.0	0.3	0.4	1.0	-2.3	0.2	-4.2	-3.8	-2.9	-0.3	-7.2	-1.2	-1.0	-13.9	23.8	-3.9	-11.3	-64.2
topTag sig eff. ($t\bar{t}$ ME)	-0.7	-0.2	-0.4	-0.9	0.8	-0.3	-0.1	-0.2	0.3	100.0	-0.3	-0.2	0.5	-2.1	1.4	1.1	1.1	1.0	0.3	0.2	0.1	1.2	-3.2	-1.1	1.9	-25.1
topTag sig eff. ($t\bar{t}$ stat.)	-0.9	-0.3	-0.5	-1.0	1.0	-0.4	-0.1	-0.2	0.4	-0.3	100.0	-0.2	0.8	-2.8	1.7	1.4	1.4	1.2	0.4	0.3	0.1	1.3	-3.6	-2.0	1.1	-31.1
XStW+jets	-0.2	0.1	-0.4	-0.2	-0.4	-0.1	-0.3	-0.0	1.0	-0.2	-0.2	100.0	8.1	-3.5	-1.4	3.3	0.2	-3.3	4.3	1.5	0.6	20.7	-17.2	3.5	-8.0	-10.3
Wt diagram subtraction	1.1	-0.5	1.3	0.7	0.7	0.4	0.6	0.2	-2.3	0.5	0.8	8.1	100.0	15.7	1.4	-12.1	-2.3	6.5	-9.5	-7.0	-1.2	-26.8	15.4	34.5	18.7	9.3
ttb up to +50%	-5.9	-0.4	-2.8	-4.3	4.2	-0.9	-1.1	-1.6	0.2	-2.1	-2.8	-3.5	15.7	100.0	1.3	13.9	2.3	6.0	-1.2	4.5	0.8	0.7	8.8	-48.6	43.5	9.9
tt+ ≥ 1 b 4FS vs. 5FS	5.3	1.6	2.5	5.0	-3.8	2.1	0.4	1.3	-4.2	1.4	1.7	-1.4	1.4	1.3	100.0	-29.4	-46.3	-7.5	-15.5	-8.0	0.2	5.8	-7.8	-5.1	9.6	-0.7
tt+ ≥ 1 b NLO gen.	3.6	0.2	2.3	2.6	-1.1	1.1	0.5	0.9	-3.8	1.1	1.4	3.3	-12.1	13.9	-29.4	100.0	-24.6	-0.0	-14.8	-10.2	-0.7	2.3	-4.6	27.2	-1.5	-1.8
tt+ ≥ 1 b PS & had.	4.1	1.1	2.0	4.0	-2.6	2.0	0.4	1.0	-2.9	1.1	1.4	0.2	-2.3	2.3	-46.3	-24.6	100.0	-4.6	-11.1	-7.7	0.4	9.1	-7.3	-26.6	10.5	-2.3
ttbar reweighting w/ H7jets	3.2	1.3	1.7	4.8	-5.5	2.1	0.3	0.9	-0.3	1.0	1.2	-3.3	6.5	6.0	-7.5	-0.0	-4.6	100.0	6.2	2.3	0.0	4.3	7.6	6.3	-44.5	18.0
tt+ ≥ 1 c NLO gen.	1.3	0.2	1.9	1.2	0.5	0.2	0.1	0.4	-7.2	0.3	0.4	4.3	-9.5	-1.2	-15.5	-14.8	-11.1	6.2	100.0	-8.3	-2.2	-56.3	11.6	-1.4	-4.3	2.7
tt+ ≥ 1 c PS & had.	0.9	-0.3	0.5	-0.2	0.6	-0.0	0.1	0.2	-1.2	0.2	0.3	1.5	-7.0	4.5	-8.0	-10.2	-7.7	2.3	-8.3	100.0	-0.2	-0.8	-32.0	-6.5	0.6	-1.0
tt PDF05	0.4	0.1	0.6	1.0	-0.7	0.5	0.0	0.1	-1.0	0.1	0.1	0.6	-1.2	0.8	0.2	-0.7	0.4	0.0	-2.2	-0.2	100.0	-6.1	8.6	-0.8	-0.9	27.1
tt+light NLO gen.	1.7	4.0	-6.8	-2.6	-8.2	-7.9	2.0	0.8	-13.9	1.2	1.3	20.7	-26.8	0.7	5.8	2.3	9.1	4.3	-56.3	-0.8	-6.1	100.0	-33.7	-27.3	-0.4	-5.4
tt+light PS & had.	-9.2	-6.6	-21.4	-42.9	31.6	-26.2	-2.2	-3.3	23.8	-3.2	-3.6	-17.2	15.4	-8.8	-7.8	-4.6	-7.3	7.6	11.6	-32.0	8.6	-33.7	100.0	23.7	-7.8	0.1
μ_{Wp}	-0.7	2.1	0.7	1.2	-0.8	2.2	-0.9	-0.9	-3.9	-1.1	-2.0	3.5	34.5	-48.6	-5.1	27.2	-26.6	6.3	-1.4	-6.5	-0.8	-27.3	23.7	100.0	-31.0	23.0
k(tt+ ≥ 1 b)	42.8	21.1	-2.3	-9.6	6.0	-30.3	-14.6	7.5	-11.3	1.9	1.1	-8.0	18.7	43.5	9.6	-1.5	10.5	44.5	-4.3	0.6	-0.9	-0.4	-7.8	-31.0	100.0	-20.2
k(tt+light)	-15.7	-8.2	0.3	2.4	-1.1	10.3	-37.7	-22.9	-64.2	-25.1	-31.1	-10.3	9.3	-9.9	-0.7	-1.8	-2.3	18.0	2.7	-1.0	27.1	-5.4	0.1	23.0	-20.2	100.0

(b) Correlation matrix

Figure 96: Signal strength and normalization factors (top) and correlation matrix (bottom) for the 1200 GeV W'_R mass hypotheses.

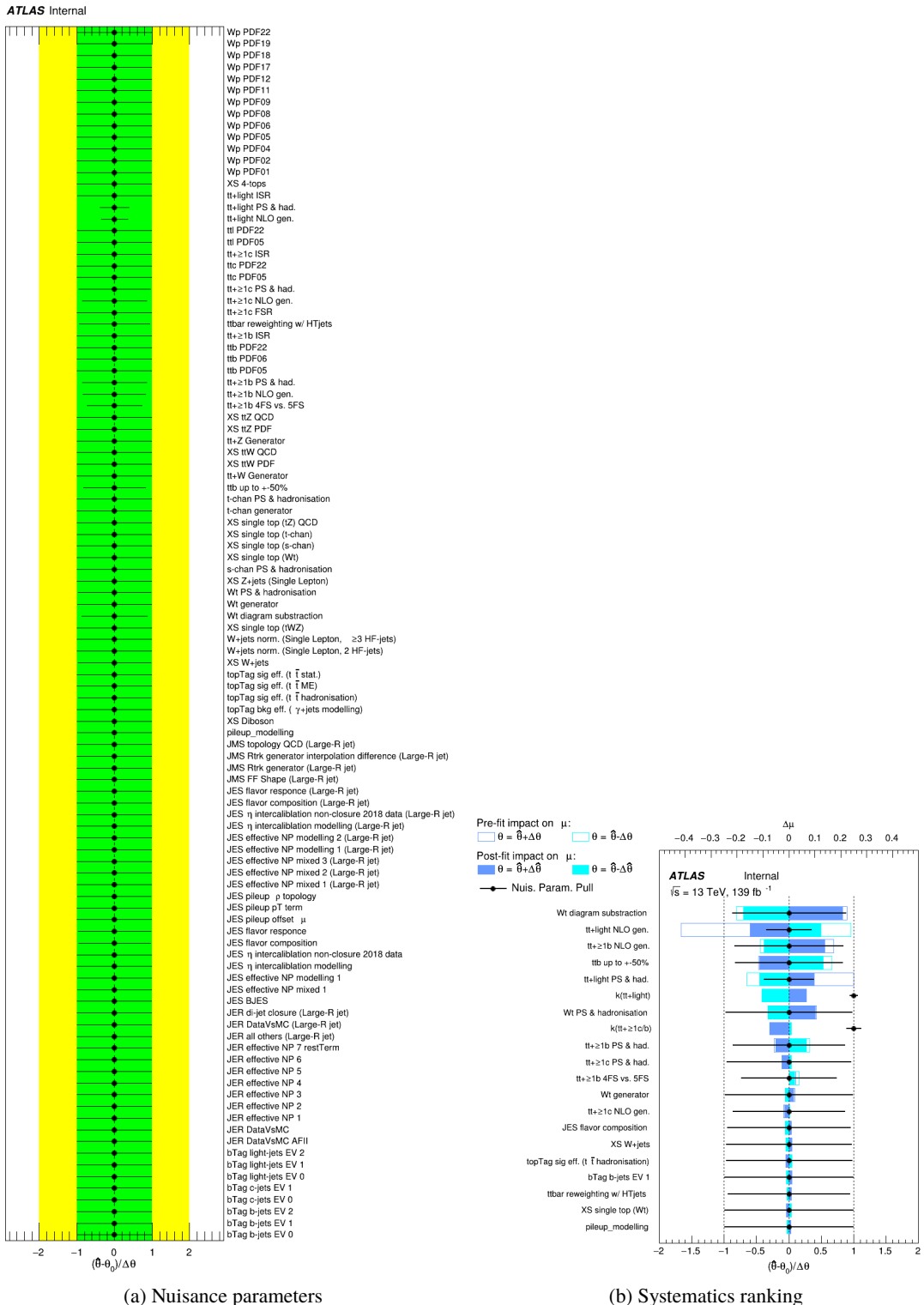
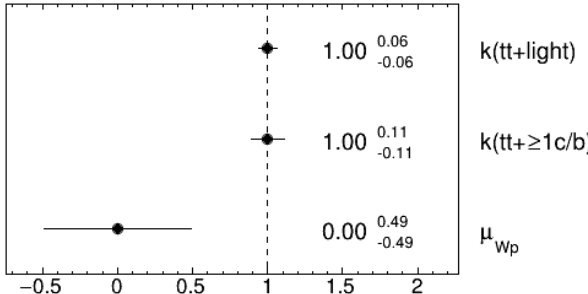


Figure 97: Nuisance parameters (left) and ranking plot (right) of the effect of various nuisance parameters before and after the fit for the 1400 GeV W'_R mass hypotheses.

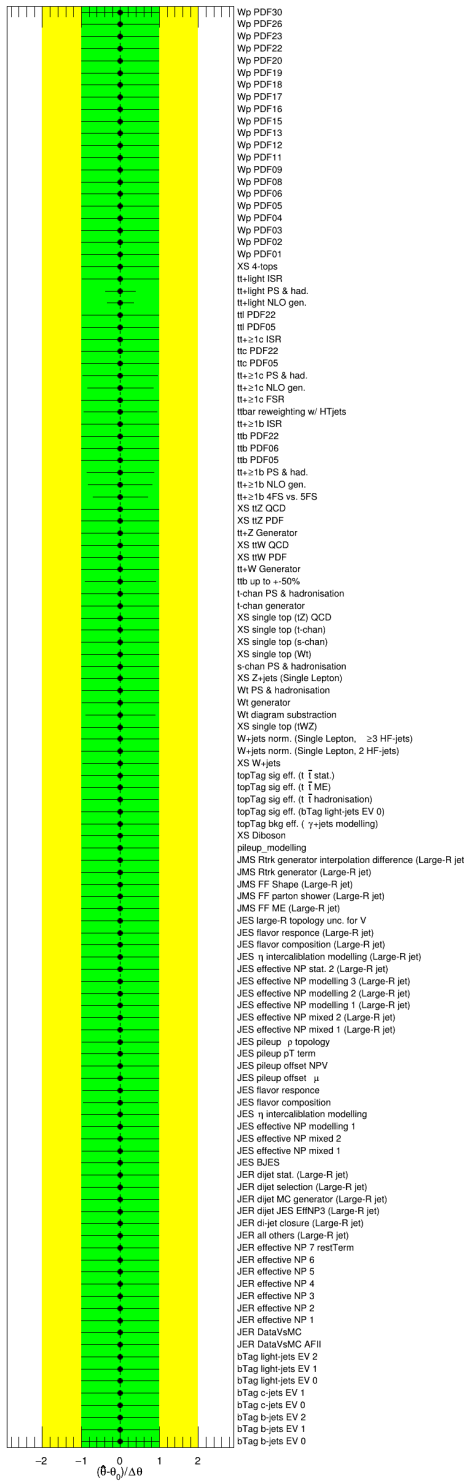
ATLAS Internal**ATLAS Internal**

	bTag b-jets EV 0	bTag b-jets EV 1	JES effective NP modeling 1	JES flavor composition	JES flavor response	JES pileup topology	tive NP modelling 1 (Large-R jet)	ablation modelling (Large-R jet)	topTag sig eff. ($t\bar{t}$ hadronisation)	topTag sig eff. ($t\bar{t}$ ME)	topTag sig eff. ($t\bar{t}$ stat.)	XS W+jets	W diagram subtraction	ttb up to +50%	tt+≥1b 4FS vs. 5FS	tt+≥1b NLO gen.	tt+≥1b PS & had.	ttbar reweighting w/ Higgs	tt+≥1c NLO gen.	tt+≥1c PS & had.	tt PDF05	tt+light NLO gen.	tt+light PS & had.	μ_{Wp}	k(tt+≥1c/b)	k(tt+light)
100.0	-0.5	-1.1	-2.6	2.4	-1.3	-0.2	-0.4	1.0	-0.5	-0.6	0.1	0.2	-3.5	3.2	2.1	1.9	2.0	-0.3	-0.5	0.4	6.1	-12.1	0.7	44.9	-16.7	
-0.5	100.0	-0.4	-1.0	1.0	-0.5	-0.1	-0.2	0.4	-0.2	-0.2	0.1	-0.9	0.1	1.4	-0.1	0.9	1.3	0.1	-0.5	0.1	4.4	-7.2	2.1	21.7	-8.4	
-1.1	-0.4	100.0	-4.4	3.2	-2.8	-0.0	-0.4	2.7	-0.4	-0.5	-0.5	0.2	-3.7	0.9	2.7	1.7	0.0	0.5	0.2	0.9	-4.6	-20.8	1.0	-1.7	-0.4	
-2.6	-1.0	-4.4	100.0	7.1	-5.4	-0.1	-0.9	4.7	-0.9	-1.1	-0.7	-0.3	-8.3	1.7	4.2	3.2	2.0	-1.4	-0.4	1.6	-0.9	-40.8	2.4	-9.7	1.8	
2.4	1.0	3.2	7.1	100.0	4.0	0.2	0.8	-3.2	0.8	1.0	-0.1	1.2	7.3	-1.0	-1.9	-1.5	-3.6	2.3	1.5	-1.1	-9.2	30.6	-0.9	5.9	-1.0	
-1.3	-0.5	-2.8	-5.4	4.0	100.0	0.0	-0.4	2.9	-0.4	-0.5	-0.5	-0.4	-4.6	0.2	2.4	1.9	0.3	-1.1	0.1	1.0	-7.4	-24.0	1.3	-31.1	10.2	
-0.2	-0.1	-0.0	-0.1	0.2	0.0	100.0	-0.0	0.1	-0.0	-0.0	-0.3	0.3	-0.4	-0.4	-0.3	-0.3	0.3	0.0	-0.3	-0.0	3.1	-3.2	0.1	-14.8	-37.9	
-0.4	-0.2	-0.4	-0.9	0.8	-0.4	-0.0	100.0	0.4	-0.1	-0.2	0.1	0.2	-1.4	1.3	1.1	0.8	0.6	-0.1	-0.1	0.1	1.3	-3.5	-0.2	7.8	-23.1	
1.0	0.4	2.7	4.7	-3.2	2.9	0.1	0.4	100.0	0.4	0.5	1.2	-0.6	1.7	-4.6	-5.7	-4.2	1.2	-6.1	-1.7	-1.5	-13.2	21.9	-2.3	-11.9	-63.8	
-0.5	-0.2	-0.4	-0.9	0.8	-0.4	-0.0	-0.1	0.4	100.0	-0.2	-0.0	0.4	-1.8	1.4	1.2	0.9	0.6	-0.2	-0.1	0.1	1.9	-3.5	-0.3	2.2	-25.4	
-0.6	-0.2	-0.5	-1.1	1.0	-0.5	-0.0	-0.2	0.5	-0.2	100.0	-0.0	0.7	-2.5	1.8	1.7	1.0	0.7	-0.3	-0.0	0.2	2.1	-4.0	-1.0	1.5	-31.5	
0.1	0.1	-0.5	-0.7	-0.1	-0.5	-0.3	0.1	1.2	-0.0	-0.0	100.0	7.2	-2.4	-2.8	2.5	0.4	-4.2	3.7	1.0	0.6	21.5	-17.7	2.6	-6.9	-11.3	
0.2	-0.9	0.2	-0.3	1.2	-0.4	0.3	0.2	-0.6	0.4	0.7	7.2	100.0	2.0	3.7	-14.9	3.1	8.9	-5.4	-0.6	-0.9	-26.2	17.2	47.0	17.8	7.7	
-3.5	0.1	-3.7	-8.3	7.3	-4.6	-0.4	-1.4	1.7	-1.8	-2.5	-2.4	20.0	100.0	-3.3	17.3	-3.5	-1.5	-8.0	-0.9	1.5	7.7	-5.2	-27.0	45.0	-11.5	
3.2	1.4	0.9	1.7	-1.0	0.2	-0.4	1.3	-4.6	1.4	1.8	-2.8	3.7	-3.3	100.0	-40.7	-47.4	-6.7	-14.0	-12.4	-1.1	7.5	-2.6	-1.9	7.5	1.0	
2.1	-0.1	2.7	4.2	-1.9	2.4	-0.3	1.1	-5.7	1.2	1.7	2.5	-14.9	17.3	-40.7	100.0	-24.8	5.7	-8.4	-8.8	-2.2	3.9	-9.3	23.6	-2.5	-0.8	
1.9	0.9	1.7	3.2	-1.5	1.9	-0.3	0.8	-4.2	0.9	1.0	0.4	3.1	-3.5	-47.4	-24.8	100.0	-1.0	-6.9	-10.0	-1.2	0.8	0.3	-12.5	3.8	1.9	
2.0	1.3	0.0	2.0	-3.6	0.3	0.3	0.6	1.2	0.6	0.7	-4.2	8.9	-1.5	-6.7	5.7	-1.0	100.0	6.1	4.9	0.6	-3.1	16.7	1.9	-46.3	18.6	
-0.3	0.1	0.5	-1.4	2.3	-1.1	0.0	-0.1	-6.1	-0.2	-0.3	3.7	-5.4	-8.0	-14.0	-8.4	-6.9	6.1	100.0	-6.9	-1.9	-6.2	21.8	-1.9	-6.4	4.3	
-0.5	-0.5	0.2	-0.4	1.5	0.1	-0.3	-0.1	-1.7	-0.1	-0.0	1.0	-0.6	-0.9	-12.4	-8.8	-10.0	4.9	-6.9	100.0	-0.6	-7.0	-27.3	-4.0	-2.6	2.1	
0.4	0.1	0.9	1.6	-1.1	1.0	-0.0	0.1	-1.5	0.1	0.2	0.6	-0.9	1.5	-1.1	-2.2	-1.2	0.6	-1.9	-0.6	100.0	-4.8	6.8	-0.8	-1.0	27.5	
6.1	4.4	-4.6	-0.9	-9.2	-7.4	3.1	1.3	-13.2	1.9	2.1	21.5	-26.2	7.7	7.5	3.9	0.8	-3.1	-62.2	-7.0	-4.8	100.0	-41.0	-27.6	7.2	-8.8	
-12.1	-7.2	-20.8	-40.8	30.6	-24.0	-3.2	-3.5	21.9	-3.5	-4.0	-17.7	17.2	-5.2	-2.6	-9.3	0.3	16.7	21.8	6.8	-41.0	100.0	21.0	-11.5	2.8		
0.7	2.1	1.0	2.4	-0.9	1.3	0.1	-0.2	-2.3	-0.3	-1.0	2.6	47.0	-27.0	-1.9	23.6	-12.5	1.9	-1.9	-4.0	-0.8	-27.6	21.0	100.0	-12.1	16.2	
44.9	21.7	-1.7	-9.7	5.9	-31.1	-14.8	7.8	-11.9	2.2	1.5	-6.9	17.8	45.0	7.5	-2.5	3.8	-46.3	-6.4	-2.6	-1.0	7.2	-11.5	-12.1	100.0	-20.3	
-16.7	-8.4	-0.4	1.8	-1.0	10.2	-37.9	-23.1	-63.8	-25.4	-31.5	-11.3	7.7	-11.5	1.0	-0.8	1.9	18.6	4.3	2.1	27.5	-8.8	2.8	16.2	-20.3	100.0	

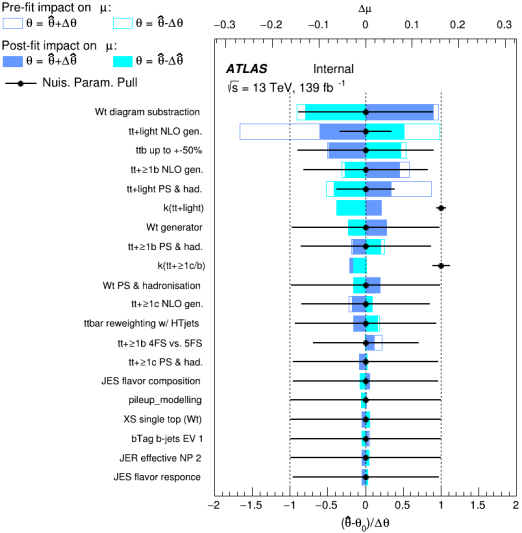
(b) Correlation matrix

Figure 98: Signal strength and normalization factors (top) and correlation matrix (bottom) for the 1400 GeV W'_R mass hypotheses.

ATLAS Internal



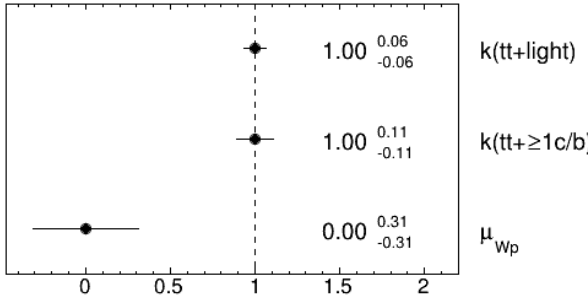
(a) Nuisance parameters



(b) Systematics ranking

Figure 99: Nuisance parameters (left) and ranking plot (right) of the effect of various nuisance parameters before and after the fit for the 1600 GeV W'_R mass hypotheses.

ATLAS Internal



(a) Norm. factors

ATLAS Internal

	bTag b-jets EV 0	bTag b-jets EV 1	JES effective NP modelling 1	JES flavor composition	JES flavor response	JES pileup p topology	tive NP modelling 1 (Large-R jet)	calibration modelling (Large-R jet)	topTag sig eff. ($t\bar{t}$ hadronisation)	topTag sig eff. ($t\bar{t}$ ME)	topTag sig eff. ($t\bar{t}$ stat.)	Wt diagram subtraction	tt up to +50%	tt+>1b 4FS vs. 5FS	tt+>1b NLO gen.	tt+>1b PS & had.	ttbar reweighting w/ HT jets	tt+>1c NLO gen.	tt+>1c PS & had.	tt PDF05	tt+light NLO gen.	tt+light PS & had.	μ_{W_p}	k($t\bar{t}+\geq 1c/b$)	k($t\bar{t}+\text{light}$)
bTag b-jets EV 0	100.0	-0.5	-1.2	-2.8	2.8	-1.4	-0.3	-0.4	1.1	-0.5	-0.6	0.5	-3.6	3.4	3.6	2.1	1.5	0.6	-0.1	0.5	4.4	-11.1	1.2	45.6	-16.6
bTag b-jets EV 1	-0.5	100.0	-0.4	-1.1	1.1	-0.5	-0.1	-0.2	0.4	-0.2	-0.2	-0.4	-0.7	0.6	-0.0	0.5	1.2	0.5	-0.4	0.2	4.0	-6.8	2.6	21.9	-8.2
JES effective NP modelling 1	-1.2	-0.4	100.0	-3.5	3.1	-2.4	-0.2	-0.4	2.2	-0.4	-0.4	1.2	-1.8	-0.2	4.3	0.7	0.2	3.1	0.3	0.8	-7.5	-21.4	1.4	-1.0	-0.1
JES flavor composition	-2.8	-1.1	-3.5	100.0	6.5	-4.3	-0.5	-0.8	3.8	-0.9	-1.1	0.8	-4.3	7.2	8.3	5.2	3.2	3.5	-0.0	1.3	-7.7	-40.3	3.2	-9.1	2.3
JES flavor response	2.8	1.1	3.1	6.5	100.0	3.9	0.5	0.8	-3.1	0.9	1.1	-1.1	5.8	-0.5	-6.3	-1.0	-3.3	-1.8	0.5	-1.1	-2.8	28.9	-2.0	5.0	-1.4
JES pileup p topology	-1.4	-0.5	-2.4	-4.3	3.9	100.0	-0.2	-0.4	2.4	-0.4	-0.5	1.4	-2.0	-1.3	4.9	0.6	0.7	2.6	0.3	0.8	-11.7	-24.3	1.6	-30.2	10.6
tive NP modelling 1 (Large-R jet)	-0.3	-0.1	-0.2	-0.5	0.5	-0.2	100.0	-0.1	0.3	-0.1	-0.1	1.1	-1.2	0.4	1.3	0.3	-0.1	0.0	0.1	0.1	1.3	-1.6	-1.5	-14.7	-37.6
calibration modelling (Large-R jet)	-0.4	-0.2	-0.4	-0.8	0.8	-0.4	-0.1	100.0	0.4	-0.1	-0.2	0.1	-0.8	0.5	0.6	0.4	0.6	0.3	-0.1	0.1	1.7	-3.9	1.2	8.0	-23.0
topTag sig eff. ($t\bar{t}$ hadronisation)	1.1	0.4	2.2	3.8	-3.1	2.4	0.3	0.4	100.0	0.4	0.5	-2.3	1.2	2.8	-7.5	-2.1	1.1	9.0	-1.5	-1.3	-10.1	22.2	-2.1	-12.6	64.0
topTag sig eff. ($t\bar{t}$ ME)	-0.5	-0.2	-0.4	-0.9	0.9	-0.4	-0.1	-0.1	0.4	100.0	-0.2	0.4	-1.5	1.0	1.2	0.6	0.4	-0.0	-0.0	0.1	1.9	-3.6	-0.3	2.4	-25.3
topTag sig eff. ($t\bar{t}$ stat.)	-0.6	-0.2	-0.4	-1.1	1.1	-0.5	-0.1	-0.2	0.5	-0.2	100.0	0.7	-1.9	1.3	1.7	0.8	0.5	-0.1	-0.0	0.2	2.1	-4.2	-1.2	1.7	-31.3
Wt diagram subtraction	0.5	-0.4	1.2	0.8	-1.1	1.4	1.1	0.1	-2.3	0.4	0.7	100.0	8.6	7.3	-15.1	2.2	9.9	-5.8	-3.5	-1.2	-28.0	17.3	50.2	15.4	10.2
tt up to +50%	-3.6	-0.7	-1.8	-4.3	5.8	-2.0	-1.2	-0.8	1.2	-1.5	-1.9	8.6	100.0	3.7	11.1	-0.9	-2.6	-7.9	-0.9	0.8	15.0	-15.4	-27.3	44.3	-13.9
tt+>1b 4FS vs. 5FS	3.4	0.6	-0.2	7.2	-0.5	-1.3	0.4	0.5	-2.8	1.0	1.3	7.3	3.7	100.0	-33.2	-55.3	-7.5	-1.1	-6.1	-0.5	-7.0	-1.7	3.6	10.6	-0.2
tt+>1b NLO gen.	3.6	-0.0	4.3	8.3	-6.3	4.9	1.3	0.6	-7.5	1.2	1.7	-15.1	11.1	-33.2	100.0	-22.4	11.6	-14.1	-12.7	-2.9	9.1	-14.4	18.6	-6.7	1.0
tt+>1b PS & had.	2.1	0.5	0.7	5.2	-1.0	0.6	0.3	0.4	-2.1	0.6	0.8	2.2	-0.9	-55.3	-22.4	100.0	-2.1	-5.7	-6.5	-0.7	-1.4	0.3	-10.2	4.0	0.2
ttbar reweighting w/ HT jets	1.5	1.2	0.2	3.2	-3.3	0.7	-0.1	0.6	1.1	0.4	0.5	9.9	-2.6	-7.5	11.6	-2.1	100.0	7.8	5.7	0.6	-9.4	18.0	-8.3	-45.6	18.9
tt+>1c NLO gen.	0.6	0.5	3.1	3.5	-1.8	2.6	0.0	0.3	-9.0	-0.0	-0.1	-5.8	-7.9	-1.1	-14.1	-5.7	7.8	100.0	-9.6	-3.1	-59.7	13.5	-7.0	-7.7	5.7
tt+>1c PS & had.	-0.1	-0.4	0.3	-0.0	0.5	0.3	0.1	-0.1	-1.5	-0.0	-0.0	-3.5	-0.9	-6.1	-12.7	-6.5	5.7	-9.6	100.0	-0.7	-3.2	-29.0	-3.0	-4.2	1.5
tt PDF05	0.5	0.2	0.8	1.3	-1.1	0.8	0.1	0.1	-1.3	0.1	0.2	-1.2	0.8	-0.5	-2.9	-0.7	0.6	-3.1	-0.7	100.0	-3.6	7.0	-0.6	-1.3	27.2
tt+light NLO gen.	4.4	4.0	-7.5	-7.7	-2.8	-11.7	1.3	1.7	-10.1	1.9	2.1	-28.0	15.0	-7.0	9.1	-1.4	-9.4	-59.7	-3.2	-3.6	100.0	-33.7	-29.4	12.9	-12.3
tt+light PS & had.	-11.1	-6.8	-21.4	-40.3	28.9	-24.3	-1.6	-3.9	22.2	-3.6	-4.2	17.3	-15.4	-1.7	-14.4	0.3	18.0	13.5	-29.0	7.0	-33.7	100.0	19.4	-15.3	3.5
μ_{W_p}	1.2	2.6	1.4	3.2	-2.0	1.6	-1.5	1.2	-2.1	-0.3	-1.2	50.2	-27.3	3.6	18.6	-10.2	-8.3	-7.0	-3.0	-0.6	-29.4	19.4	100.0	-3.1	14.0
k($t\bar{t}+\geq 1c/b$)	45.6	21.9	-1.0	-9.1	5.0	-30.2	-14.7	8.0	-12.6	2.4	1.7	15.4	44.3	10.6	-6.7	4.0	-45.6	-7.7	-4.2	-1.3	12.9	-15.3	-3.1	100.0	-20.1
k($t\bar{t}+\text{light}$)	-16.6	-8.2	-0.1	2.3	-1.4	10.6	-37.6	-23.0	-64.0	25.3	-31.3	10.2	-13.9	-0.2	1.0	0.2	18.9	5.7	1.5	27.2	-12.3	3.5	14.0	-20.1	100.0

(b) Correlation matrix

Figure 100: Signal strength and normalization factors (top) and correlation matrix (bottom) for the 1600 GeV W'_R mass hypotheses.

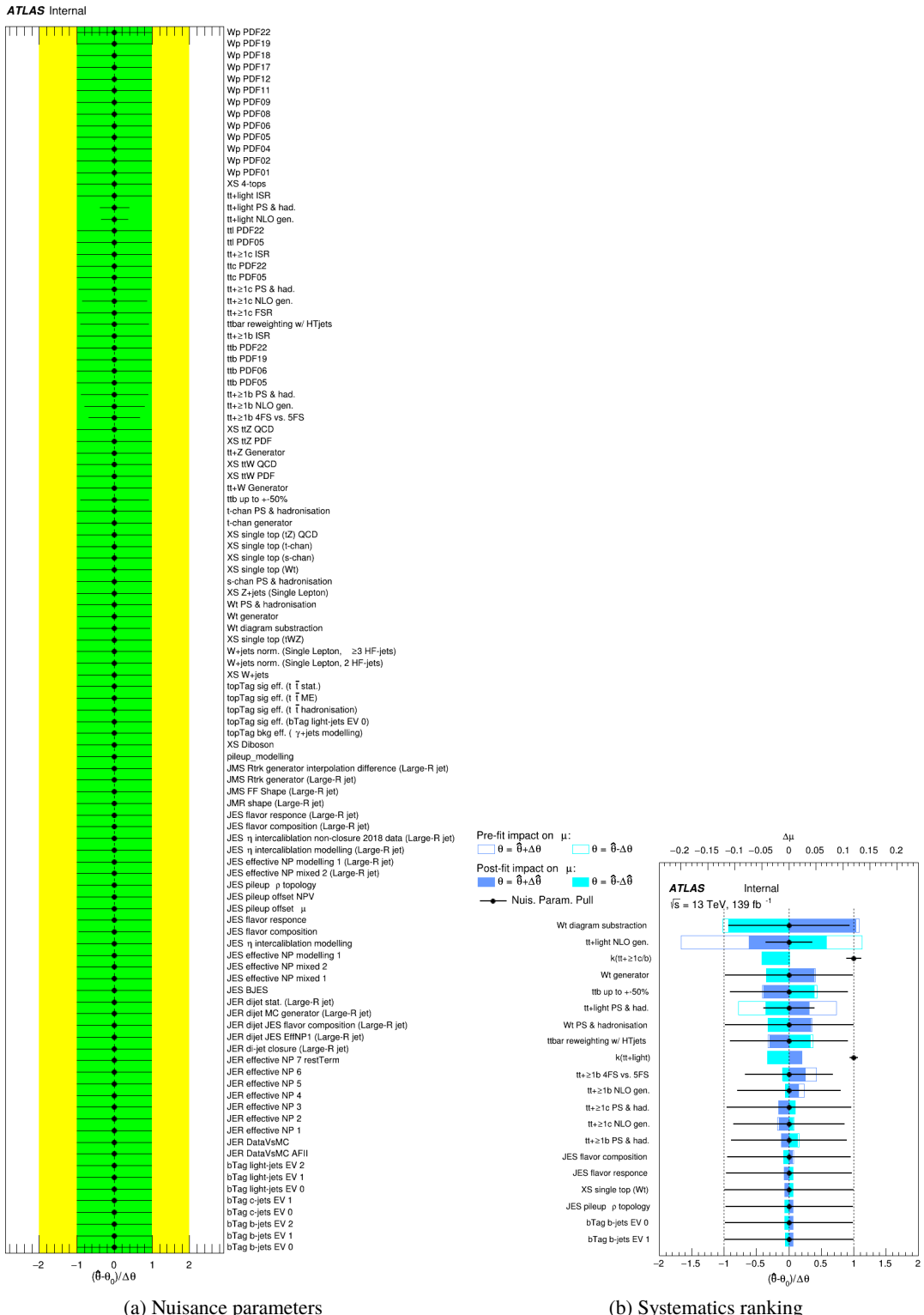
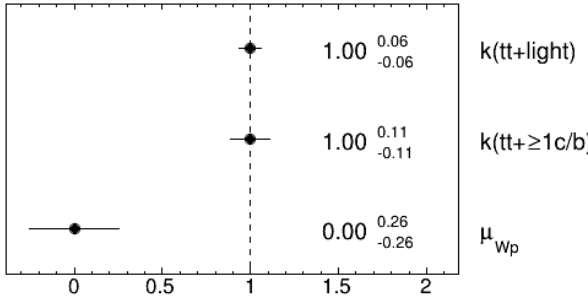


Figure 101: Nuisance parameters (left) and ranking plot (right) of the effect of various nuisance parameters before and after the fit for the 1800 GeV W'_R mass hypotheses.

ATLAS Internal



(a) Norm. factors

ATLAS Internal

	bTag b-jets EV 0	-0.5	-1.0	-2.6	2.4	-1.2	-0.3	-0.5	0.8	-0.5	-0.6	-0.0	0.3	-2.9	3.8	3.0	2.1	1.4	0.2	-0.4	0.4	5.3	-12.0	3.0	45.7	-16.5
bTag b-jets EV 1	-0.5	100.0	-0.4	-1.1	1.0	-0.5	-0.1	-0.2	0.3	-0.2	-0.2	0.0	-0.2	-0.4	0.9	-0.2	0.5	1.5	0.2	-0.4	0.2	4.1	-6.9	2.8	21.9	-8.1
JES effective NP modeling 1	-1.0	-0.4	100.0	-2.8	2.7	-2.1	-0.1	-0.4	1.8	-0.3	-0.4	-0.3	1.2	-2.5	1.0	4.6	1.8	0.2	1.1	-0.2	0.6	-5.8	-22.1	1.2	-1.2	0.2
JES flavor composition	-2.6	-1.1	-2.8	100.0	5.0	-3.4	-0.3	-0.9	3.0	-0.8	-1.0	0.5	-1.3	-3.1	21.5	7.1	9.0	6.0	2.5	0.1	1.0	-7.4	-39.2	3.4	-10.4	2.5
JES flavor response	2.4	1.0	2.7	5.0	100.0	3.3	0.4	0.9	-2.2	0.8	1.0	-0.4	-1.0	6.4	-1.7	-5.7	-2.5	-3.2	1.7	1.5	-0.8	-5.9	31.1	-3.2	5.2	-1.8
JES pileup p topology	-1.2	-0.5	-2.1	-3.4	3.3	100.0	-0.1	-0.4	1.9	-0.4	-0.4	-0.1	1.2	-3.1	0.9	5.5	2.7	1.2	-0.3	0.0	0.6	-9.4	-25.0	3.0	-30.8	10.9
tree NP modelling 1 (Large-R jet)	-0.3	-0.1	-0.1	-0.3	0.4	-0.1	100.0	-0.1	0.2	-0.0	-0.1	-0.3	0.5	-0.8	0.2	0.7	0.3	-0.1	-0.1	0.0	2.1	-2.3	-1.1	-14.7	37.6	
ablation modelling (Large-R jet)	-0.5	-0.2	-0.4	-0.9	0.9	-0.4	-0.1	100.0	0.3	-0.2	-0.2	0.0	0.2	-1.2	1.3	1.5	0.8	0.2	-0.0	-0.1	0.1	1.0	-3.5	-0.4	8.1	22.9
topTag sig eff. (t T hadronisation)	0.8	0.3	1.8	3.0	-2.2	1.9	0.2	0.3	100.0	0.3	0.4	1.0	-1.9	1.1	-4.3	-5.6	-2.5	0.4	-6.9	-0.7	-1.1	-12.7	24.1	-2.7	-12.2	43.9
topTag sig eff. (t T ME)	-0.5	-0.2	-0.3	-0.8	0.8	-0.4	-0.0	-0.2	0.3	100.0	-0.2	-0.0	0.2	-1.2	1.3	1.1	0.7	0.4	-0.1	-0.2	0.1	2.1	-3.9	0.1	2.4	-25.3
topTag sig eff. (t T stat.)	-0.6	-0.2	-0.4	-1.0	1.0	-0.4	-0.1	-0.2	0.4	-0.2	100.0	-0.1	0.3	-1.6	1.5	1.5	0.8	0.3	-0.1	-0.2	0.1	2.5	-4.5	-0.8	1.7	-31.3
XW+jets	-0.0	0.0	-0.3	0.5	-0.4	-0.1	-0.3	0.0	1.0	-0.0	-0.1	100.0	5.8	-1.8	-2.5	4.1	1.5	-4.5	3.6	0.6	0.5	20.8	-18.6	-1.7	-6.8	-11.4
Wt diagram subtraction	0.3	-0.2	1.2	-1.3	-1.0	1.2	0.5	0.2	-1.9	0.2	0.3	5.8	100.0	8.7	7.8	-13.4	-1.9	10.6	-4.4	-2.2	-0.9	-32.4	21.1	53.1	18.6	11.0
tbt up to +50%	-2.9	-0.4	-2.5	-3.1	6.4	-3.1	-0.8	-1.2	1.1	-1.2	-1.6	-1.8	8.7	100.0	-0.9	14.2	0.6	-7.1	-5.4	-1.7	0.6	13.3	-15.5	-19.0	45.7	-14.6
tt+geq1b 4FS vs. 5FS	3.8	0.9	1.0	21.5	-1.7	0.9	0.2	1.3	-4.3	1.3	1.5	-2.5	7.8	-0.9	100.0	-31.7	-42.2	-9.0	-16.6	-10.0	-1.2	6.4	-16.1	8.8	7.6	0.9
tt+geq1b NLO gen.	3.0	-0.2	4.6	7.1	-5.7	5.5	0.7	1.5	-5.6	1.1	1.5	4.1	-13.4	14.2	-31.7	100.0	-27.3	17.3	-7.3	-11.3	-2.4	3.4	-12.0	3.8	-6.8	0.0
tt+geq1b PS & had.	2.1	0.5	1.8	9.0	-2.5	2.7	0.3	0.8	-2.5	0.7	0.8	1.5	-1.9	0.6	-42.2	-27.3	100.0	-0.4	-4.2	-7.7	-1.1	1.7	-4.4	-6.1	0.7	-0.2
ttbar reweighting w/ HT jets	1.4	1.5	0.2	6.0	-3.2	1.2	-0.1	0.2	0.4	0.4	0.3	-4.5	10.6	-7.1	-9.0	17.3	-0.4	100.0	5.4	3.4	0.3	-10.6	17.1	-14.5	-45.4	19.8
tt+geq1c NLO gen.	0.2	0.2	1.1	2.5	1.7	-0.3	-0.1	-0.0	-6.9	-0.1	-0.1	3.6	-4.4	-5.4	-16.6	-7.3	-4.2	5.4	100.0	-7.8	-2.3	-0.1	17.7	-5.4	-4.8	4.3
tt+geq1c PS & had.	-0.4	-0.4	-0.2	0.1	1.5	0.0	-0.1	-0.1	-0.7	-0.2	-0.2	0.6	-2.2	-1.7	-10.0	-11.3	-7.7	3.4	-7.8	100.0	-0.4	-6.1	-27.0	-6.4	-2.9	1.1
tt PDF05	0.4	0.2	0.6	1.0	-0.8	0.6	0.0	0.1	-1.1	0.1	0.1	0.5	-0.9	0.6	-1.2	-2.4	-1.1	0.3	-2.3	-0.4	100.0	-4.7	7.8	-1.2	-1.1	27.0
tt+light NLO gen.	5.3	4.1	-5.8	-7.4	-5.9	-9.4	2.1	1.0	-12.7	2.1	2.5	20.8	-32.4	13.3	6.4	3.4	1.7	-10.6	-61.2	-6.1	-4.7	100.0	-37.9	-28.7	10.2	-11.4
tt+light PS & had.	-12.0	-6.9	-22.1	-39.2	31.1	-25.0	-2.3	-3.5	24.1	-3.9	-4.5	-18.6	21.1	-15.5	-16.1	-12.0	-4.4	17.1	17.7	-27.0	7.8	-37.9	100.0	16.1	-13.0	3.2
μ_{Wp}	3.0	2.8	1.2	3.4	-3.2	3.0	-1.1	-0.4	-2.7	0.1	-0.8	-1.7	53.1	-19.0	8.8	3.8	-6.1	-14.5	-5.4	-6.4	-1.2	-28.7	16.1	100.0	9.3	12.2
$k(t+geq1b)$	45.7	21.9	-1.2	-10.4	5.2	-30.8	-14.7	8.1	-12.2	2.4	1.7	-6.8	18.6	45.7	7.6	-6.8	0.7	45.4	-4.8	-2.9	-1.1	10.2	-13.0	9.3	100.0	-19.6
$k(t+light)$	-16.5	-8.1	0.2	2.5	-1.8	10.9	-37.6	-22.9	-63.9	-25.3	-31.3	-11.4	11.0	-14.6	0.9	0.0	-0.2	19.8	4.3	1.1	27.0	-11.4	3.2	12.2	-19.6	100.0

(b) Correlation matrix

Figure 102: Signal strength and normalization factors (top) and correlation matrix (bottom) for the 1800 GeV W'_R mass hypotheses.

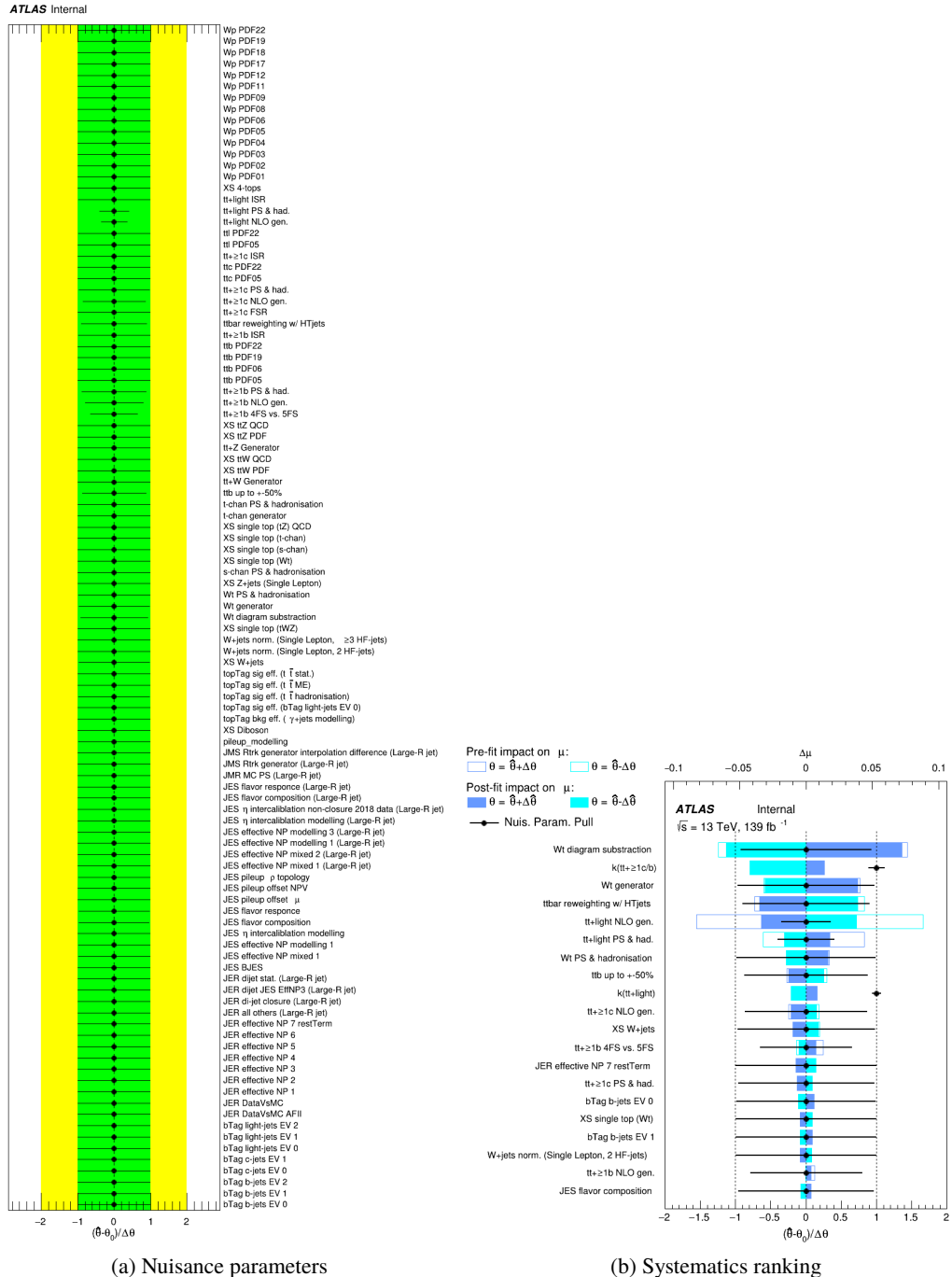
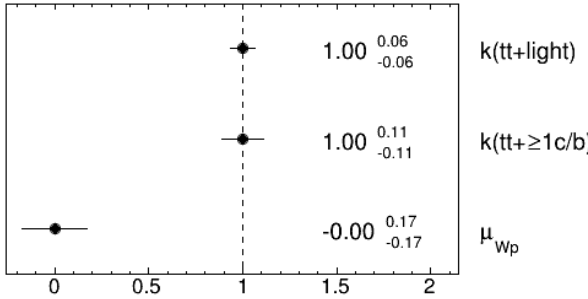


Figure 103: Nuisance parameters (left) and ranking plot (right) of the effect of various nuisance parameters before and after the fit for the 2000 GeV W'_R mass hypotheses.

ATLAS Internal

(a) Norm. factors

ATLAS Internal

	bTag b-jets EV 0	-0.5	-0.9	2.2	2.2	-1.1	-0.2	-0.4	0.7	-0.4	-0.5	0.2	0.2	-2.0	1.8	1.3	1.2	1.7	0.2	-0.7	0.3	7.1	-13.2	3.5	46.3	-16.7
bTag b-jets EV 1	-0.5	100.0	-0.4	-1.0	0.9	-0.5	-0.1	-0.2	0.3	-0.2	-0.3	-0.2	-0.4	1.0	-0.4	0.5	1.4	-0.0	-0.4	0.2	4.4	-6.9	2.7	22.2	-8.2	
JES effective NP modeling 1	-0.9	-0.4	100.0	-2.8	2.4	-2.0	-0.1	-0.3	1.5	-0.3	-0.4	0.5	0.8	-1.5	0.2	3.4	1.0	0.1	1.9	-0.3	0.6	-4.8	-22.6	1.0	-0.8	-0.1
JES flavor composition	-2.2	-1.0	-2.8	100.0	4.9	-3.6	-0.3	-0.8	2.8	-0.8	-0.9	-1.0	-0.0	-3.3	13.4	6.8	6.7	4.1	0.5	-1.2	1.0	-3.6	-41.2	2.3	-9.1	2.2
JES flavor response	2.2	0.9	2.4	4.9	100.0	3.1	0.4	0.8	-1.8	0.8	1.0	-0.7	-1.3	5.6	1.6	-3.1	-0.0	-2.4	0.2	1.9	-0.7	-7.3	32.1	-1.3	4.3	-1.6
JES pileup p topology	-1.1	-0.5	-2.0	-3.6	3.1	100.0	-0.1	-0.4	1.5	-0.4	-0.5	-0.1	0.4	-1.6	0.3	4.9	2.0	0.5	1.0	0.0	0.6	-8.7	-25.5	1.0	-30.3	10.5
tive NP modelling 1 (Large-R jet)	-0.2	-0.1	-0.1	-0.3	0.4	-0.1	100.0	-0.1	0.2	-0.1	-0.1	0.6	0.3	-0.9	0.1	0.8	0.2	-0.2	0.1	-0.1	0.0	1.9	-2.2	-1.1	-14.8	-37.6
ablation modelling (Large-R jet)	-0.4	-0.2	-0.3	-0.8	0.8	-0.4	-0.1	100.0	0.2	-0.1	-0.2	0.2	0.2	-0.8	0.9	1.0	0.6	0.3	0.1	-0.2	0.1	1.5	-3.8	0.4	8.3	-23.0
topTag sig eff. ($t\bar{t}$ hadronisation)	0.7	0.3	1.5	2.8	-1.8	1.5	0.2	0.2	100.0	0.2	0.3	-1.2	-1.6	1.9	-5.5	-3.0	-1.7	-0.1	-6.7	-0.1	-1.0	-14.0	24.4	-1.4	-11.7	-64.0
topTag sig eff. ($t\bar{t}$ ME)	-0.4	-0.2	-0.3	-0.8	0.8	-0.4	-0.1	-0.1	0.2	100.0	-0.2	0.3	0.2	-1.1	1.0	1.0	0.6	0.3	0.0	-0.2	0.1	2.2	-3.9	0.3	2.6	-25.3
topTag sig eff. ($t\bar{t}$ stat.)	-0.5	-0.2	-0.4	-0.9	1.0	-0.5	-0.1	-0.2	0.3	-0.2	100.0	0.5	0.4	-1.4	1.3	1.5	0.7	0.2	-0.0	-0.2	0.1	2.4	-4.5	-0.5	2.0	-31.4
Wt diagram subtraction	0.2	-0.3	0.5	-1.0	-0.7	-0.1	0.6	0.2	-1.2	0.3	0.5	100.0	-0.7	8.7	6.5	-11.3	1.3	12.4	-8.7	-1.0	-0.6	-29.6	20.0	44.2	19.4	9.8
Wt generator	0.2	-0.2	0.8	-0.0	-1.3	0.4	0.3	0.2	-1.6	0.2	0.4	-7.5	100.0	6.1	3.6	-7.7	2.1	7.5	-6.6	-0.3	-0.6	-11.6	7.2	21.3	-4.4	5.9
ttb up to +50%	-2.0	-0.4	-1.5	-3.3	5.6	-1.6	-0.9	-0.8	1.9	-1.1	-1.4	8.7	6.1	100.0	5.0	7.0	-1.3	-9.0	-2.1	-2.6	0.5	10.4	-14.1	-7.8	44.8	-14.5
tt+≥1b 4FS vs. 5FS	1.8	1.0	0.2	13.4	1.6	0.3	0.1	0.9	-5.5	1.0	1.3	6.5	3.6	5.0	100.0	-38.5	-53.5	-9.4	1.0	-2.9	-1.2	-0.6	-12.1	4.1	10.0	0.8
tt+≥1b NLO gen.	1.3	-0.4	3.4	6.8	-3.1	4.9	0.8	1.0	-3.0	1.0	1.5	-11.3	-7.7	7.0	-38.5	100.0	-26.2	21.2	-14.0	-10.8	-2.2	4.7	-7.8	0.6	-11.6	1.2
tt+≥1b PS & had.	1.2	0.5	1.0	6.7	-0.0	2.0	0.2	0.6	-1.7	0.6	0.7	1.3	2.1	-1.3	-53.5	-26.2	100.0	-1.1	-1.9	-5.4	-1.0	-2.4	-0.3	-1.7	0.8	0.5
ttbar reweighting w/ H7jets	1.7	1.4	0.1	4.1	-2.4	0.5	-0.2	0.3	-0.1	0.3	0.2	12.4	7.5	-9.0	-9.4	21.2	-1.1	100.0	10.6	5.4	0.3	-18.5	20.8	-21.6	-45.1	20.5
tt+≥1c NLO gen.	0.2	-0.0	1.9	0.5	0.2	1.0	0.1	0.1	-6.7	0.0	-0.0	-8.7	-6.6	-2.1	1.0	-14.0	-1.9	10.6	100.0	-7.8	-2.5	-60.4	17.7	-6.0	-7.8	3.8
tt+≥1c PS & had.	-0.7	-0.4	-0.3	-1.2	1.9	0.0	-0.1	-0.2	-0.1	-0.2	-0.1	-0.3	-2.6	-2.9	-10.8	-5.4	5.4	-7.8	100.0	-0.5	-9.4	-22.6	-3.5	-4.3	1.5	
tt PDF05	0.3	0.2	0.6	1.0	-0.7	0.6	0.0	0.1	-1.0	0.1	0.1	-0.6	-0.6	0.5	-1.2	-2.2	-1.0	0.3	-2.5	-0.5	100.0	-4.9	7.8	-0.7	-1.2	27.2
tt+light NLO gen.	7.1	4.4	-4.8	-3.6	-7.3	-8.7	1.9	1.5	-14.0	2.2	2.4	-29.6	-11.6	10.4	-0.6	4.7	-2.4	-18.5	-60.4	-9.4	-4.9	100.0	-40.5	-22.0	13.5	-10.8
tt+light PS & had.	-13.2	-6.9	-22.6	-41.2	32.1	-25.5	-2.2	-3.8	24.4	-3.9	-4.5	20.0	7.2	-14.1	-12.1	-7.8	-0.3	20.8	17.7	-22.6	7.8	-40.5	100.0	10.8	-14.2	2.9
μ_{W_p}	3.5	2.7	1.0	2.3	-1.3	1.0	-1.1	0.4	-1.4	0.3	-0.5	44.2	21.3	-7.8	4.1	0.6	-1.7	-21.6	-6.0	-3.5	-0.7	-22.0	10.8	100.0	18.4	6.1
$k(t\bar{t}+1c/b)$	46.3	22.2	-0.8	-9.1	4.3	-30.3	-14.8	8.3	-11.7	2.6	2.0	19.4	-4.4	44.8	10.0	-11.6	0.8	-45.1	-7.8	-4.3	-1.2	13.5	-14.2	18.4	100.0	-19.6
$k(t\bar{t}+\text{light})$	-16.7	-8.2	-0.1	2.2	-1.6	10.5	-37.6	-23.0	-64.0	-25.3	-31.4	9.8	5.9	-14.5	0.8	1.2	0.5	20.5	3.8	1.5	27.2	-10.8	2.9	6.1	-19.6	100.0

(b) Correlation matrix

Figure 104: Signal strength and normalization factors (top) and correlation matrix (bottom) for the 2000 GeV W'_R mass hypotheses.

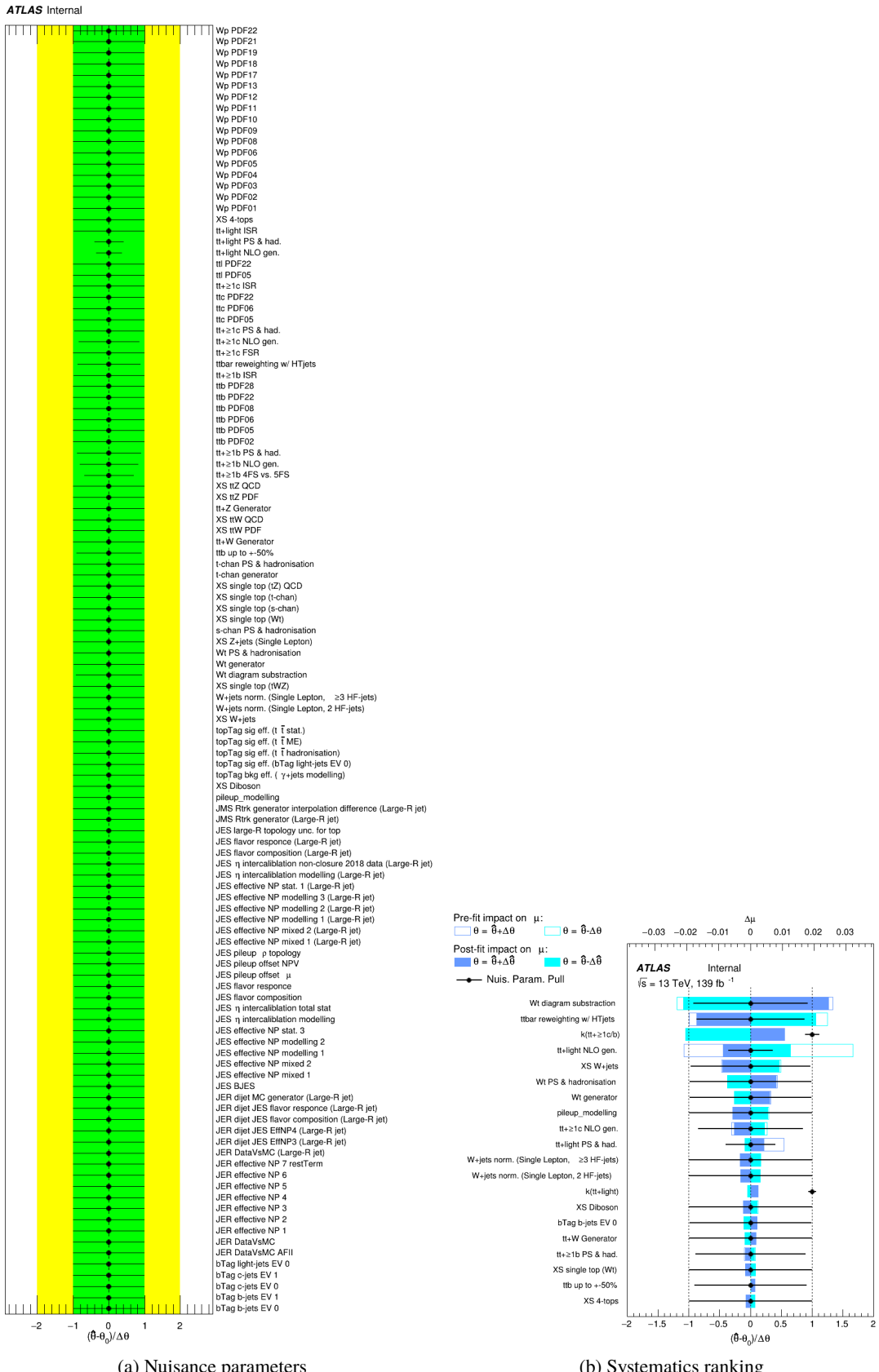
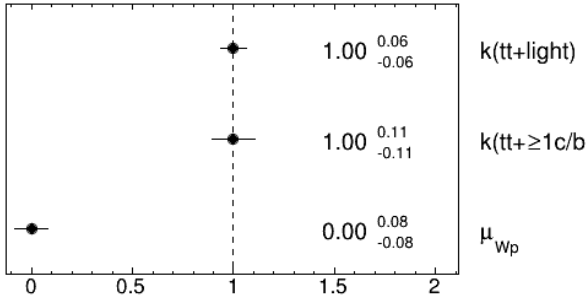


Figure 105: Nuisance parameters (left) and ranking plot (right) of the effect of various nuisance parameters before and after the fit for the 2500 GeV W'_R mass hypotheses.
22nd March 2023 – 00:45

ATLAS Internal

(a) Norm. factors

ATLAS Internal

	bTag b-jets EV 0	bTag b-jets EV 1	JES effective NP modelling 1	JES flavor composition	JES flavor response	JES pileup p topology	tive NP modelling 1 (Large-R jet)	calibration modelling (Large-R jet)	topTag sig eff. ($t\bar{t}$ hadronisation)	topTag sig eff. ($t\bar{t}$ ME)	topTag sig eff. ($t\bar{t}$ stat.)	Wt diagram subtraction	tt up to +50%	tt+>1b 4FS vs. 5FS	tt+>1b NLO gen.	tt+>1b PS & had.	ttbar reweighting w/ HT jets	tt+>1c NLO gen.	tt+>1c PS & had.	tt PDF05	tt+light NLO gen.	tt+light PS & had.	μ_{W_p}	$k(t\bar{t}+\geq 1 c/b)$	$k(t\bar{t}+\text{light})$
bTag b-jets EV 0	100.0	-0.6	-1.0	-2.3	2.4	-1.1	-0.2	-0.4	0.7	-0.4	-0.5	-0.4	-1.5	0.8	0.9	0.7	2.3	0.9	-0.9	0.4	7.3	-13.3	2.6	46.1	-16.7
bTag b-jets EV 1	-0.6	100.0	-0.5	-1.1	1.1	-0.6	-0.1	-0.2	0.3	-0.2	-0.2	-0.2	-0.8	0.4	0.4	0.4	1.1	0.4	-0.4	0.2	3.5	-6.4	1.3	22.4	-8.1
JES effective NP modelling 1	-1.0	-0.5	100.0	-2.9	2.3	-1.7	-0.1	-0.3	1.6	-0.3	-0.4	-0.1	-1.3	2.2	2.6	1.2	0.7	2.2	-0.8	0.6	-5.0	-22.3	-0.2	-1.2	-0.0
JES flavor composition	-2.3	-1.1	-2.9	100.0	5.1	-3.3	-0.2	-0.8	2.7	-0.8	-0.9	-1.2	-1.9	16.1	5.9	7.4	5.4	1.1	-1.6	0.9	-4.2	-40.6	1.6	-9.2	2.2
JES flavor response	2.4	1.1	2.3	5.1	100.0	2.9	0.3	0.8	-1.9	0.8	1.0	0.7	4.8	-2.1	-3.6	-1.3	-3.0	-0.7	2.3	-0.7	-6.2	31.2	-1.2	4.7	-1.5
JES pileup p topology	-1.1	-0.6	-1.7	-3.3	2.9	100.0	-0.1	-0.4	1.5	-0.4	-0.4	-0.1	-2.1	2.4	3.2	1.4	0.7	1.1	-1.2	0.5	-8.8	-25.5	-0.1	-30.6	10.7
tive NP modelling 1 (Large-R jet)	-0.2	-0.1	-0.1	-0.2	0.3	-0.1	100.0	-0.1	0.1	-0.1	-0.1	0.5	-0.7	0.0	0.5	0.2	-0.1	0.1	-0.1	0.0	2.2	-2.4	-0.8	-14.9	-37.6
calibration modelling (Large-R jet)	-0.4	-0.2	-0.3	-0.8	0.8	-0.4	-0.1	100.0	0.3	-0.1	-0.2	0.0	-0.7	0.8	0.9	0.5	0.4	0.3	-0.2	0.1	1.5	-3.8	0.1	8.3	-23.0
topTag sig eff. ($t\bar{t}$ hadronisation)	0.7	0.3	1.6	2.7	-1.9	1.5	0.1	0.3	100.0	0.2	0.3	-1.5	0.3	3.0	-2.5	-1.0	-0.6	-6.9	0.0	-1.0	-14.9	25.3	-1.7	12.1	63.9
topTag sig eff. ($t\bar{t}$ ME)	-0.4	-0.2	-0.3	-0.8	0.8	-0.4	-0.1	-0.1	0.2	100.0	-0.2	0.2	-0.9	0.7	0.9	0.5	0.3	0.2	-0.3	0.1	2.3	-3.9	-0.1	2.6	-25.3
topTag sig eff. ($t\bar{t}$ stat.)	-0.5	-0.2	-0.4	-0.9	1.0	-0.4	-0.1	-0.2	0.3	-0.2	100.0	0.3	-1.3	0.9	1.2	0.6	0.2	0.2	-0.4	0.1	2.6	-4.6	-0.7	2.0	-31.4
Wt diagram subtraction	-0.4	-0.2	0.1	-1.2	0.7	-0.1	0.5	0.0	-1.5	0.2	0.3	100.0	4.5	1.4	-9.2	-1.2	12.5	-8.0	-1.3	-0.6	-32.0	20.8	31.3	18.7	10.3
tt up to +50%	-1.5	-0.8	-1.3	-1.9	4.8	-2.1	-0.7	-0.7	0.3	-0.9	-1.3	4.5	100.0	-3.5	12.1	0.3	-10.5	-2.4	-3.1	0.4	16.5	-18.8	1.5	45.9	-15.2
tt+>1b 4FS vs. 5FS	0.8	0.4	2.2	16.1	-2.1	2.4	0.0	0.8	-3.0	0.7	0.9	1.4	-3.5	100.0	-39.6	-51.1	-5.2	-1.0	-6.5	-1.0	-0.8	-11.8	-0.3	1.7	2.1
tt+>1b NLO gen.	0.9	0.4	2.6	5.9	-3.6	3.2	0.5	0.9	-2.5	0.9	1.2	-9.2	12.1	-39.6	100.0	-23.7	24.1	-17.7	-5.6	-1.8	5.9	-8.2	0.5	-10.1	0.8
tt+>1b PS & had.	0.7	0.4	1.2	7.4	-1.3	1.4	0.2	0.5	-1.0	0.5	0.6	-1.2	0.3	-51.1	-23.7	100.0	1.2	-3.2	-3.9	-0.7	-0.6	-1.2	-2.0	-0.8	0.2
ttbar reweighting w/ HT jets	2.3	1.1	0.7	5.4	-3.0	0.7	-0.1	0.4	-0.6	0.3	0.2	12.5	-10.5	-5.2	24.1	1.2	100.0	11.2	4.1	0.1	-20.8	21.7	-22.6	-44.1	20.6
tt+>1c NLO gen.	0.9	0.4	2.2	1.1	-0.7	1.1	0.1	0.3	-6.9	0.2	0.2	-8.0	-2.4	-1.0	-17.7	-3.2	11.2	100.0	-7.2	-2.8	-56.5	14.6	-6.1	-7.5	3.6
tt+>1c PS & had.	-0.9	-0.4	-0.8	-1.6	2.3	-1.2	-0.1	-0.2	0.0	-0.3	-0.4	-1.3	-3.1	-6.5	-5.6	-3.9	4.1	-7.2	100.0	-0.1	-11.0	-20.8	-1.1	-3.9	1.4
tt PDF05	0.4	0.2	0.6	0.9	-0.7	0.5	0.0	0.1	-1.0	0.1	0.1	-0.6	0.4	-1.0	-1.8	-0.7	0.1	-2.8	-0.1	100.0	-4.9	7.9	-0.7	-1.1	27.1
tt+light NLO gen.	7.3	3.5	-5.0	-4.2	-6.2	-8.8	2.2	1.5	-14.9	2.3	2.6	-32.0	16.5	-0.8	5.9	-0.6	-20.8	-56.5	-11.0	-4.9	100.0	-40.5	-14.0	16.2	-11.8
tt+light PS & had.	-13.3	-6.4	-22.3	-40.6	31.2	-25.5	-2.4	-3.8	25.3	-3.9	-4.6	20.8	-18.8	-11.8	-8.2	-1.2	21.7	14.6	-20.8	7.9	-40.5	100.0	4.4	-16.1	3.4
μ_{W_p}	2.6	1.3	-0.2	1.6	-1.2	-0.1	-0.8	0.1	-1.7	-0.1	-0.7	31.3	1.5	-0.3	0.5	-2.0	-22.6	-6.1	-1.1	-0.7	-14.0	4.4	100.0	21.7	2.9
$k(t\bar{t}+\geq 1 c/b)$	46.1	22.4	-1.2	-9.2	4.7	-30.6	-14.9	8.3	-12.1	2.6	2.0	18.7	45.9	1.7	-10.1	-0.8	-44.1	-7.5	-3.9	-1.1	16.2	-16.1	21.7	100.0	-19.7
$k(t\bar{t}+\text{light})$	-16.7	-8.1	-0.0	2.2	-1.5	10.7	-37.6	-23.0	-63.9	25.3	-31.4	10.3	-15.2	2.1	0.8	0.2	20.6	3.6	1.4	27.1	-11.8	3.4	2.9	-19.7	100.0

(b) Correlation matrix

Figure 106: Signal strength and normalization factors (top) and correlation matrix (bottom) for the 2500 GeV W'_R mass hypotheses.

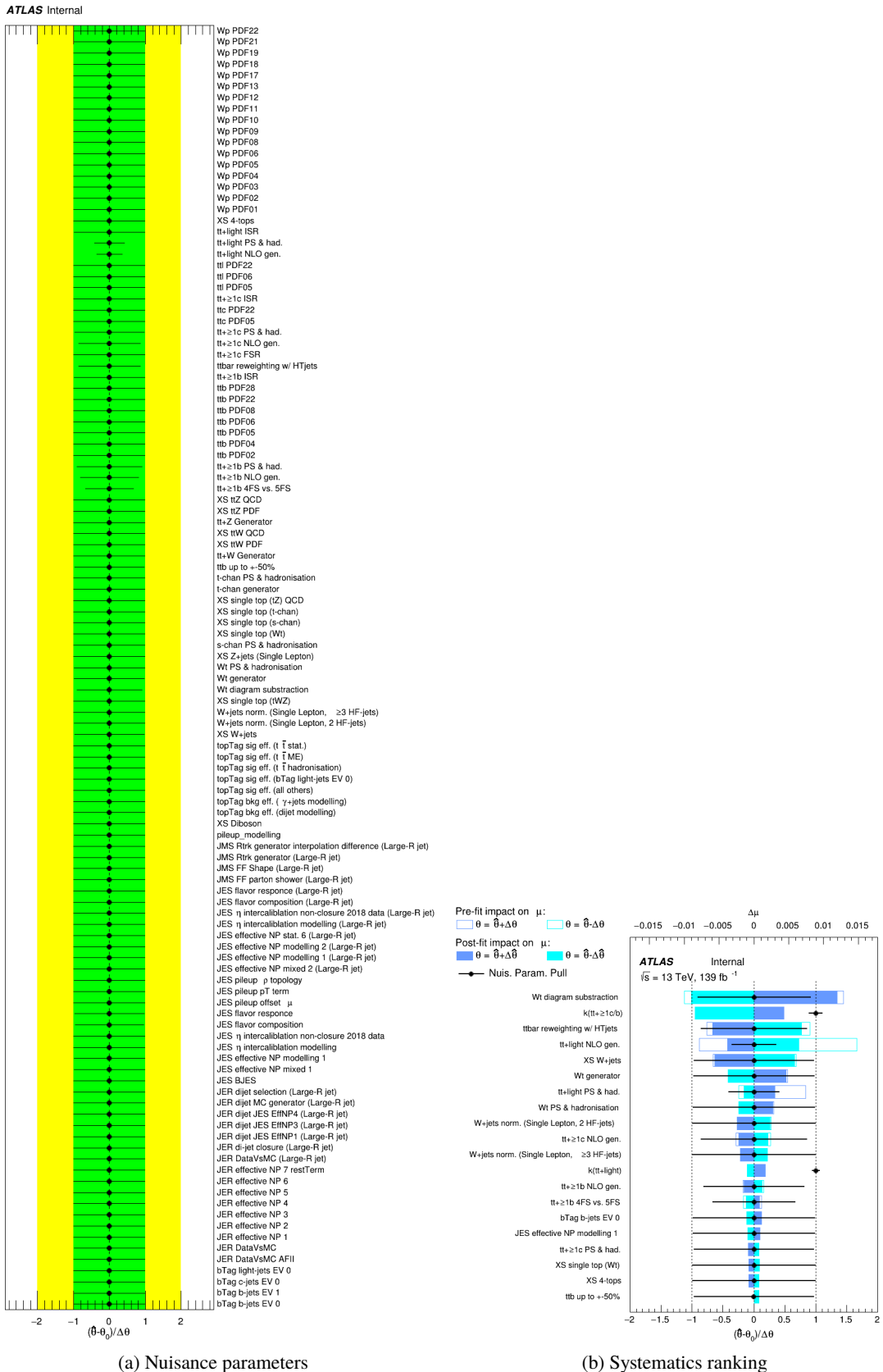
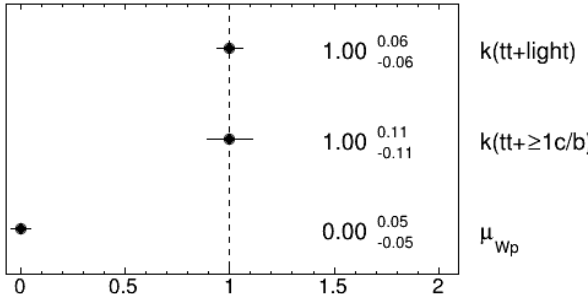


Figure 107: Nuisance parameters (left) and ranking plot (right) of the effect of various nuisance parameters before and after the fit for the 3000 GeV W'_R mass hypotheses.

ATLAS Internal



(a) Norm. factors

ATLAS Internal

	bTag b-jets EV 0	bTag b-jets EV 1	JES effective NP modelling 1	JES flavor composition	JES flavor response	JES pileup p topology	utive NP modelling 1 (Large-R jet)	calibration modelling (Large-R jet)	topTag sig eff. ($t\bar{t}$ hadronisation)	topTag sig eff. ($t\bar{t}$ ME)	topTag sig eff. ($t\bar{t}$ stat.)	Wt diagram subtraction	ttb up to +50%	tt+>1b 4FS vs. 5FS	tt+>1b NLO gen.	tt+>1b PS & had.	ttbar reweighting w/ HT jets	tt+>1c NLO gen.	tt PDF05	tt+light NLO gen.	tt+light PS & had.	μ_{W_p}	k($t\bar{t} + \geq 1 c/b$)	k($t\bar{t}$ +light)	
bTag b-jets EV 0	100.0	-0.5	-0.9	-2.2	2.2	-1.0	-0.2	-0.4	0.7	-0.4	-0.5	-0.3	-1.9	1.3	1.4	1.2	1.8	0.2	0.3	6.9	-13.1	2.3	47.1	-16.8	
bTag b-jets EV 1	-0.5	100.0	-0.4	-1.0	1.0	-0.5	-0.1	-0.2	0.3	-0.2	-0.2	-0.2	-0.8	0.5	0.2	0.4	1.3	-0.0	0.2	3.8	-6.6	1.2	22.7	-8.1	
JES effective NP modelling 1	-0.9	-0.4	100.0	-2.8	1.9	-1.4	-0.1	-0.3	1.5	-0.3	-0.3	-0.5	-1.0	3.0	2.1	1.6	1.6	1.5	0.5	-3.8	-22.5	1.9	-1.8	-0.1	
JES flavor composition	-2.2	-1.0	-2.8	100.0	4.2	-2.9	-0.2	-0.9	2.3	-0.7	-0.9	-1.9	-3.8	18.2	5.7	7.0	5.0	-0.2	0.8	-3.0	-40.2	0.4	-10.2	2.5	
JES flavor response	2.2	1.0	1.9	4.2	100.0	2.8	0.4	0.7	-2.0	0.7	0.9	0.4	3.8	1.9	-0.8	0.7	-2.9	-0.0	-0.6	-8.5	32.8	-0.9	4.2	-1.3	
JES pileup p topology	-1.0	-0.5	-1.4	-2.9	2.8	100.0	-0.2	-0.4	1.5	-0.3	-0.4	0.2	-1.7	1.1	1.9	0.3	0.1	0.7	0.4	-7.7	-25.9	-0.8	-30.5	10.6	
utive NP modelling 1 (Large-R jet)	-0.2	-0.1	-0.1	-0.2	0.4	-0.2	100.0	-0.0	0.2	-0.0	-0.0	0.8	-0.6	-0.2	0.6	0.1	-0.5	0.1	-0.0	1.9	-2.3	-1.0	-14.8	-37.8	
calibration modelling (Large-R jet)	-0.4	-0.2	-0.3	-0.9	0.7	-0.4	-0.0	100.0	0.2	-0.1	-0.2	0.1	-0.7	1.8	1.2	0.9	0.1	0.1	0.1	1.1	-3.5	-0.2	8.6	-23.0	
topTag sig eff. ($t\bar{t}$ hadronisation)	0.7	0.3	1.5	2.3	-2.0	1.5	0.2	0.2	100.0	0.3	0.3	-1.6	0.4	-0.5	-1.6	0.2	-0.5	-6.8	-1.0	-15.6	25.5	-1.3	-12.4	-64.0	
topTag sig eff. ($t\bar{t}$ ME)	-0.4	-0.2	-0.3	-0.7	0.7	-0.3	-0.0	-0.1	0.3	100.0	-0.1	0.2	-0.8	0.7	0.7	0.5	0.3	-0.0	0.1	2.4	-4.1	-0.0	2.8	-25.4	
topTag sig eff. ($t\bar{t}$ stat.)	-0.5	-0.2	-0.3	-0.9	0.9	-0.4	-0.0	-0.2	0.3	-0.1	100.0	0.5	-1.0	0.9	1.0	0.6	0.2	0.0	0.1	2.7	-4.8	-0.5	2.2	-31.4	
Wt diagram subtraction	-0.3	-0.2	-0.5	-1.9	0.4	0.2	0.8	0.1	-1.6	0.2	0.5	100.0	3.7	7.7	7.3	-7.0	-0.1	13.7	-9.4	-0.7	31.6	21.1	25.0	18.2	9.9
ttb up to +50%	-1.9	-0.8	-1.0	-3.8	3.8	-1.7	-0.6	-0.7	0.4	-0.8	-1.0	3.7	100.0	6.7	4.1	3.1	-0.7	-2.2	0.3	18.8	-18.0	-0.0	43.3	-14.9	
tt+>1b 4FS vs. 5FS	1.3	0.5	3.0	18.2	1.9	1.1	-0.2	1.8	-0.5	0.7	0.9	7.3	6.7	100.0	-40.7	-44.1	-0.9	-0.9	-1.1	-5.4	-10.4	2.4	6.7	0.3	
tt+>1b NLO gen.	1.4	0.2	2.1	5.7	-0.8	1.9	0.6	1.2	-1.6	0.7	1.0	-7.0	4.1	-40.7	100.0	-23.7	25.8	-17.1	-1.4	3.3	-2.7	-3.6	-12.7	1.8	
tt+>1b PS & had.	1.2	0.4	1.6	7.0	0.7	0.3	0.1	0.9	0.2	0.5	0.6	-0.1	3.1	-44.1	-23.7	100.0	1.8	-2.0	-0.6	-3.9	2.1	-0.8	1.3	-1.0	
ttbar reweighting w/ HT jets	1.8	1.3	1.6	5.0	-2.9	0.1	-0.5	0.1	-0.5	0.3	0.2	13.7	-0.7	-0.9	25.8	1.8	100.0	15.7	0.1	-25.1	22.3	-13.8	-39.9	19.6	
tt+>1c NLO gen.	0.2	-0.0	1.5	-0.2	-0.0	0.7	0.1	0.1	-6.8	-0.0	0.0	-9.4	-2.2	-0.9	-17.1	-2.0	15.7	100.0	-2.3	-55.7	16.7	-4.8	-10.8	4.4	
tt PDF05	0.3	0.2	0.5	0.8	-0.6	0.4	-0.0	0.1	-1.0	0.1	0.1	-0.7	0.3	-1.1	-1.4	-0.6	0.1	-2.3	100.0	-5.3	8.1	-0.5	-1.2	27.1	
tt+light NLO gen.	6.9	3.8	-3.8	-3.0	-8.5	-7.7	1.9	1.1	-15.6	2.4	2.7	-31.6	18.8	-5.4	3.3	-3.9	-25.1	-55.7	-5.3	100.0	-44.5	-12.2	19.5	-12.0	
tt+light PS & had.	-13.1	-6.6	-22.5	40.2	32.8	-25.9	-2.3	-3.5	25.5	-4.1	-4.8	21.1	-18.0	-10.4	-2.7	2.1	22.3	16.7	8.1	-44.5	100.0	5.7	-16.2	3.2	
μ_{W_p}	2.3	1.2	1.9	0.4	-0.9	-0.8	-1.0	-0.2	-1.3	-0.0	-0.5	25.0	-0.0	2.4	-3.6	-0.8	-13.8	-4.8	-0.5	-12.2	5.7	-10.0	16.2	3.6	
k($t\bar{t} + \geq 1 c/b$)	47.1	22.7	-1.8	-10.2	4.2	-30.5	-14.8	8.6	-12.4	2.8	2.2	18.2	43.3	6.7	-12.7	1.3	-39.9	-10.8	-1.2	19.5	-16.2	16.2	100.0	-19.6	
k($t\bar{t}$ +light)	-16.8	-8.1	-0.1	2.5	-1.3	10.6	-37.8	-23.0	-64.0	-25.4	-31.4	9.9	-14.9	0.3	1.8	-1.0	19.6	4.4	27.1	-12.0	3.2	3.6	-19.6	100.0	

(b) Correlation matrix

Figure 108: Signal strength and normalization factors (top) and correlation matrix (bottom) for the 3000 GeV W'_R mass hypotheses.

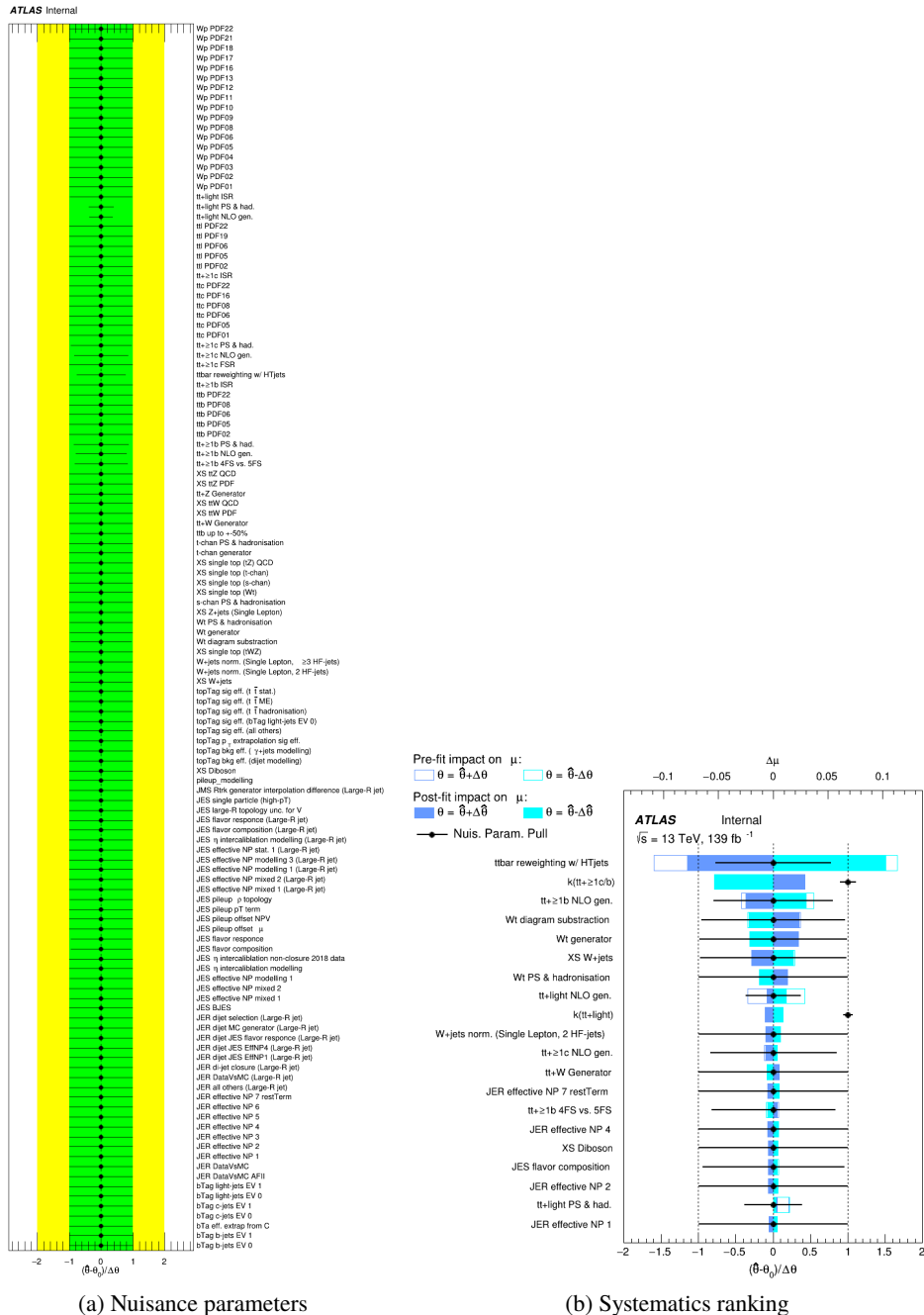
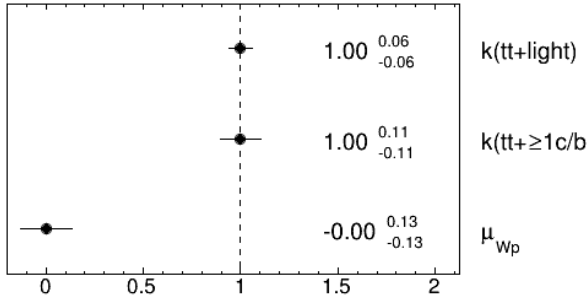


Figure 109: Nuisance parameters (left) and ranking plot (right) of the effect of various nuisance parameters before and after the fit for the 4000 GeV W'_R mass hypotheses.

ATLAS Internal



(a) Norm. factors

ATLAS Internal

	bTag b-jets EV 0	bTag b-jets EV 1	JES flavor composition	JES flavor response	JES pileup p topology	ive NP modelling 1 (Large-R jet)	alibration modelling (Large-R jet)	topTag sig eff. ($t\bar{t}$ hadronisation)	topTag sig eff. ($t\bar{t}$ TME)	topTag sig eff. ($t\bar{t}$ stat.)	XS W+jets	Wt diagram subtraction	tt up to +50%	tt+>1b 4FS vs. 5FS	tt+>1b NLO gen.	tt+>1b PS & had.	ttbar reweighting w/ HT jets	tt+>1c NLO gen.	tt+>1c PS & had.	tt PDF05	tt-light NLO gen.	tt-light PS & had.	μ_{W_p}	$k(tt+\geq 1 c/b)$	$k(tt+\text{light})$
bTag b-jets EV 0	100.0	-0.7	-4.5	3.4	-1.7	-0.2	-0.5	1.8	-0.5	-0.7	0.5	-1.4	-1.5	7.3	-0.8	5.1	4.9	2.9	0.2	0.3	3.2	-8.8	-2.3	46.0	-17.0
bTag b-jets EV 1	-0.7	100.0	-1.3	1.1	-0.5	-0.1	-0.2	0.5	-0.2	-0.2	-0.1	0.0	-0.6	1.2	-0.2	0.8	1.3	0.2	-0.3	0.1	3.4	-6.5	1.9	23.2	-8.2
JES flavor composition	-4.5	-1.3	100.0	8.3	-5.2	-0.3	-1.0	4.2	-1.0	-1.3	1.0	-1.5	-1.7	14.3	7.1	11.1	3.0	4.0	0.5	0.9	-9.4	-36.5	-3.3	-9.3	1.3
JES flavor response	3.4	1.1	8.3	100.0	4.3	0.3	0.9	-2.9	0.9	1.2	-0.9	1.3	2.1	-10.6	-6.5	-8.2	0.3	-0.4	0.2	-0.7	-1.6	27.1	-0.4	2.9	0.1
JES pileup p topology	-1.7	-0.5	-5.2	4.3	100.0	-0.1	-0.5	2.0	-0.4	-0.5	0.5	-0.3	-0.2	6.2	6.3	5.4	-0.9	0.8	0.3	0.5	-11.3	-23.2	-0.6	-30.6	9.9
ive NP modelling 1 (Large-R jet)	-0.2	-0.1	-0.3	0.3	-0.1	100.0	-0.0	0.3	-0.0	0.0	-0.2	0.2	-0.4	0.5	0.3	0.4	0.0	0.1	-0.1	-0.0	2.3	-2.5	-0.5	-15.3	-37.9
alibration modelling (Large-R jet)	-0.5	-0.2	-1.0	0.9	-0.5	-0.0	100.0	0.4	-0.1	-0.1	0.1	-0.2	-0.4	1.0	0.0	0.7	0.2	0.2	-0.2	0.1	1.7	-3.9	-0.4	8.7	-23.3
topTag sig eff. ($t\bar{t}$ hadronisation)	1.8	0.5	4.2	-2.9	2.0	0.3	0.4	100.0	0.4	0.5	0.7	-1.0	0.2	-7.2	-3.3	-4.4	-1.9	-8.5	-1.0	-1.1	-10.6	22.2	2.3	-1.3	-64.3
topTag sig eff. ($t\bar{t}$ TME)	-0.5	0.2	-1.0	0.9	-0.4	0.0	-0.1	0.4	100.0	0.1	-0.0	-0.1	0.5	1.0	0.0	0.7	0.5	0.2	-0.2	0.0	2.6	-4.2	0.2	2.8	-25.6
topTag sig eff. ($t\bar{t}$ stat.)	-0.7	-0.2	-1.3	1.2	-0.5	0.0	-0.1	0.5	-0.1	100.0	0.0	-0.2	-0.7	1.3	0.0	0.9	0.3	0.2	-0.3	0.1	3.0	-4.9	-1.2	2.2	-31.8
XS W+jets	0.5	-0.1	1.0	-0.9	0.5	-0.2	0.1	0.7	-0.0	0.0	100.0	4.6	-1.8	-0.2	2.8	0.4	-1.0	3.4	0.2	0.5	20.5	-20.3	-14.6	-8.8	-11.0
Wt diagram subtraction	-1.4	0.0	-1.5	1.3	-0.3	0.2	-0.2	-1.0	-0.1	-0.2	4.6	100.0	-0.4	1.6	-10.9	-1.4	3.5	-7.4	-2.0	-0.9	-37.7	25.7	19.1	23.4	10.9
tt up to +50%	-1.5	-0.6	-1.7	2.1	-0.2	-0.4	-0.4	0.2	-0.5	-0.7	-1.8	-0.4	100.0	-6.2	-10.4	-8.4	-2.7	-2.4	-5.7	0.1	32.4	-31.2	-0.4	44.6	-16.3
tt+>1b 4FS vs. 5FS	7.3	1.2	14.3	-10.6	6.2	0.5	1.0	-7.2	1.0	1.3	-0.2	1.6	-6.2	100.0	-26.5	-36.3	-6.1	-16.2	-12.4	-1.0	5.1	-15.4	3.8	3.7	2.6
tt+>1b NLO gen.	-0.8	-0.2	7.1	-6.5	6.3	0.3	0.0	-3.3	-0.0	0.0	2.8	-10.9	-10.4	26.5	100.0	-29.8	25.0	-9.5	-14.1	-1.6	-6.6	-2.2	-23.3	-20.5	6.0
tt+>1b PS & had.	5.1	0.8	11.1	-8.2	5.4	0.4	0.7	-4.4	0.7	0.9	0.4	-1.4	-6.4	-36.3	-29.8	100.0	-2.1	-11.7	-12.1	-0.7	9.5	-12.1	1.4	-0.6	2.0
ttbar reweighting w/ HT jets	4.9	1.3	3.0	0.3	-0.9	0.0	0.2	-1.9	0.5	0.3	-1.0	3.5	-2.7	-6.1	25.0	-2.1	100.0	1.3	1.4	0.4	-10.9	15.7	-78.1	-36.3	15.6
tt+>1c NLO gen.	2.9	0.2	4.0	-0.4	0.8	0.1	0.2	-8.5	0.2	0.2	3.4	-7.4	-2.4	-16.2	-9.5	-11.7	1.3	100.0	-9.0	-2.1	52.6	8.9	-4.2	-1.5	3.1
tt+>1c PS & had.	0.2	-0.3	0.5	0.2	0.3	-0.1	-0.2	-1.0	-0.2	-0.3	0.2	-2.0	-5.7	-12.4	-14.1	-12.1	1.4	-9.0	100.0	-0.2	-2.8	-30.4	-0.9	-3.8	1.9
tt PDF05	0.3	0.1	0.9	-0.7	0.5	-0.0	0.1	-1.1	0.0	0.1	0.5	-0.9	0.1	-1.0	-1.6	-0.7	0.4	-2.1	-0.2	100.0	-5.1	8.5	0.0	-1.5	27.3
tt-light NLO gen.	3.2	3.4	-9.4	-1.6	-11.3	2.3	1.7	-10.6	2.6	3.0	20.5	-37.7	32.4	5.1	-6.6	9.5	-10.9	-52.6	-2.8	-5.1	100.0	-38.7	-8.4	14.0	-16.6
tt-light PS & had.	-8.8	-6.5	-36.5	27.1	-23.2	-2.5	-3.9	22.2	-4.2	-4.9	-20.3	25.7	-31.2	-15.4	-2.2	-12.1	15.7	8.9	-30.4	8.5	-38.7	100.0	1.4	-14.2	7.2
μ_{W_p}	-2.3	1.9	-3.3	-0.4	-0.6	-0.5	-0.4	2.3	0.2	-1.2	-14.6	19.1	-0.4	3.8	-23.3	1.4	-78.1	-4.2	-0.9	0.0	-8.4	1.4	100.0	37.5	-5.8
$k(tt+\geq 1 c/b)$	46.0	23.2	-9.3	2.9	-30.6	-15.3	8.7	-11.3	2.8	2.2	-8.8	23.4	44.6	3.7	-20.5	-0.6	-36.3	-1.5	-3.8	-1.5	14.0	-14.2	37.5	100.0	-17.4
$k(tt+\text{light})$	-17.0	-8.2	1.3	0.1	9.9	-37.9	-23.3	-64.3	-25.6	-31.8	-11.0	10.9	-16.3	2.6	6.0	2.0	15.6	3.1	1.9	27.3	-16.6	7.2	-5.8	-17.4	100.0

(b) Correlation matrix

Figure 110: Signal strength and normalization factors (top) and correlation matrix (bottom) for the 4000 GeV W'_R mass hypotheses.

865 7.3.3 Post-fit plots

866 Figure 118 to 120 show the post-fit plots for each H^+ mass hypotheses. Similarly, Figure 121 to 129 and
 867 Figure 130 to 138 show the post-fit plots for each W'_L and W'_R mass hypotheses, respectively.

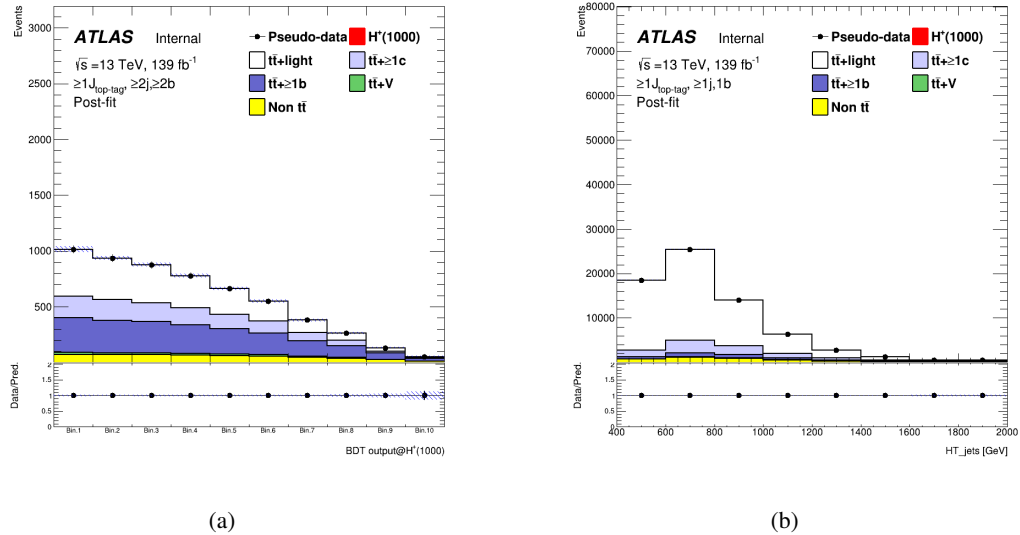


Figure 111: Post-fit plots in the SR (left) and CR (right) for 1000 GeV mass hypothesis of H^+ signal.

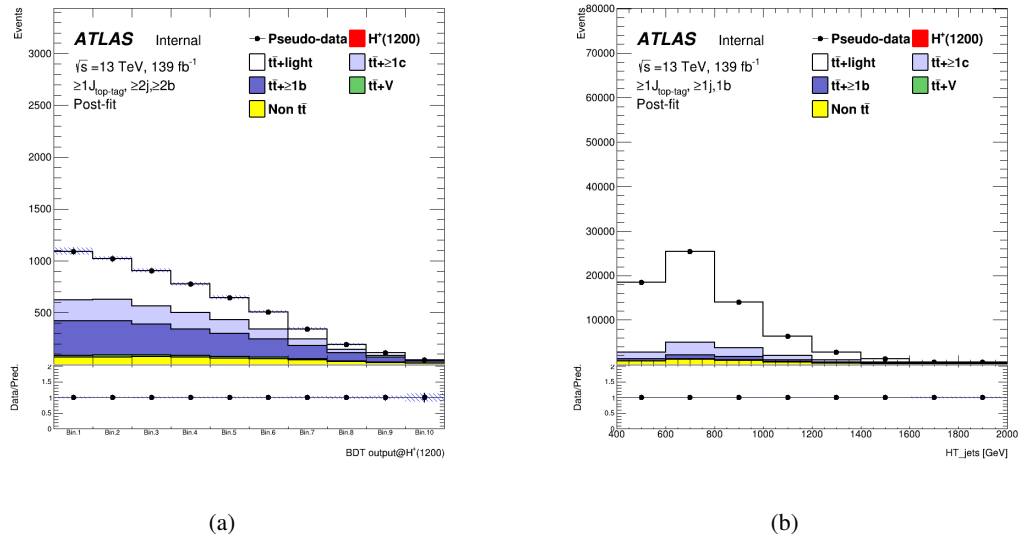


Figure 112: Post-fit plots in the SR (left) and CR (right) for 1200 GeV mass hypothesis of H^+ signal.

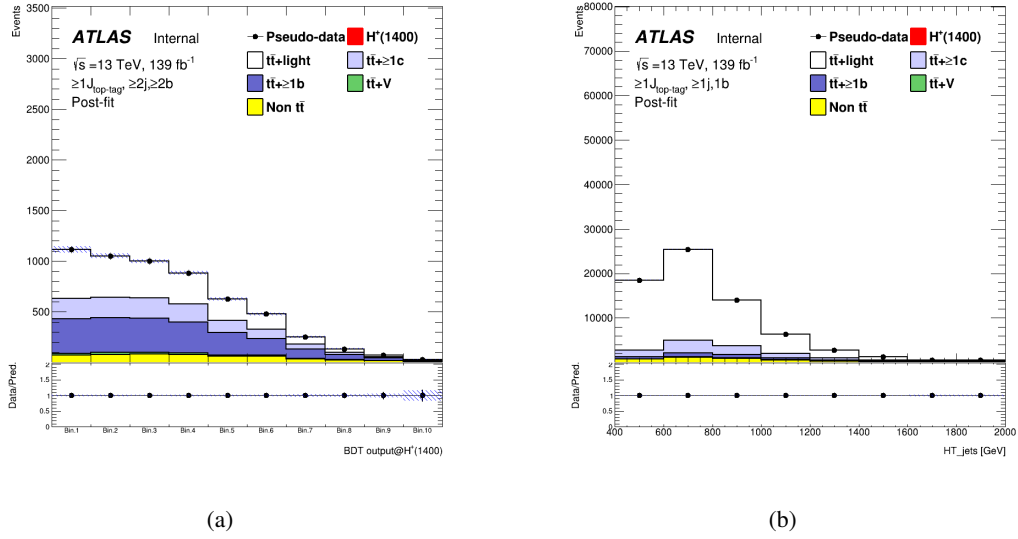


Figure 113: Post-fit plots in the SR (left) and CR (right) for 1400 GeV mass hypothesis of H^+ signal.

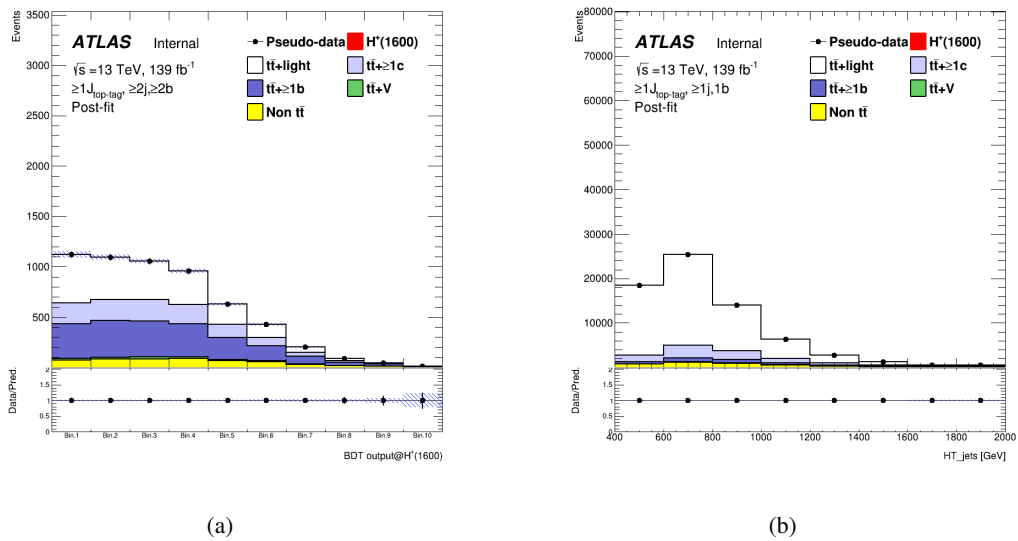


Figure 114: Post-fit plots in the SR (left) and CR (right) for 1600 GeV mass hypothesis of H^+ signal.

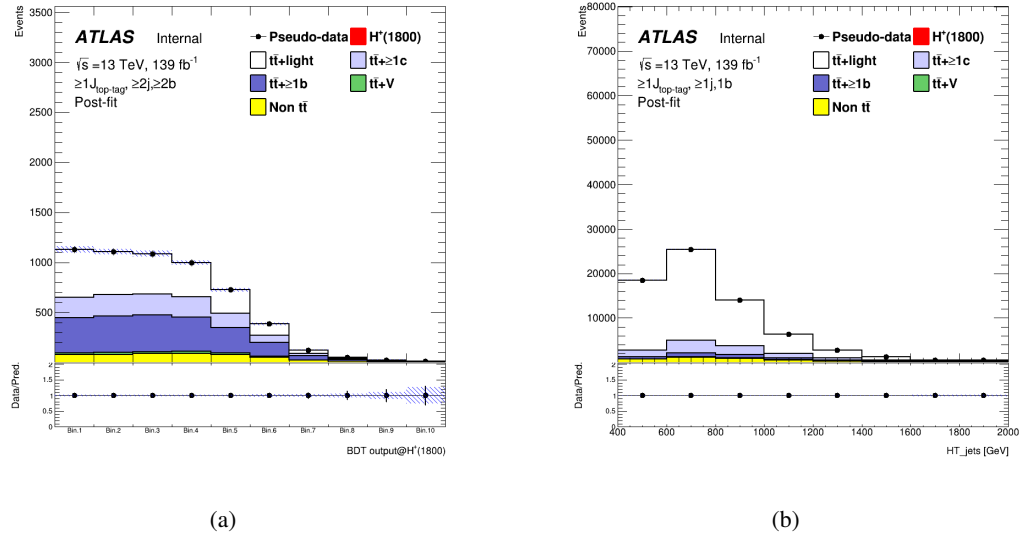


Figure 115: Post-fit plots in the SR (left) and CR (right) for 1800 GeV mass hypothesis of H^+ signal.

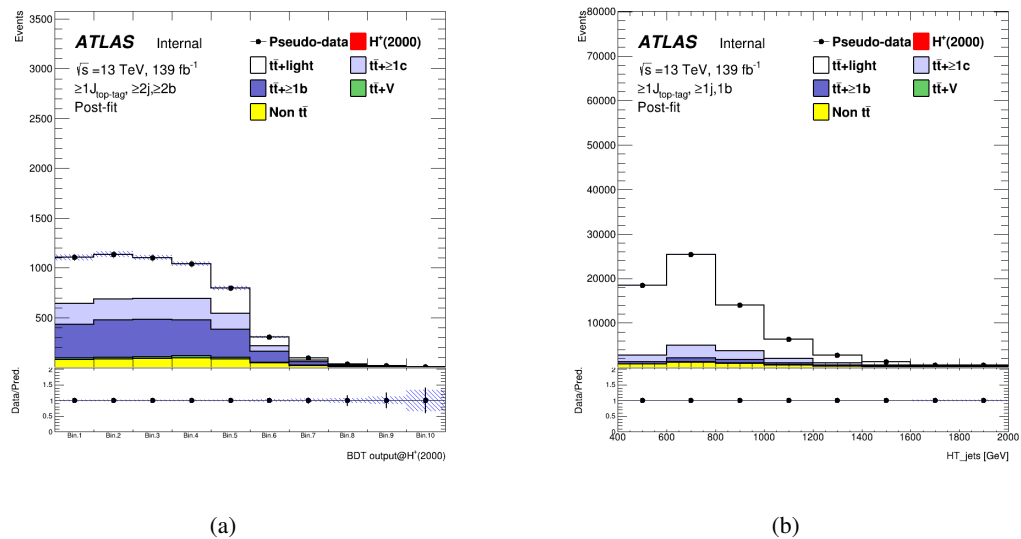


Figure 116: Post-fit plots in the SR (left) and CR (right) for 2000 GeV mass hypothesis of H^+ signal.

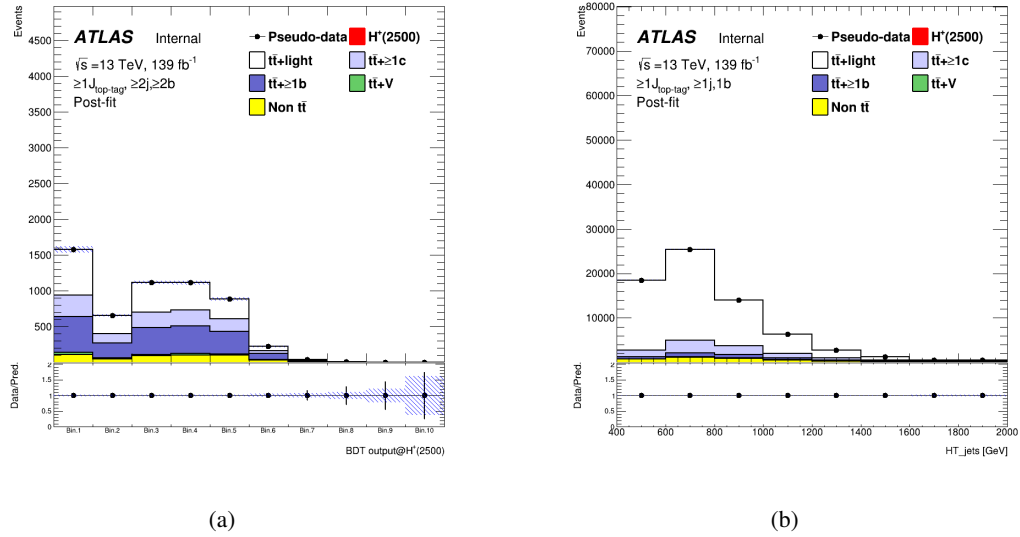


Figure 117: Post-fit plots in the SR (left) and CR (right) for 2500 GeV mass hypothesis of H^+ signal.

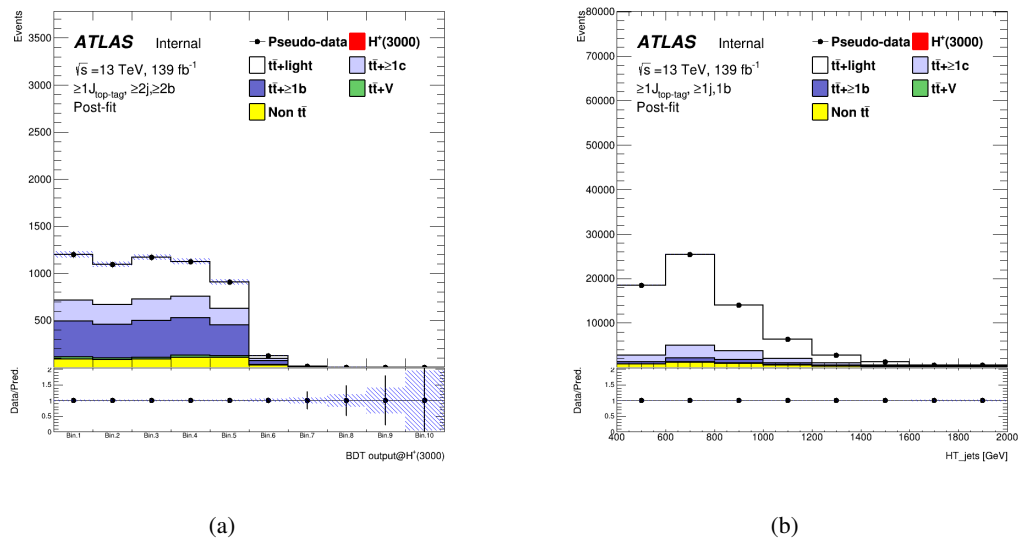


Figure 118: Post-fit plots in the SR (left) and CR (right) for 3000 GeV mass hypothesis of H^+ signal.

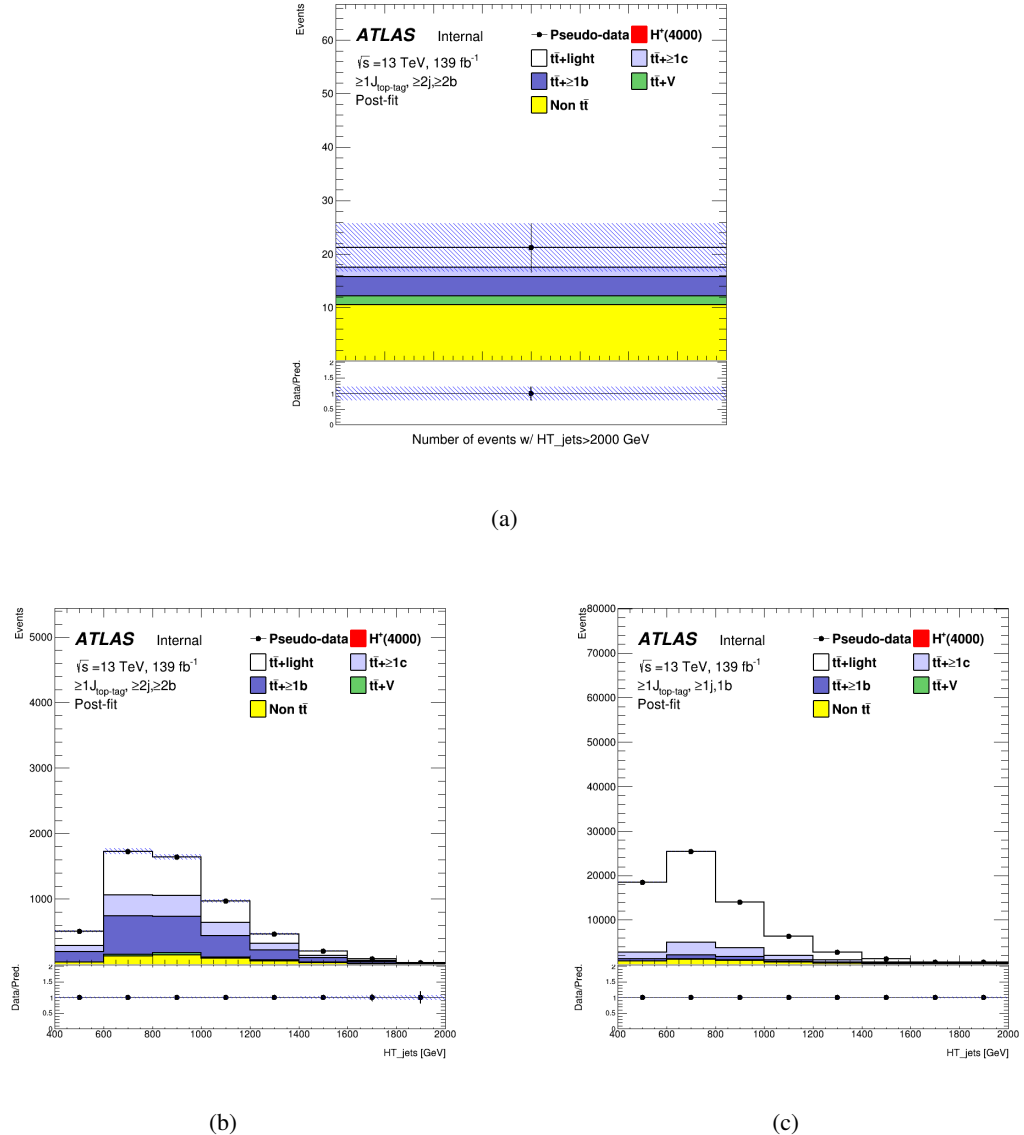


Figure 119: Post-fit plots in the SR (top), CR1 (bottom-left), and CR2 (bottom-right) for 4000 GeV mass hypothesis of H^+ signal.

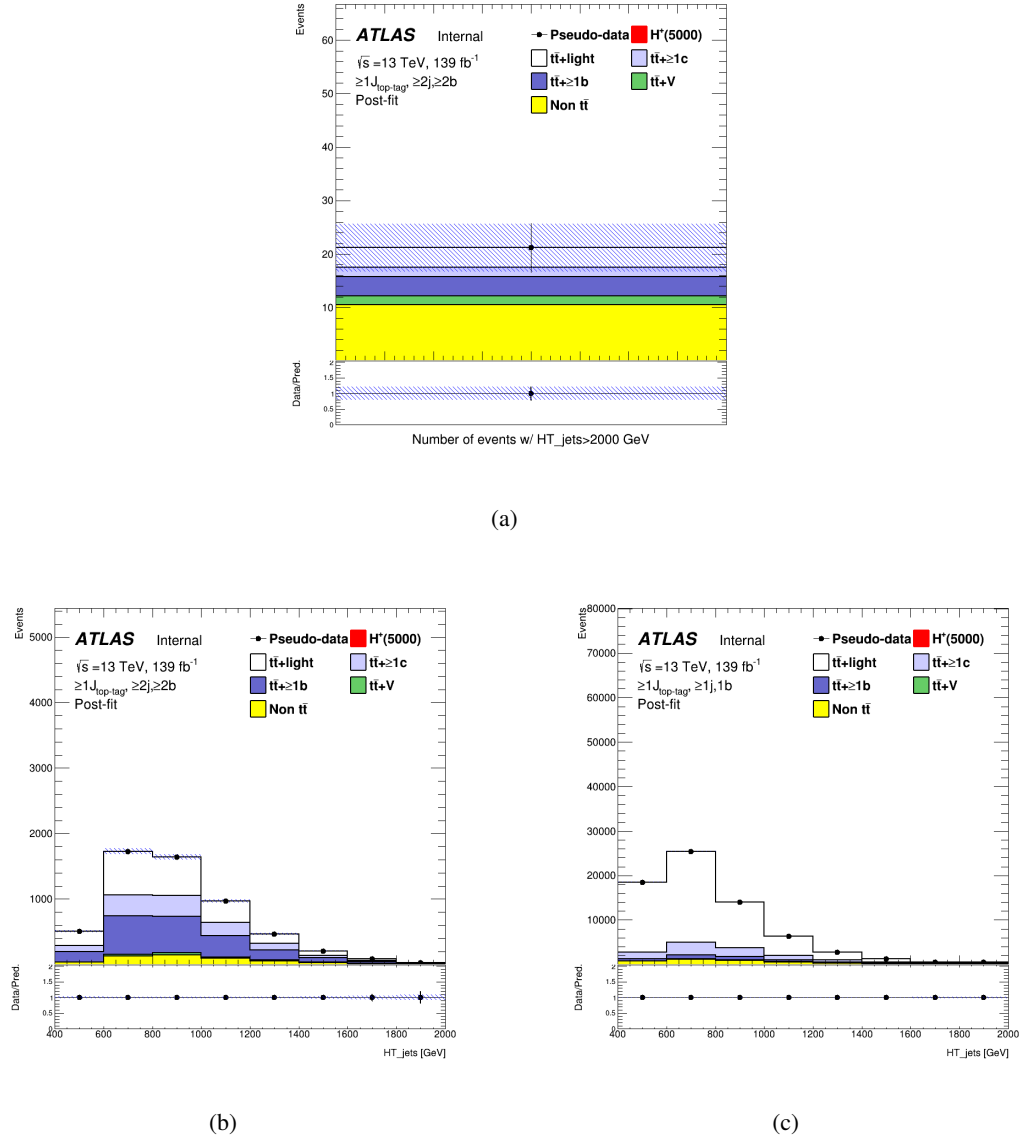


Figure 120: Post-fit plots in the SR (top), CR1 (bottom-left), and CR2 (bottom-right) for 5000 GeV mass hypothesis of H^+ signal.

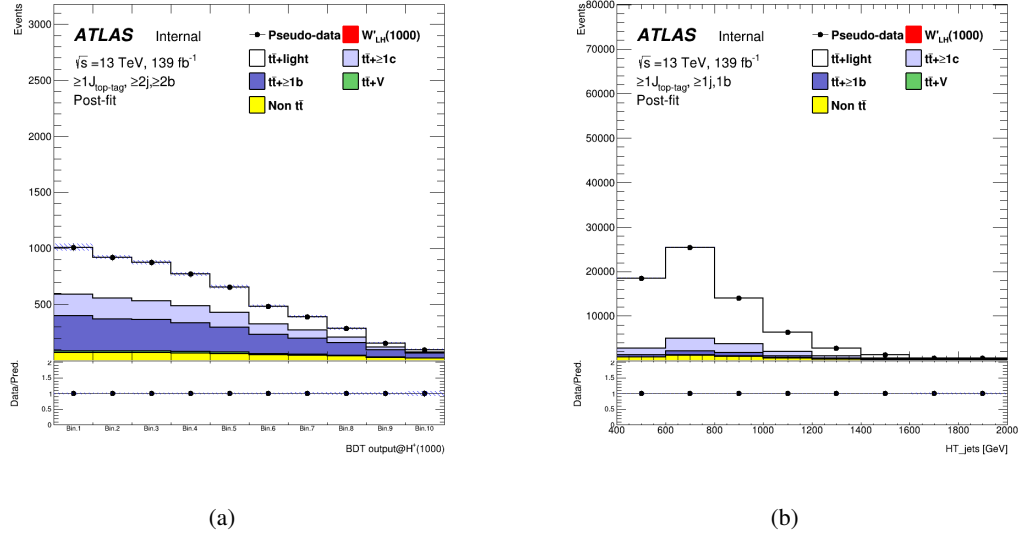


Figure 121: Post-fit plots in the SR (left) and SR (right) for 1000 GeV mass hypothesis of W'_L signal.

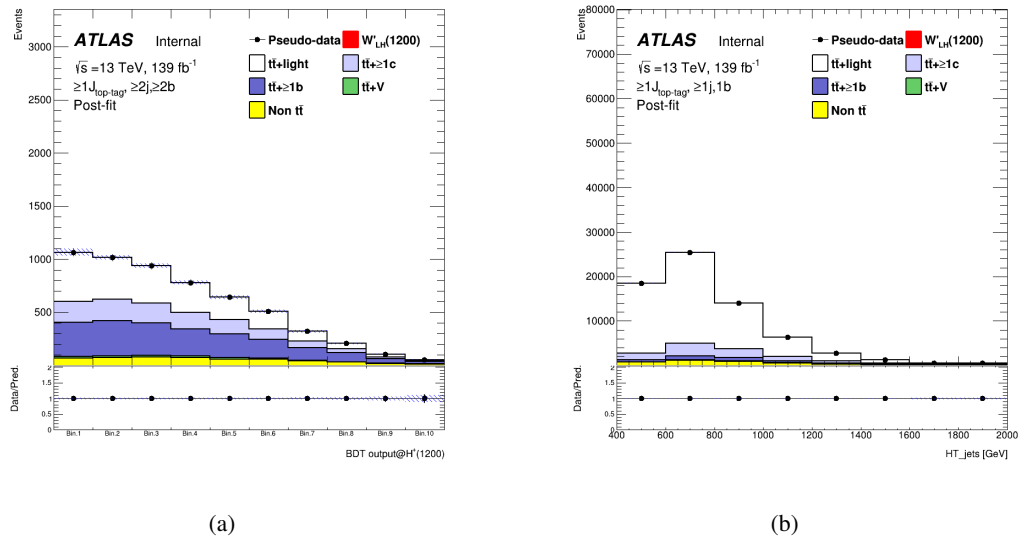


Figure 122: Post-fit plots in the SR (left) and SR (right) for 1200 GeV mass hypothesis of W'_L signal.

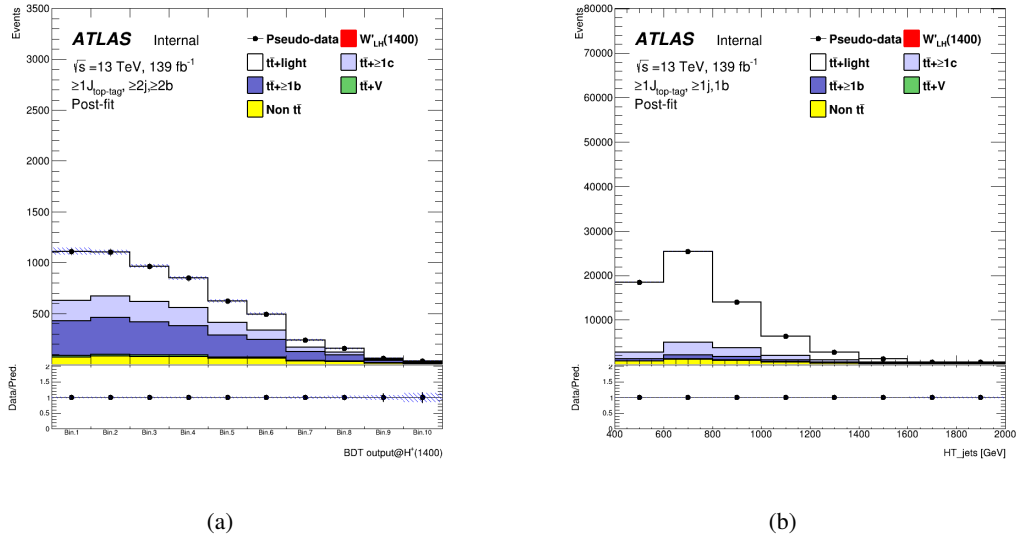


Figure 123: Post-fit plots in the SR (left) and CR (right) for 1400 GeV mass hypothesis of W'_L signal.

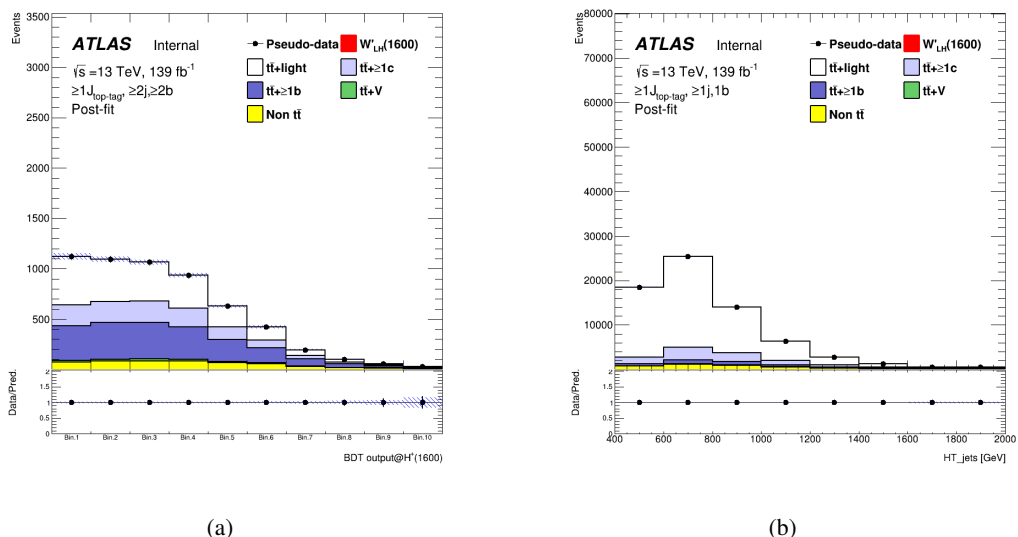


Figure 124: Post-fit plots in the SR (left) and CR (right) for 1600 GeV mass hypothesis of W'_L signal.

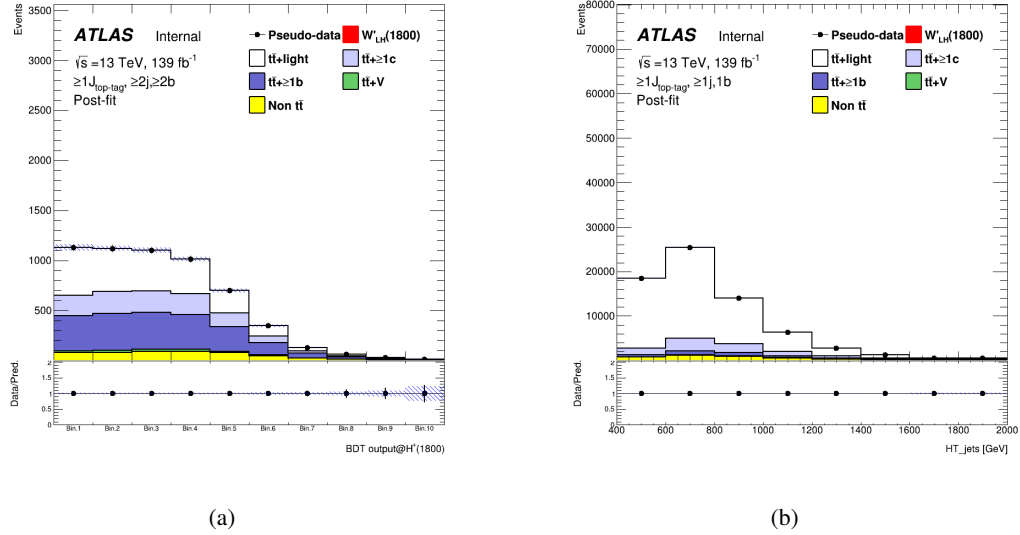


Figure 125: Post-fit plots in the SR (left) and CR (right) for 1800 GeV mass hypothesis of W'_L signal.

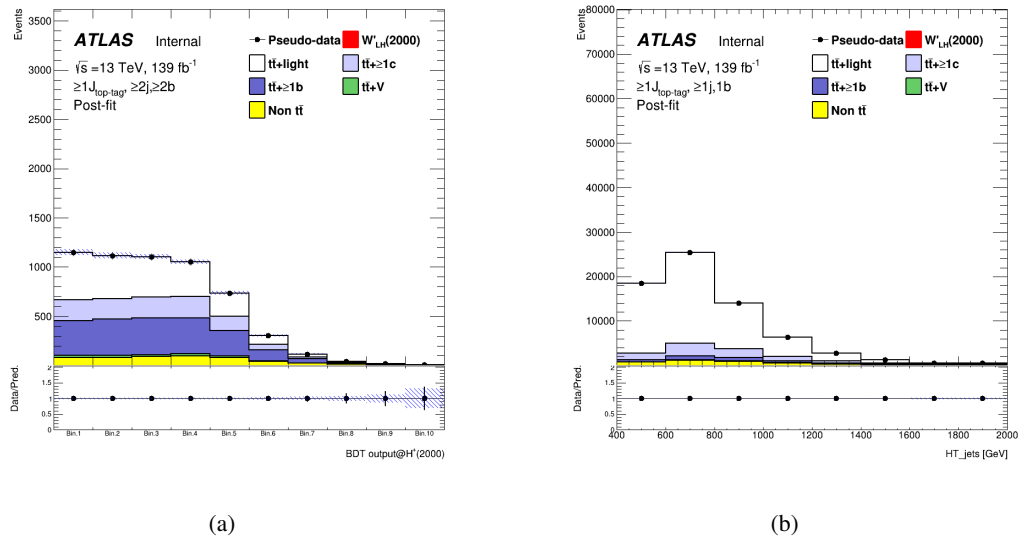


Figure 126: Post-fit plots in the SR (left) and CR (right) for 2000 GeV mass hypothesis of W'_L signal.

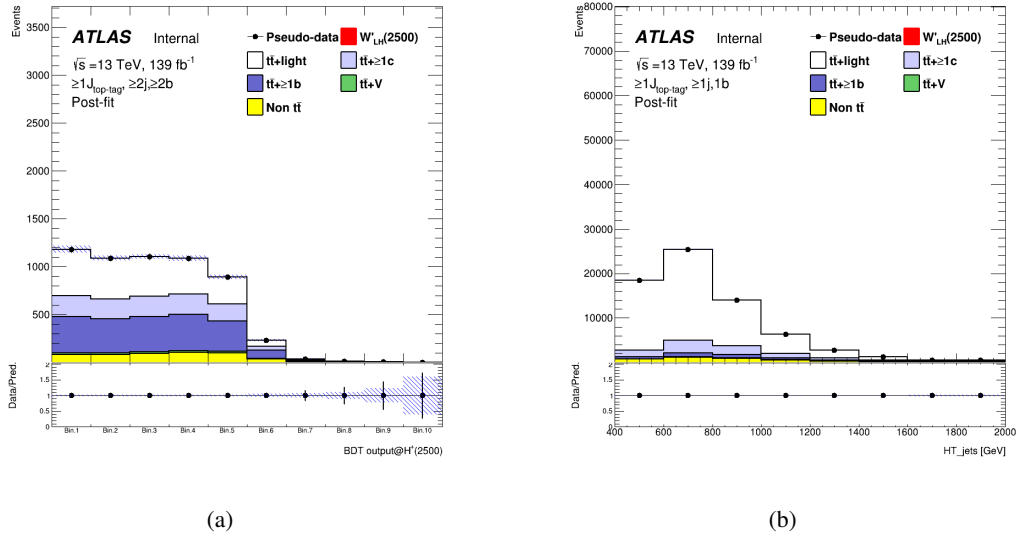


Figure 127: Post-fit plots in the SR (left) and CR (right) for 2500 GeV mass hypothesis of W'_L signal.

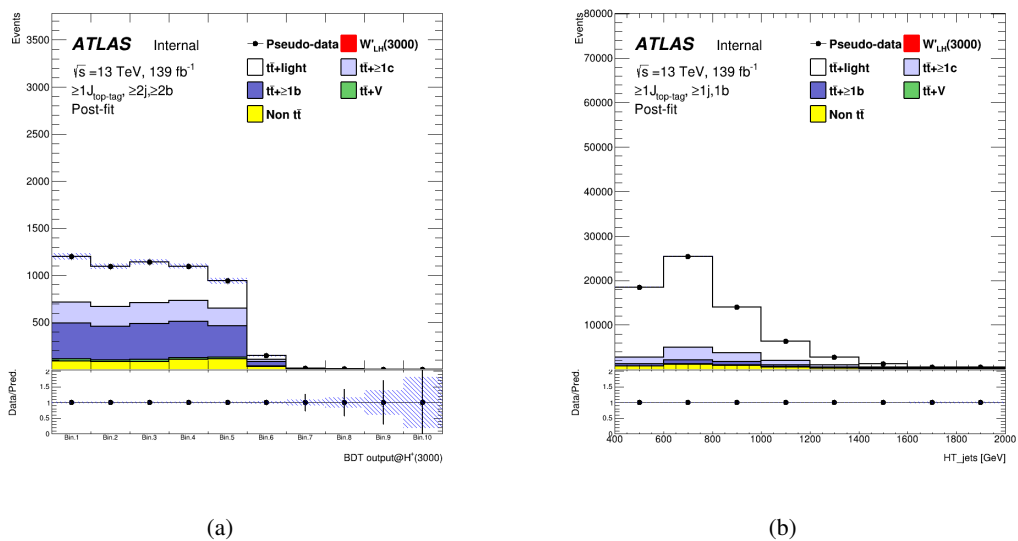


Figure 128: Post-fit plots in the SR (left) and CR (right) for 3000 GeV mass hypothesis of W_L' signal.

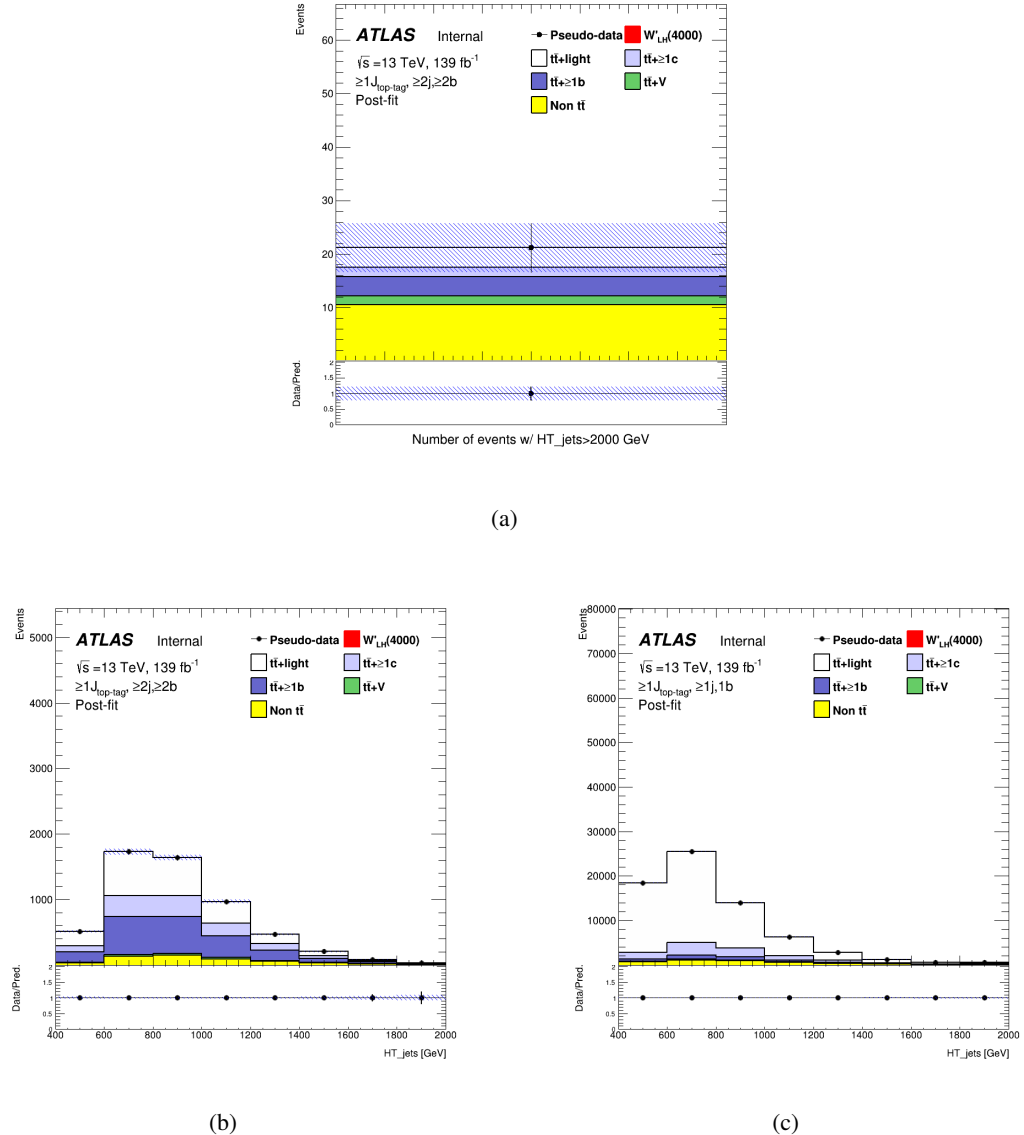


Figure 129: Post-fit plots in the SR (top), CR1 (bottom-left), and CR2 (bottom-right) for 4000 GeV mass hypothesis of W'_L signal.

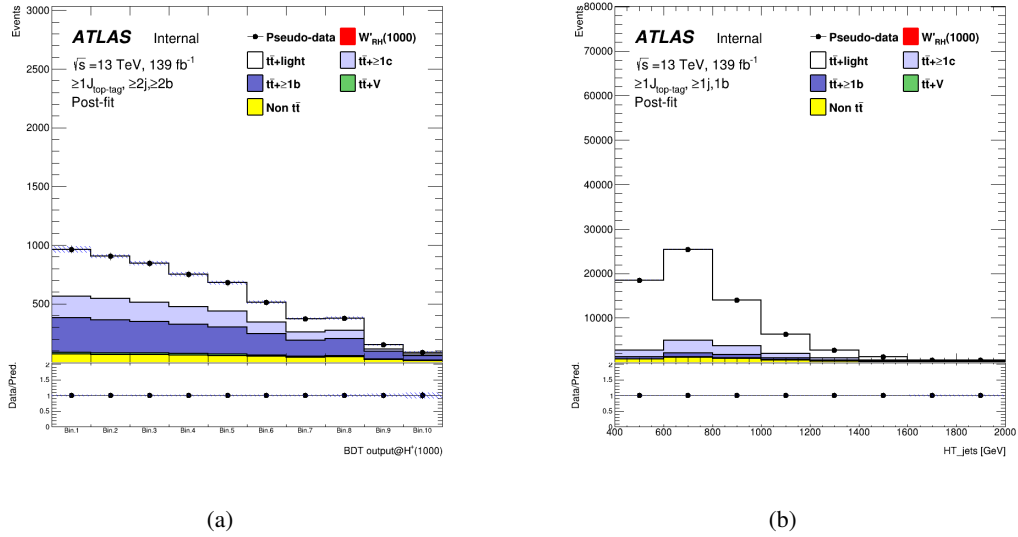


Figure 130: Post-fit plots in the SR (left) and CR (right) for 1000 GeV mass hypothesis of W'_R signal.

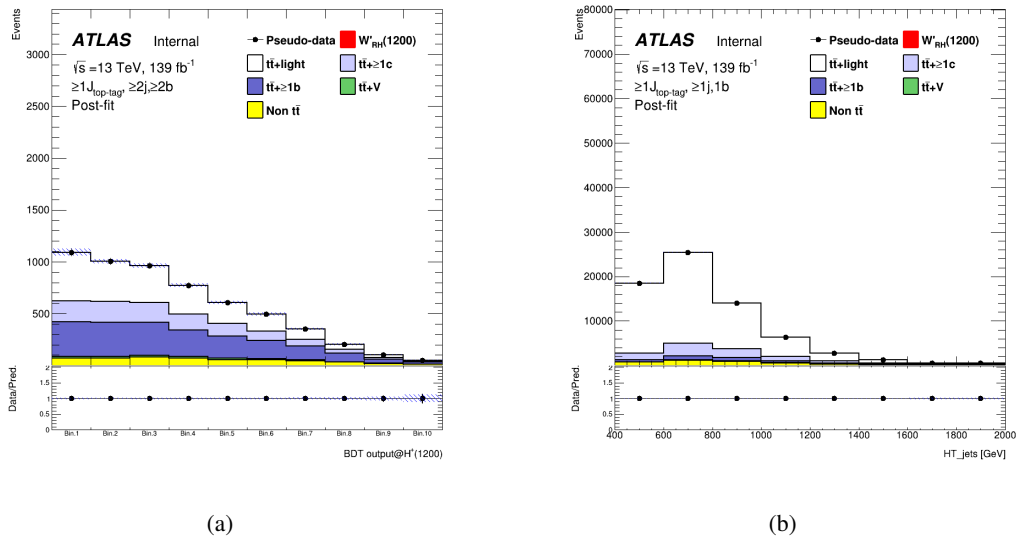


Figure 131: Post-fit plots in the SR (left) and CR (right) for 1200 GeV mass hypothesis of W'_R signal.

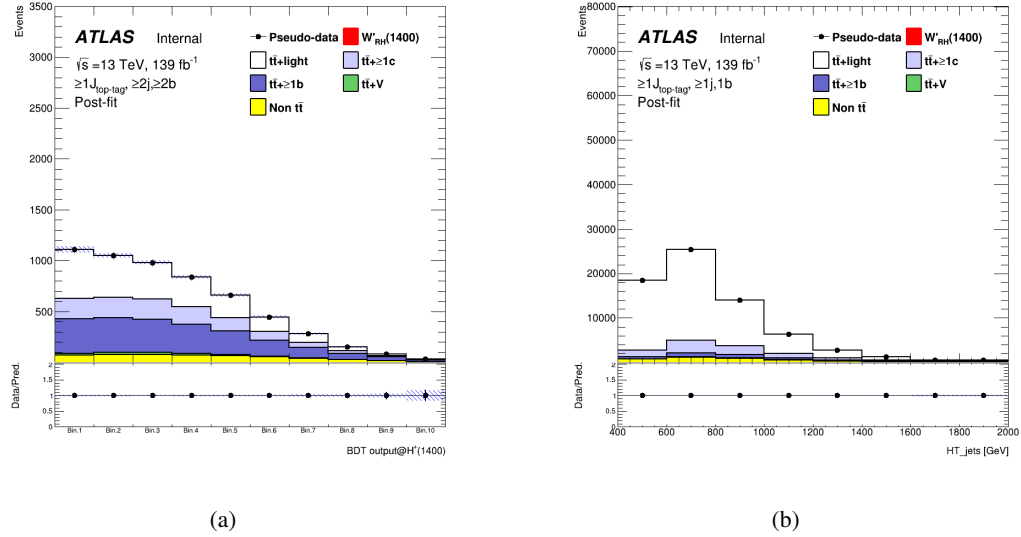


Figure 132: Post-fit plots in the SR (left) and CR (right) for 1400 GeV mass hypothesis of W'_R signal.

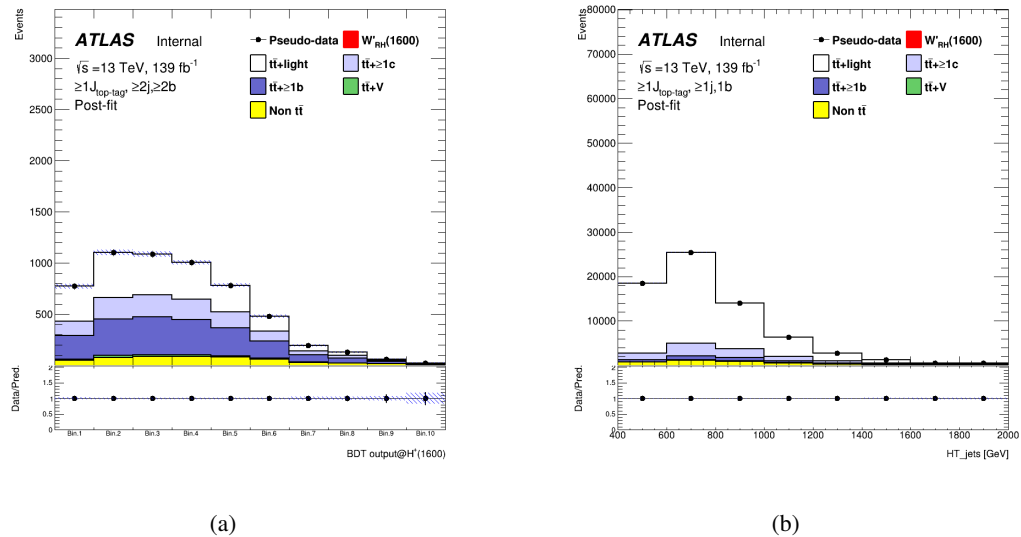


Figure 133: Post-fit plots in the SR (left) and CR (right) for 1600 GeV mass hypothesis of W'_R signal.

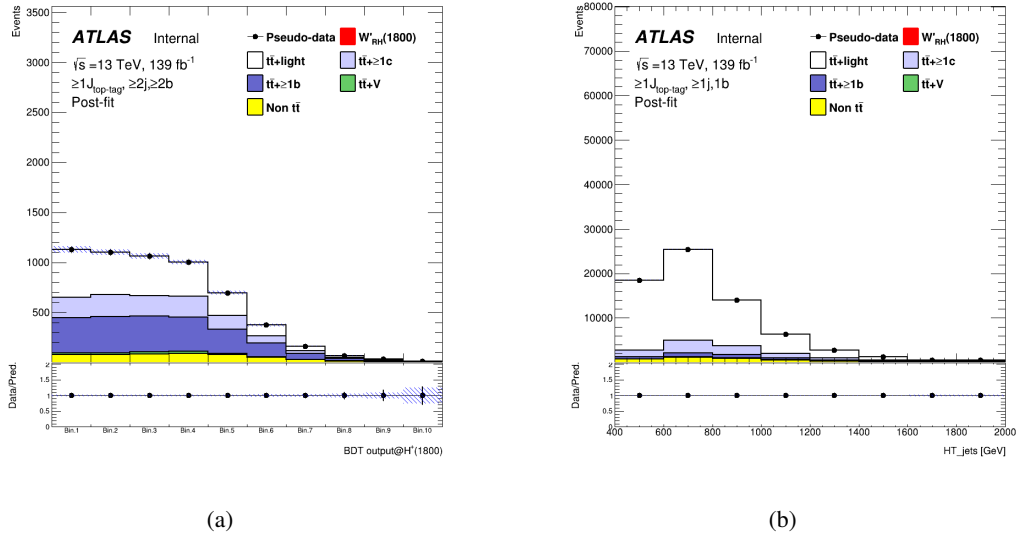


Figure 134: Post-fit plots in the SR (left) and CR (right) for 1800 GeV mass hypothesis of W'_R signal.

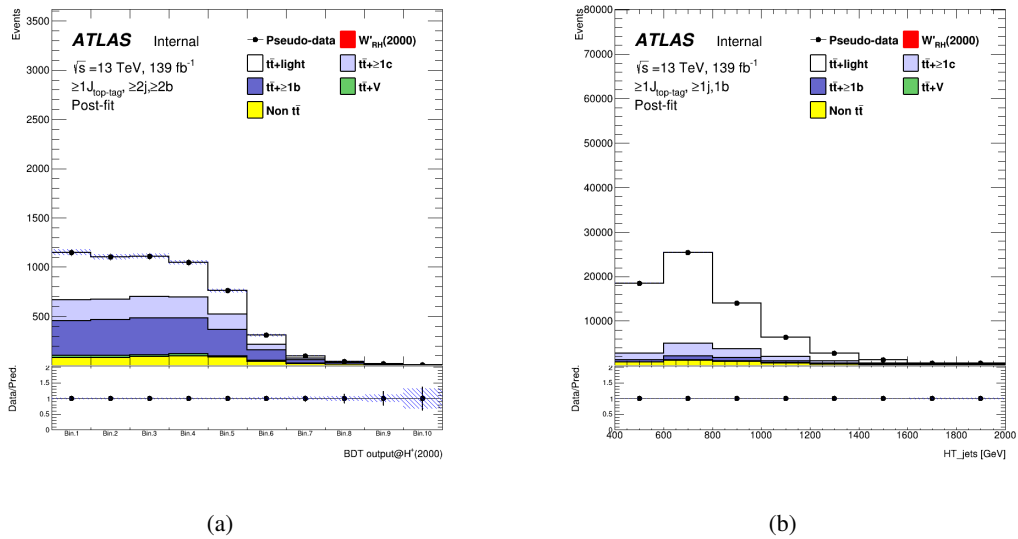


Figure 135: Post-fit plots in the SR (left) and CR (right) for 2000 GeV mass hypothesis of W'_R signal.

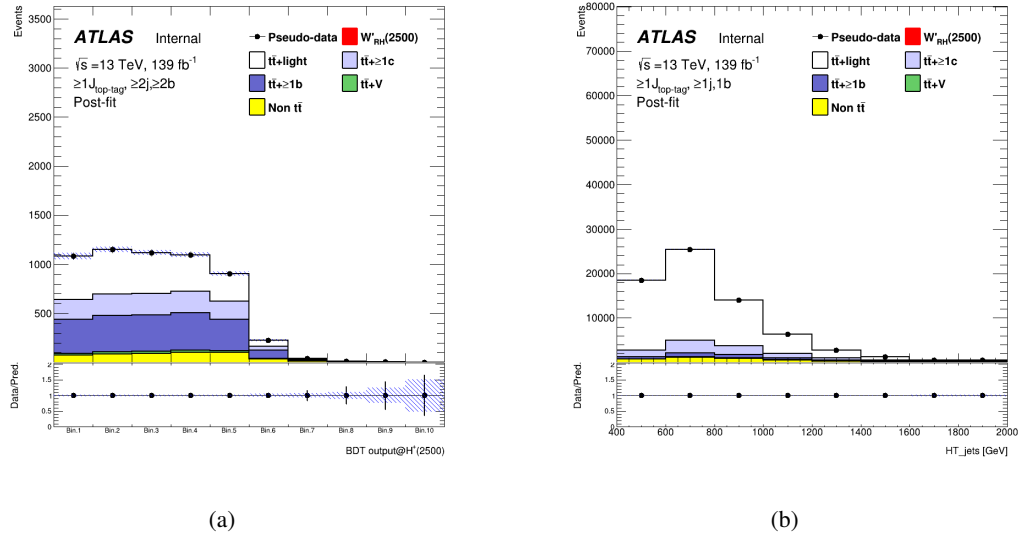


Figure 136: Post-fit plots in the SR (left) and CR (right) for 2500 GeV mass hypothesis of W'_R signal.

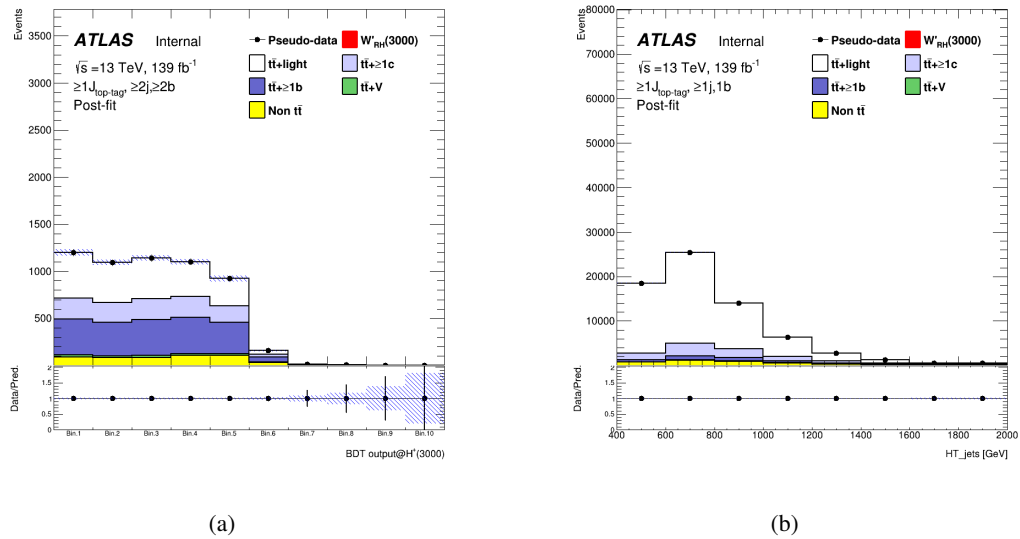


Figure 137: Post-fit plots in the SR (left) and CR (right) for 3000 GeV mass hypothesis of W'_R signal.

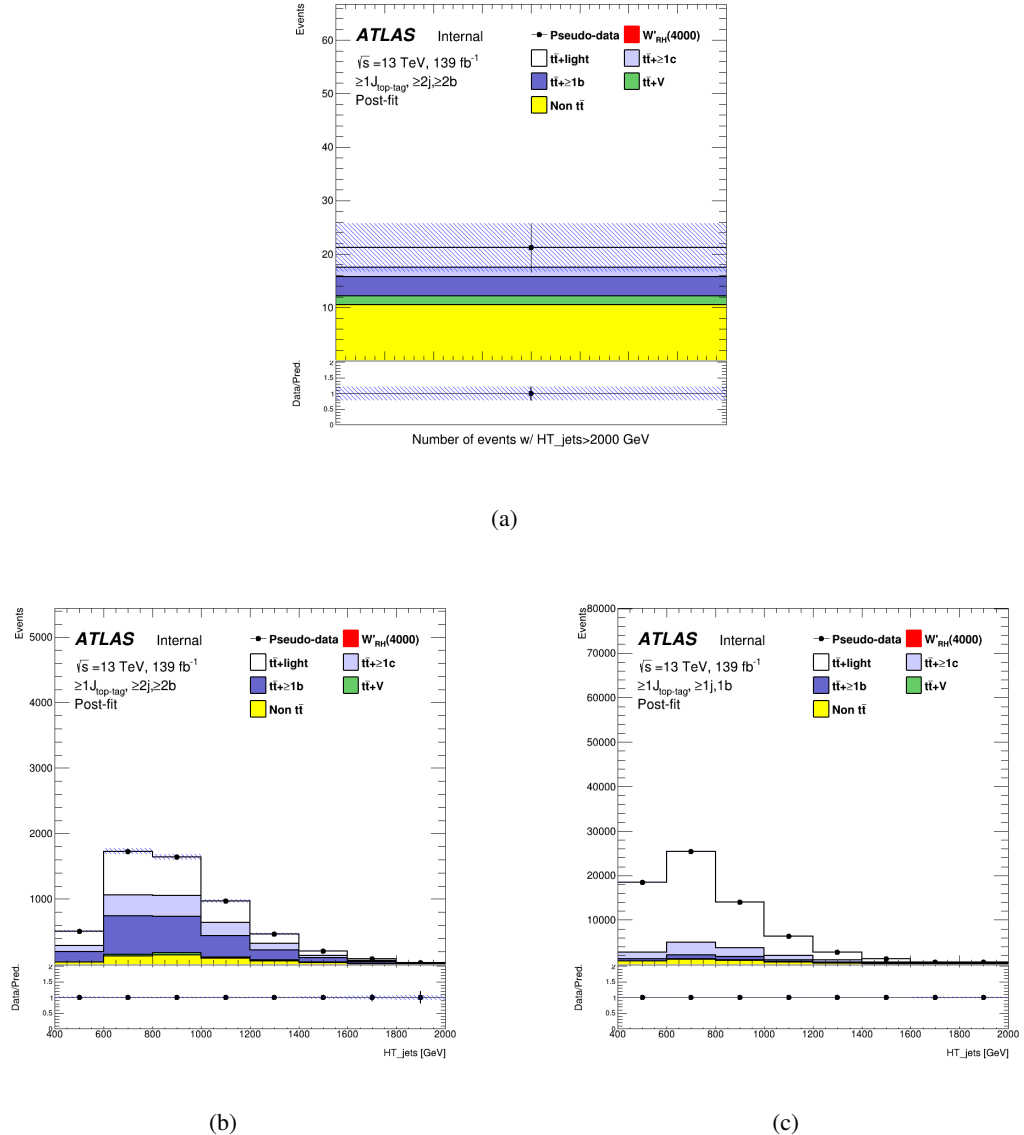


Figure 138: Post-fit plots in the SR (top), CR1 (bottom-left), and CR2 (bottom-right) for 4000 GeV mass hypothesis of W'_R signal.

868 7.3.4 Asimov fit results summary

869 Figure 139 to Figure 141 shows the fitted signal strength and $t\bar{t} + \text{light}$ and $t\bar{t} + \geq 1c/b$ normalization factors
870 as a function of the signal mass hypothesis of the Asimov fit.

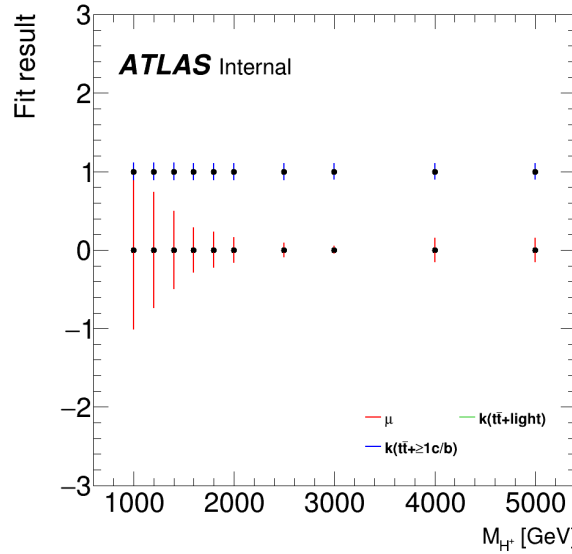


Figure 139: Fitted signal strength and $t\bar{t} + \text{light}$ and $t\bar{t} + \geq 1 c/b$ normalisation factors as a function of the H^+ mass hypothesis of the Asimov fit

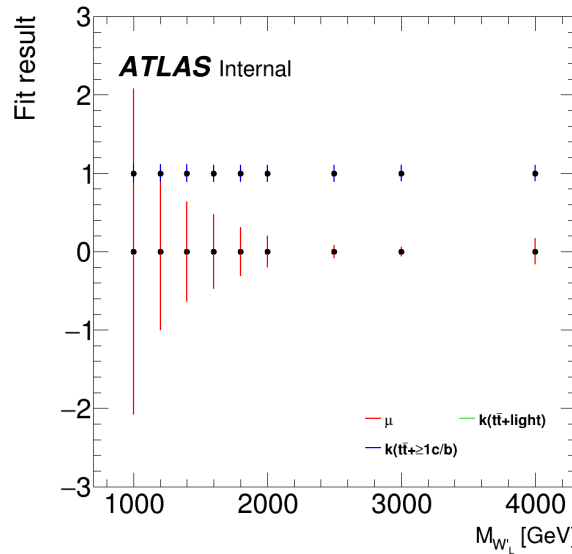


Figure 140: Fitted signal strength and $t\bar{t} + \text{light}$ and $t\bar{t} + \geq 1 c/b$ normalisation factors as a function of the W'_L mass hypothesis of the Asimov fit

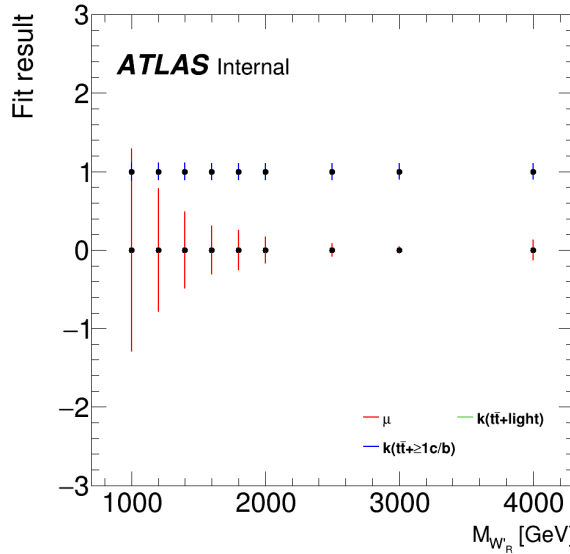


Figure 141: Fitted signal strength and $t\bar{t} + \text{light}$ and $t\bar{t} + \geq 1 c/b$ normalisation factors as a function of the W'_R mass hypothesis of the Asimov fit

871 7.4 Data fit

872 7.4.1 Pre-fit plots

873 The following section performs fitting to collision data with and without the signal strength fixed to zero
 874 (background-only (BOnly) and signal+background (S+B) fits) using blinding. Figure 152 to 160 show the
 875 pre-fit plots for each H^+ mass hypothesis.

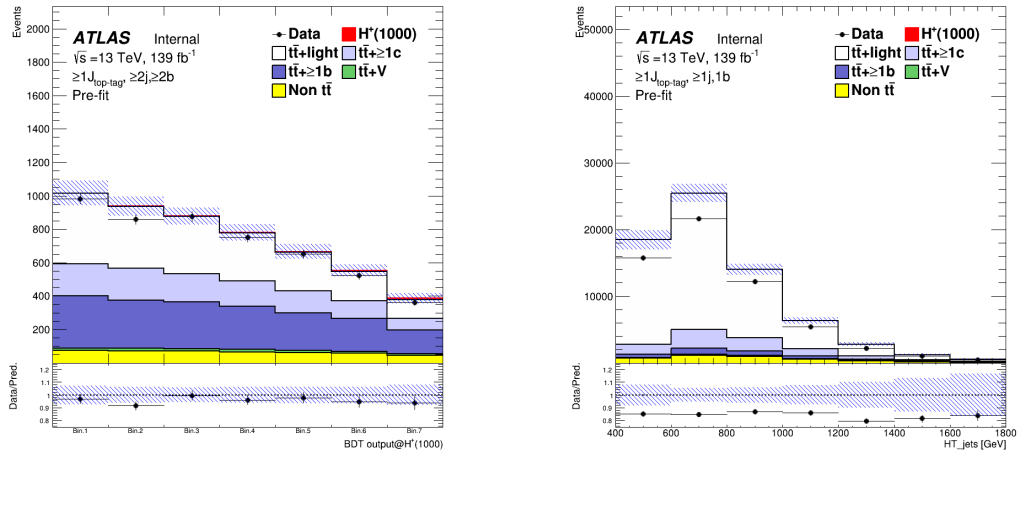


Figure 142: Pre-fit plots in the SR (left) and CR (right) for 1000 GeV mass hypothesis of H^+ signal. Blinding bins aren't plotted.

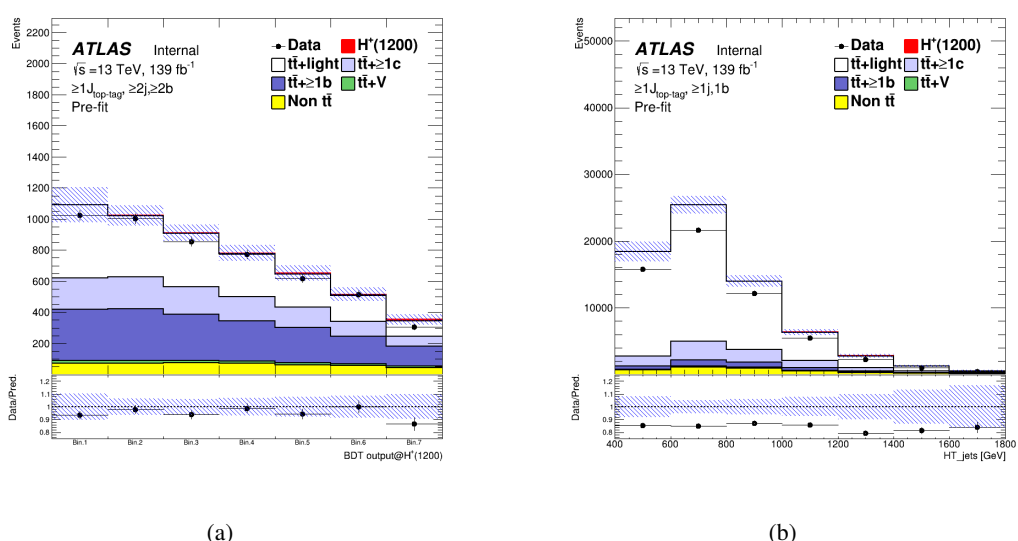


Figure 143: Pre-fit plots in the SR (left) and CR (right) for 1200 GeV mass hypothesis of H^+ signal. Blinding bins aren't plotted.

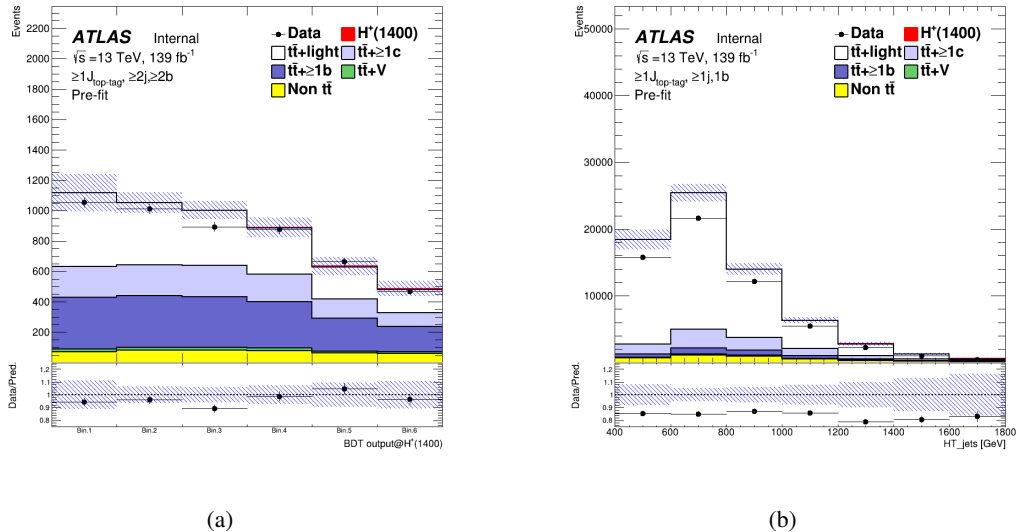


Figure 144: Pre-fit plots in the SR (left) and CR (right) for 1400 GeV mass hypothesis of H^+ signal. Blinding bins aren't plotted.

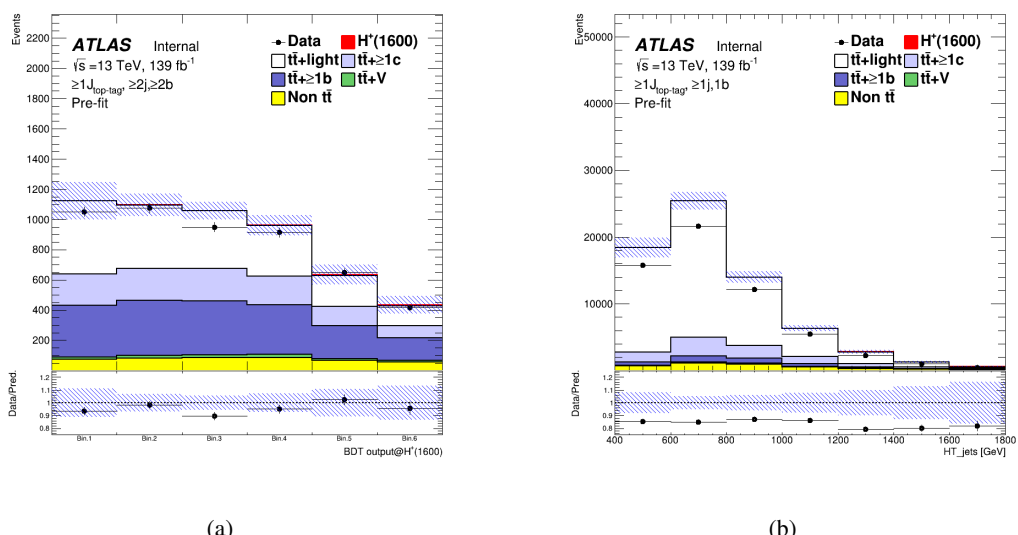


Figure 145: Pre-fit plots in the SR (left) and CR (right) for 1600 GeV mass hypothesis of H^+ signal. Blinding bins aren't plotted.

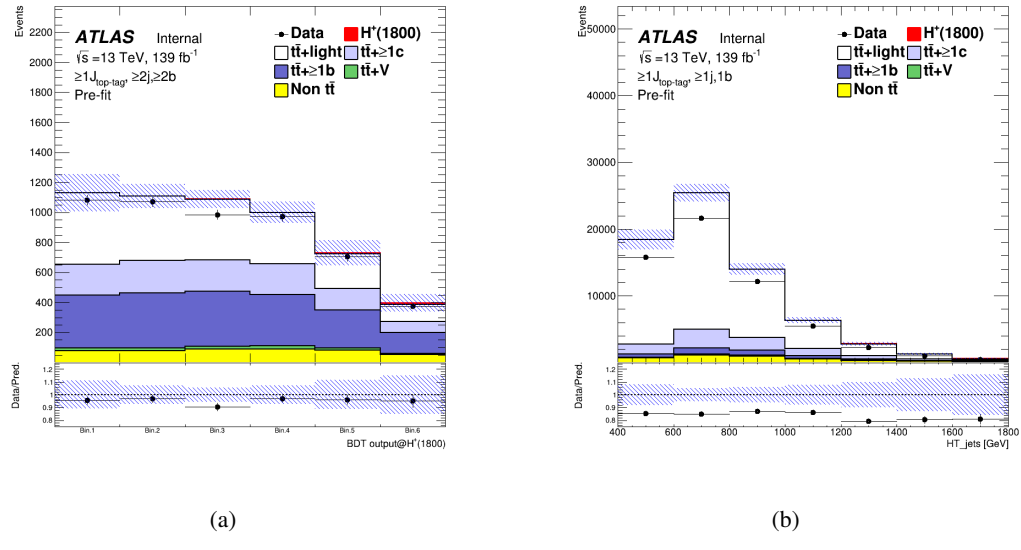


Figure 146: Pre-fit plots in the SR (left) and CR (right) for 1800 GeV mass hypothesis of H^+ signal. Blinding bins aren't plotted.

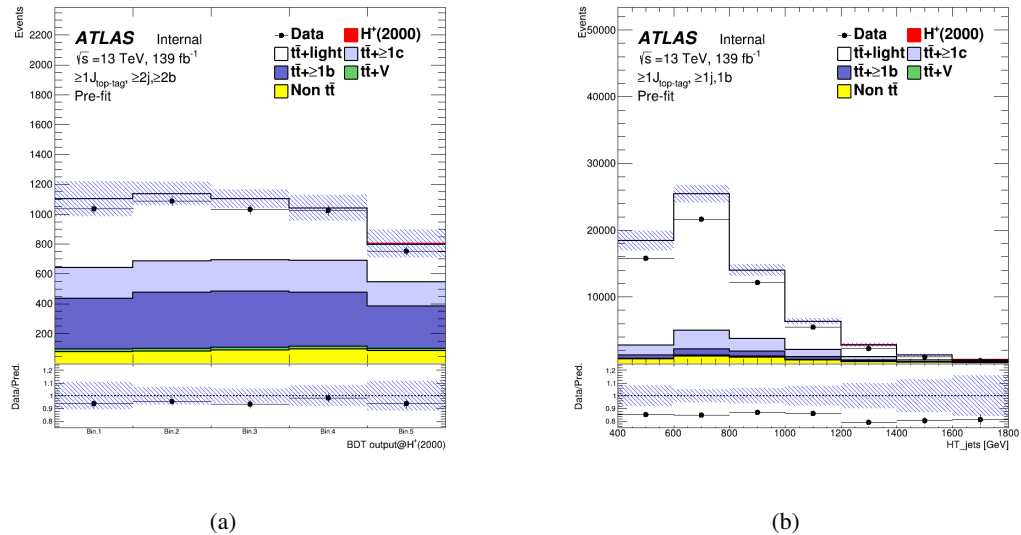


Figure 147: Pre-fit plots in the SR (left) and CR (right) for 2000 GeV mass hypothesis of H^+ signal. Blinding bins aren't plotted.

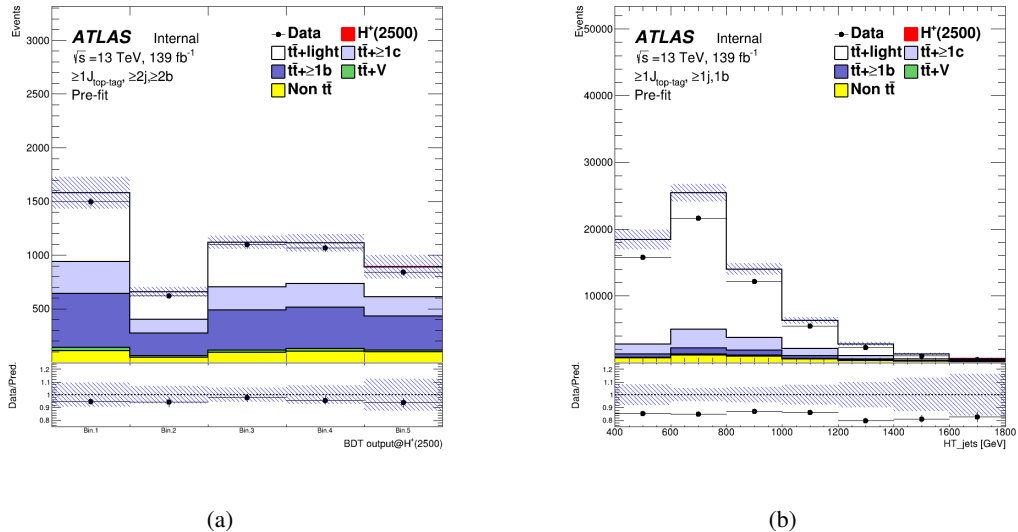


Figure 148: Pre-fit plots in the SR (left) and CR (right) for 2500 GeV mass hypothesis of H^+ signal. Blinding bins aren't plotted.

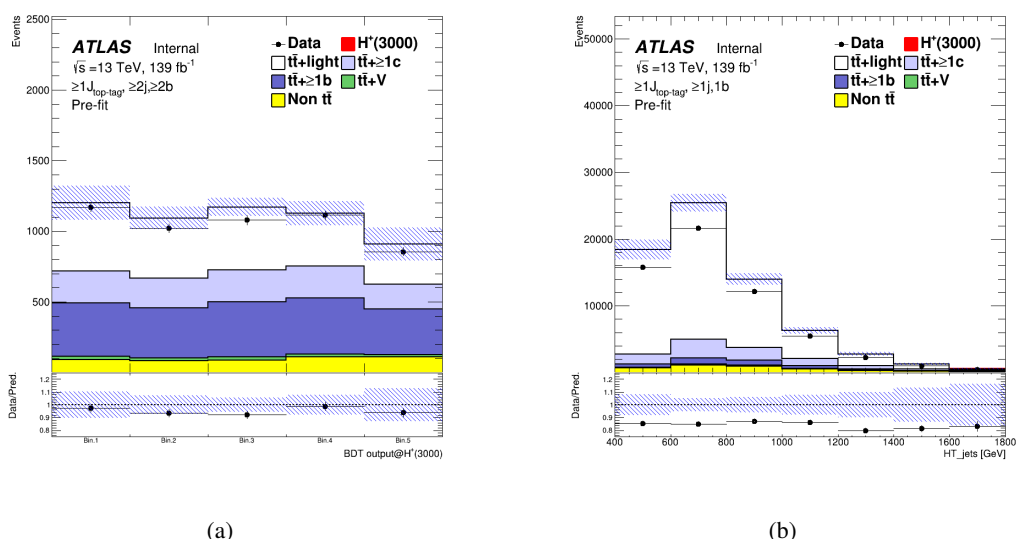


Figure 149: Pre-fit plots in the SR (left) and CR (right) for 3000 GeV mass hypothesis of H^+ signal. Blinding bins aren't plotted.

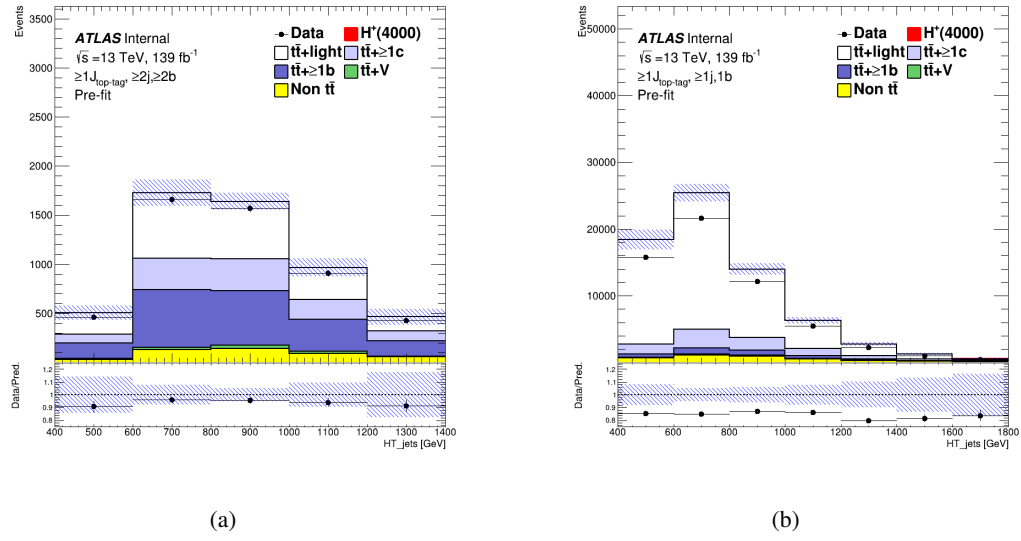


Figure 150: Pre-fit plots in the CR1 (left) and CR2 (right) for 4000 GeV mass hypothesis of H^+ signal. Blinding bins aren't plotted.

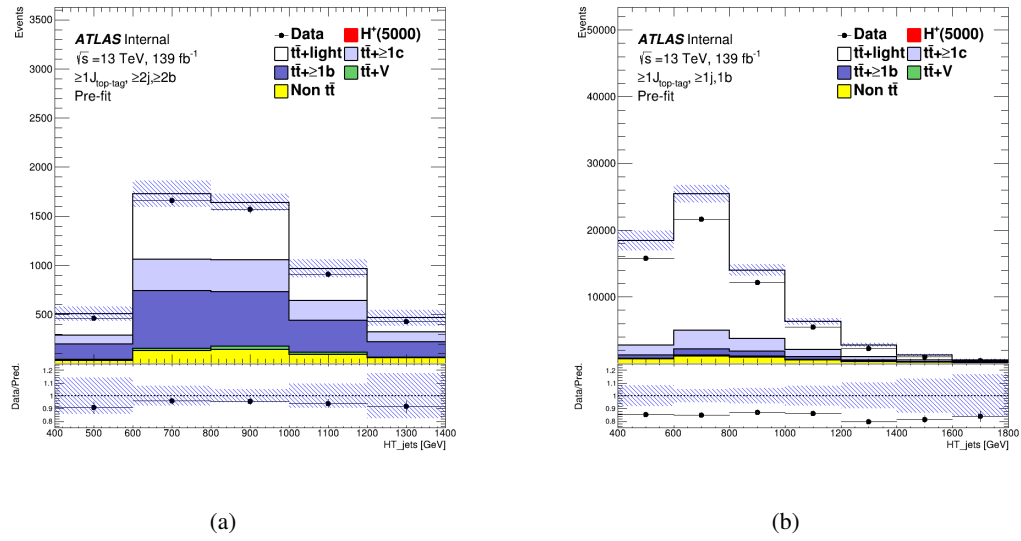
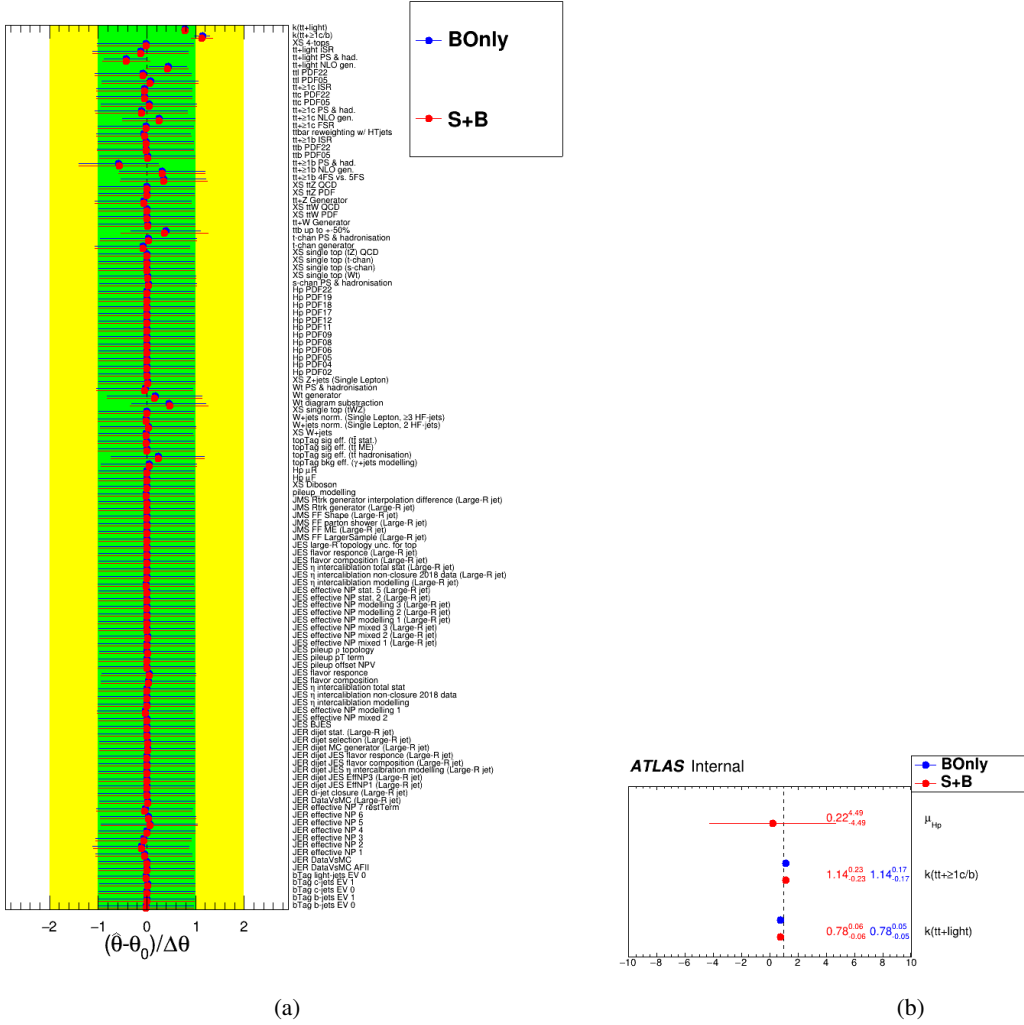


Figure 151: Pre-fit plots in the CR1 (left) and CR2 (right) for 5000 GeV mass hypothesis of H^+ signal. Blinding bins aren't plotted.

876 7.4.2 Fit results

877 The results of BOnly and S+B fits are presented. Figures 152 to 161 show the nuisance parameters and
 878 normalization factors for each H^+ mass hypothesis.

ATLAS InternalFigure 152: Nuisance parameters (left) and Norm. factors (right) for the 1000 GeV H^+ mass hypotheses.

ATLAS Internal

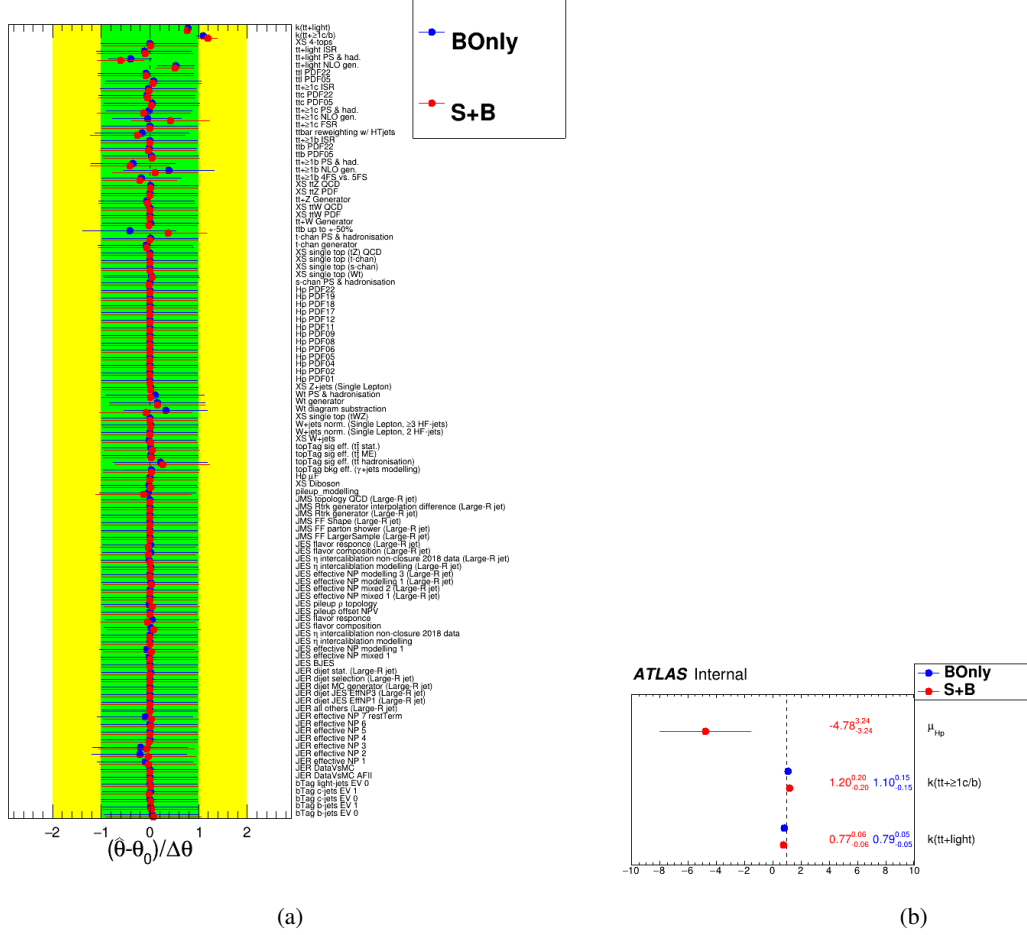


Figure 153: Nuisance parameters (left) and Norm. factors (right) for the 1200 GeV H^+ mass hypotheses.

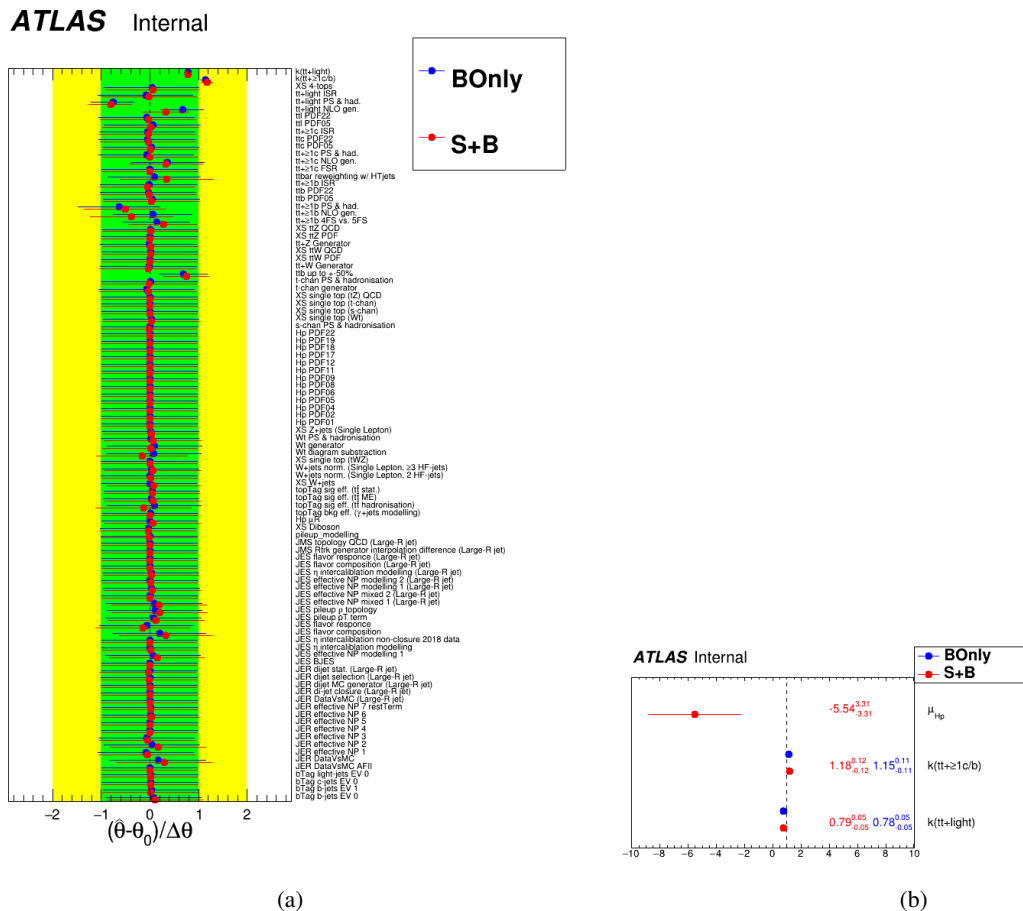
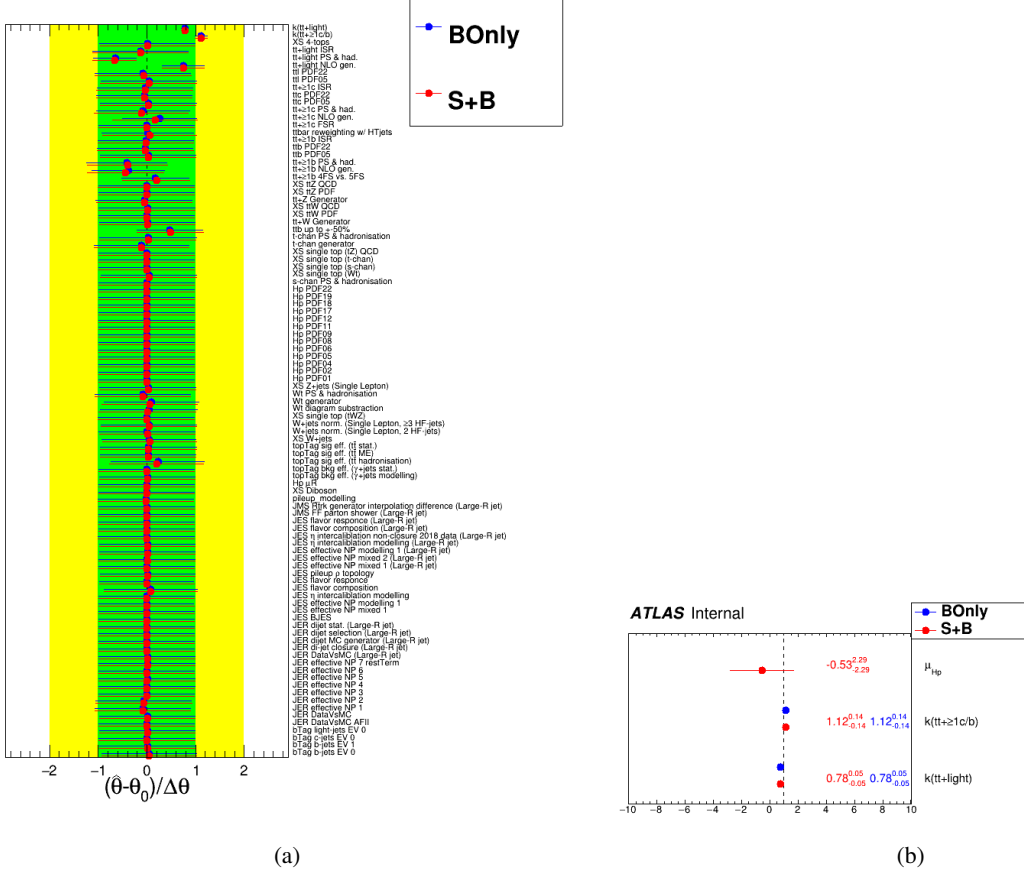
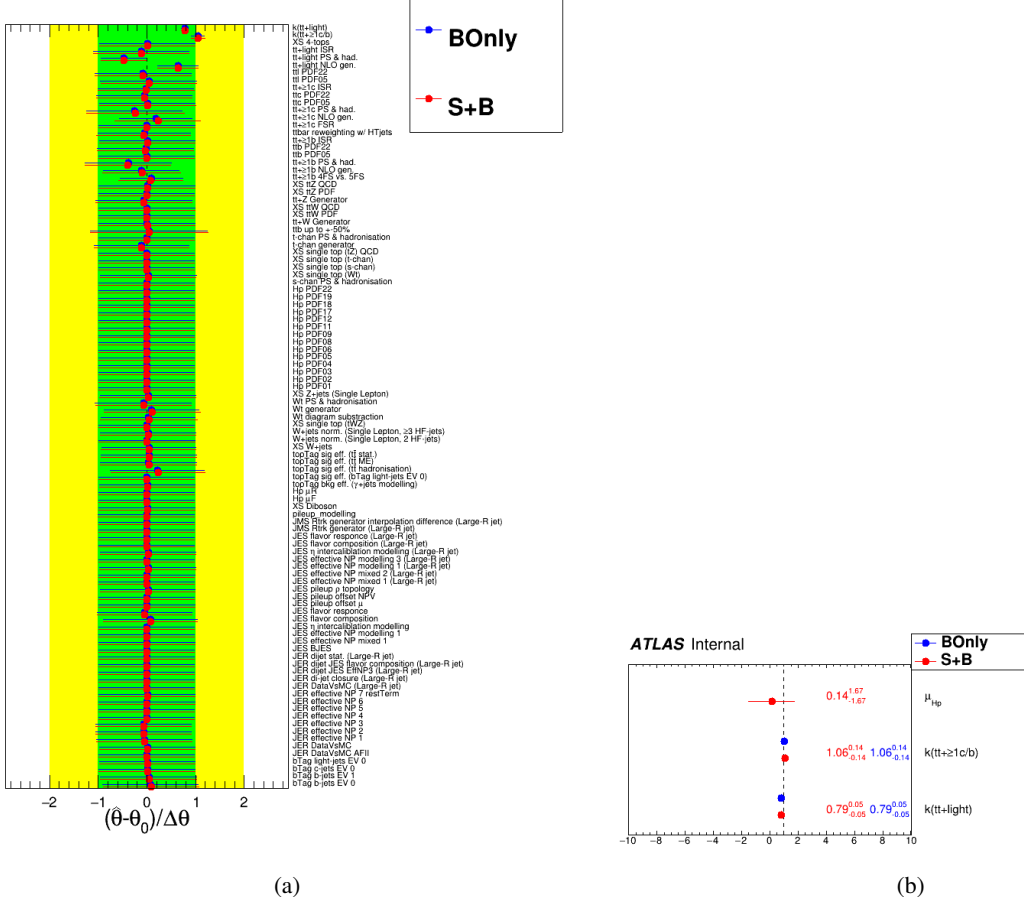


Figure 154: Nuisance parameters (left) and Norm. factors (right) for the 1400 GeV H^+ mass hypotheses.

ATLAS InternalFigure 155: Nuisance parameters (left) and Norm. factors (right) for the 1600 GeV H^+ mass hypotheses.

ATLAS InternalFigure 156: Nuisance parameters (left) and Norm. factors (right) for the 1800 GeV H^+ mass hypotheses.

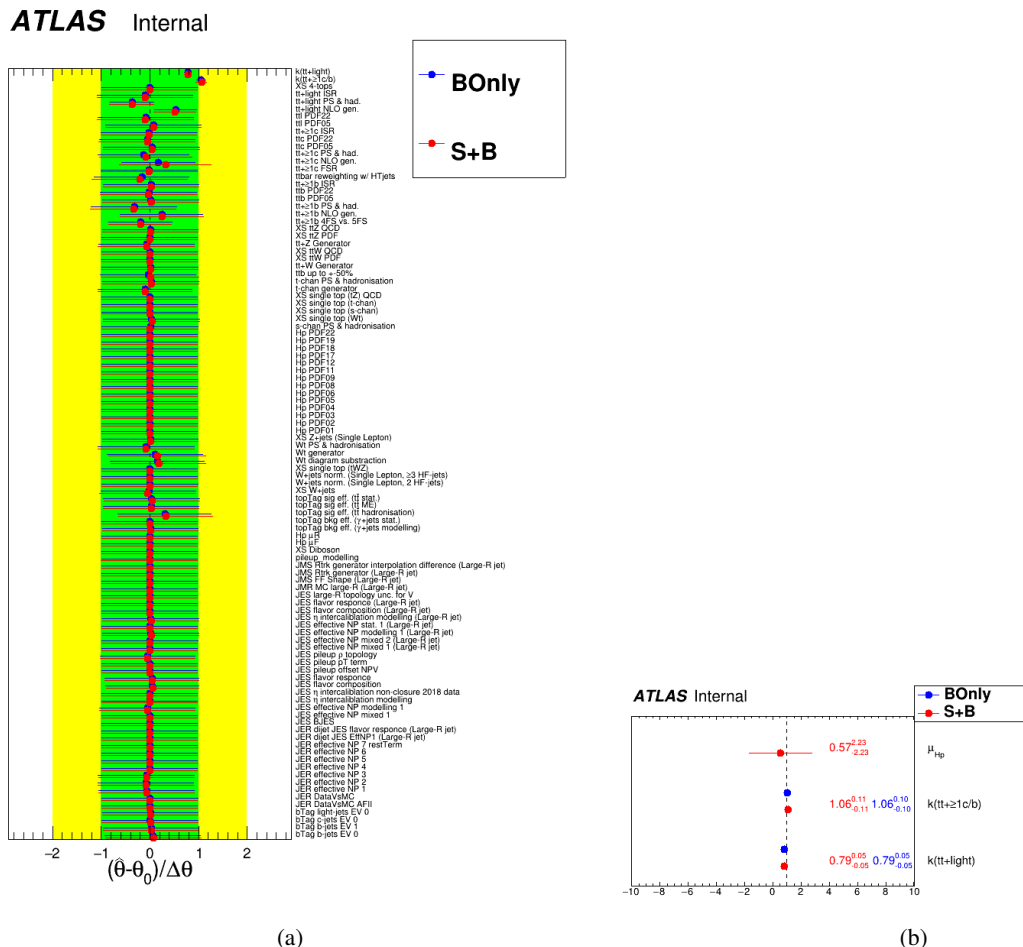
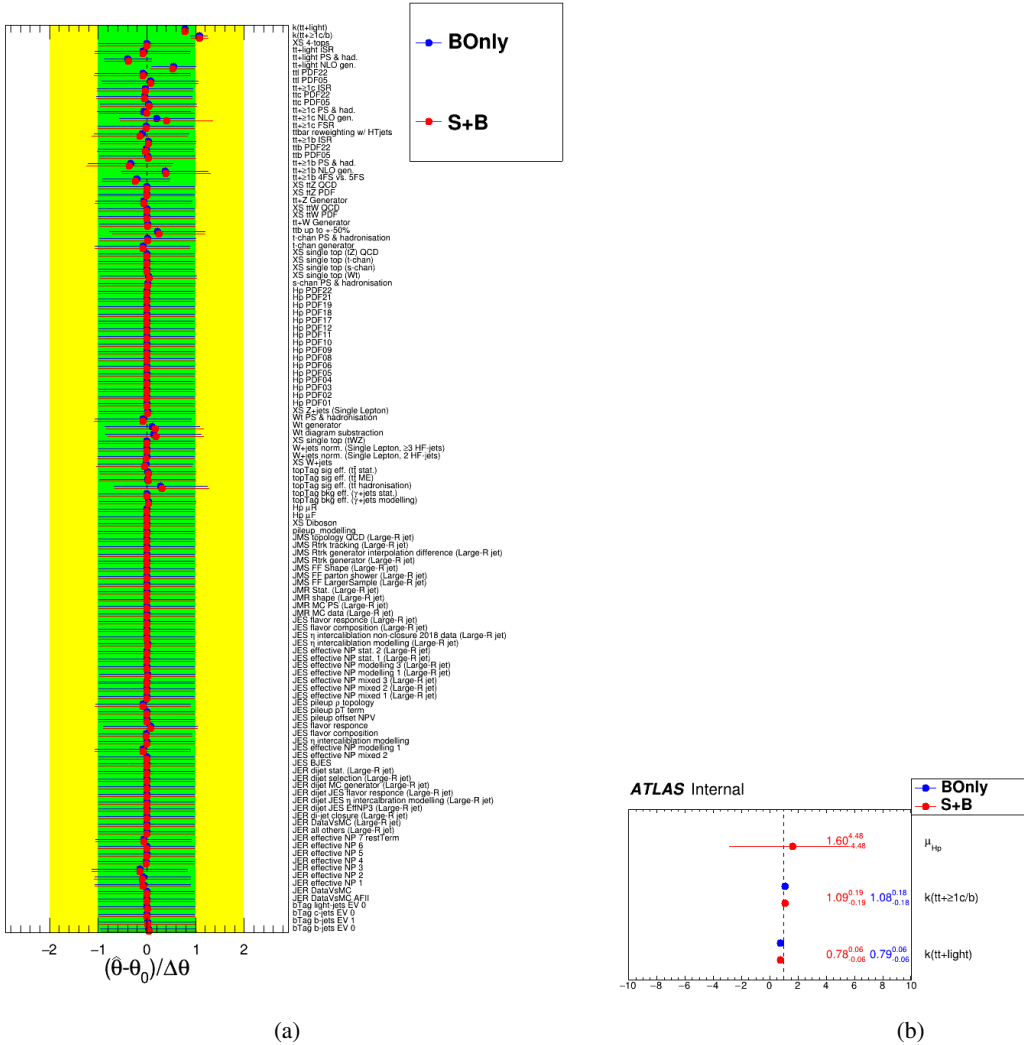


Figure 157: Nuisance parameters (left) and Norm. factors (right) for the 2000 GeV H^+ mass hypotheses.

ATLAS InternalFigure 158: Nuisance parameters (left) and Norm. factors (right) for the 2500 GeV H^+ mass hypotheses.

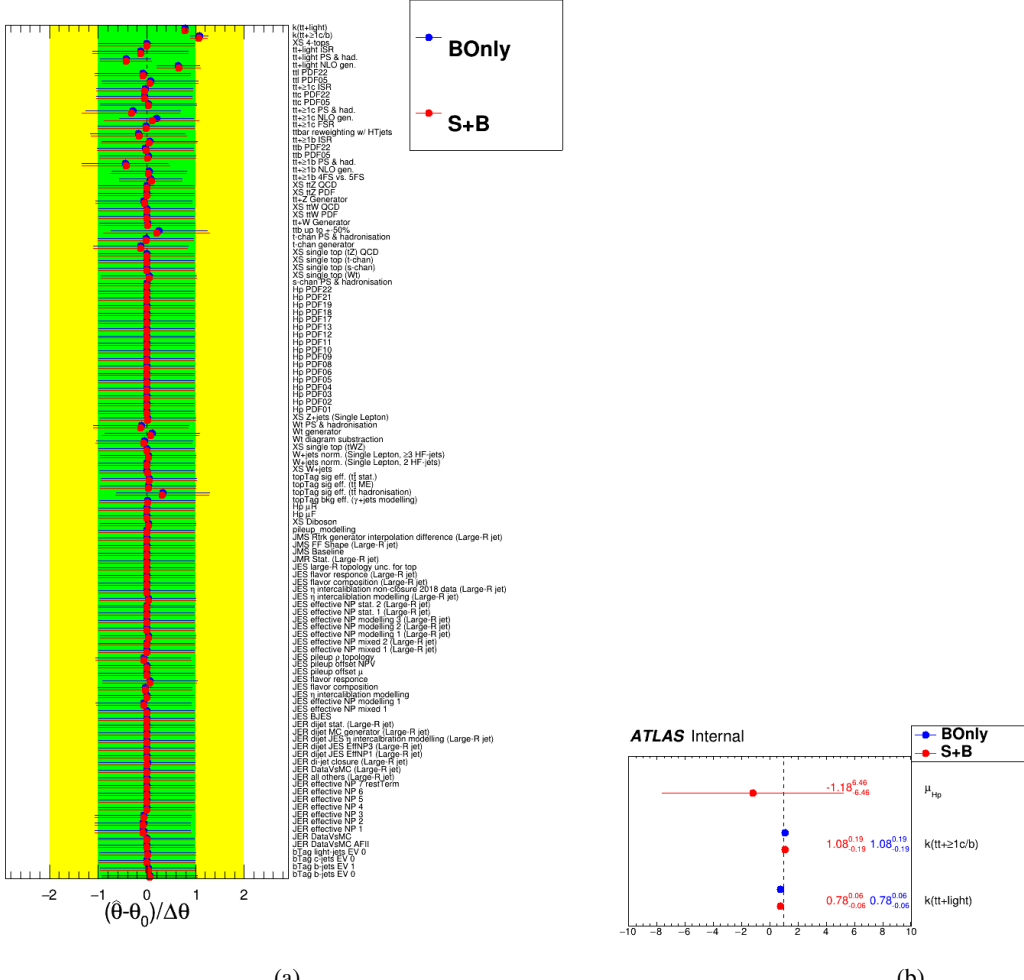
ATLAS Internal

Figure 159: Nuisance parameters (left) and Norm. factors (right) for the 3000 GeV H^+ mass hypotheses.

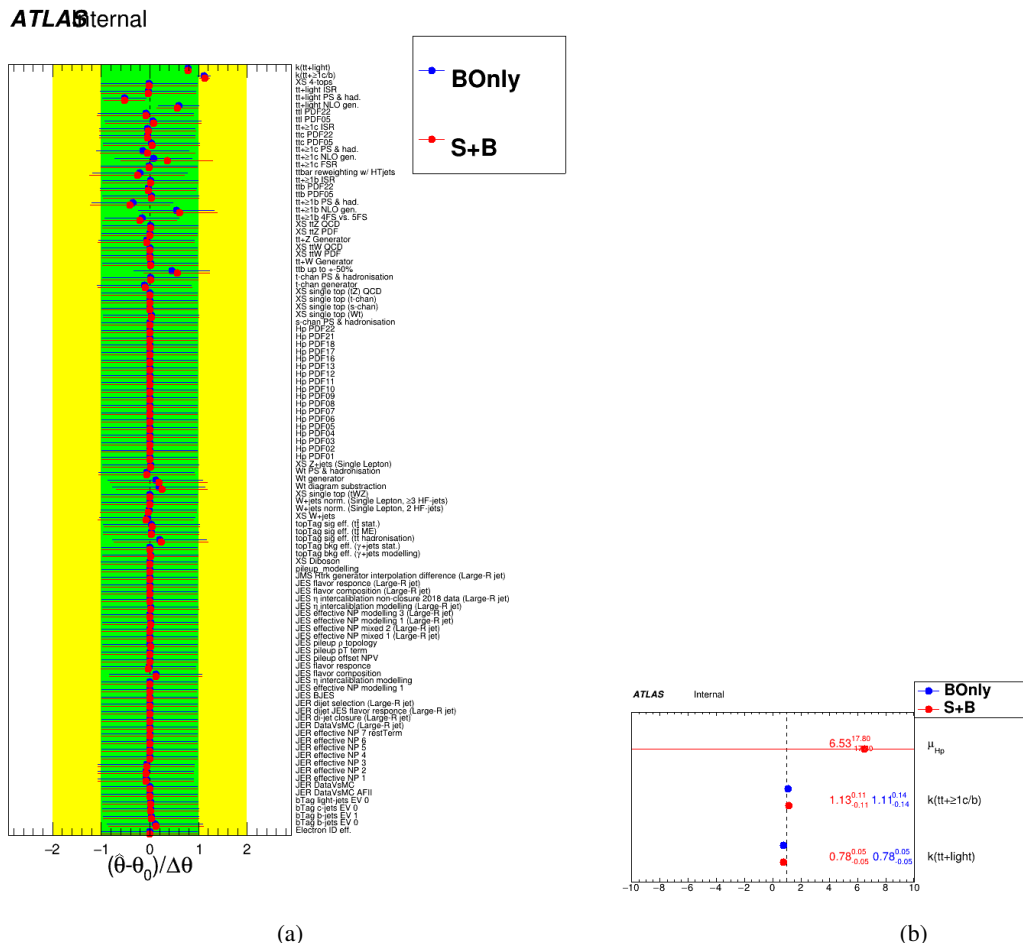
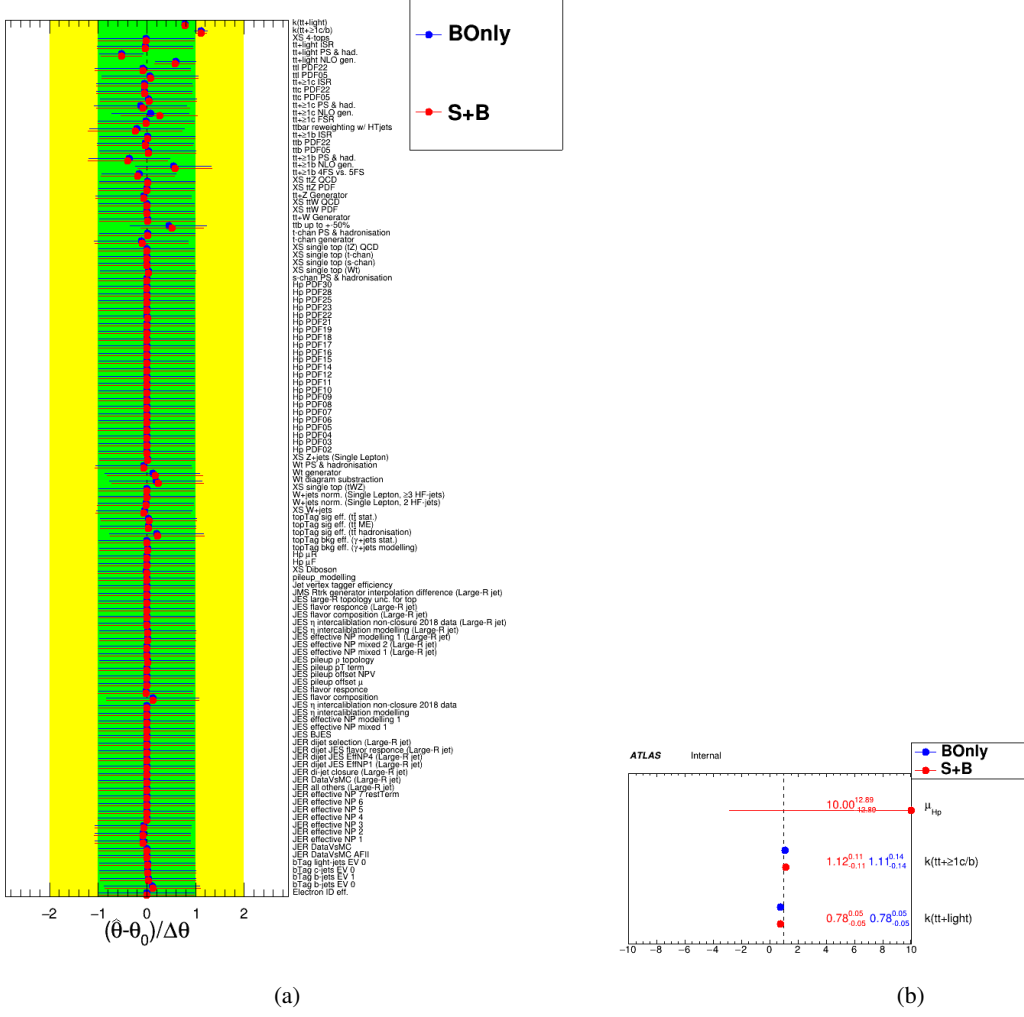
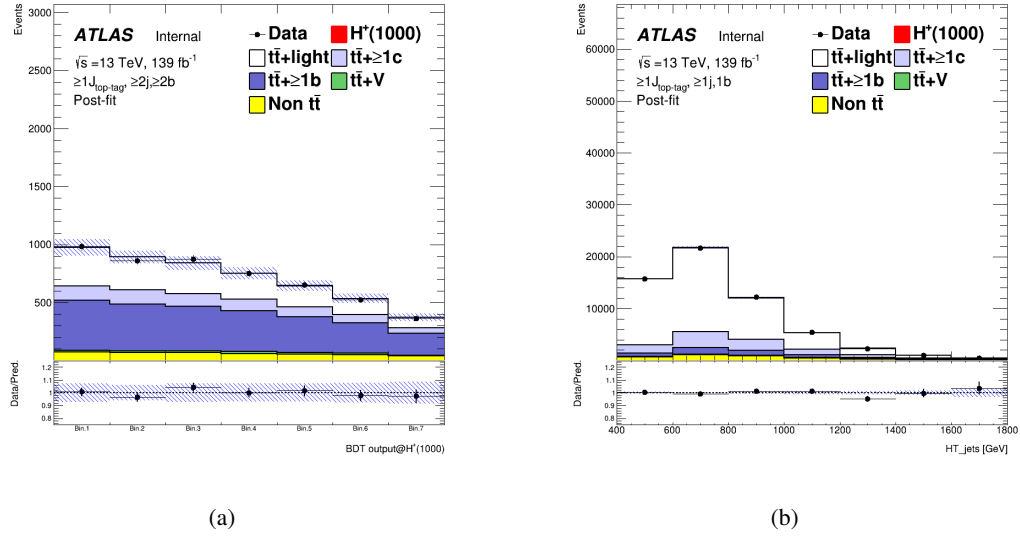
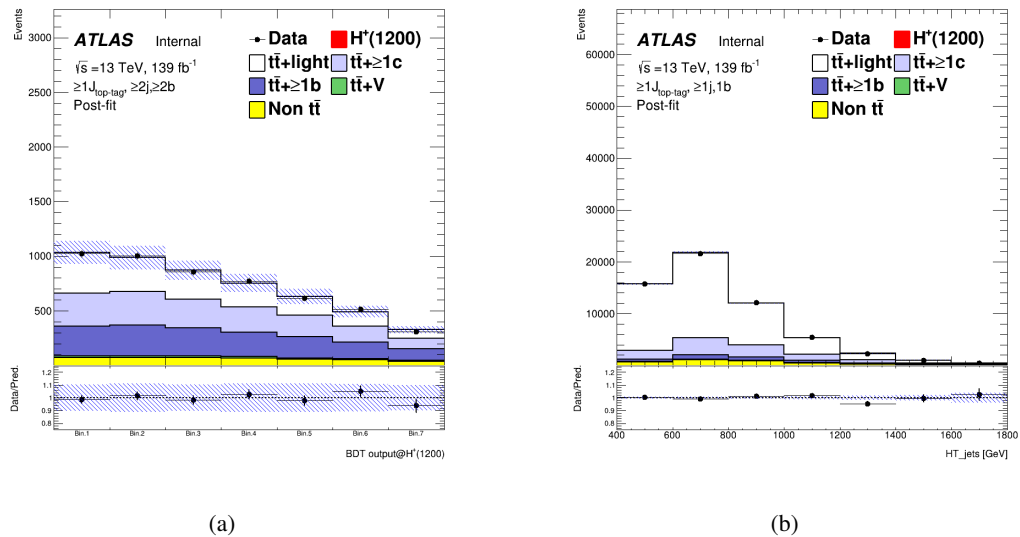


Figure 160: Nuisance parameters (left) and Norm. factors (right) for the 4000 GeV H^+ mass hypotheses.

ATLAS Internal

Figure 161: Nuisance parameters (left) and Norm. factors (right) for the 5000 GeV H^+ mass hypotheses.

879 **7.5 Post-fit plots**Figure 162: Post-fit (BOnly) plots in the SR (left) and CR (right) for 1000 GeV mass hypothesis of H^+ signal.Figure 163: Post-fit (BOnly) plots in the SR (left) and CR (right) for 1200 GeV mass hypothesis of H^+ signal.

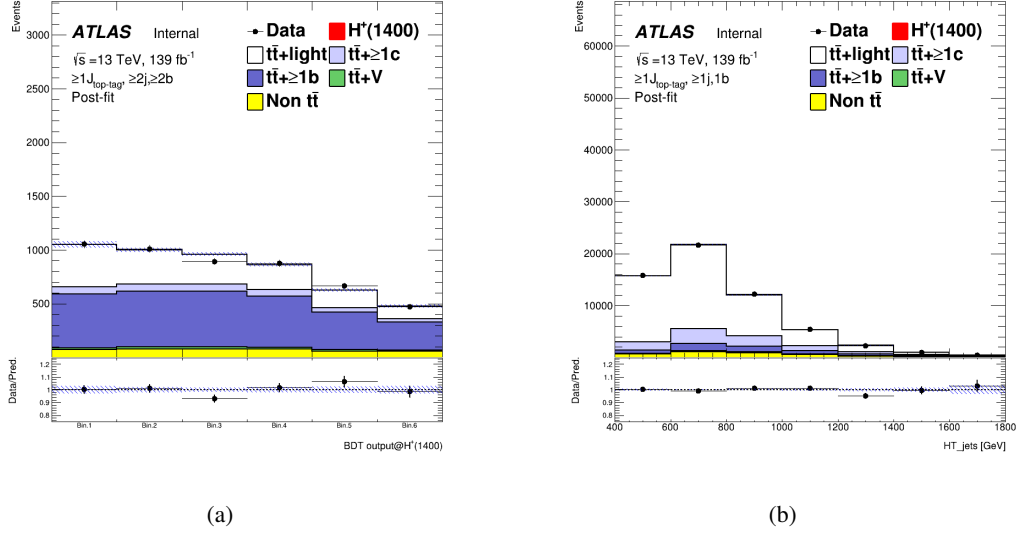


Figure 164: Post-fit (BOnly) plots in the SR (left) and CR (right) for 1400 GeV mass hypothesis of H^+ signal.

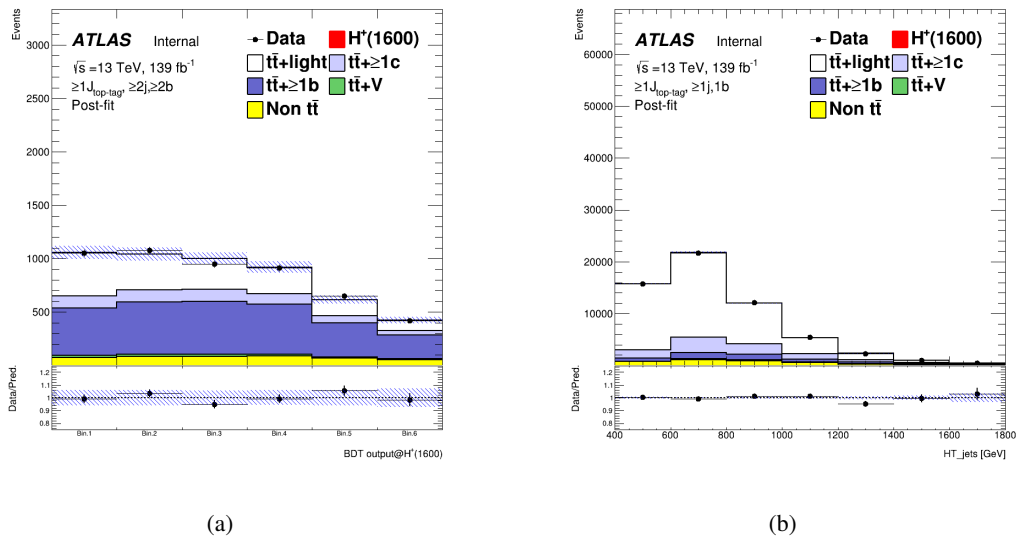


Figure 165: Post-fit (BOnly) plots in the SR (left) and CR (right) for 1600 GeV mass hypothesis of H^+ signal.

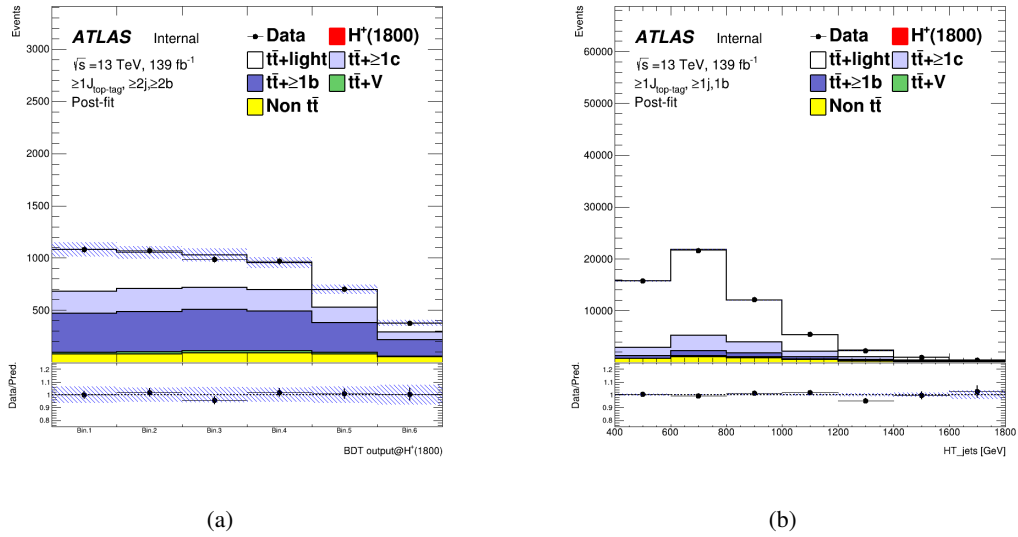


Figure 166: Post-fit (BOnly) plots in the SR (left) and CR (right) for 1800 GeV mass hypothesis of H^+ signal.

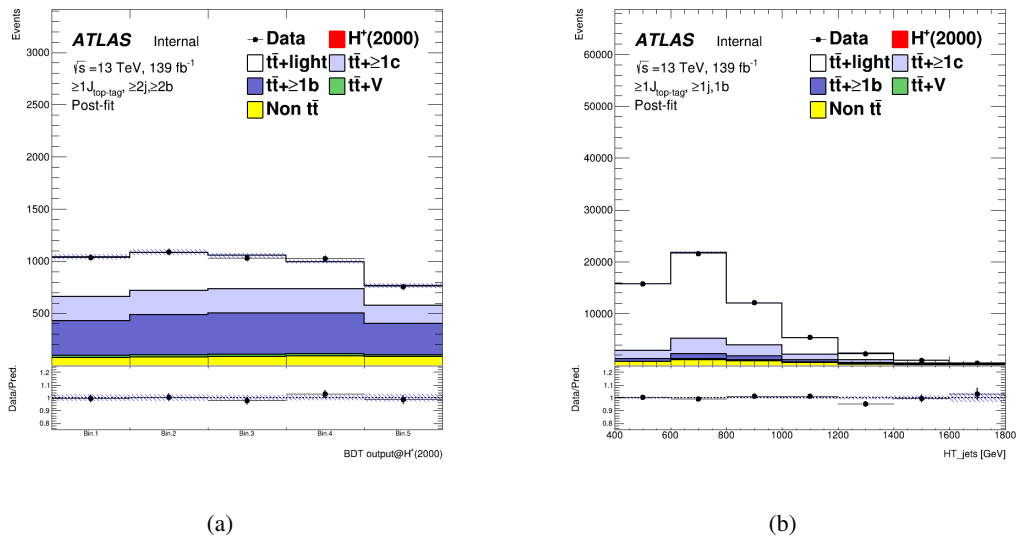


Figure 167: Post-fit (BOnly) plots in the SR (left) and CR (right) for 2000 GeV mass hypothesis of H^+ signal.

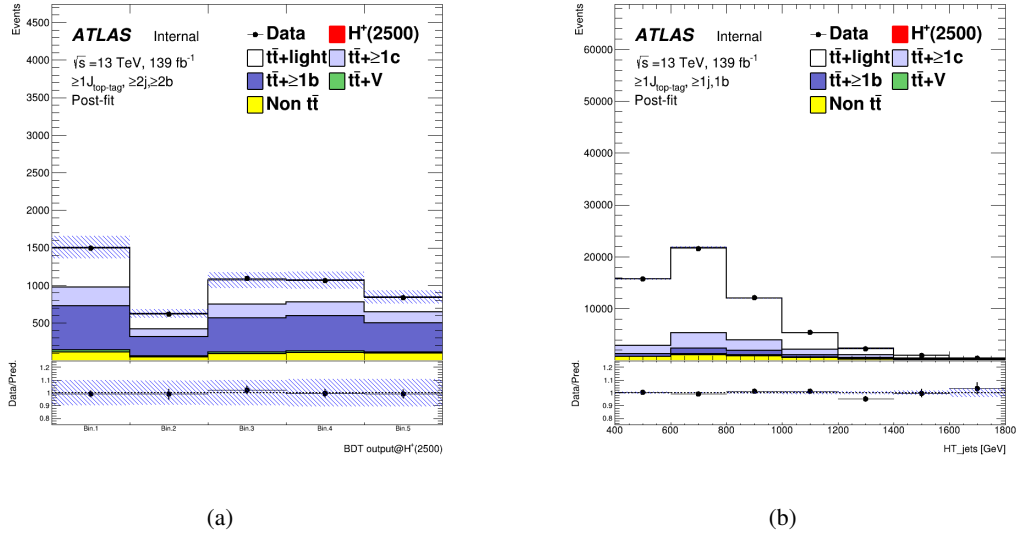


Figure 168: Post-fit (BOnly) plots in the SR (left) and CR (right) for 2500 GeV mass hypothesis of H^+ signal.

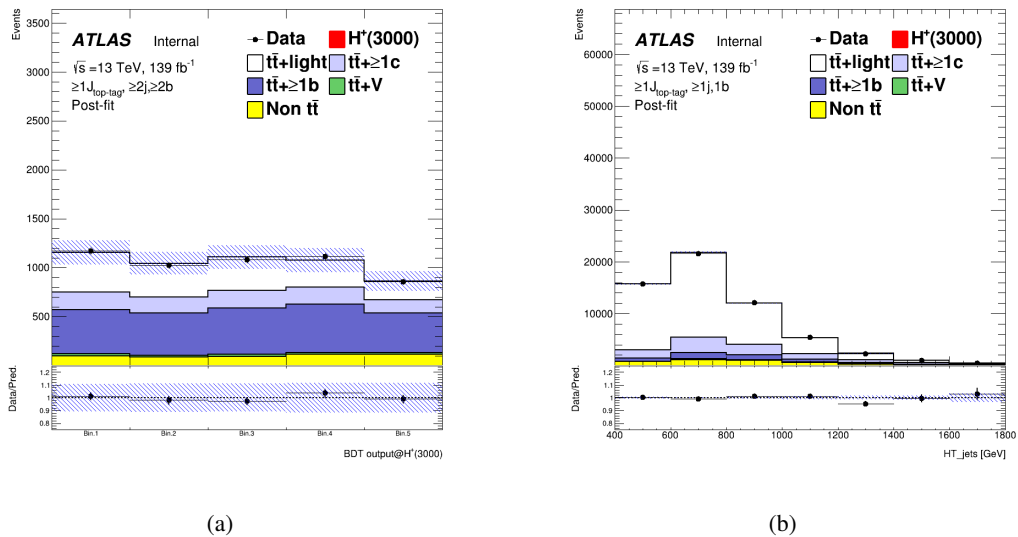


Figure 169: Post-fit (BOnly) plots in the SR (left) and CR (right) for 3000 GeV mass hypothesis of H^+ signal.

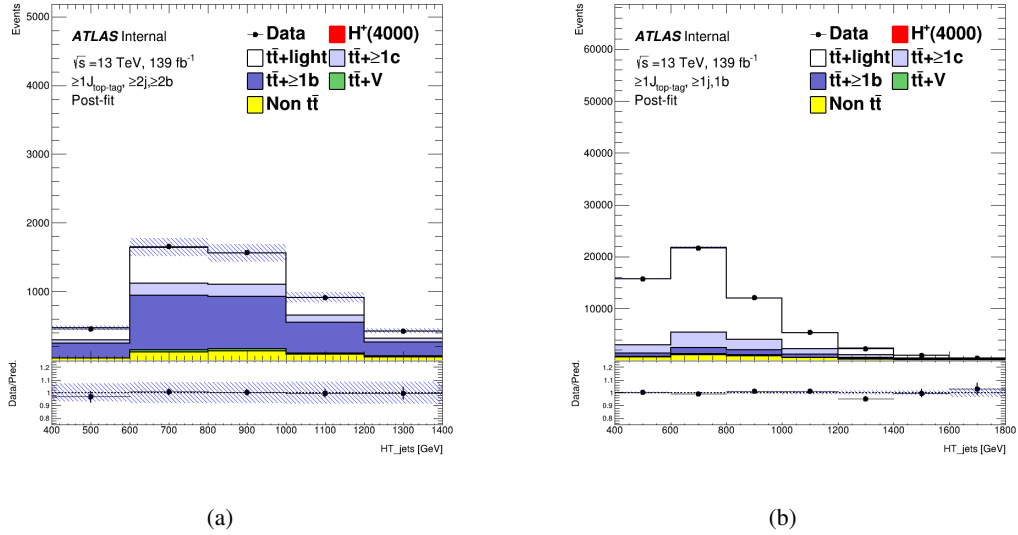


Figure 170: Post-fit (BOnly) plots in the SR (left) and CR (right) for 4000 GeV mass hypothesis of H^+ signal.

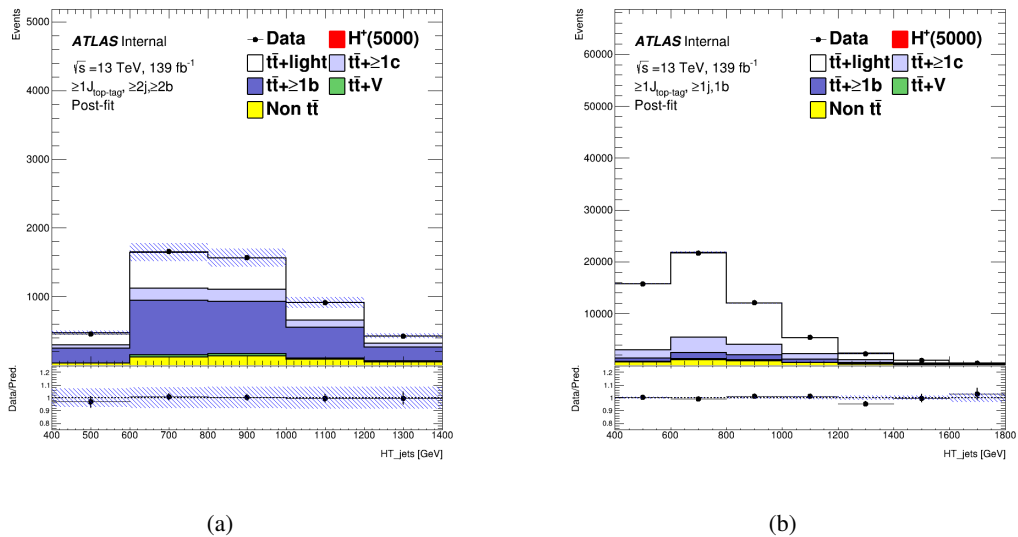


Figure 171: Post-fit (BOnly) plots in the SR (left) and CR (right) for 5000 GeV mass hypothesis of H^+ signal.

880 7.6 Upper cross-section limits as a function of signal mass

881 The 95% confidence level (CL) upper limit for each production of $H^+ \rightarrow tb$ and $W'_{\text{L/R}} \rightarrow tb$ in association
 882 with a top quark and a bottom quark using the CL_S method is shown in Figure 172 to 174. The expected
 883 upper limits for H^+ signals are set between 0.0958 to 0.0069 pb in the mass range of $1000 \leq M_{H^+} \leq 5000$
 884 GeV. The ones for W'_L (W'_R) are set between 0.1743 (0.1111) to 0.0080 (0.0061) pb in the mass range of
 885 $1000 \leq M_{W'} \leq 4000$ GeV.

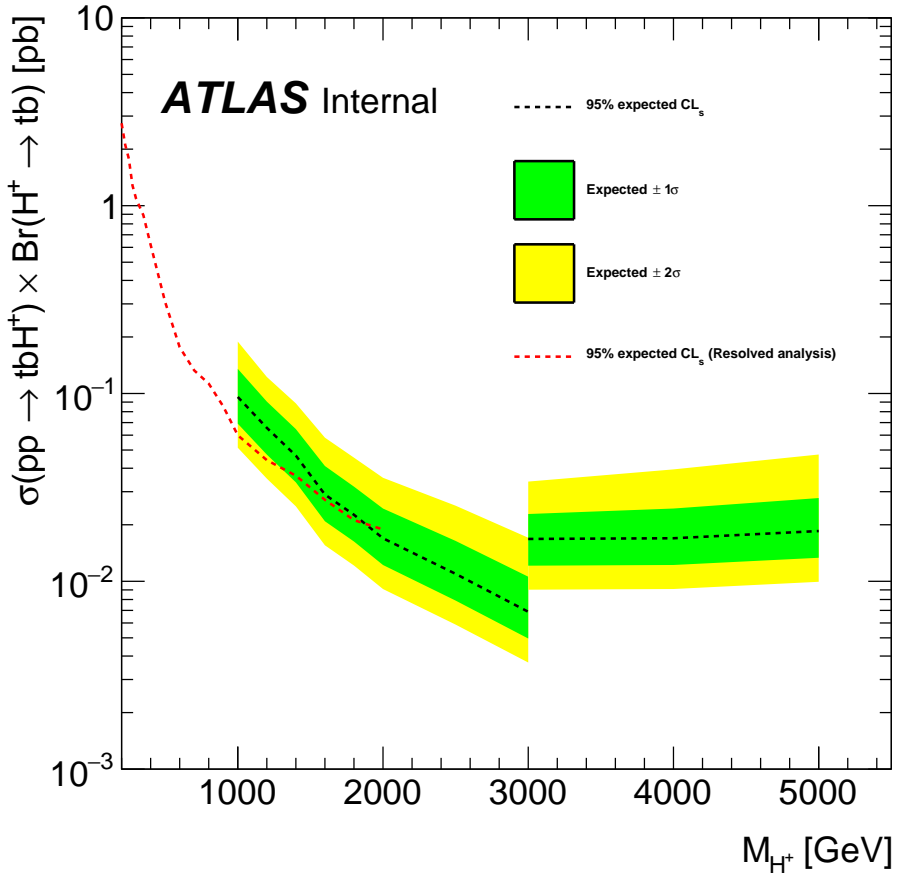


Figure 172: Expected limit for the production of $H^+ \rightarrow tb$ in association with a top quark and a bottom quark. The bands surrounding the expected limit show the 68% and 95% confidence intervals. The expected limit from ATLAS search using Run2 full data with the resolved channel is also shown[25].

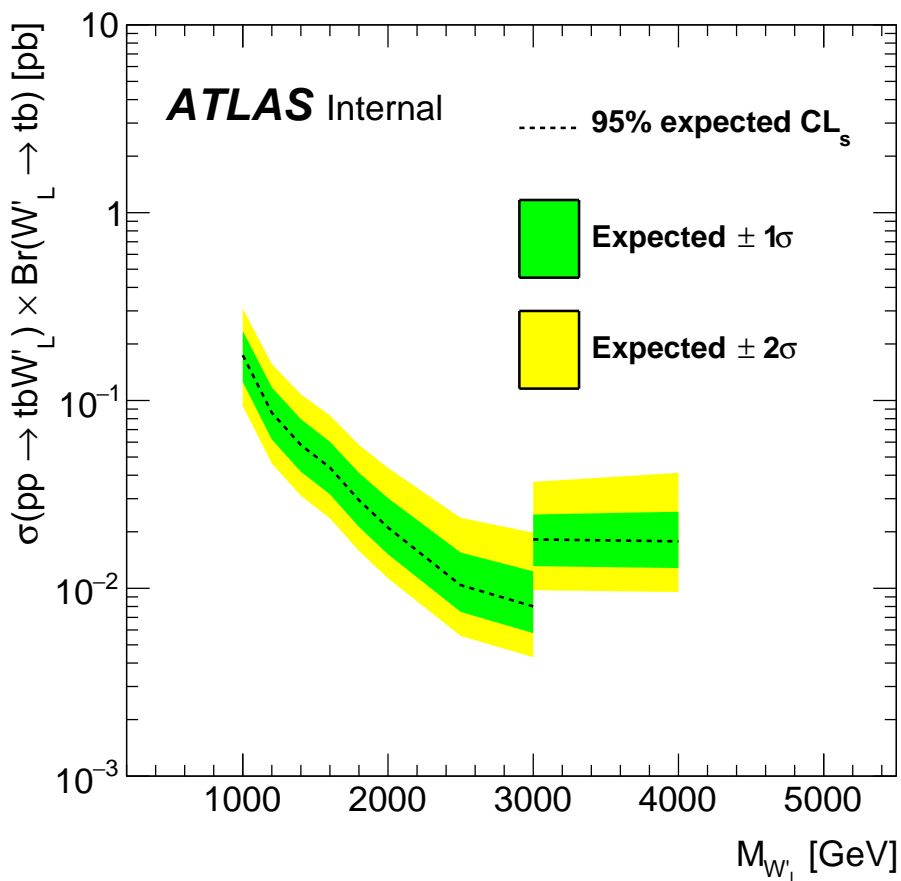


Figure 173: Expected limit for the production of $W'_L \rightarrow tb$ in association with a top quark and a bottom quark. The bands surrounding the expected limit show the 68% and 95% confidence intervals.

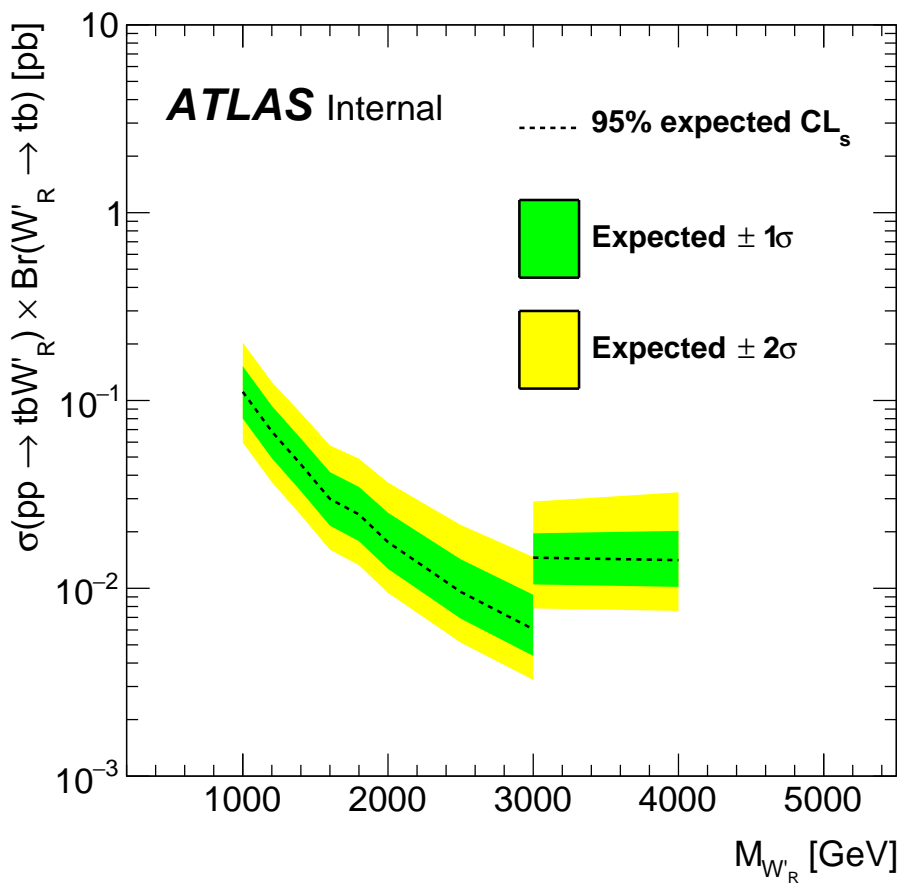


Figure 174: Expected limit for the production of $W'_R \rightarrow tb$ in association with a top quark and a bottom quark. The bands surrounding the expected limit show the 68% and 95% confidence intervals.

886 8 Summary and Conclusions

887 We have performed a search for charged Higgs boson H^+ as well as W' bosons produced in association with
888 a top quark and a bottom quark, and decaying into a top quark and a bottom quark, in the lepton-plus-jets
889 final state, in the regime where the top quark from the parent boson is highly boosted to be reconstructed as
890 a top-tagged large- R jet. The H^+ signals are investigated in the mass ranges of $1000 \leq m_{H^+} \leq 5000$ GeV,
891 while The W' signals are done in the mass range of $1000 \leq m_{W'_{LR}} \leq 4000$ GeV. The expected upper limits
892 for H^+ signals are set between 0.0958 to 0.0069 pb. The ones for W'_L (W'_R) are set between 0.1743 (0.1111)
893 to 0.0080 (0.0060) pb.

894 References

- 895 [1] G. Aad et al., *Measurements of differential cross-sections in top-quark pair events with a high*
 896 *transverse momentum top quark and limits on beyond the Standard Model contributions to top-quark*
 897 *pair production with the ATLAS detector at $\sqrt{s} = 13$ TeV*, Journal of High Energy Physics **2022**
 898 (2022) 1.
- 899 [2] ATLAS Collaboration, *Observation of a new particle in the search for the Standard Model Higgs*
 900 *boson with the ATLAS detector at the LHC*, Phys. Lett. B **716** (2012) 1, arXiv: [1207.7214](#) [hep-ex].
- 902 [3] CMS Collaboration, *Observation of a new boson at a mass of 125 GeV with the CMS experiment*
 903 *at the LHC*, Phys. Lett. B **716** (2012) 30, arXiv: [1207.7235](#) [hep-ex].
- 904 [4] ATLAS and CMS Collaborations, *Combined Measurement of the Higgs Boson Mass in pp*
 905 *Collisions at $\sqrt{s} = 7$ and 8 TeV with the ATLAS and CMS Experiments*, Phys. Rev. Lett. **114**
 906 (2015) 191803, arXiv: [1503.07589](#) [hep-ex].
- 907 [5] T. D. Lee, *A Theory of Spontaneous T Violation*, Phys. Rev. **D 8** (1973).
- 908 [6] G. Branco, P. Ferreira, L. Lavoura, M. Rebelo and M. Sher et al., *Theory and phenomenology of*
 909 *two-Higgs-doublet models*, Phys. Rept. **516** (2012), arXiv: [1106.0034](#) [hep-ph].
- 910 [7] K. Inoue, A. Kakuto, H. Komatsu and S. Takeshita, *Aspects of Grand Unified Models with Softly*
 911 *Broken Supersymmetry*, Prog.Theor.Phys. **68** (1982).
- 912 [8] T. Cheng and L.-F. Li, *Neutrino Masses, Mixings and Oscillations in $SU(2) \times U(1)$ Models of*
 913 *Electroweak Interactions*, Phys. Rev. **D 22** (1980).
- 914 [9] J. Schechter and J. Valle, *Neutrino Masses in $SU(2) \times U(1)$ Theories*, Phys. Rev. **D 22** (1980).
- 915 [10] G. Lazarides, Q. Shafi and C. Wetterich, *Proton Lifetime and Fermion Masses in an $SO(10)$ Model*,
 916 Nucl. Phys. B **181** (1981).
- 917 [11] R. Mohapatra and G. Senjanovic, *Neutrino Masses and Mixings in Gauge Models with Spontaneous*
 918 *Parity Violation*, Phys. Rev. **D 23** (1981).
- 919 [12] M. Magg and C. Wetterich, *Neutrino Mass Problem and Gauge Hierarchy*, Phys. Lett. **B 94** (1980).
- 920 [13] ATLAS Collaboration, *Search for charged Higgs bosons decaying via $H^\pm \rightarrow \tau\nu$ in $t\bar{t}$ events using*
 921 *pp collision data at $\sqrt{s} = 7$ TeV with the ATLAS detector*, JHEP **06** (2012) 039, arXiv: [1204.2760](#)
 922 [hep-ex].
- 923 [14] ATLAS Collaboration, *Search for charged Higgs bosons through the violation of lepton universality*
 924 *in $t\bar{t}$ events using pp collision data at $\sqrt{s} = 7$ TeV with the ATLAS experiment*, JHEP **03** (2013) 076,
 925 arXiv: [1212.3572](#) [hep-ex].
- 926 [15] ATLAS Collaboration, *Search for charged Higgs bosons decaying via $H^\pm \rightarrow \tau^\pm\nu$ in fully hadronic*
 927 *final states using pp collision data at $\sqrt{s} = 8$ TeV with the ATLAS detector*, JHEP **03** (2015) 088,
 928 arXiv: [1412.6663](#) [hep-ex].
- 929 [16] CMS Collaboration, *Search for a light charged Higgs boson in top quark decays in pp collisions at*
 930 *$\sqrt{s} = 7$ TeV*, JHEP **07** (2012) 143, arXiv: [1205.5736](#) [hep-ex].
- 931 [17] CMS Collaboration, *Search for a charged Higgs boson in pp collisions at $\sqrt{s} = 8$ TeV*, JHEP **11**
 932 (2015) 018, arXiv: [1508.07774](#) [hep-ex].

- [18] ATLAS Collaboration, *Search for charged Higgs bosons decaying via $H^\pm \rightarrow \tau^\pm \nu_\tau$ in the $\tau+jets$ and $\tau+lepton$ final states with 36fb^{-1} of pp collision data recorded at $\sqrt{s} = 13\text{ TeV}$ with the ATLAS experiment*, *JHEP* **09** (2018) 139, arXiv: [1807.07915 \[hep-ex\]](#).
- [19] ATLAS Collaboration, *Search for a light charged Higgs boson in the decay channel $H^+ \rightarrow c\bar{s}$ in $t\bar{t}$ events using pp collisions at $\sqrt{s} = 7\text{ TeV}$ with the ATLAS detector*, *Eur. Phys. J. C* **73** (2013) 2465, arXiv: [1302.3694 \[hep-ex\]](#).
- [20] CMS Collaboration, *Search for a light charged Higgs boson decaying to $c\bar{s}$ in pp collisions at $\sqrt{s} = 8\text{ TeV}$* , *JHEP* **12** (2015) 178, arXiv: [1510.04252 \[hep-ex\]](#).
- [21] CMS Collaboration, *Search for a charged Higgs boson decaying to charm and bottom quarks in proton–proton collisions at $\sqrt{s} = 8\text{ TeV}$* , *JHEP* **11** (2018) 115, arXiv: [1808.06575 \[hep-ex\]](#).
- [22] ATLAS Collaboration, *Search for charged Higgs bosons in the $H^\pm \rightarrow tb$ decay channel in pp collisions at $\sqrt{s} = 8\text{ TeV}$ using the ATLAS detector*, *JHEP* **03** (2016) 127, arXiv: [1512.03704 \[hep-ex\]](#).
- [23] ATLAS Collaboration, *Search for charged Higgs bosons produced in association with a top quark and decaying via $H^\pm \rightarrow \tau\nu$ using pp collision data recorded at $\sqrt{s} = 13\text{ TeV}$ by the ATLAS detector*, *Phys. Lett. B* **759** (2016) 555, arXiv: [1603.09203 \[hep-ex\]](#).
- [24] ATLAS Collaboration, *Search for charged Higgs bosons decaying into top and bottom quarks at $\sqrt{s} = 13\text{ TeV}$ with the ATLAS detector*, *JHEP* **11** (2018) 085, arXiv: [1808.03599 \[hep-ex\]](#) (cit. on pp. 6, 54).
- [25] ATLAS Collaboration, *Search for a charged Higgs bosons decaying into a top-quark and a bottom-quark at $\sqrt{s} = 13\text{ TeV}$ with the ATLAS detector*, *JHEP* **16** (2021) 145, arXiv: [2102.10076 \[hep-ex\]](#) (cit. on pp. 6, 7, 21, 37, 54, 170).
- [26] CMS Collaboration, *Search for a charged Higgs boson decaying into top and bottom quarks in events with electrons or muons in proton–proton collisions at $\sqrt{s} = 13\text{ TeV}$* , *JHEP* **01** (2020) 096, arXiv: [1908.09206 \[hep-ex\]](#).
- [27] CMS Collaboration, *Search for charged Higgs bosons decaying into a top and a bottom quark in the all-jet final state of pp collisions at $\sqrt{s} = 13\text{ TeV}$* , (2020), arXiv: [2001.07763 \[hep-ex\]](#).
- [28] ATLAS Collaboration, *Search for dijet resonances in events with an isolated charged lepton using $\sqrt{s} = 13\text{ TeV}$ proton–proton collision data collected by the ATLAS detector*, *JHEP* **06** (2020) 151, arXiv: [2002.11325 \[hep-ex\]](#).
- [29] ATLAS Collaboration, *Search for a Charged Higgs Boson Produced in the Vector-Boson Fusion Mode with Decay $H^\pm \rightarrow W^\pm Z$ using pp Collisions at $\sqrt{s} = 8\text{ TeV}$ with the ATLAS Experiment*, *Phys. Rev. Lett.* **114** (2015) 231801, arXiv: [1503.04233 \[hep-ex\]](#).
- [30] CMS Collaboration, *Search for charged Higgs bosons produced via vector boson fusion and decaying into a pair of W and Z bosons using pp collisions at $\sqrt{s} = 13\text{ TeV}$* , *Phys. Rev. Lett.* **119** (2017) 141802, arXiv: [1705.02942 \[hep-ex\]](#).
- [31] K. R. Dienes, E. Dudas and T. Gherghetta, *Grand unification at intermediate mass scales through extra dimensions*, *Nuclear Physics B* **537** (1999) 47.
- [32] S. Weinberg, *Implications of dynamical symmetry breaking: an addendum*, *Physical Review D* **19** (1979) 1277.
- [33] L. Susskind, *Dynamics of spontaneous symmetry breaking in the Weinberg-Salam theory*, *Physical Review D* **20** (1979) 2619.

- 975 [34] S. Dimopoulos and L. Susskind, *Mass without scalars*, Nuclear Physics B **155** (1979) 237.
- 976 [35] E. Eichten and K. Lane, *Dynamical breaking of weak interaction symmetries*, Physics Letters B **90**
977 (1980) 125.
- 978 [36] D. J. Muller and S. Nandi, *Topflavor: a separate SU(2) for the third family*, Physics Letters B **383**
979 (1996) 345.
- 980 [37] G. Burdman, B. A. Dobrescu and E. Ponton, *Resonances from two universal extra dimensions*,
981 Physical Review D **74** (2006) 075008.
- 982 [38] E. Malkawi, T. Tait and C.-P. Yuan, *A model of strong flavor dynamics for the top quark*, Physics
983 Letters B **385** (1996) 304.
- 984 [39] J. C. Pati and A. Salam, *Lepton number as the fourth "color"*, Physical Review D **10** (1974) 275.
- 985 [40] C. T. Hill, *Topcolor assisted technicolor*, Physics Letters B **345** (1995) 483.
- 986 [41] V. M. Abazov et al., *Search for $W \rightarrow tb$ resonances with left-and right-handed couplings to
987 fermions*, Physics Letters B **699** (2011) 145.
- 988 [42] T. Aaltonen et al., *Search for the Production of Narrow $t\bar{b}$ Resonances in 1.9 fb-1 of $p\bar{p}$ Collisions
989 at $s = 1.96$ TeV*, Physical review letters **103** (2009) 041801.
- 990 [43] CMS Collaboration, *Search for a W' boson decaying to a bottom quark and a top quark in pp
991 collisions at $\sqrt{s} = 7$ TeV*, Phys. Lett. B **718** (2013) 1229, arXiv: [1208.0956 \[hep-ex\]](https://arxiv.org/abs/1208.0956).
- 992 [44] CMS Collaboration, *Search for $W' \rightarrow tb$ decays in the lepton+jets final state in pp collisions at
993 $\sqrt{s} = 8$ TeV*, JHEP **05** (2014) 108, arXiv: [1402.2176 \[hep-ex\]](https://arxiv.org/abs/1402.2176).
- 994 [45] CMS Collaboration, *Search for heavy resonances decaying to a top quark and a bottom quark in
995 the lepton+jets final state in proton–proton collisions at 13 TeV*, Phys. Lett. B **777** (2018) 39, arXiv:
996 [1708.08539 \[hep-ex\]](https://arxiv.org/abs/1708.08539).
- 997 [46] CMS Collaboration, *Search for W' bosons decaying to a top and a bottom quark at $\sqrt{s} = 13$ TeV in
998 the hadronic final state*, Phys. Lett. B **820** (2021) 136535, arXiv: [2104.04831 \[hep-ex\]](https://arxiv.org/abs/2104.04831).
- 999 [47] ATLAS Collaboration, *Search for $W' \rightarrow t\bar{b}$ in the lepton plus jets final state in proton–proton
1000 collisions at a centre-of-mass energy of $\sqrt{s} = 8$ TeV with the ATLAS detector*, Phys. Lett. B **743**
1001 (2015) 235, arXiv: [1410.4103 \[hep-ex\]](https://arxiv.org/abs/1410.4103).
- 1002 [48] ATLAS Collaboration, *Search for $W' \rightarrow tb \rightarrow qqbb$ decays in pp collisions at $\sqrt{s} = 8$ TeV with
1003 the ATLAS detector*, Eur. Phys. J. C **75** (2015) 165, arXiv: [1408.0886 \[hep-ex\]](https://arxiv.org/abs/1408.0886).
- 1004 [49] ATLAS Collaboration, *Search for $W' \rightarrow tb$ decays in the hadronic final state using pp collisions
1005 at $\sqrt{s} = 13$ TeV with the ATLAS detector*, Phys. Lett. B **781** (2018) 327, arXiv: [1801.07893
1006 \[hep-ex\]](https://arxiv.org/abs/1801.07893).
- 1007 [50] ATLAS Collaboration, *Search for vector-boson resonances decaying to a top quark and bottom
1008 quark in the lepton plus jets final state in pp collisions at $\sqrt{s} = 13$ TeV with the ATLAS detector*,
1009 Phys. Lett. B **788** (2019) 347, arXiv: [1807.10473 \[hep-ex\]](https://arxiv.org/abs/1807.10473).
- 1010 [51] ATLAS Collaboration, *Luminosity determination in pp collisions at $\sqrt{s} = 13$ TeV using the ATLAS
1011 detector at the LHC*, ATLAS-CONF-2019-021, 2019, URL: <https://cds.cern.ch/record/2677054> (cit. on pp. 8, 50).
- 1013 [52] *LuminosityForPhysics twiki page*, URL: <https://twiki.cern.ch/twiki/bin/viewauth/Atlas/LuminosityForPhysics>.

- 1015 [53] *Web directory for GoodRunsLists in atlas-groupdata area*, URL: <https://atlas-groupdata.web.cern.ch/atlas-groupdata/GoodRunsLists>.
- 1016
- 1017 [54] C. Degrande, M. Ubiali, M. Wiesemann and M. Zaro, *Heavy charged Higgs boson production at the LHC*, **JHEP** **10** (2015) 145, arXiv: [1507.02549 \[hep-ph\]](https://arxiv.org/abs/1507.02549).
- 1018
- 1019 [55] J. Alwall et al., *The automated computation of tree-level and next-to-leading order differential cross sections, and their matching to parton shower simulations*, **JHEP** **07** (2014) 079, arXiv: [1405.0301 \[hep-ph\]](https://arxiv.org/abs/1405.0301) (cit. on pp. 9, 57).
- 1020
- 1021
- 1022 [56] R. D. Ball et al., *Parton distributions with LHC data*, **Nucl. Phys. B** **867** (2013) 244, arXiv: [1207.1303 \[hep-ph\]](https://arxiv.org/abs/1207.1303).
- 1023
- 1024 [57] R. D. Ball et al., *Parton distributions for the LHC run II*, **JHEP** **04** (2015) 040, arXiv: [1410.8849 \[hep-ph\]](https://arxiv.org/abs/1410.8849).
- 1025
- 1026 [58] T. Sjöstrand, S. Mrenna and P. Skands, *A brief introduction to PYTHIA 8.1*, **Comput. Phys. Commun.** **178** (2008) 852, arXiv: [0710.3820 \[hep-ph\]](https://arxiv.org/abs/0710.3820).
- 1027
- 1028 [59] ATLAS Collaboration, *ATLAS Pythia 8 tunes to 7 TeV data*, ATL-PHYS-PUB-2014-021, 2014, URL: <https://cds.cern.ch/record/1966419> (cit. on pp. 9, 56).
- 1029
- 1030 [60] M. Flechl, M. Klees, M. Krämer, M. Spira and M. Ubiali, *Improved cross-section predictions for heavy charged Higgs boson production at the LHC*, **Physical Review D** **91** (2015), URL: <http://dx.doi.org/10.1103/PhysRevD.91.075015>, ISSN:1550-2368.
- 1031
- 1032
- 1033 [61] S. Dittmaier, M. Krämer, M. Spira and M. Walser, *Charged-Higgs-boson production at the LHC:Next-to-leading-order supersymmetric QCD corrections*, **Physical Review D** **83** (2011), URL: <http://dx.doi.org/10.1103/PhysRevD.83.055005>, ISSN:1550-2368.
- 1034
- 1035
- 1036 [62] E. Berger, T. Han, J. Jiang and T. Plehn, *Associated production of a top quark and a charged Higgs boson*, **Physical Review D** **71** (2005), URL: <http://dx.doi.org/10.1103/PhysRevD.71.115012>, ISSN:1550-2368.
- 1037
- 1038
- 1039 [63] P. Nason, *A new method for combining NLO QCD with shower Monte Carlo algorithms*, **JHEP** **11** (2004) 040, arXiv: [hep-ph/0409146](https://arxiv.org/abs/hep-ph/0409146).
- 1040
- 1041 [64] S. Frixione, P. Nason and C. Oleari, *Matching NLO QCD computations with parton shower simulations: the POWHEG method*, **JHEP** **11** (2007) 070, arXiv: [0709.2092 \[hep-ph\]](https://arxiv.org/abs/0709.2092).
- 1042
- 1043 [65] S. Alioli, P. Nason, C. Oleari and E. Re, *A general framework for implementing NLO calculations in shower Monte Carlo programs: the POWHEG BOX*, **JHEP** **06** (2010) 043, arXiv: [1002.2581 \[hep-ph\]](https://arxiv.org/abs/1002.2581).
- 1044
- 1045
- 1046 [66] J. Campbell, R. Ellis, P. Nason and E. Re, *Top-pair production and decay at NLO matched with parton showers*, **JHEP** **04** (2015), arXiv: [1412.1828 \[hep-ph\]](https://arxiv.org/abs/1412.1828).
- 1047
- 1048 [67] ATLAS Collaboration, *Studies on top-quark Monte Carlo modelling for Top2016*, ATL-PHYS-PUB-2016-020, 2016, URL: <https://cds.cern.ch/record/2216168>.
- 1049
- 1050 [68] T. Sjöstrand et al., *An introduction to PYTHIA 8.2*, **Comput. Phys. Commun.** **191** (2015) 159, arXiv: [1410.3012 \[hep-ph\]](https://arxiv.org/abs/1410.3012).
- 1051
- 1052 [69] M. Bahr et al., *Herwig++ physics and manual*, **Eur. Phys. J. C** **58** (2008) 639, arXiv: [0803.0883 \[hep-ph\]](https://arxiv.org/abs/0803.0883).
- 1053
- 1054 [70] J. Bellm et al., *Herwig 7.0/Herwig++ 3.0 release note*, **Eur. Phys. J. C** **76** (2016) 196, arXiv: [1512.01178 \[hep-ph\]](https://arxiv.org/abs/1512.01178).
- 1055

- [71] ATLAS Collaboration, *Studies on top-quark Monte Carlo modelling with Sherpa and MG5_aMC@NLO*, ATL-PHYS-PUB-2017-007, 2017, URL: <https://cds.cern.ch/record/2261938>.
- [72] H. B. Hartanto, B. Jäger, L. Reina and D. Wackerlo, *Higgs boson production in association with top quarks in the POWHEG BOX*, Phys. Rev. D **91** (2015) 094003, arXiv: [1501.04498 \[hep-ph\]](https://arxiv.org/abs/1501.04498).
- [73] E. Bothmann et al., *Event Generation with Sherpa 2.2*, SciPost Phys. **7** (2019) 034, arXiv: [1905.09127 \[hep-ph\]](https://arxiv.org/abs/1905.09127).
- [74] S. Catani, F. Krauss, R. Kuhn and B. R. Webber, *QCD Matrix Elements + Parton Showers*, JHEP **11** (2001) 063, arXiv: [hep-ph/0109231](https://arxiv.org/abs/hep-ph/0109231).
- [75] S. Höche, F. Krauss, S. Schumann and F. Siegert, *QCD matrix elements and truncated showers*, JHEP **05** (2009) 053, arXiv: [0903.1219 \[hep-ph\]](https://arxiv.org/abs/0903.1219).
- [76] R. Frederix, E. Re and P. Torrielli, *Single-top t-channel hadroproduction in the four-flavour scheme with POWHEG and aMC@NLO*, JHEP **09** (2012) 130, arXiv: [1207.5391 \[hep-ph\]](https://arxiv.org/abs/1207.5391).
- [77] S. Frixione, E. Laenen, P. Motylinski and B. R. Webber, *Angular correlations of lepton pairs from vector boson and top quark decays in Monte Carlo simulations*, JHEP **04** (2007) 081, arXiv: [hep-ph/0702198](https://arxiv.org/abs/hep-ph/0702198).
- [78] P. Artoisenet, R. Frederix, O. Mattelaer and R. Rietkerk, *Automatic spin-entangled decays of heavy resonances in Monte Carlo simulations*, JHEP **03** (2013) 015, arXiv: [1212.3460 \[hep-ph\]](https://arxiv.org/abs/1212.3460).
- [79] S. Frixione, E. Laenen, P. Motylinski, C. D. White and B. R. Webber, *Single-top hadroproduction in association with a W boson*, JHEP **07** (2008) 029, arXiv: [0805.3067 \[hep-ph\]](https://arxiv.org/abs/0805.3067) (cit. on pp. 13, 14, 56).
- [80] ATLAS Collaboration, *Measurement of the production cross-section of a single top quark in association with a Z boson in proton–proton collisions at 13 TeV with the ATLAS detector*, Phys. Lett. B **780** (2018) 557, arXiv: [1710.03659 \[hep-ex\]](https://arxiv.org/abs/1710.03659).
- [81] J. Pumplin et al., *New Generation of Parton Distributions with Uncertainties from Global QCD Analysis*, JHEP **07** (2002) 012, arXiv: [hep-ph/0201195](https://arxiv.org/abs/hep-ph/0201195).
- [82] R. Frederix, D. Pagani and M. Zaro, *Large NLO corrections in $t\bar{t}W^\pm$ and $t\bar{t}\bar{t}$ hadroproduction from supposedly subleading EW contributions*, JHEP **02** (2018) 031, arXiv: [1711.02116 \[hep-ph\]](https://arxiv.org/abs/1711.02116).
- [83] T. Gleisberg and S. Höche, *Comix, a new matrix element generator*, JHEP **12** (2008) 039, arXiv: [0808.3674 \[hep-ph\]](https://arxiv.org/abs/0808.3674).
- [84] F. Caccioli, P. Maierhöfer and S. Pozzorini, *Scattering Amplitudes with Open Loops*, Phys. Rev. Lett. **108** (2012) 111601, arXiv: [1111.5206 \[hep-ph\]](https://arxiv.org/abs/1111.5206).
- [85] A. Denner, S. Dittmaier and L. Hofer, *Collier: A fortran-based complex one-loop library in extended regularizations*, Comput. Phys. Commun. **212** (2017) 220, arXiv: [1604.06792 \[hep-ph\]](https://arxiv.org/abs/1604.06792).
- [86] S. Schumann and F. Krauss, *A parton shower algorithm based on Catani–Seymour dipole factorisation*, JHEP **03** (2008) 038, arXiv: [0709.1027 \[hep-ph\]](https://arxiv.org/abs/0709.1027).
- [87] J.-C. Winter, F. Krauss and G. Soff, *A modified cluster-hadronization model*, Eur. Phys. J. C **36** (2004) 381, arXiv: [hep-ph/0311085](https://arxiv.org/abs/hep-ph/0311085).
- [88] S. Höche, F. Krauss, M. Schönherr and F. Siegert, *A critical appraisal of NLO+PS matching methods*, JHEP **09** (2012) 049, arXiv: [1111.1220 \[hep-ph\]](https://arxiv.org/abs/1111.1220).
- [89] S. Höche, F. Krauss, M. Schönherr and F. Siegert, *QCD matrix elements + parton showers. The NLO case*, JHEP **04** (2013) 027, arXiv: [1207.5030 \[hep-ph\]](https://arxiv.org/abs/1207.5030).

- [90] E. Bothmann, M. Schönher and S. Schumann, *Reweighting QCD matrix-element and parton-shower calculations*, *Eur. Phys. J. C* **76** (2016) 590, arXiv: [1606.08753 \[hep-ph\]](https://arxiv.org/abs/1606.08753).
- [91] ATLAS Collaboration, *Electron reconstruction and identification efficiency measurements with the ATLAS detector using the 2011 LHC proton–proton collision data*, *Eur. Phys. J. C* **74** (2014) 2941, arXiv: [1404.2240 \[hep-ex\]](https://arxiv.org/abs/1404.2240) (cit. on p. 16).
- [92] ATLAS Collaboration, *Electron efficiency measurements with the ATLAS detector using the 2015 LHC proton–proton collision data*, ATLAS-CONF-2016-024, 2016, URL: <https://cds.cern.ch/record/2157687> (cit. on p. 16).
- [93] *Lepton isolation recommendations*, URL: <https://twiki.cern.ch/twiki/bin/viewauth/AtlasProtected/IsolationSelectionTool> (cit. on p. 16).
- [94] ATLAS Collaboration, *Muon reconstruction performance of the ATLAS detector in proton–proton collision data at $\sqrt{s} = 13\text{ TeV}$* , *Eur. Phys. J. C* **76** (2016) 292, arXiv: [1603.05598 \[hep-ex\]](https://arxiv.org/abs/1603.05598) (cit. on pp. 16, 51).
- [95] ATLAS Collaboration, *Reconstruction, Energy Calibration, and Identification of Hadronically Decaying Tau Leptons in the ATLAS Experiment for Run-2 of the LHC*, ATL-PHYS-PUB-2015-045, 2015, URL: <https://cds.cern.ch/record/2064383> (cit. on p. 16).
- [96] M. Cacciari, G. P. Salam and G. Soyez, *The anti- k_t jet clustering algorithm*, *JHEP* **04** (2008) 063, arXiv: [0802.1189 \[hep-ph\]](https://arxiv.org/abs/0802.1189) (cit. on p. 16).
- [97] ATLAS Collaboration, *Jet reconstruction and performance using particle flow with the ATLAS Detector*, *Eur. Phys. J. C* **77** (2017) 466, arXiv: [1703.10485 \[hep-ex\]](https://arxiv.org/abs/1703.10485) (cit. on p. 16).
- [98] ATLAS Collaboration, *Jet energy scale and resolution measured in proton–proton collisions at $\sqrt{s} = 13\text{ TeV}$ with the ATLAS detector*, (2020), arXiv: [2007.02645 \[hep-ex\]](https://arxiv.org/abs/2007.02645) (cit. on p. 16).
- [99] ATLAS Collaboration, *Performance of pile-up mitigation techniques for jets in pp collisions at $\sqrt{s} = 8\text{ TeV}$ using the ATLAS detector*, *Eur. Phys. J. C* **76** (2016) 581, arXiv: [1510.03823 \[hep-ex\]](https://arxiv.org/abs/1510.03823) (cit. on pp. 17, 51).
- [100] ATLAS Collaboration, *ATLAS b-jet identification performance and efficiency measurement with $t\bar{t}$ events in pp collisions at $\sqrt{s} = 13\text{ TeV}$* , *Eur. Phys. J. C* **79** (2019) 970, arXiv: [1907.05120 \[hep-ex\]](https://arxiv.org/abs/1907.05120) (cit. on pp. 17, 53).
- [101] ATLAS Collaboration, *Topological cell clustering in the ATLAS calorimeters and its performance in LHC Run 1*, *Eur. Phys. J. C* **77** (2017) 490, arXiv: [1603.02934 \[hep-ex\]](https://arxiv.org/abs/1603.02934) (cit. on p. 17).
- [102] D. Krohn, J. Thaler and L.-T. Wang, *Jet trimming*, *Journal of High Energy Physics* **2010** (2010) 84, URL: [https://link.springer.com/article/10.1007/JHEP02\(2010\)084](https://link.springer.com/article/10.1007/JHEP02(2010)084), ISSN:1029-8479 (cit. on p. 17).
- [103] S. Catani, Y. Dokshitzer, M. Seymour and B. Webber, *Longitudinally invariant K(t) clustering algorithms for hadron-hadron collisions*, *Nuclear Physics B* **406** (1993) 187, URL: <https://www.sciencedirect.com/science/article/pii/055032139390166M>, ISSN:0550-3213 (cit. on p. 17).
- [104] ATLAS Collaboration, *Identification of boosted, hadronically decaying W bosons and comparisons with ATLAS data taken at $\sqrt{s} = 8\text{ TeV}$* , *Eur. Phys. J. C* **76** (2016) 154, arXiv: [1510.05821 \[hep-ex\]](https://arxiv.org/abs/1510.05821) (cit. on p. 17).
- [105] ATLAS Collaboration, *Jet mass reconstruction with the ATLAS Detector in early Run 2 data*, ATLAS-CONF-2016-035, 2016, URL: <https://cds.cern.ch/record/2200211> (cit. on p. 17).

- [106] JetEtMiss group, *Twiki: JetUncertaintiesRel21ConsolidatedLargeRScaleRes*, URL: <https://twiki.cern.ch/twiki/bin/view/AtlasProtected/JetUncertaintiesRel21ConsolidatedLargeRS>
- [107] ATLAS Collaboration, *Boosted hadronic vector boson and top quark tagging with ATLAS using Run 2 data*, ATL-PHYS-PUB-2020-017, 2020, URL: <https://cds.cern.ch/record/2724149> (cit. on pp. 17, 53).
- [108] J. Thaler and K. Van Tilburg, *Identifying Boosted Objects with N-subjettiness*, **JHEP** **03** (2011) 015, arXiv: [1011.2268 \[hep-ph\]](https://arxiv.org/abs/1011.2268) (cit. on p. 17).
- [109] J. Thaler and L.-T. Wang, *Strategies to Identify Boosted Tops*, **JHEP** **07** (2008) 092, arXiv: [0806.0023 \[hep-ph\]](https://arxiv.org/abs/0806.0023) (cit. on p. 17).
- [110] A. Larkoski, G. Salam and J. Thaler, *Energy Correlation Functions for Jet Substructure*, **JHEP** **06** (2013) 108, arXiv: [1305.0007 \[hep-ph\]](https://arxiv.org/abs/1305.0007) (cit. on p. 17).
- [111] D. Adams and et al., *Recommendations of the Physics Objects and Analysis Harmonisation Study Groups 2014*, ATL-PHYS-INT-2014-018, 2014, URL: <https://cds.cern.ch/record/1743654> (cit. on p. 18).
- [112] *Documentation of the ATLAS AssociationUtils package*, URL: <https://gitlab.cern.ch/atlas/athena/blob/release/21.2.86/PhysicsAnalysis/AnalysisCommon/AssociationUtils/README.rst> (cit. on p. 18).
- [113] J. Gallicchio and Y.-T. Chien, *Quit Using Pseudorapidity, Transverse Energy, and Massless Constituents*, 2018, arXiv: [1802.05356 \[hep-ph\]](https://arxiv.org/abs/1802.05356) (cit. on p. 18).
- [114] A. Hoecker et al., *TMVA - Toolkit for Multivariate Data Analysis*, 2007, arXiv: [physics/0703039 \[physics.data-an\]](https://arxiv.org/abs/physics/0703039) (cit. on p. 23).
- [115] *Automatic binning implematation in TTHFitter*. URL: https://indico.cern.ch/event/455289/contributions/1953694/attachments/1209081/1762963/Calvet_binning_Htop_160108.pdf (cit. on pp. 40, 58).
- [116] G. Avoni and et al., *The new LUCID-2 detector for luminosity measurement and monitoring in ATLAS*, **JINST** **13** (2018) P07017 (cit. on p. 50).
- [117] ATLAS Collaboration, *Measurement of the Inelastic Proton–Proton Cross Section at $\sqrt{s} = 13\text{ TeV}$ with the ATLAS Detector at the LHC*, **Phys. Rev. Lett.** **117** (2016) 182002, arXiv: [1606.02625 \[hep-ex\]](https://arxiv.org/abs/1606.02625) (cit. on p. 50).
- [118] ATLAS Collaboration, *Electron reconstruction and identification in the ATLAS experiment using the 2015 and 2016 LHC proton–proton collision data at $\sqrt{s} = 13\text{ TeV}$* , **Eur. Phys. J. C** **79** (2019) 639, arXiv: [1902.04655 \[hep-ex\]](https://arxiv.org/abs/1902.04655) (cit. on p. 51).
- [119] ATLAS Collaboration, *Electron and photon performance measurements with the ATLAS detector using the 2015–2017 LHC proton–proton collision data*, **JINST** **14** (2019) P12006, arXiv: [1908.00005 \[hep-ex\]](https://arxiv.org/abs/1908.00005) (cit. on p. 51).
- [120] ATLAS Collaboration, *Jet energy scale measurements and their systematic uncertainties in proton–proton collisions at $\sqrt{s} = 13\text{ TeV}$ with the ATLAS detector*, **Phys. Rev. D** **96** (2017) 072002, arXiv: [1703.09665 \[hep-ex\]](https://arxiv.org/abs/1703.09665) (cit. on p. 51).
- [121] ATLAS Collaboration, *Determination of jet calibration and energy resolution in proton–proton collisions at $\sqrt{s} = 8\text{ TeV}$ using the ATLAS detector*, (2019), arXiv: [1910.04482 \[hep-ex\]](https://arxiv.org/abs/1910.04482) (cit. on p. 51).

- [122] ATLAS Collaboration, *In situ calibration of large-radius jet energy and mass in 13 TeV proton–proton collisions with the ATLAS detector*, *Eur. Phys. J. C* **79** (2019) 135, arXiv: [1807.09477 \[hep-ex\]](#) (cit. on p. 52).
- [123] ATLAS Collaboration, *Measurement of the ATLAS Detector Jet Mass Response using Forward Folding with 80fb^{-1} of $\sqrt{s} = 13\text{ TeV}$ pp data*, ATLAS-CONF-2020-022, 2020, URL: <https://cds.cern.ch/record/2724442> (cit. on p. 52).
- [124] ATLAS Collaboration, *Measurement of b-tagging efficiency of c-jets in $t\bar{t}$ events using a likelihood approach with the ATLAS detector*, ATLAS-CONF-2018-001, 2018, URL: <https://cds.cern.ch/record/2306649> (cit. on p. 53).
- [125] ATLAS Collaboration, *Calibration of light-flavour b-jet mistagging rates using ATLAS proton–proton collision data at $\sqrt{s} = 13\text{ TeV}$* , ATLAS-CONF-2018-006, 2018, URL: <https://cds.cern.ch/record/2314418> (cit. on p. 53).
- [126] ATLAS Collaboration, *Performance of top-quark and W-boson tagging with ATLAS in Run 2 of the LHC*, *Eur. Phys. J. C* **79** (2019) 375, arXiv: [1808.07858 \[hep-ex\]](#) (cit. on p. 53).
- [127] J. Butterworth et al., *PDF4LHC recommendations for LHC Run II*, *J. Phys. G* **43** (2016) 023001, arXiv: [1510.03865 \[hep-ph\]](#) (cit. on p. 53).
- [128] D. de Florian et al., *Handbook of LHC Higgs Cross Sections: 4. Deciphering the Nature of the Higgs Sector*, (2016), arXiv: [1610.07922 \[hep-ph\]](#) (cit. on p. 56).
- [129] R. Raitio and W. W. Wada, *Higgs Boson Production at Large Transverse Momentum in QCD*, *Phys. Rev. D* **19** (1979) (cit. on p. 56).
- [130] W. Beenakker and et al., *NLO QCD corrections to t anti-t H production in hadron collisions*, *Nucl. Phys. B* **653** (2003), arXiv: [hep-ph/0211352 \[hep-ph\]](#) (cit. on p. 56).
- [131] S. Dawson, C. Jackson, L. H. Orr, L. Reina and D. Wackerlo, *Associated Higgs production with top quarks at the large hadron collider: NLO QCD corrections*, *Phys. Rev. D* **68** (2003), arXiv: [hep-ph/0305087 \[hep-ph\]](#) (cit. on p. 56).
- [132] Y. Zhang, W.-G. Ma, R.-Y. Zhang, C. Chen and L. Guo, *QCD NLO and EW NLO corrections to $t\bar{t}H$ production with top quark decays at hadron collider*, *Phys. Lett. B* **738** (2014), arXiv: [1407.1110 \[hep-ph\]](#) (cit. on p. 56).
- [133] S. Frixione, V. Hirschi, D. Pagani, H.-S. Shao and M. Zaro, *Electroweak and QCD corrections to top-pair hadroproduction in association with heavy bosons*, *JHEP* **06** (2015), arXiv: [1504.03446 \[hep-ph\]](#) (cit. on p. 56).
- [134] LHCTopWG, *NLO single-top channel cross sections*, 2017, URL: <https://twiki.cern.ch/twiki/bin/view/LHCPhysics/SingleTopRefXsec> (cit. on p. 56).
- [135] A. D. Martin, W. J. Stirling, R. S. Thorne and G. Watt, *Parton distributions for the LHC*, *Eur. Phys. J. C* **63** (2009) 189, arXiv: [0901.0002 \[hep-ph\]](#) (cit. on p. 56).
- [136] A. D. Martin, W. Stirling, R. Thorne and G. Watt, *Uncertainties on α_S in global PDF analyses and implications for predicted hadronic cross sections*, *Eur. Phys. J. C* **64** (2009) 653, arXiv: [0905.3531 \[hep-ph\]](#) (cit. on p. 56).
- [137] M. Aliev et al., *HATHOR – HArdonic Top and Heavy quarks crOss section calculatoR*, *Comput. Phys. Commun.* **182** (2011) 1034, arXiv: [1007.1327 \[hep-ph\]](#) (cit. on p. 56).

- 1220 [138] P. Kant et al., *HatHor for single top-quark production: Updated predictions and uncertainty*
1221 *estimates for single top-quark production in hadronic collisions*, Comput. Phys. Commun. **191**
1222 (2015) 74, arXiv: [1406.4403 \[hep-ph\]](https://arxiv.org/abs/1406.4403) (cit. on p. 56).
- 1223 [139] LHCHXSWG1, *Recommended predictions for $t\bar{t}V$ cross sections*, URL: https://twiki.cern.ch/twiki/bin/view/LHCPhysics/LHCHXSWGTT#Plans_for_YR4 (cit. on p. 56).
- 1225 [140] J. M. Campbell and R. K. Ellis, *$t\bar{t}W^{+-}$ production and decay at NLO*, JHEP **07** (2012), arXiv:
1226 [1204.5678 \[hep-ph\]](https://arxiv.org/abs/1204.5678) (cit. on p. 56).
- 1227 [141] ATLAS PMG Top processes twiki page, URL: <https://twiki.cern.ch/twiki/bin/view/AtlasProtected/PmgTopProcesses> (cit. on p. 57).
- 1229 [142] ATLAS Collaboration, *Multi-boson simulation for 13 TeV ATLAS analyses*, ATL-PHYS-PUB-
1230 2016-002, 2016, URL: <https://cds.cern.ch/record/2119986> (cit. on p. 57).

1231 Appendices

1232 A TOPQ1 DAOD list

1233 A.1 Data

1234 Table 20 is the TOPQ1 DAOD list for data sample in this analysis.

data15_13TeV.AllYear.physics_Main.PhysCont.DAOD_TOPQ1.grp15_v01_p4513
data16_13TeV.AllYear.physics_Main.PhysCont.DAOD_TOPQ1.grp16_v01_p4513
data17_13TeV.AllYear.physics_Main.PhysCont.DAOD_TOPQ1.grp17_v01_p4513
data18_13TeV.AllYear.physics_Main.PhysCont.DAOD_TOPQ1.grp18_v01_p4513

Table 20: TOPQ1 DAOD list for data sample in this analysis.

1235 A.2 $\bar{t}bH^+$

1236 Table 21 is the TOPQ1 DAOD list for H^+ sample in this analysis.

Nominal
mc16_13TeV.450004.aMcAtNloPythia8EvtGen_A14NNPDF23LO_Hplus4FS_H1000_tb.deriv.DAOD_TOPQ1.e7137_s3126_r9364_p4514
mc16_13TeV.450598.aMcAtNloPythia8EvtGen_A14NNPDF23LO_Hplus4FS_H1200_tb.deriv.DAOD_TOPQ1.e7429_s3126_r9364_p4514
mc16_13TeV.450599.aMcAtNloPythia8EvtGen_A14NNPDF23LO_Hplus4FS_H1400_tb.deriv.DAOD_TOPQ1.e7429_s3126_r9364_p4514
mc16_13TeV.450600.aMcAtNloPythia8EvtGen_A14NNPDF23LO_Hplus4FS_H1600_tb.deriv.DAOD_TOPQ1.e7429_s3126_r9364_p4514
mc16_13TeV.450601.aMcAtNloPythia8EvtGen_A14NNPDF23LO_Hplus4FS_H1800_tb.deriv.DAOD_TOPQ1.e7429_s3126_r9364_p4514
mc16_13TeV.450602.aMcAtNloPythia8EvtGen_A14NNPDF23LO_Hplus4FS_H2000_tb.deriv.DAOD_TOPQ1.e7429_s3126_r9364_p4514
mc16_13TeV.451490.aMcAtNloPythia8EvtGen_A14NNPDF23LO_Hplus4FS_H2500_tb.deriv.DAOD_TOPQ1.e7970_s3126_r9364_p4514
mc16_13TeV.451491.aMcAtNloPythia8EvtGen_A14NNPDF23LO_Hplus4FS_H3000_tb.deriv.DAOD_TOPQ1.e7970_s3126_r9364_p4514
mc16_13TeV.508710.MGPy8EG_A14NNPDF30_Hplus4FS_H4000_tb.deriv.DAOD_TOPQ1.e8276_s3126_r9364_p4514
mc16_13TeV.508711.MGPy8EG_A14NNPDF30_Hplus4FS_H5000_tb.deriv.DAOD_TOPQ1.e8276_s3126_r9364_p4514

Table 21: TOPQ1 DAOD list for H^+ sample in this analysis.

1237 A.3 $\bar{t}bW'$

1238 Table 22 is the TOPQ1 DAOD list for the W' sample in this analysis.

Nominal
mc16_13TeV.510889.MGPy8EG_WprimeTbTb_lep_LH_1000_10.deriv.DAOD_TOPQ1.e8470_s3126_r9364_p4514
mc16_13TeV.510890.MGPy8EG_WprimeTbTb_lep_LH_1200_10.deriv.DAOD_TOPQ1.e8470_s3126_r9364_p4514
mc16_13TeV.510891.MGPy8EG_WprimeTbTb_lep_LH_1400_10.deriv.DAOD_TOPQ1.e8470_s3126_r9364_p4514
mc16_13TeV.510892.MGPy8EG_WprimeTbTb_lep_LH_1600_10.deriv.DAOD_TOPQ1.e8470_s3126_r9364_p4514
mc16_13TeV.510893.MGPy8EG_WprimeTbTb_lep_LH_1800_10.deriv.DAOD_TOPQ1.e8470_s3126_r9364_p4514
mc16_13TeV.510894.MGPy8EG_WprimeTbTb_lep_LH_2000_10.deriv.DAOD_TOPQ1.e8470_s3126_r9364_p4514
mc16_13TeV.510895.MGPy8EG_WprimeTbTb_lep_LH_2500_10.deriv.DAOD_TOPQ1.e8470_s3126_r9364_p4514
mc16_13TeV.510896.MGPy8EG_WprimeTbTb_lep_LH_3000_10.deriv.DAOD_TOPQ1.e8470_s3126_r9364_p4514
mc16_13TeV.510897.MGPy8EG_WprimeTbTb_lep_LH_4000_10.deriv.DAOD_TOPQ1.e8470_s3126_r9364_p4514
mc16_13TeV.510898.MGPy8EG_WprimeTbTb_lep_RH_1000_10.deriv.DAOD_TOPQ1.e8470_s3126_r9364_p4514
mc16_13TeV.510899.MGPy8EG_WprimeTbTb_lep_RH_1200_10.deriv.DAOD_TOPQ1.e8470_s3126_r9364_p4514
mc16_13TeV.510900.MGPy8EG_WprimeTbTb_lep_RH_1400_10.deriv.DAOD_TOPQ1.e8470_s3126_r9364_p4514
mc16_13TeV.510901.MGPy8EG_WprimeTbTb_lep_RH_1600_10.deriv.DAOD_TOPQ1.e8470_s3126_r9364_p4514
mc16_13TeV.510902.MGPy8EG_WprimeTbTb_lep_RH_1800_10.deriv.DAOD_TOPQ1.e8470_s3126_r9364_p4514
mc16_13TeV.510903.MGPy8EG_WprimeTbTb_lep_RH_2000_10.deriv.DAOD_TOPQ1.e8470_s3126_r9364_p4514
mc16_13TeV.510904.MGPy8EG_WprimeTbTb_lep_RH_2500_10.deriv.DAOD_TOPQ1.e8470_s3126_r9364_p4514
mc16_13TeV.510905.MGPy8EG_WprimeTbTb_lep_RH_3000_10.deriv.DAOD_TOPQ1.e8470_s3126_r9364_p4514
mc16_13TeV.510906.MGPy8EG_WprimeTbTb_lep_RH_4000_10.deriv.DAOD_TOPQ1.e8470_s3126_r9364_p4514

Table 22: TOPQ1 DAOD list for W' sample in this analysis.

1239 **A.4 $t\bar{t} + \text{jets}$**

1240 Table 23 is the TOPQ1 DAOD list for $t\bar{t} + \text{jets}$ sample in this analysis.

Nominal
mc16_13TeV.410470.PhPy8EG_A14_ttbar_hdamp258p75_nonallhad.deriv.DAOD_TOPQ1.e6337_s3126_r9364_p4514
mc16_13TeV.410471.PhPy8EG_A14_ttbar_hdamp258p75_allhad.deriv.DAOD_TOPQ1.e6337_s3126_r9364_p4514
mc16_13TeV.411073.PhPy8EG_A14_ttbar_hdamp258p75_ljets_BBFilt.deriv.DAOD_TOPQ1.e6798_s3126_r9364_p4514
mc16_13TeV.411074.PhPy8EG_A14_ttbar_hdamp258p75_ljets_BFiltBBVeto.deriv.DAOD_TOPQ1.e6798_s3126_r9364_p4514
mc16_13TeV.411075.PhPy8EG_A14_ttbar_hdamp258p75_ljets_CFiltBVeto.deriv.DAOD_TOPQ1.e6798_s3126_r9364_p4514
mc16_13TeV.411076.PhPy8EG_A14_ttbar_hdamp258p75_dil_BBFilt.deriv.DAOD_TOPQ1.e6798_s3126_r9364_p4514
mc16_13TeV.411077.PhPy8EG_A14_ttbar_hdamp258p75_dil_BFiltBBVeto.deriv.DAOD_TOPQ1.e6798_s3126_r9364_p4514
mc16_13TeV.411078.PhPy8EG_A14_ttbar_hdamp258p75_dil_CFiltBVeto.deriv.DAOD_TOPQ1.e6798_s3126_r9364_p4514
Reference
mc16_13TeV.410470.PhPy8EG_A14_ttbar_hdamp258p75_nonallhad.deriv.DAOD_TOPQ1.e6337_a875_r9364_p4514
mc16_13TeV.410471.PhPy8EG_A14_ttbar_hdamp258p75_allhad.deriv.DAOD_TOPQ1.e6337_a875_r9364_p4514
mc16_13TeV.411073.PhPy8EG_A14_ttbar_hdamp258p75_ljets_BBFilt.deriv.DAOD_TOPQ1.e6798_a875_r9364_p4514
mc16_13TeV.411074.PhPy8EG_A14_ttbar_hdamp258p75_ljets_BFiltBBVeto.deriv.DAOD_TOPQ1.e6798_a875_r9364_p4514
mc16_13TeV.411075.PhPy8EG_A14_ttbar_hdamp258p75_ljets_CFiltBVeto.deriv.DAOD_TOPQ1.e6798_a875_r9364_p4514
mc16_13TeV.411076.PhPy8EG_A14_ttbar_hdamp258p75_dil_BBFilt.deriv.DAOD_TOPQ1.e6798_a875_r9364_p4514
mc16_13TeV.411077.PhPy8EG_A14_ttbar_hdamp258p75_dil_BFiltBBVeto.deriv.DAOD_TOPQ1.e6798_a875_r9364_p4514
mc16_13TeV.411078.PhPy8EG_A14_ttbar_hdamp258p75_dil_CFiltBVeto.deriv.DAOD_TOPQ1.e6798_a875_r9364_p4514
Alternative
mc16_13TeV.410557.PowhegHerwig7EvtGen_H7UE_tt_hdamp258p75_704_SingleLep.deriv.DAOD_TOPQ1.e6366_a875_r9364_p4514
mc16_13TeV.410558.PowhegHerwig7EvtGen_H7UE_tt_hdamp258p75_704_dil.deriv.DAOD_TOPQ1.e6366_a875_r9364_p4514
mc16_13TeV.411082.PhHerwig7EG_H7UE_ttbar_hdamp258p75_ljets_BBFilt.deriv.DAOD_TOPQ1.e6799_a875_r9364_p4514
mc16_13TeV.411083.PhHerwig7EG_H7UE_ttbar_hdamp258p75_ljets_BFiltBBVeto.deriv.DAOD_TOPQ1.e6799_a875_r9364_p4514
mc16_13TeV.411084.PhHerwig7EG_H7UE_ttbar_hdamp258p75_ljets_CFiltBVeto.deriv.DAOD_TOPQ1.e6799_a875_r9364_p4514
mc16_13TeV.411085.PhHerwig7EG_H7UE_ttbar_hdamp258p75_dil_BBFilt.deriv.DAOD_TOPQ1.e6799_a875_r9364_p4514
mc16_13TeV.411086.PhHerwig7EG_H7UE_ttbar_hdamp258p75_dil_BFiltBBVeto.deriv.DAOD_TOPQ1.e6799_a875_r9364_p4514
mc16_13TeV.411087.PhHerwig7EG_H7UE_ttbar_hdamp258p75_dil_CFiltBVeto.deriv.DAOD_TOPQ1.e6799_a875_r9364_p4514
mc16_13TeV.411088.PhHerwig7EG_H7UE_ttbar_hdamp258p75_allhad_BBFilt.deriv.DAOD_TOPQ1.e6799_a875_r9364_p4514
mc16_13TeV.411089.PhHerwig7EG_H7UE_ttbar_hdamp258p75_allhad_BFiltBBVeto.deriv.DAOD_TOPQ1.e6799_a875_r9364_p4514
mc16_13TeV.411090.PhHerwig7EG_H7UE_ttbar_hdamp258p75_allhad_CFiltBVeto.deriv.DAOD_TOPQ1.e6799_a875_r9364_p4514
mc16_13TeV.410464.aMcAtNloPy8EvtGen_MEN30NLO_A14N23LO_ttbar_noShWe_SingleLep.deriv.DAOD_TOPQ1.e6762_a875_r9364_p4514
mc16_13TeV.410465.aMcAtNloPy8EvtGen_MEN30NLO_A14N23LO_ttbar_noShWe_dil.deriv.DAOD_TOPQ1.e6762_a875_r9364_p4514
mc16_13TeV.410466.aMcAtNloPy8EvtGen_MEN30NLO_A14N23LO_ttbar_noShWe_AllHadronic.deriv.DAOD_TOPQ1.e6762_a875_r9364_p4514
mc16_13TeV.412066.aMcAtNloPy8EG_A14_ttbar_hdamp258p75_ljets_BBFilt.deriv.DAOD_TOPQ1.e7129_a875_r9364_p4514
mc16_13TeV.412067.aMcAtNloPy8EG_A14_ttbar_hdamp258p75_ljets_BFiltBBVeto.deriv.DAOD_TOPQ1.e7129_a875_r9364_p4514
mc16_13TeV.412068.aMcAtNloPy8EG_A14_ttbar_hdamp258p75_ljets_CFiltBVeto.deriv.DAOD_TOPQ1.e7129_a875_r9364_p4514
mc16_13TeV.412069.aMcAtNloPy8EG_A14_ttbar_hdamp258p75_dil_BBFilt.deriv.DAOD_TOPQ1.e7129_a875_r9364_p4514
mc16_13TeV.412070.aMcAtNloPy8EG_A14_ttbar_hdamp258p75_dil_BFiltBBVeto.deriv.DAOD_TOPQ1.e7129_a875_r9364_p4514
mc16_13TeV.412071.aMcAtNloPy8EG_A14_ttbar_hdamp258p75_dil_CFiltBVeto.deriv.DAOD_TOPQ1.e7129_a875_r9364_p4514

Table 23: TOPQ1 DAOD list for $t\bar{t}$ + jets sample in this analysis.

1241 A.5 $t\bar{t}H$

1242 Table 24 is the TOPQ1 DAOD list for $t\bar{t}H$ sample in this analysis.

Nominal	
mc16_13TeV.346343.PhPy8EG_A14NNPDF23_NNPDF30ME_ttH125_allhad.deriv.DAOD_TOPQ1.e7148_s3126_r9364_p4514	
mc16_13TeV.346344.PhPy8EG_A14NNPDF23_NNPDF30ME_ttH125_semilep.deriv.DAOD_TOPQ1.e7148_s3126_r9364_p4514	
mc16_13TeV.346345.PhPy8EG_A14NNPDF23_NNPDF30ME_ttH125_dilep.deriv.DAOD_TOPQ1.e7148_s3126_r9364_p4514	
Reference	
mc16_13TeV.346343.PhPy8EG_A14NNPDF23_NNPDF30ME_ttH125_allhad.deriv.DAOD_TOPQ1.e7148_a875_r9364_p4514	
mc16_13TeV.346344.PhPy8EG_A14NNPDF23_NNPDF30ME_ttH125_semilep.deriv.DAOD_TOPQ1.e7148_a875_r9364_p4514	
mc16_13TeV.346345.PhPy8EG_A14NNPDF23_NNPDF30ME_ttH125_dilep.deriv.DAOD_TOPQ1.e7148_a875_r9364_p4514	
Alternative	
mc16_13TeV.346443.aMcAtNloPythia8EvtGen_ttH_noShWe_dilep.deriv.DAOD_TOPQ1.e7310_a875_r9364_p4514	
mc16_13TeV.346444.aMcAtNloPythia8EvtGen_ttH_noShWe_semilep.deriv.DAOD_TOPQ1.e7310_a875_r9364_p4514	
mc16_13TeV.346445.aMcAtNloPythia8EvtGen_ttH_noShWe_allhad.deriv.DAOD_TOPQ1.e7310_a875_r9364_p4514	
mc16_13TeV.346346.PhH7EG_H7UE_NNPDF30ME_ttH125_allhad.deriv.DAOD_TOPQ1.e7148_a875_r9364_p4514	
mc16_13TeV.346347.PhH7EG_H7UE_NNPDF30ME_ttH125_semilep.deriv.DAOD_TOPQ1.e7148_a875_r9364_p4514	
mc16_13TeV.346348.PhH7EG_H7UE_NNPDF30ME_ttH125_dilep.deriv.DAOD_TOPQ1.e7148_a875_r9364_p4514	

Table 24: TOPQ1 DAOD list for $t\bar{t}H$ sample in this analysis.

1243 **A.6 $t\bar{t}V$**

1244 Table 25 is the TOPQ1 DAOD list for $t\bar{t}V$ sample in this analysis.

Nominal	
mc16_13TeV.410155.aMcAtNloPythia8EvtGen_MEN30NLO_A14N23LO_ttW.deriv.DAOD_TOPQ1.e5070_s3126_r9364_p4514	
mc16_13TeV.410156.aMcAtNloPythia8EvtGen_MEN30NLO_A14N23LO_ttZnunu.deriv.DAOD_TOPQ1.e5070_s3126_r9364_p4514	
mc16_13TeV.410157.aMcAtNloPythia8EvtGen_MEN30NLO_A14N23LO_ttZqq.deriv.DAOD_TOPQ1.e5070_s3126_r9364_p4514	
mc16_13TeV.410218.aMcAtNloPythia8EvtGen_MEN30NLO_A14N23LO_ttee.deriv.DAOD_TOPQ1.e5070_s3126_r9364_p4514	
mc16_13TeV.410219.aMcAtNloPythia8EvtGen_MEN30NLO_A14N23LO_ttmumu.deriv.DAOD_TOPQ1.e5070_s3126_r9364_p4514	
mc16_13TeV.410220.aMcAtNloPythia8EvtGen_MEN30NLO_A14N23LO_ttautau.deriv.DAOD_TOPQ1.e5070_s3126_r9364_p4514	
mc16_13TeV.410276.aMcAtNloPythia8EvtGen_MEN30NLO_A14N23LO_tee_mll_1_5.deriv.DAOD_TOPQ1.e6087_s3126_r9364_p4514	
mc16_13TeV.410277.aMcAtNloPythia8EvtGen_MEN30NLO_A14N23LO_ttmumu_mll_1_5.deriv.DAOD_TOPQ1.e6087_s3126_r9364_p4514	
mc16_13TeV.410278.aMcAtNloPythia8EvtGen_MEN30NLO_A14N23LO_ttautau_mll_1_5.deriv.DAOD_TOPQ1.e6087_s3126_r9364_p4514	
Alternative	
mc16_13TeV.410142.Sherpa_NNPDF30NNLO_ttll_mll5.deriv.DAOD_TOPQ1.e4686_s3126_r9364_p4514	
mc16_13TeV.410143.Sherpa_NNPDF30NNLO_ttZnnqq.deriv.DAOD_TOPQ1.e4686_s3126_r9364_p4514	
mc16_13TeV.410144.Sherpa_NNPDF30NNLO_ttW.deriv.DAOD_TOPQ1.e4686_s3126_r9364_p4514	

Table 25: TOPQ1 DAOD list for $t\bar{t}V$ sample in this analysis.

1245 **A.7 Single top**

1246 Table 26 is the TOPQ1 DAOD list for single top sample in this analysis.

Nominal
mc16_13TeV.410644.PowhegPythia8EvtGen_A14_singletop_schan_lept_top.deriv.DAOD_TOPQ1.e6527_s3126_r9364_p4514
mc16_13TeV.410645.PowhegPythia8EvtGen_A14_singletop_schan_lept_antitop.deriv.DAOD_TOPQ1.e6527_s3126_r9364_p4514
mc16_13TeV.410646.PowhegPythia8EvtGen_A14_Wt_DR_inclusive_top.deriv.DAOD_TOPQ1.e6552_s3126_r9364_p4514
mc16_13TeV.410647.PowhegPythia8EvtGen_A14_Wt_DR_inclusive_antitop.deriv.DAOD_TOPQ1.e6552_s3126_r9364_p4514
mc16_13TeV.410658.PhPy8EG_A14_tchan_BW50_lept_top.deriv.DAOD_TOPQ1.e6671_s3126_r9364_p4514
mc16_13TeV.410659.PhPy8EG_A14_tchan_BW50_lept_antitop.deriv.DAOD_TOPQ1.e6671_s3126_r9364_p4514
Reference
mc16_13TeV.410644.PowhegPythia8EvtGen_A14_singletop_schan_lept_top.deriv.DAOD_TOPQ1.e6527_a875_r9364_p4514
mc16_13TeV.410645.PowhegPythia8EvtGen_A14_singletop_schan_lept_antitop.deriv.DAOD_TOPQ1.e6527_a875_r9364_p4514
mc16_13TeV.410646.PowhegPythia8EvtGen_A14_Wt_DR_inclusive_top.deriv.DAOD_TOPQ1.e6552_a875_r9364_p4514
mc16_13TeV.410647.PowhegPythia8EvtGen_A14_Wt_DR_inclusive_antitop.deriv.DAOD_TOPQ1.e6552_a875_r9364_p4514
mc16_13TeV.410658.PhPy8EG_A14_tchan_BW50_lept_top.deriv.DAOD_TOPQ1.e6671_a875_r9364_p4514
mc16_13TeV.410659.PhPy8EG_A14_tchan_BW50_lept_antitop.deriv.DAOD_TOPQ1.e6671_a875_r9364_p4514
Alternative
mc16_13TeV.410654.PowhegPythia8EvtGen_A14_Wt_DS_inclusive_top.deriv.DAOD_TOPQ1.e6552_s3126_r9364_p4514
mc16_13TeV.410655.PowhegPythia8EvtGen_A14_Wt_DS_inclusive_antitop.deriv.DAOD_TOPQ1.e6552_s3126_r9364_p4514
mc16_13TeV.411032.PowhegHerwig7EvtGen_H7UE_704_tchan_lept_antitop.deriv.DAOD_TOPQ1.e6719_a875_r9364_p4514
mc16_13TeV.411033.PowhegHerwig7EvtGen_H7UE_704_tchan_lept_top.deriv.DAOD_TOPQ1.e6719_a875_r9364_p4514
mc16_13TeV.411034.PhHerwig7EG_H7UE_singletop_schan_lept_top.deriv.DAOD_TOPQ1.e6734_a875_r9364_p4514
mc16_13TeV.411035.PhHerwig7EG_H7UE_singletop_schan_lept_antitop.deriv.DAOD_TOPQ1.e6734_a875_r9364_p4514
mc16_13TeV.411036.PowhegHerwig7EvtGen_H7UE_Wt_DR_inclusive_top.deriv.DAOD_TOPQ1.e6702_a875_r9364_p4514
mc16_13TeV.411037.PowhegHerwig7EvtGen_H7UE_Wt_DR_inclusive_antitop.deriv.DAOD_TOPQ1.e6702_a875_r9364_p4514
mc16_13TeV.412002.aMcAtNloPythia8EvtGen_HThalfscale_tW_inclusive.deriv.DAOD_TOPQ1.e6817_a875_r9364_p4514
mc16_13TeV.412004.aMcAtNloPy8EG_tchan_NLO.deriv.DAOD_TOPQ1.e6888_a875_r9364_p4514

Table 26: TOPQ1 DAOD list for single top sample in this analysis.

1247 A.8 tH

1248 Table 27 is the TOPQ1 DAOD list for tH sample in this analysis.

Nominal
mc16_13TeV.346676.aMcAtNloPythia8EvtGen_tHjb125_4fl_CPalpha_0.deriv.DAOD_TOPQ1.e7815_a875_r9364_p4514
mc16_13TeV.346678.aMcAtNloPythia8EvtGen_tWH125_4fl_CPalpha_0.deriv.DAOD_TOPQ1.e7816_a875_r9364_p4514

Table 27: TOPQ1 DAOD list for tH sample in this analysis.

1249 A.9 Rare t processes

1250 Table 28 is the TOPQ1 DAOD list for rare t processes' sample in this analysis.

Nominal
mc16_13TeV.410560.MadGraphPythia8EvtGen_A14_tZ_4fl_tchan_noAllHad.deriv.DAOD_TOPQ1.e5803_s3126_r9364_p4514
mc16_13TeV.410408.aMcAtNloPythia8EvtGen_tWZ_Ztoll_minDR1.deriv.DAOD_TOPQ1.e6423_s3126_r9364_p4514
mc16_13TeV.412043.aMcAtNloPythia8EvtGen_A14NNPDF31_SM4topsNLO.deriv.DAOD_TOPQ1.e7101_a875_r9364_p4514

Table 28: TOPQ1 DAOD list for rare processes' sample in this analysis.

1251 A.10 Vector bosons plus jets

1252 A.10.1 $W + \text{jets}$

1253 Table 29 is the TOPQ1 DAOD list for $W + \text{jets}$ sample in this analysis.

Nominal
mc16_13TeV.364170.Sherpa_221_NNPDF30NNLO_Wenu_MAXHTPTV0_70_CVetoBVeto.deriv.DAOD_TOPQ1.e5340_s3126_r9364_p4512
mc16_13TeV.364171.Sherpa_221_NNPDF30NNLO_Wenu_MAXHTPTV0_70_CFilterBVeto.deriv.DAOD_TOPQ1.e5340_s3126_r9364_p4512
mc16_13TeV.364172.Sherpa_221_NNPDF30NNLO_Wenu_MAXHTPTV0_70_BFilter.deriv.DAOD_TOPQ1.e5340_s3126_r9364_p4512
mc16_13TeV.364173.Sherpa_221_NNPDF30NNLO_Wenu_MAXHTPTV70_140_CVetoBVeto.deriv.DAOD_TOPQ1.e5340_s3126_r9364_p4512
mc16_13TeV.364174.Sherpa_221_NNPDF30NNLO_Wenu_MAXHTPTV70_140_CFilterBVeto.deriv.DAOD_TOPQ1.e5340_s3126_r9364_p4512
mc16_13TeV.364175.Sherpa_221_NNPDF30NNLO_Wenu_MAXHTPTV70_140_BFilter.deriv.DAOD_TOPQ1.e5340_s3126_r9364_p4512
mc16_13TeV.364176.Sherpa_221_NNPDF30NNLO_Wenu_MAXHTPTV140_280_CVetoBVeto.deriv.DAOD_TOPQ1.e5340_s3126_r9364_p4512
mc16_13TeV.364177.Sherpa_221_NNPDF30NNLO_Wenu_MAXHTPTV140_280_CFilterBVeto.deriv.DAOD_TOPQ1.e5340_s3126_r9364_p4512
mc16_13TeV.364178.Sherpa_221_NNPDF30NNLO_Wenu_MAXHTPTV140_280_BFilter.deriv.DAOD_TOPQ1.e5340_s3126_r9364_p4512
mc16_13TeV.364179.Sherpa_221_NNPDF30NNLO_Wenu_MAXHTPTV280_500_CVetoBVeto.deriv.DAOD_TOPQ1.e5340_s3126_r9364_p4512
mc16_13TeV.364180.Sherpa_221_NNPDF30NNLO_Wenu_MAXHTPTV280_500_CFilterBVeto.deriv.DAOD_TOPQ1.e5340_s3126_r9364_p4512
mc16_13TeV.364181.Sherpa_221_NNPDF30NNLO_Wenu_MAXHTPTV280_500_BFilter.deriv.DAOD_TOPQ1.e5340_s3126_r9364_p4512
mc16_13TeV.364182.Sherpa_221_NNPDF30NNLO_Wenu_MAXHTPTV500_1000.deriv.DAOD_TOPQ1.e5340_s3126_r9364_p4512
mc16_13TeV.364183.Sherpa_221_NNPDF30NNLO_Wenu_MAXHTPTV1000_E_CMS.deriv.DAOD_TOPQ1.e5340_s3126_r9364_p4512
mc16_13TeV.364156.Sherpa_221_NNPDF30NNLO_Wmumu_MAXHTPTV0_70_CVetoBVeto.deriv.DAOD_TOPQ1.e5340_s3126_r9364_p4512
mc16_13TeV.364157.Sherpa_221_NNPDF30NNLO_Wmumu_MAXHTPTV0_70_CFilterBVeto.deriv.DAOD_TOPQ1.e5340_s3126_r9364_p4512
mc16_13TeV.364158.Sherpa_221_NNPDF30NNLO_Wmumu_MAXHTPTV0_70_BFilter.deriv.DAOD_TOPQ1.e5340_s3126_r9364_p4512
mc16_13TeV.364159.Sherpa_221_NNPDF30NNLO_Wmumu_MAXHTPTV70_140_CVetoBVeto.deriv.DAOD_TOPQ1.e5340_s3126_r9364_p4512
mc16_13TeV.364160.Sherpa_221_NNPDF30NNLO_Wmumu_MAXHTPTV70_140_CFilterBVeto.deriv.DAOD_TOPQ1.e5340_s3126_r9364_p4512
mc16_13TeV.364161.Sherpa_221_NNPDF30NNLO_Wmumu_MAXHTPTV70_140_BFilter.deriv.DAOD_TOPQ1.e5340_s3126_r9364_p4512
mc16_13TeV.364162.Sherpa_221_NNPDF30NNLO_Wmumu_MAXHTPTV140_280_CVetoBVeto.deriv.DAOD_TOPQ1.e5340_s3126_r9364_p4512
mc16_13TeV.364163.Sherpa_221_NNPDF30NNLO_Wmumu_MAXHTPTV140_280_CFilterBVeto.deriv.DAOD_TOPQ1.e5340_s3126_r9364_p4512
mc16_13TeV.364164.Sherpa_221_NNPDF30NNLO_Wmumu_MAXHTPTV140_280_BFilter.deriv.DAOD_TOPQ1.e5340_s3126_r9364_p4512
mc16_13TeV.364165.Sherpa_221_NNPDF30NNLO_Wmumu_MAXHTPTV280_500_CVetoBVeto.deriv.DAOD_TOPQ1.e5340_s3126_r9364_p4512
mc16_13TeV.364166.Sherpa_221_NNPDF30NNLO_Wmumu_MAXHTPTV280_500_CFilterBVeto.deriv.DAOD_TOPQ1.e5340_s3126_r9364_p4512
mc16_13TeV.364167.Sherpa_221_NNPDF30NNLO_Wmumu_MAXHTPTV280_500_BFilter.deriv.DAOD_TOPQ1.e5340_s3126_r9364_p4512
mc16_13TeV.364168.Sherpa_221_NNPDF30NNLO_Wmumu_MAXHTPTV500_1000.deriv.DAOD_TOPQ1.e5340_s3126_r9364_p4512
mc16_13TeV.364169.Sherpa_221_NNPDF30NNLO_Wmumu_MAXHTPTV1000_E_CMS.deriv.DAOD_TOPQ1.e5340_s3126_r9364_p4512
mc16_13TeV.364184.Sherpa_221_NNPDF30NNLO_Wtaunu_MAXHTPTV0_70_CVetoBVeto.deriv.DAOD_TOPQ1.e5340_s3126_r9364_p4512
mc16_13TeV.364185.Sherpa_221_NNPDF30NNLO_Wtaunu_MAXHTPTV0_70_CFilterBVeto.deriv.DAOD_TOPQ1.e5340_s3126_r9364_p4512
mc16_13TeV.364186.Sherpa_221_NNPDF30NNLO_Wtaunu_MAXHTPTV0_70_BFilter.deriv.DAOD_TOPQ1.e5340_s3126_r9364_p4512
mc16_13TeV.364187.Sherpa_221_NNPDF30NNLO_Wtaunu_MAXHTPTV70_140_CVetoBVeto.deriv.DAOD_TOPQ1.e5340_s3126_r9364_p4512
mc16_13TeV.364188.Sherpa_221_NNPDF30NNLO_Wtaunu_MAXHTPTV70_140_CFilterBVeto.deriv.DAOD_TOPQ1.e5340_s3126_r9364_p4512
mc16_13TeV.364189.Sherpa_221_NNPDF30NNLO_Wtaunu_MAXHTPTV70_140_BFilter.deriv.DAOD_TOPQ1.e5340_s3126_r9364_p4512
mc16_13TeV.364190.Sherpa_221_NNPDF30NNLO_Wtaunu_MAXHTPTV140_280_CVetoBVeto.deriv.DAOD_TOPQ1.e5340_s3126_r9364_p4512
mc16_13TeV.364191.Sherpa_221_NNPDF30NNLO_Wtaunu_MAXHTPTV140_280_CFilterBVeto.deriv.DAOD_TOPQ1.e5340_s3126_r9364_p4512
mc16_13TeV.364192.Sherpa_221_NNPDF30NNLO_Wtaunu_MAXHTPTV140_280_BFilter.deriv.DAOD_TOPQ1.e5340_s3126_r9364_p4512
mc16_13TeV.364193.Sherpa_221_NNPDF30NNLO_Wtaunu_MAXHTPTV280_500_CVetoBVeto.deriv.DAOD_TOPQ1.e5340_s3126_r9364_p4512
mc16_13TeV.364194.Sherpa_221_NNPDF30NNLO_Wtaunu_MAXHTPTV280_500_CFilterBVeto.deriv.DAOD_TOPQ1.e5340_s3126_r9364_p4512
mc16_13TeV.364195.Sherpa_221_NNPDF30NNLO_Wtaunu_MAXHTPTV280_500_BFilter.deriv.DAOD_TOPQ1.e5340_s3126_r9364_p4512
mc16_13TeV.364196.Sherpa_221_NNPDF30NNLO_Wtaunu_MAXHTPTV500_1000.deriv.DAOD_TOPQ1.e5340_s3126_r9364_p4512
mc16_13TeV.364197.Sherpa_221_NNPDF30NNLO_Wtaunu_MAXHTPTV1000_E_CMS.deriv.DAOD_TOPQ1.e5340_s3126_r9364_p4512

Table 29: TOPQ1 DAOD list for $W + \text{jets}$ sample in this analysis.

¹²⁵⁴ **A.10.2 $Z + \text{jets}$**

¹²⁵⁵ Table 30 is the TOPQ1 DAOD list for $Z + \text{jets}$ sample in this analysis.

Nominal

Table 30: TOPQ1 DAOD list for $Z + \text{jets}$ sample in this analysis.

A.11 Diboson

¹²⁵⁶ Table 31 is the TOPQ1 DAOD list for diboson sample in this analysis.

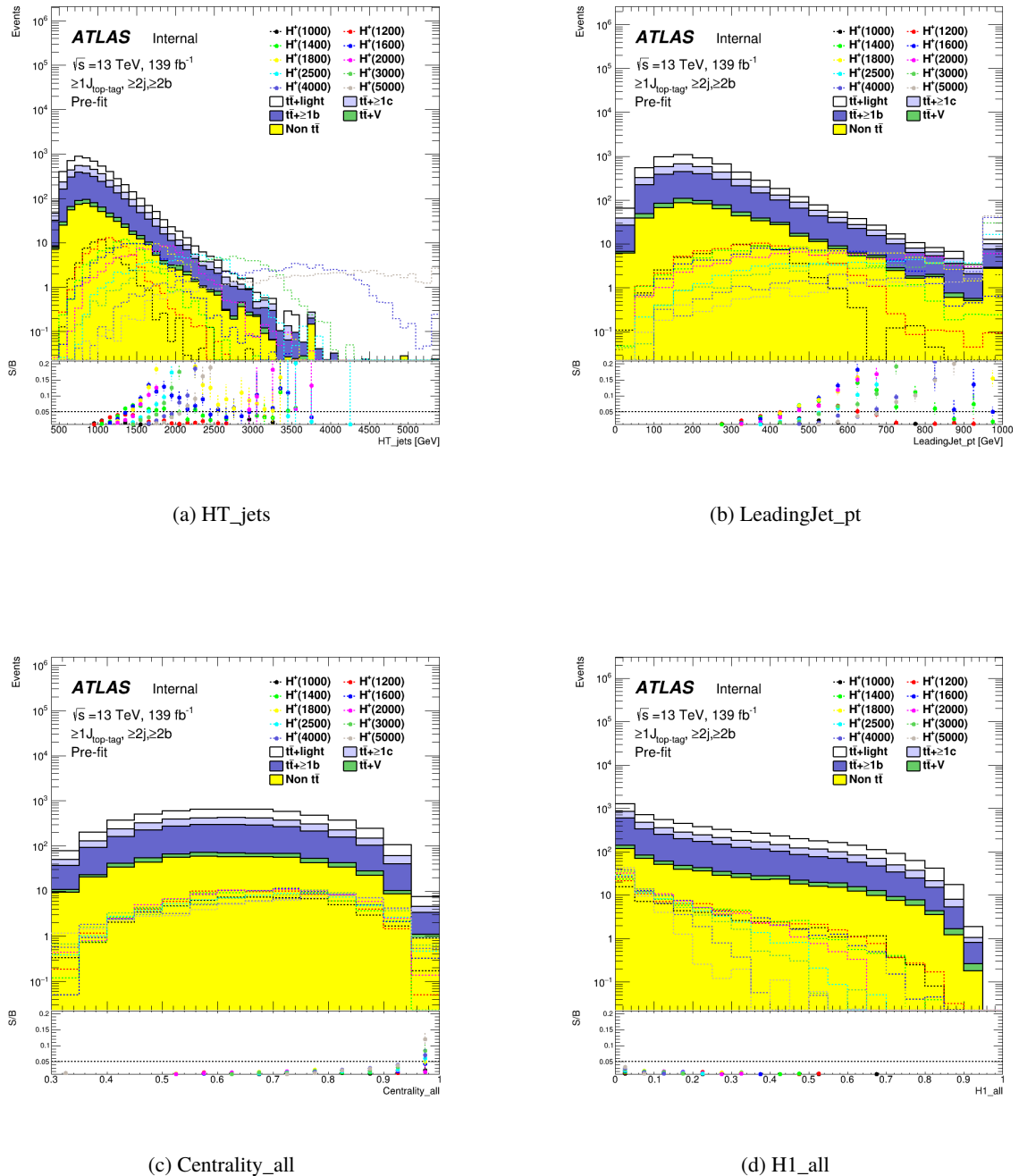
Nominal
mc16_13TeV.364250.Sherpa_222_NNPDF30NNLO_llll.deriv.DAOD_TOPQ1.e5894_s3126_r9364_p4512
mc16_13TeV.364253.Sherpa_222_NNPDF30NNLO_lllv.deriv.DAOD_TOPQ1.e5916_s3126_r9364_p4512
mc16_13TeV.364254.Sherpa_222_NNPDF30NNLO_llvv.deriv.DAOD_TOPQ1.e5916_s3126_r9364_p4512
mc16_13TeV.364255.Sherpa_222_NNPDF30NNLO_lvvv.deriv.DAOD_TOPQ1.e5916_s3126_r9364_p4512
mc16_13TeV.364288.Sherpa_222_NNPDF30NNLO_llll_lowMllPtComplement.deriv.DAOD_TOPQ1.e6096_s3126_r9364_p4512
mc16_13TeV.364289.Sherpa_222_NNPDF30NNLO_lllv_lowMllPtComplement.deriv.DAOD_TOPQ1.e6133_s3126_r9364_p4512
mc16_13TeV.364290.Sherpa_222_NNPDF30NNLO_llvv_lowMllPtComplement.deriv.DAOD_TOPQ1.e6096_s3126_r9364_p4512
mc16_13TeV.363355.Sherpa_221_NNPDF30NNLO_ZqqZv.deriv.DAOD_TOPQ1.e5525_s3126_r9364_p4512
mc16_13TeV.363356.Sherpa_221_NNPDF30NNLO_ZqqZll.deriv.DAOD_TOPQ1.e5525_s3126_r9364_p4512
mc16_13TeV.363357.Sherpa_221_NNPDF30NNLO_WqqZvv.deriv.DAOD_TOPQ1.e5525_s3126_r9364_p4512
mc16_13TeV.363358.Sherpa_221_NNPDF30NNLO_WqqZll.deriv.DAOD_TOPQ1.e5525_s3126_r9364_p4512
mc16_13TeV.363359.Sherpa_221_NNPDF30NNLO_WpqqWmlv.deriv.DAOD_TOPQ1.e5583_s3126_r9364_p4512
mc16_13TeV.363360.Sherpa_221_NNPDF30NNLO_WplvWmqq.deriv.DAOD_TOPQ1.e5983_s3126_r9364_p4512
mc16_13TeV.363489.Sherpa_221_NNPDF30NNLO_WlvZqq.deriv.DAOD_TOPQ1.e5525_s3126_r9364_p4512
mc16_13TeV.363494.Sherpa_221_NNPDF30NNLO_vvvv.deriv.DAOD_TOPQ1.e5332_s3126_r9364_p4512
mc16_13TeV.364283.Sherpa_222_NNPDF30NNLO_llljjj_EW6.deriv.DAOD_TOPQ1.e6055_s3126_r9364_p4512
mc16_13TeV.364284.Sherpa_222_NNPDF30NNLO_lllvjj_EW6.deriv.DAOD_TOPQ1.e6055_s3126_r9364_p4512
mc16_13TeV.364285.Sherpa_222_NNPDF30NNLO_llvvjj_EW6.deriv.DAOD_TOPQ1.e6055_s3126_r9364_p4512
mc16_13TeV.364287.Sherpa_222_NNPDF30NNLO_llvlij_ss_EW6.deriv.DAOD_TOPQ1.e6055_s3126_r9364_p4512
mc16_13TeV.345705.Sherpa_222_NNPDF30NNLO_ggllll_0M41130.deriv.DAOD_TOPQ1.e6213_s3126_r9364_p4512
mc16_13TeV.345706.Sherpa_222_NNPDF30NNLO_ggllll_130M41.deriv.DAOD_TOPQ1.e6213_s3126_r9364_p4512
mc16_13TeV.345723.Sherpa_222_NNPDF30NNLO_ggllvvZZ.deriv.DAOD_TOPQ1.e6213_s3126_r9364_p4512

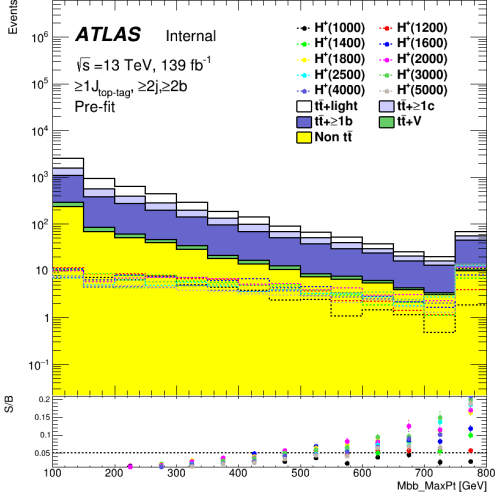
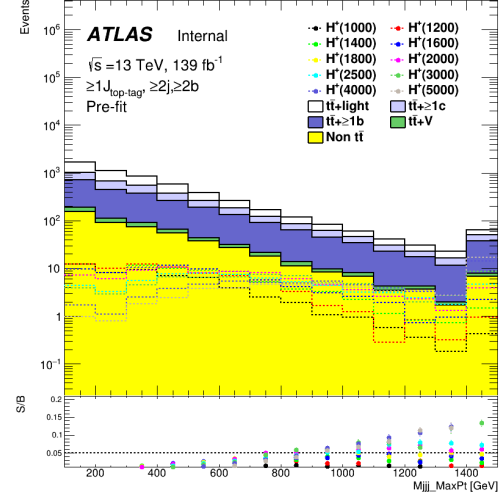
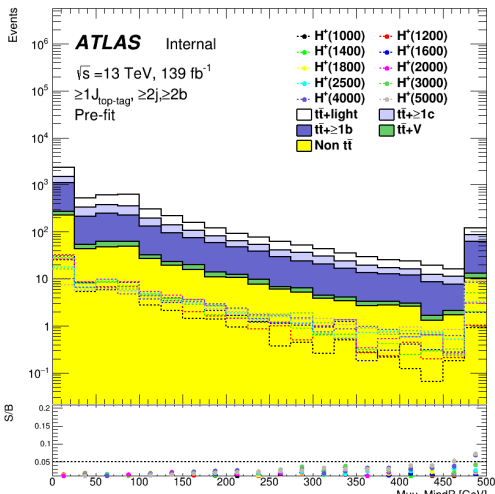
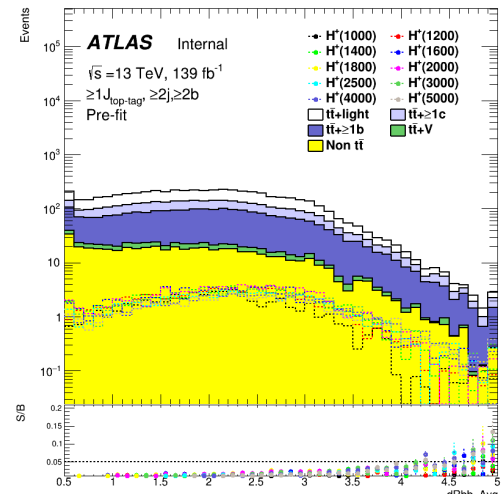
Table 31: TOPQ1 DAOD list for diboson sample in this analysis.

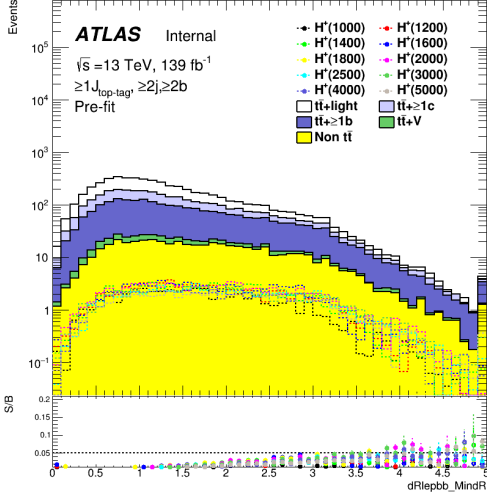
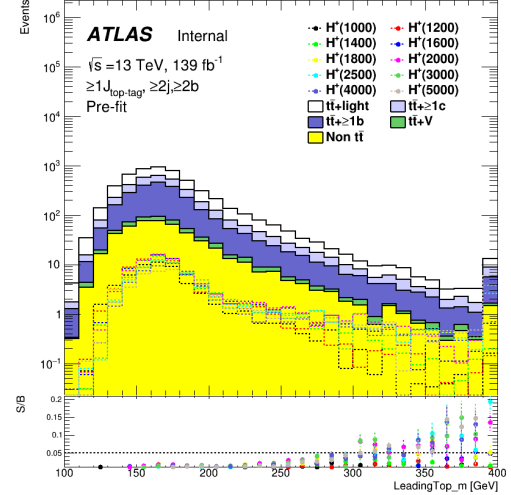
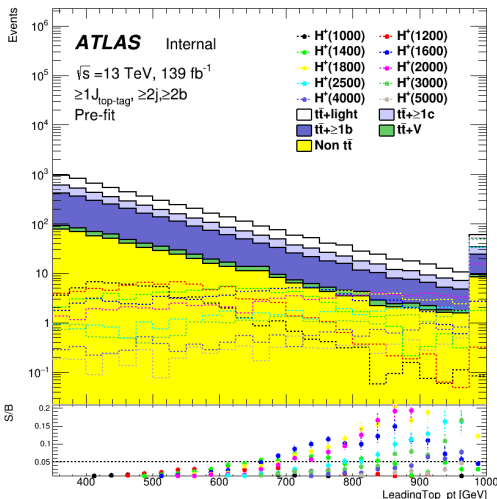
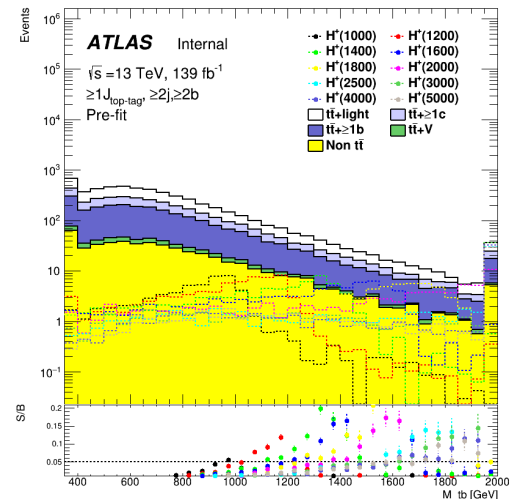
1258 B Signal/background comparisons

1259 B.1 BDT input variables

1260 Figures 176 compare the shape of the variables included in the BDT for all H^+ signal masses and background
 1261 in the SR.



(e) $M_{bb, \text{MaxPt}}$ (f) $M_{jjj, \text{MaxPt}}$ (g) $\mu_{uu, \text{MindR}}$ (h) $dR_{bb, \text{Avg}}$

(i) $dR_{\text{lepb_MindR}}$ (j) LeadingTop_m (k) LeadingTop_pt (l) M_{tb}

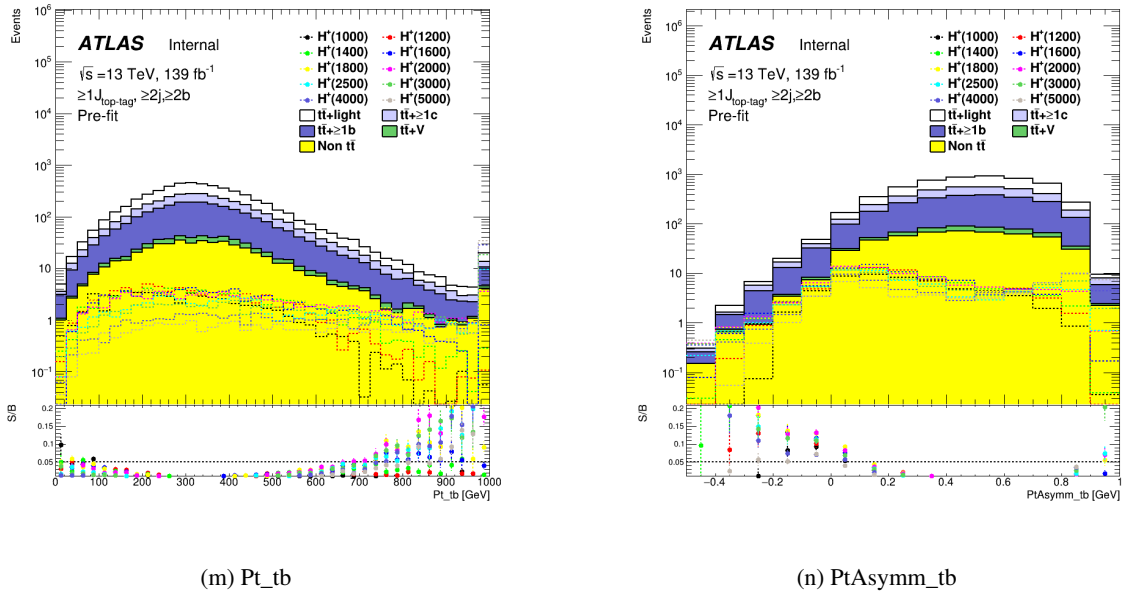
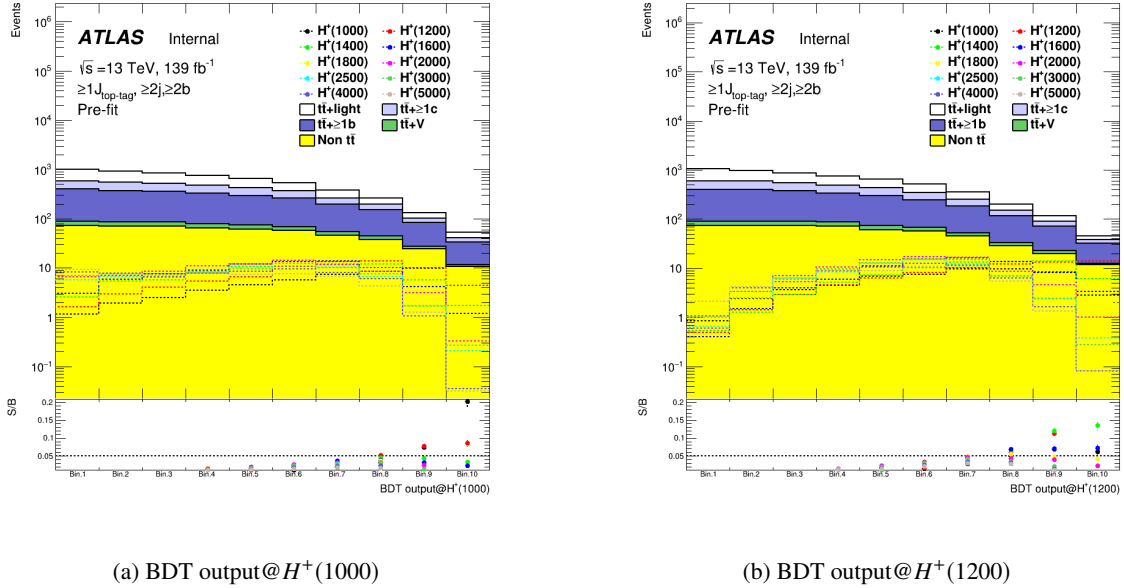
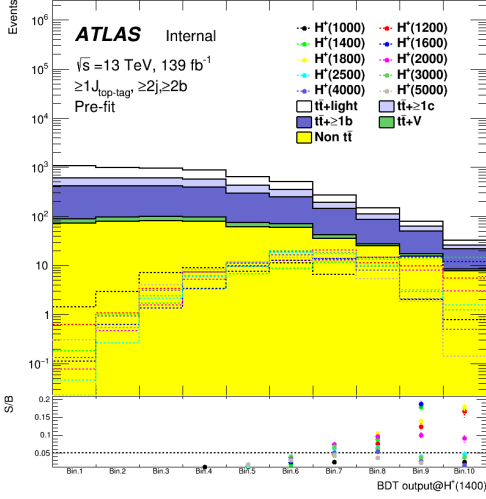
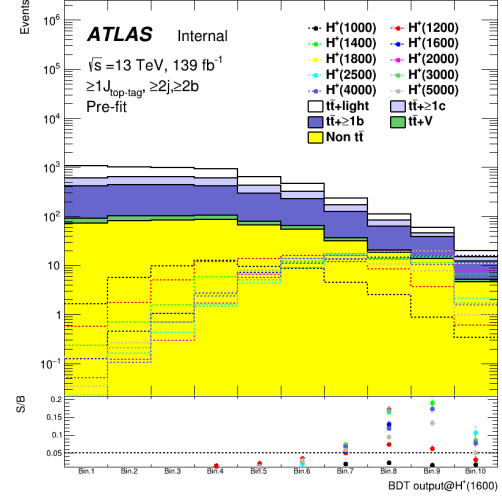
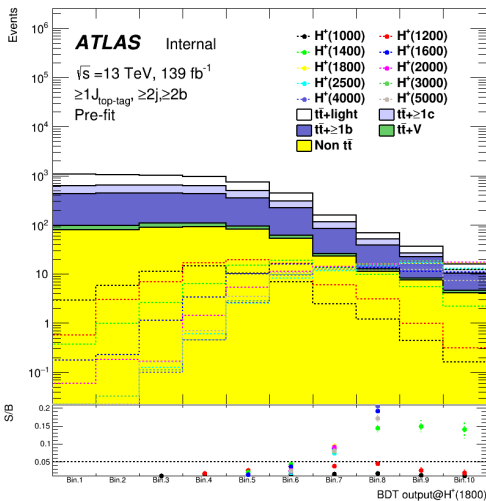
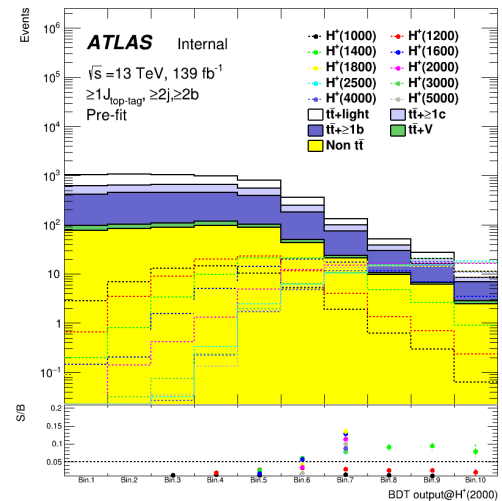


Figure 174: Comparison of the kinematic variables included in the BDT in the SR for the various H^+ signal masses between signal and background.

1262 B.2 BDT outputs

Figures 175(a) to 175(h) compare the shape of BDT outputs for all H^+ signal masses and background in the SR.



(c) BDT output@ $H^+(1400)$ (d) BDT output@ $H^+(1600)$ (e) BDT output@ $H^+(1800)$ (f) BDT output@ $H^+(2000)$

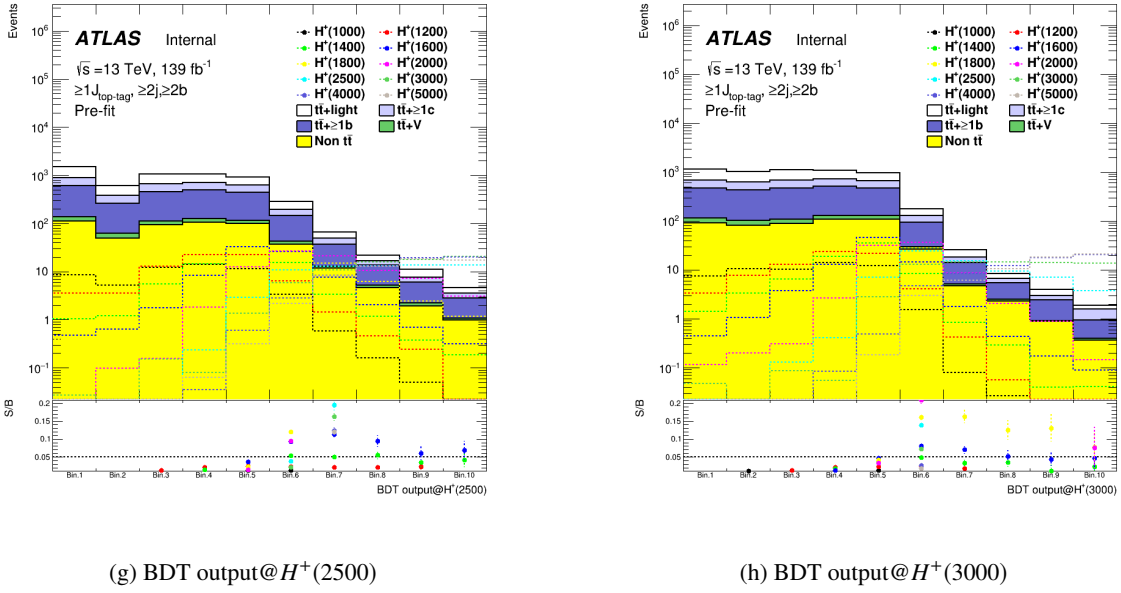


Figure 175: Comparison of BDT outputs in the SR for the various H^+ signal masses between signal and background.

1265 B.3 H_T^{jets} in the CR

1266 Figure 176 compares the shape of H_T^{jets} for all H^+ signal masses and background in the CR.

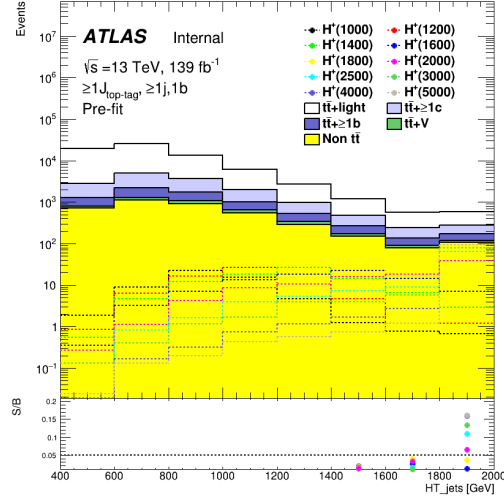


Figure 176: Comparison of H_T^{jets} in the CR for the various H^+ signal masses between signal and background.

1267 **C Fit test**

1268 **C.1 Data fit with $t\bar{t}$ + light constrained**

1269 **C.1.1 Pre-fit plots**

1270 This section tests data fits with $t\bar{t}$ + light constrained to the result of $t\bar{t}$ cross-section measurement
 1271 using boosted top-quarks in ℓ + jets channel [1]. The analysis obtained the fiducial cross-sections of
 1272 $\sigma_{\text{data}} = 1.267 \pm 0.005 \pm 0.053$ and $\sigma_{\text{MC}} = 1.481 + 0.091 - 0.083$ from collision data and $t\bar{t}$ MC (PP8),
 1273 respectively. From these results, the normalization of $t\bar{t}$ MC (PP8) is expected to be as follows:

$$\frac{\sigma_{\text{data}}}{\sigma_{\text{MC}}} \sim 0.856 + 0.074 - 0.070 \quad (3)$$

1274 We perform fitting to data (BOnly) with $t\bar{t}$ + light fixed after scaling by 0.856. The uncertainties of $\pm 1\sigma$
 1275 are introduced as an NP. Figure 177 to 181 show the pre-fit plots for each H^+ mass hypothesis.

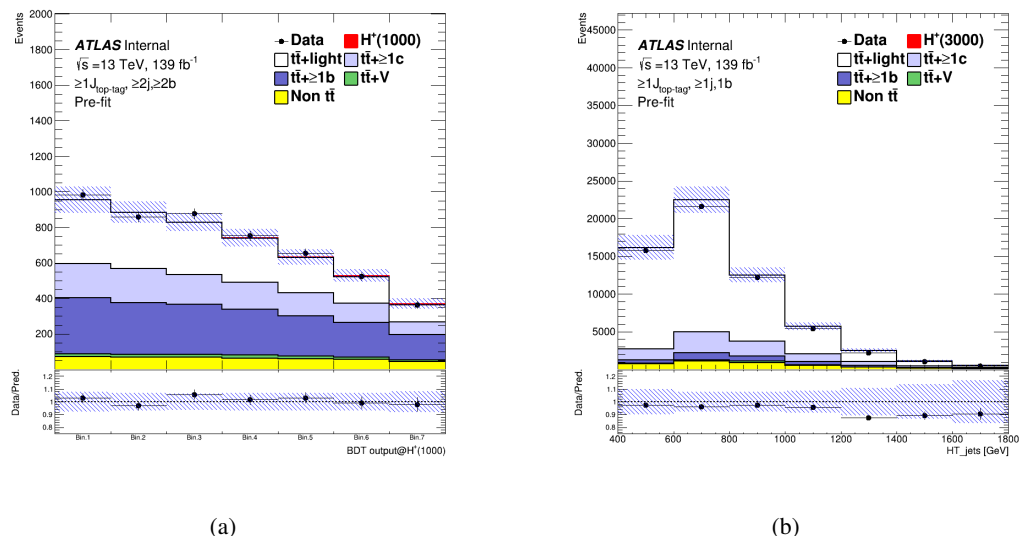


Figure 177: Pre-fit plots in the SR (left) and CR (right) for 1000 GeV mass hypothesis of H^+ signal. The blinded bins aren't plotted. $t\bar{t}$ + light MC events are scaled by 0.856. The uncertainties of $+0.074$ and -0.070 are included as systematics. The scale factor and uncertainties are the ratio of fiducial cross-sections of collision data and $t\bar{t}$ MC (PP8), which are obtained by $t\bar{t}$ cross-section measurement analysis using boosted top-quarks in ℓ + jets channel.

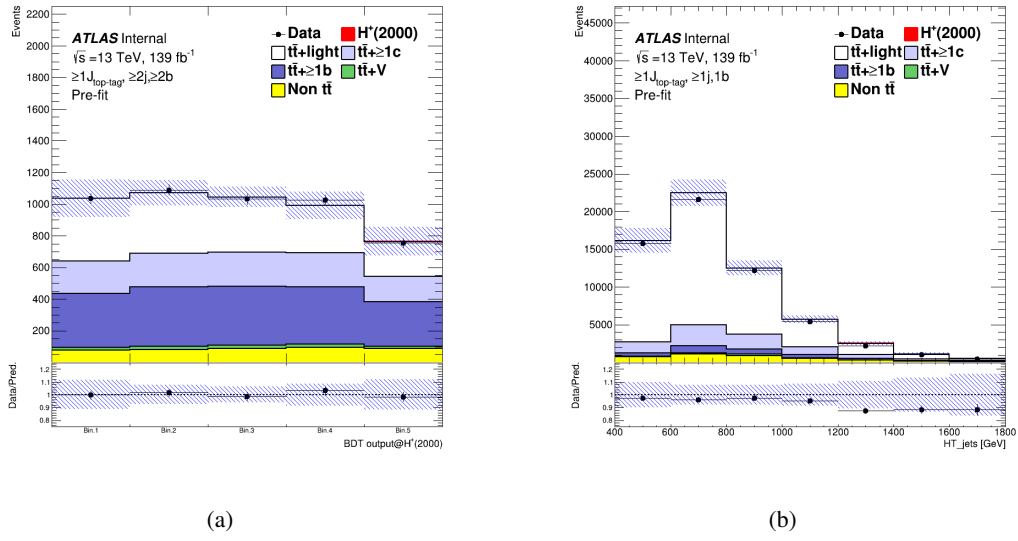


Figure 178: Pre-fit plots in the SR (left) and CR (right) for 2000 GeV mass hypothesis of H^+ signal. The blinded bins aren't plotted. $t\bar{t}$ + light MC events are scaled by 0.856. The uncertainties of +0.074 and -0.070 are included as systematics. The scale factor and uncertainties are the ratio of fiducial cross-sections of collision data and $t\bar{t}$ MC (PP8), which are obtained by $t\bar{t}$ cross-section measurement analysis using boosted top-quarks in ℓ + jets channel.

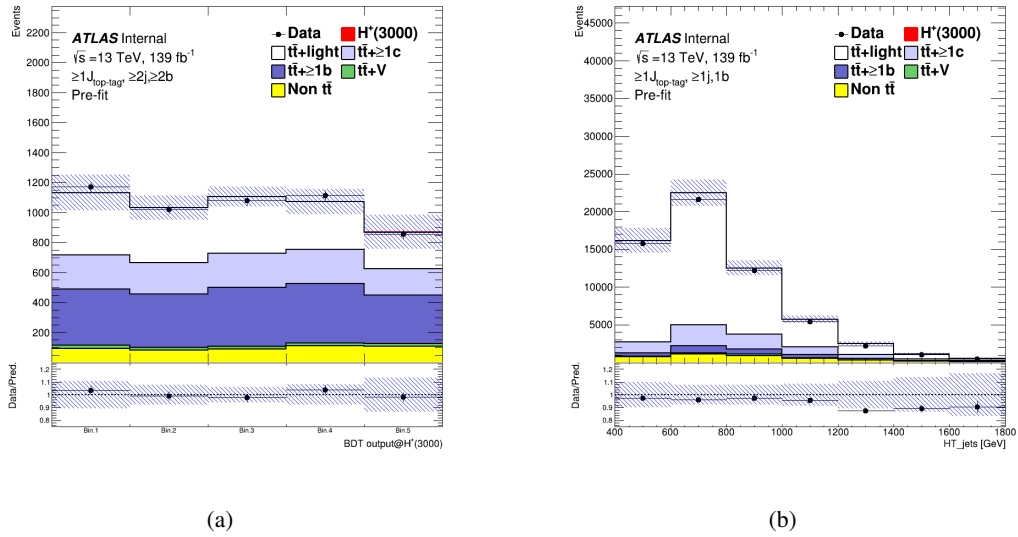


Figure 179: Pre-fit plots in the SR (left) and CR (right) for 3000 GeV mass hypothesis of H^+ signal. The blinded bins aren't plotted. $t\bar{t}$ + light MC events are scaled by 0.856. The uncertainties of +0.074 and -0.070 are included as systematics. The scale factor and uncertainties are the ratio of fiducial cross-sections of collision data and $t\bar{t}$ MC (PP8), which are obtained by $t\bar{t}$ cross-section measurement analysis using boosted top-quarks in ℓ + jets channel.

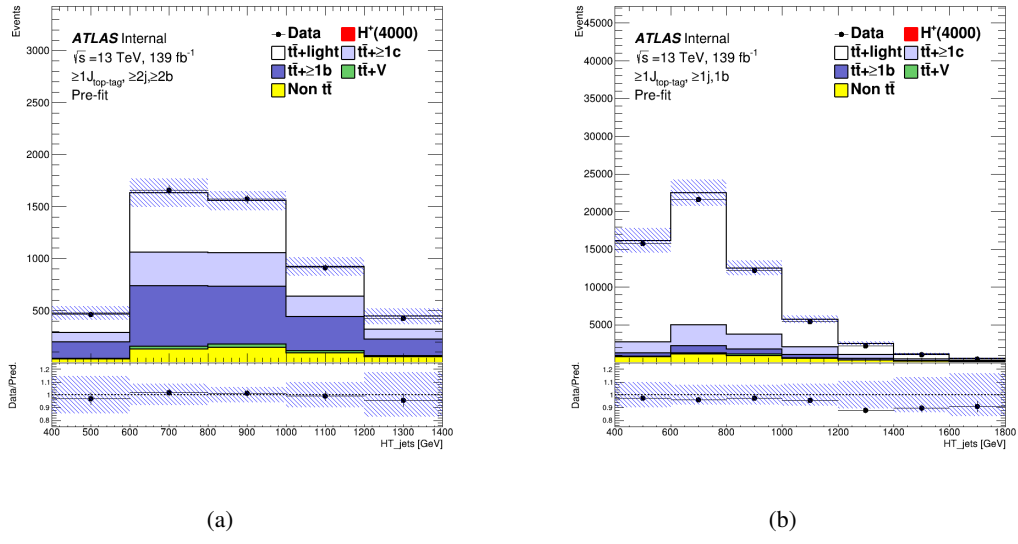


Figure 180: Pre-fit plots in the CR1 (left) and CR2 (right) for 4000 GeV mass hypothesis of H^+ signal. The blinded bins aren't plotted. $t\bar{t}$ + light MC events are scaled by 0.856. The uncertainties of $+0.074$ and -0.070 are included as systematics. The scale factor and uncertainties are the ratio of fiducial cross-sections of collision data and $t\bar{t}$ MC (PP8), which are obtained by $t\bar{t}$ cross-section measurement analysis using boosted top-quarks in $\ell + \text{jets}$ channel.

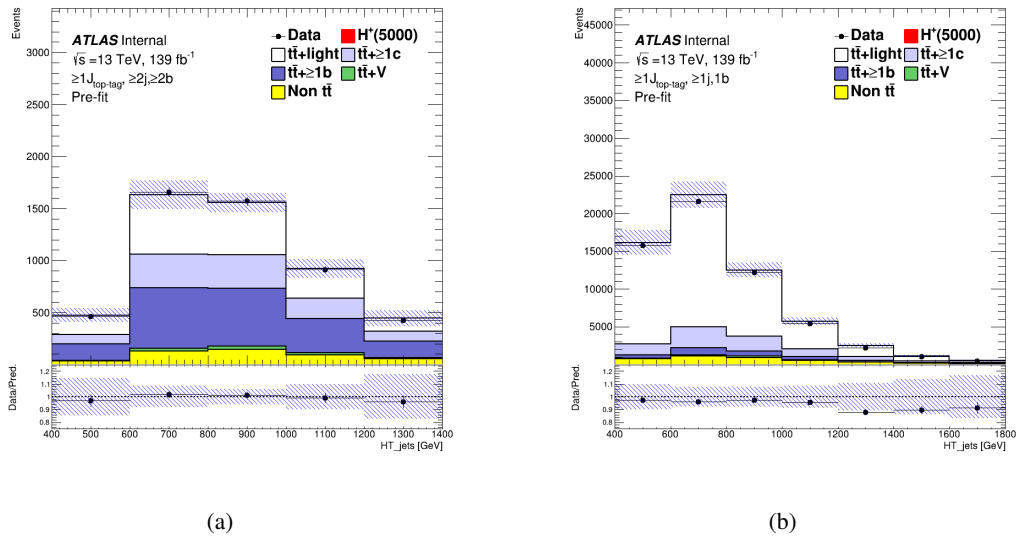
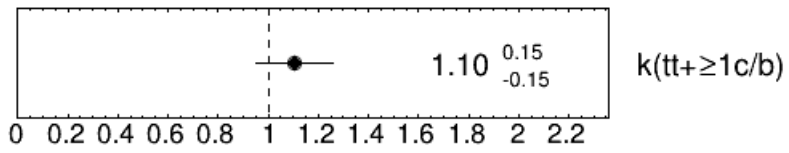


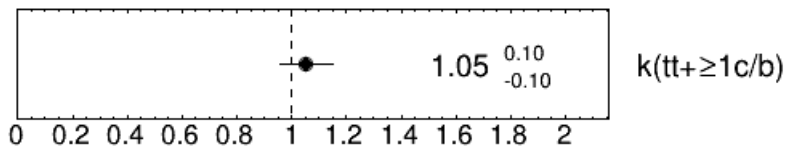
Figure 181: Pre-fit plots in the CR1 (left) and CR2 (right) for 5000 GeV mass hypothesis of H^+ signal. The blinded bins aren't plotted. $t\bar{t}$ + light MC events are scaled by 0.856. The uncertainties of $+0.074$ and -0.070 are included as systematics. The scale factor and uncertainties are the ratio of fiducial cross-sections of collision data and $t\bar{t}$ MC (PP8), which are obtained by $t\bar{t}$ cross-section measurement analysis using boosted top-quarks in $\ell + \text{jets}$ channel.

1276 C.1.2 Fit results

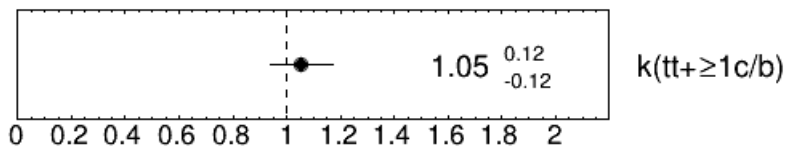
1277 Figure 182(a) to 182(e) show the BOnly fit result of $t\bar{t}$ + HF normalization for each H^+ signal mass
1278 hypothesis. These results are consistent with the results with $t\bar{t}$ + light free-floating in the fit (Section
1279 7.4.2).

ATLAS Internal

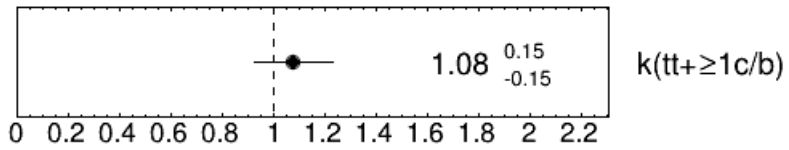
(a)

ATLAS Internal

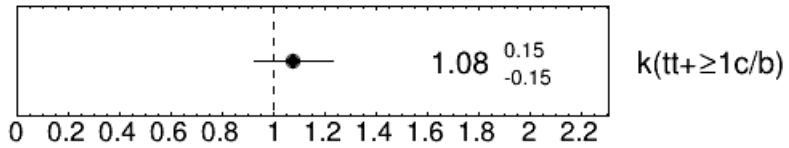
(b)

ATLAS Internal

(c)

ATLAS Internal

(d)

ATLAS Internal

(e)

Figure 182: BOnly fit results of $t\bar{t} + \text{HF}$ normalization for from 1000 to 5000 GeV H^+ signal mass hypotheses.